Associative exchange reactions of boron or nitrogen containing bonds and design of vitrimers

Max Roettger

Université Pierre et Marie Curie

École doctorale 397

Laboratoire Matière Molle et Chimie – UMR 7167

Associative Exchange Reactions of Boron or Nitrogen Containing Bonds and Design of Vitrimers

---

Par Max ROETTGER

Thèse de doctorat de Physique et Chimie des matériaux

Dirigée par Ludwik Leibler et Renaud Nicolaÿ

Présentée et soutenue publiquement le 13 décembre 2016

Devant un jury composé de :

M. E. W. (Bert) MEIJER	Rapporteur
M. Christian LIGOURE	Rapporteur
M. Ludovic JULLIEN	Examinateur
M. Jacques LALEVEE	Examinateur
M. Renaud NICOLAY	Co-Directeur de thèse
M. Ludwik LEIBLER	Directeur de thèse

Université Pierre et Marie Curie

École doctorale 397

Laboratoire Matière Molle et Chimie – UMR 7167

Associative Exchange Reactions of Boron or Nitrogen Containing Bonds and Design of Vitrimers

---

Par Max ROETTGER

Thèse de doctorat de Physique et Chimie des matériaux

Dirigée par Ludwik Leibler et Renaud Nicolaÿ

Présentée et soutenue publiquement le 13 décembre 2016

Devant un jury composé de :

M. E. W. (Bert) MEIJER	Rapporteur
M. Christian LIGOURE	Rapporteur
M. Ludovic JULLIEN	Examinateur
M. Jacques LALEVEE	Examinateur
M. Renaud NICOLAY	Co-Directeur de thèse
M. Ludwik LEIBLER	Directeur de thèse

Acknowledgements

The work presented here would have not been possible without the guidance and support of many people. I want to thank

Ludwik Leibler for supervision, advice, motivation and enthusiasm.

Renaud Nicolaÿ for supervision, patience, a friendly ear, guidance and knowledge.

Maud for patience, affection and her ability to raise my moral.

Ella for all the joy.

My siblings, parents and parents in law for good times in Paris and support.

My friends, Malick Diedhiou, Mario Majic, Miguel Pozo, Bastian Schmidt, Nurettin Aygün, Mani Daneshvar-Talebi, Georgios Dodekatos, Nick Kopp and Ole Springer for the solid and reliable friendship.

Jun Mougnier and Reda Agnaou for the good time in the office, on the football field and in Paris.

Marie-France Boucher, François Tournilhac, Corinne Soulié-Ziakovic, Anne-Claire Dumas, Marie Noëlle Rager for help in the lab.

The whole laboratory of Chemistry and Soft Matter, especially Fanny, Adrien, Coralie, Jeremy, Remy, Aurelie, Lise, Remy and Marie for their help and the good atmosphere.

Benoit, Jean-Christophe and Antoine for help with research.

Magda, Anne-Hélène, Marcos, David and Yuri from Sassypol for the time we spent together.

J.-C. Flores, C. Tzschucke, F. Wudl, Y. Cheng, R. Horn, O. Korup, M. Geske, P. Haenggi, F. Brandt, N. Bianci, C. Ducho, B. Schmidtgall for the teaching and dicussions.

Rupert, Nick, Stephan, Jan, Johanna, Linda and Jasmine for company.

Abbreviations and Variables

AIBN	Azobisisobutyronitrile
APCI	Atmospheric pressure chemical ionization
ATRP	Atom- transfer radical polymerization
BHT	Butylated hydroxytoluene
COF	Covalent adaptable frameworks
Cp	Cyclopentadiene
CTA	Chain-transfer agent
Đ	Dispersity
DA	Diels-Alder
DCC	Dynamic covalent chemistry
DCM	Dichloromethane
DIPEA	*N,-N*-Diisopropylethylamine
DMA	Dynamic mechanical analysis
DMAP	4-Dimethylaminopyridine
DMF	Dimethylformamide
DSC	Differential scanning calorimetry
Ea	Activation energy
Eq	Equivalent
Et_2O	Diethyl ether
FID	Flame ionization detector
GC	Gas chromatography
GC/MS	Gas chromatography/mass spectrometry
GPC	Gas permeation chromatography
MeCN	Acetonitrile
MeOH	Methanol
MMA	Methyl methacrylate
*n*BMA	*n*-Butyl methacrylate
NEt_3	Triethylamine
NMR	Nuclear magnetic resonance
PBMA	Poly(*n*-butyl methacrylate)
PDMS	Polydimethylsiloxanes
PMMA	Poly(methyl methacrylate)
PPBDT	2-Phenyl-2-propyl benzodithioate
PPh_3	Triphenylphosphine
ppm	Parts per million
PS	Polystyrene
*p*TSA	*p*-Toluenesulfonic acid
RAFT (polymerization)	Reversible addition-fragmentation chain-transfer (polymerization)
TCB	Trichlorobenzene
t_{eq}	Time of equilibrium
T_g	Glass transition temperature
THF	Tetrahydrofuran
T_{inj}, T_{col}, T_{det}	Injection, column, detection temperatures

TGA	Thermo-gravimetric analysis
EtOH	Ethanol
RT	Room temperature
G’	Shear storage modulus
G”	Shear loss modulus
E’	Storage modulus
E”	Loss modulus
ω	Angular frequency
T	Temperature
F	Force
l, w, d	Length, width, higth (m, mm, cm,… etc)
m	Mass (Kg, g, mg, … etc)
η	Viscosity (Pa.s)
$\eta*$	Complex viscosity (Pa.s)
σ	Stress (Pa)
τ_{rel}	Relaxation time (s)
τ_e	Shortest relaxation time
τ_d	Longest relaxation time
M_e	Mass between entanglements
γ	Deformation (%)
k_{ass}	Association rate constant
k_{diss}	Dissociation rate constant
K_{eq}	Equilibrium constant
M	Molecular mass (g/mol)
n	Molarity (mol)
c	Concentration (mol/L)
V	Volume (L)
ρ	Density (g/mL)
M_n	Number-average molar mass (g/mol)
M_w	Mass-average molar mass (g/mol)
rpm	Rounds per minute
TEMPO	2,2,6,6-Tetramethyl-1-piperidinyloxy
ρ	Monomer conversion
f	Initiator efficiency
DP_n	Number-average degree of polymerization

Table of Contents

General Introduction

General Introduction

Vitrimers are polymeric networks that contain dynamic covalent bonds in their polymer matrices. The dynamic covalent bonds present in vitrimers can undergo associative exchange reactions, which allow maintaining a constant number of crosslinks at all times and temperatures. As a results, vitrimers can combine advantageous properties of thermosets and thermoplastics. Indeed, these materials are insoluble and exhibit a rubbery plateau. Yet, they are malleable, recyclable and can be welded when heated above the polymers transition state temperature, *e.g.* T_g and/or T_m. Due to the associative mechanism of exchange reactions taking place in vitrimer matrices, the change of viscosity of vitrimers as a function of temperature follows an Arrhenius law, just like glass and in striking contrast with thermoplastics. By local heating, vitrimers can be healed or re-shaped and depending on heating time, stress relaxation mechanisms and kinetics of the covalent reshuffling bonds, a shape memory effect or a new equilibrium state can be reached. The first epoxy/acid and epoxy/anhydride vitrimers were reported in 2011 based on transesterification of β-hydroxy esters in the presence of Zn-catalysts. Since then, a lot of work has been conducted to gain deeper insights into the role of the catalyst itself and a variety of other transesterification catalysts have been tested. Vitrimer technology has been transferred to other ester-systems and welding of glass fiber composites was reported. Silica-loaded vitrimers, liquid-crystalline and hybrid systems with additional physical bonds have also been described. In addition to transesterification, several other dynamic covalent exchange reactions have been used to generate vitrimers. Transamination of vinylogous urethanes was proven to allow very fast stress relaxation and re-processability in highly crosslinked polyurethane materials.

So far, almost all of reported vitrimer systems take advantage of dynamic covalent links inherently present in the polymer backbones. This structural feature, which can be a real advantage in terms of concentration of exchangeable functional groups, has so far considerably limited the scope of polymer matrices that could be turned into vitrimers. Indeed, *ca.* 70% of the world-wide plastics produced have backbones consisting of C-C bonds only. To transfer the concept of vitrimers to the totality of existing polymer matrices, while maintaining or improving processability, an adapted concept was designed and developed in the frame of this PhD. One of the general idea of the general concept presented is to introduce dynamic covalent links as pending side groups onto polymers containing only C-C bonds in their backbones. These functionalities can then be used not only to crosslink the polymer

chains, but also to allow rapid reshuffling the network and therefore polymer processing and recycling. However, important families of carbon-based polymers such as vinyl and olefin polymers are made via chain-growth. Taking into account these facts, a crucial step for the synthesis of these new vitrimer systems is the study of dynamic covalent exchange reactions that would display the thermal and oxidative stabilities and the chemical compatibility required to prepare and process these materials multiple times. In addition, as catalysts can be expensive, toxic and sensitive to oxygen, not to mention optical issues, *e.g.* color, the use of un-catalyzed exchange chemistries is desirable. The first vitrimer systems were easily obtained from commercially available resins and in the scope of possible applications the synthetic effort of the here to be developed materials should be as small as possible. Unlike systems where the exchange reactions can happen within the polymer backbone, in the here presented vitrimers with higher molecular weight polymer chains, the occurrence of even a very few side-reactions can cause a permanent loss of the dynamic nature of the systems. Hence, to be of interest for the development of this new generation of vitrimers, the exchange reactions should be robust and generate as few side reactions as possible.

With respect to the types of investigated dynamic covalent exchange chemistries, the work conducted in the frame of this thesis can be divided into two main parts. The chapter one is a short literature review on responsive and dynamic polymer materials with a focus on systems containing dynamic covalent bonds that can undergo associative exchanges. The concept of vitrimers is presented and the latest materials are discussed. The chapter two and three are focusing on imine based systems. The chapter two presents kinetic studies performed on the targeted exchange chemistries and disclose a new exchange reaction between imine and aldehyde as well as the use of aldehyde to catalyze imine exchange. Chapter three describes the generation and characterization of vitrimers relying on imine/aldehyde exchange chemistry. This imine/aldehyde chemistry was selected because of its high rate of exchange and also because of the good availability and inexpensiveness of the chemical compounds. Thanks to its interesting properties, *e.g.* the control of the rate of reaction from very fast to very slow, the variety of possible exchanging species and the strong B-O bond, boronic esters were chosen as second dynamic covalent link. Similar to chapters two and three, chapter four is focusing on kinetic studies of boronic esters and chapter five is presenting the generation and characterization of boronic ester containing vitrimers.

Chapter 1

Literature Review

Table of Contents

Chapter 1 – Literature Review

1.1 Different families of polymers

Long before Berthelot first used the term "polymer" for polystyrene in 1866, macromolecules, *e.g.* in textile fibers, wood and sugars have played an essential role for mankind.[1] From pioneering work on Bakelite[2] rubbers (Ebonite[3]), polyethylene[4] and polyamides (Nylon[5]), to polyurethanes[6] and many others, today life is based and highly dependent on synthetic polymers. Polymers have extraordinary properties, are highly tunable in respect to their respective application, less costly than other materials, light-weight and can be produced in large quantities with high rates. They are not only essential for applications in packaging, construction, transport, electronics and clothing, but novel materials can also be a driving force for emerging technologies.[7] There are many different ways to classify polymers, one being based on the way they respond to heat. According to this classification, there are two classes of plastic materials; those who macroscopically flow when subjected to heat, named thermoplastics, and those whose shape remains unchanged when subjected to heat, named thermosets (Figure 1.1).

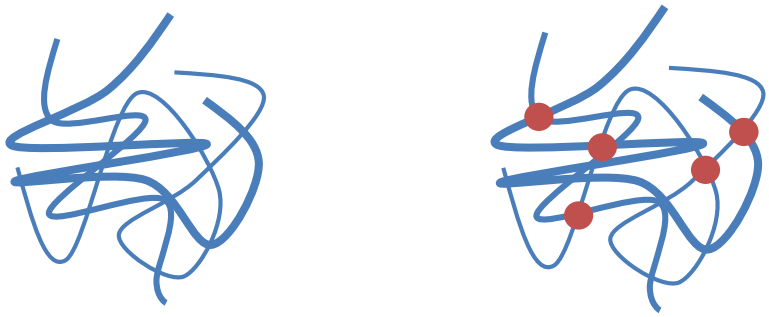

Figure 1.1. Left side: Entangled thermoplastic polymer. Right side: Crosslinked thermosetting polymer.

Thermosets are polymer materials that can be found in numerous applications, for example in coatings, composites, foamed structures, constructions, structural adhesives, biomedical and insulators for electronic packaging.[8] Due to the presence of crosslinks, this class of materials exhibits outstanding properties such as superior mechanical strength, *e.g.* high modulus, network integrity at high temperature, chemical and environmental resistance. As the name suggests, these systems are "set" by the polymerization/crosslinking process and once terminated, they cannot be re-shaped nor re-processed even at temperatures above the polymers transition temperature, *e.g.* glass transition temperature or melting temperature. These systems are usually resistant to flow even during long periods under high stresses. The fact that thermosets cannot be processed by common industrial processes such as extrusion or

injection molding combined with trapped residual stresses from the synthesis, can be a drawback, *e.g.* for rapid mass production and complex shapes. Additionally, even though long services times are targeted for applications, thermosetting polymer materials are a big issue in respect to waste production and the increasing amount of un-recyclable materials placed in landfills.[9]

Thermoplastics on the other hand, consist of linear or branched polymer chains that can flow above polymer characteristic temperatures, making them processable, recyclable and malleable.[10] Important parameters, such as the molecular weight, the topology and entanglements define the materials mechanical strength and viscosity. As these materials can be easily and efficiently processed via industrial techniques and brought into any desired shape, they can be found in a wide range of applications, such as carpets, pipes, packaging films, drink cups, toys, disposable cutlery, fabrics, gear wheels, bone cement, windows and lenses.[11] However, due to the absence of crosslinks, thermoplastics possess inferior mechanical properties as compared to their thermosets counterparts and are by definition less resistance to chemicals (soluble) and heat, potentially resulting in uncontrolled creep and lose of shape at elevated temperature.

1.2 Two different approaches to obtain repairable polymer networks

Hand in hand with the demand for new applications and high-tech polymer materials, especially in biomedical devices, energy storage and transformation, electronics, transportation industry or construction, there has been a tremendous effort to combine advantageous properties of thermosets and thermoplastics. To design crosslinked, yet repairable and recyclable networks, two different main approaches have been reported: materials can be repaired either through crack healing thanks to active chemicals present in microcapsules or other types of reservoirs,[12-15] or through the use of dynamic bonds.[16] Depending on the nature of the dynamic crosslinking bonds, the latter family can be categorized into two subgroups: systems relying on dynamic physical bonds and systems relying on dynamic covalent bonds.

1.2.1 Self-healing and reprocessing in the presence of healing agents and microcapsules

The first autonomous healing composite with embedded microcapsules containing healing agents was reported by Viswanathan and co-workers.[12] In this system, which opened the way for various other systems,[13-15] a neat epoxy network was loaded with capsules containing a polymerizable solution of monomers, which during crack formation get in contact with a dispersed catalyst triggering polymerization and resulting in bonding of the crack faces (Figure 1.2). Several criteria such as compatibility of the healing substance with the matrix, the shelf-life of the catalyst and healing agent, as well as fast and easy triggerable polymerization had to be addressed. The tested ring opening metathesis polymerization of dicyclopentadiene in the presence of Grubb's catalyst resulted in remarkably effective reconstitution of mechanical properties via self-healing in tapered double-cantilever beam specimens. This approach is autonomous: upon crack formation, no external stimuli are needed to drive self-repair. However, the process is finite: once the crack healing agent is polymerized the system loses its ability to self-repair. Additionally, the introduction of microcapsules and compatible healing agents as general approach might lead to complications with other polymer matrices and in the presence of additives, especially during high temperature processing.

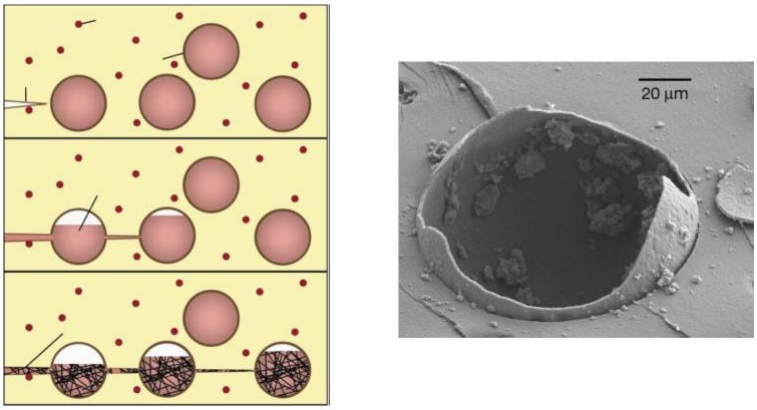

Figure 1.2. Left side: Schematic view of a self-healing composite relying on microcapsules. During crack propagation, the healing agent gets into contact with the dispersed catalyst, which triggers polymerization and bonds cracked faces. Right side: Picture of an open microcapsule.[12]

1.2.2 Self-healing and reprocessing of networks containing physical bonds

A lot of work has been performed on systems containing physical bonds, *i.e.* hydrogen-bonding, pi-pi stacking, ion- or host-guest interactions.[17,18] These materials can be responsive to external triggers such as light, pH, stress, chemicals, temperature, electric current or others

and especially the trigger-mediated decomposition of gels used for delivery purposes obtained a lot of attention. For example, Langer and co-workers reported recently the use of a pH-responsive supramolecular enteric elastomer for use as carrier medium of devices in clinical applications (see Figure 1.3).[19] Such applications necessitate the safe passage of devices into the stomach or intestines such as ingestible electronics for diagnosis and monitoring, and controlled-prolonged drug release. In case of fracture during penetration, un-degradable parts of these materials can become a real danger and thanks to stimuli-responsive supramolecular bonds the system developed was proven to be stable under acidic conditions, but fully degradable at neutral pH. A material relying on supramolecular bonds and self-organization, and displaying recoverable extensibility up to several hundred percent as well as a high creep resistance under load was designed by Leibler and co-workers.[20] In fact these systems behave like rubbers, yet they are able to efficiently self-heal at room temperature thanks to their hydrogen bonding motifs. They were generated from available, inexpensive and renewable resources such as fatty di and tri-acids and urea and their materials properties can be easily tuned by changing the ratio of the network forming molecules.

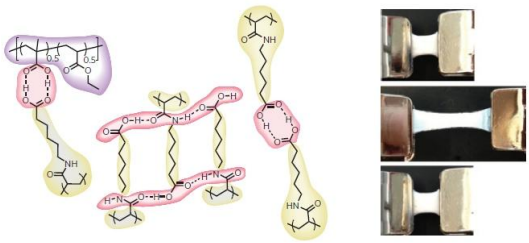

Figure 1.3. Left side: Schematic view of a supramolecular material. Right side: elasticity of the final material.[19]

Despite all effort, the most often relatively weak interaction of physical bonds as compared to chemical bonds result in several drawbacks, especially at high temperatures. The reported systems generally lack superior mechanical properties, *i.e.* creep-resistance, and often show lower chemical resistance. At elevated temperatures, the physical interactions become less pronounced and these systems can behave like thermoplastics enabling processing but also resulting in uncontrolled flow and very low modulus, comparable to those of conventional thermoplastics.

1.2.3 Self-healing and reprocessing of networks containing chemical bonds

Thanks to their covalent nature, the utilization of dynamic chemical bonds instead of dynamic physical bonds can substantially enhance the mechanical properties and chemical stabilities of materials. In general, two different classes of crosslinked materials that take advantage of

reversible (dynamic) covalent chemistry can be distinguished: systems utilizing "dissociative" mechanisms, *i.e.* reversibly crosslinking/de-crosslinking under specific conditions, and systems with "associative" mechanisms (Figure 1.4). For the latter, when the systems operate in the absence of side reactions affecting the crosslinking density and the dynamics of exchange of the covalent bonds, the materials belongs to a new class of polymeric materials coined "vitrimers".

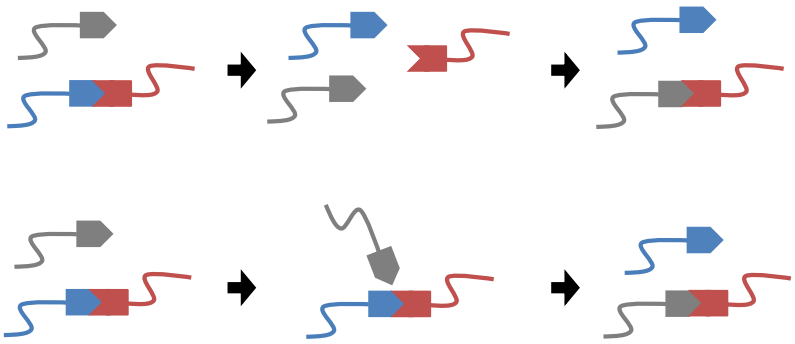

Figure 1.4. Top: Dissociative mechanism. Bond scission before bond formation results in a temporally de-bonded system. Bottom: Associative mechanism. Bond scission and formation happen at the same time via a transition state. At no time the system is de-bonded.

1.2.3.1 Materials relying on association/dissociation of reversible covalent bonds

Dissociative systems were reported using a variety of reversible covalent reactions, such as Diels-Alder (DA), thioesters, dynamic urea bonds, Schiff's bases, boronic esters and boroxines.[21-32] Especially the Diels-Alder reaction, a cycloaddition, which is known to be reversible under certain conditions, was studied in depth. For example, Wudl and co-workers reported a thermally remendable crosslinked polymeric material that behaves like classical epoxy resins at service temperatures, but can restore its properties when fractured by heating to elevated temperatures (Figure 1.5).[32, 33] Taking advantage of the relatively mild temperature and rather fast equilibrium of this maleimide/furane DA system, the degree of "open" crosslinks at 120 °C was determined to be around 30% from solid-state nuclear magnetic resonance spectroscopy. Upon cooling, the system was shown to recover its initial crosslinking degree. Similar materials, made via a solvent free method, were reported to possess healing efficiencies of more than 80%, as determined from tensile testing experiments. Other approaches were reported by Lehn and co-workers who used a bis(dicyanofumarate) in the presence of ethylene glycol based bis(fulvenes) to generate dinamers and eventually self-healing materials by the introduction of fulvene crosslinkers.[34]

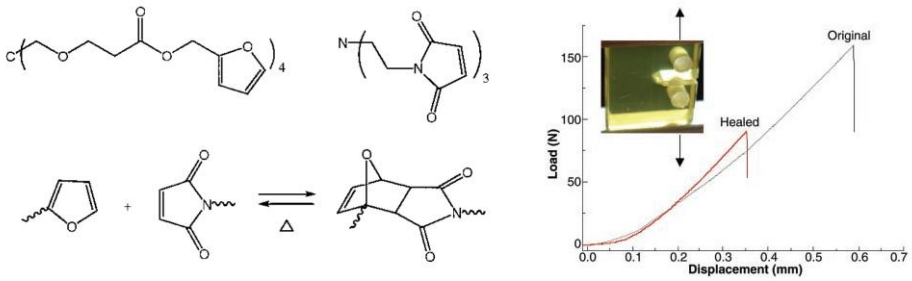

Figure 1.5. Left side: A thermo-responsive hetero-Diels-Alder reaction. Right side: Healing of a re-processable polymeric material.[32]

Barner-Kowollik and co-workers designed low temperature reversible materials using acid activated dithioesters with cyclopentadiene (Cp).[35] Addressing the relatively long life-time of the cycloadduct in the absence of catalyst, another material was presented taking advantage of accelerated association/dissociation processes thanks to the implementation of cyanodithioesters. These systems do not only show fast bonding/de-bonding cycles, but also keep their dynamic nature after several cycles of heating/cooling. Another remarkable material was reported by Sun and co-workers by combining supramolecular H-bonding mechanisms in polyurethanes with the reversible crosslinking reaction between pending *N*-maleimides and a difurane.[36] After re-processing via hot compression molding, the recycled specimen restored almost 100% of initial properties in tensile testing experiments.

Schiff's base chemistry was employed to generate crosslinked yet self-healable systems via imine or hydrazone formation. For example, Wei and co-workers reported an injectable hydrogel that could be used as cell therapy carrier thanks to its biocompatible and inexpensive preparation.[28] Target cells were encapsulated under physiological conditions during formation of the glycol chitosan polyethylene glycol gel and self-healing was demonstrated. Chen and co-workers presented the pH-dependent gelation of acylhydrazone systems using a trivalent aldehyde.[26] Cheng and co-workers combined acylhydrazone and disulfide exchanges to create environmental adaptive self-healing gels (Figure 1.6).[27] In contrast to other Schiff's base systems, the reported gels can self-heal under both acidic and basic pH conditions thanks to the complementary exchange chemistries. It was also shown that traces of aniline can enhance self-healing and that the system respond to redox-triggers.

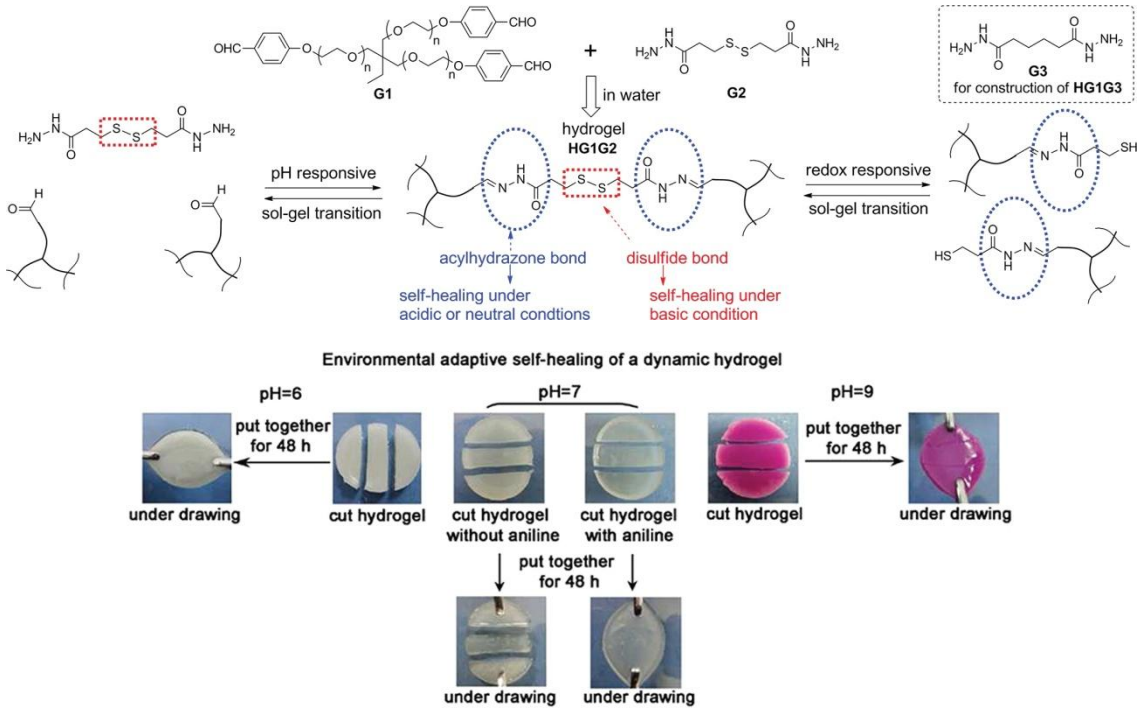

Figure 1.6. A dual responsive hydrogel. The incorporation of disulfide and acylhydrazone functionalities allows good stability under both acidic and basic conditions.[27]

A dynamic urea bond was presented by Cheng and co-workers to introduce self-healing in poly(urethane-urea) materials without the need of any catalyst or external trigger.[25] By using bulky substituents attached to the nitrogen of urea bonds, the bond is weakened and can open to result in an isocyanate and a secondary "hindered" amine, and then reform. Unmodified urea bonds bearing a hydrogen atom or less bulky groups as substituent on the nitrogen were not observed to undergo this reversible process. Although the reported material can recover more than 87% of initial stress in a tensile testing set-up, the self-healing process is rather lengthy with 12 hours at 37 °C and moduli as low as 1.22 MPa at room temperature, limiting the materials applications.

Another system with interesting properties was reported by Bowman and co-workers.[37] Polymers were generated via a thiol-ene reaction with tetra and difunctional thiols, difunctional vinyl monomers and an allyl sulfide ring-opening monomer. The resulting materials showed creep-recovery behavior upon irradiation with different wavelengths, proving that the proposed mechanism of radical induced addition-fragmentation chain transfer of allyl sulfides can be exploited to obtain dynamic materials. Matyjaszweski and co-workers took advantage of a dynamic covalent trithiocarbonate to obtain reversibly self-healing poly (methyl methacrylate) gels and *n*-butyl acrylate bulk materials (Figure 1.7).[38] The underlying concept of this approach was the utilization of radicals, generated by decomposition of an

added radical source (AIBN), by direct activation with a CuBr/L complex or, by shining light on photo-labile species.[38-40] Similar to processes found in reversible addition fragmentation chain-transfer polymerization, *i.e.* radical induced opening of S-C bonds, the trithiocarbonate moiety undergoes reshuffling leading to reversible exchange in the polymer networks. Although this method showed repeatable self-healing features, it might be limited in terms of application due to the relatively low stability of the present carbon-radicals under air and at elevated temperatures, not to mention possible recombination/termination reactions. The tested bulk materials had a very low T_g (-50 °C) and the presented approach is probably not adapted to high T_g bulk materials. By using a thiuram disulfide moiety, oxygen-stable self-healing under visible light could be achieved in a low T_g polyurethane system.[40] Another interesting system with self-healing properties thanks to thiol-disulfide exchanges was presented by the same group. Star polymers were synthesized by controlled radical polymerization (ATRP) using a bisacrylate and *n*-butyl acrylate chain extenders.[41,42] Star arms were then reversibly crosslinked by bismethcarylates bearing disulfide bonds and reversible dynamic exchange was achieved by thiol-disulfide exchange even without the addition of redox-catalysts. Self-healing of small cracks was studied and proven using atomic force microscopy and optical microscopy.

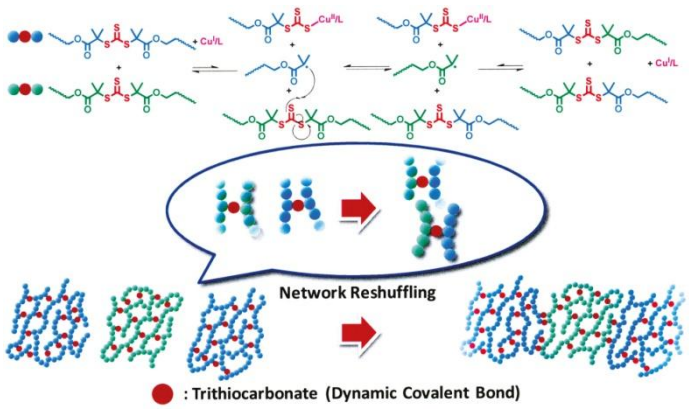

Figure 1.7. Trithiocarbonates allow network reshuffling via radical mediated processes in crosslink networks.[38]

Rowan and co-workers reported semicrystalline, covalently crosslinked polymers containing disulfide bonds.[43] The combination of photostimulation and temperature dependence of the semicrystalline domains resulted in a dual trigger-responsive material. For example, by heating, a shape memory effect was obtained due to the reorganization of the semicrystalline domains, while disulfide crosslinks remained stable. By shining light onto to specimen, scratches could efficiently be healed without undesired creep thanks to the unchanged crystalline domains.

Boronic acids and diols are known to form boronic esters by condensation. The resulting boronic esters can display low to very high stability towards hydrolysis depending on the structural characteristics of the boronic acid and diol building units. In the presence of a water trapping agent, boronic acids can also condensate into 3-membered cyclic species, called boroxines. Depending on their stability towards hydrolysis, both boronic esters and boroxines can be decomposed into the starting compounds by the addition of water. Sumerlin and co-workers introduced aromatic 5-membered boronic esters as reversible and exchangeable crosslinkers in polymeric networks made by a photoinitiated radical-based thiol-ene coupling.[29] Self-healing of materials without surface wetting with water was shown to be absent. However, when hydrolysis at the surface took place through addition of water, two pieces of bulk material could be merged and the crack between the two specimens disappeared. Due to the ubiquity of boronic esters in the system and although network stability in humid environments was observed, these systems creep at room temperature which could possibly lead to a loss of network integrity. As the above discussed poly(urethane urea) materials, they have rather low moduli, which on the one hand facilitates self-healing, but also limits application, especially to compete with existing high-modulus crosslinked materials. Feng and co-workers also took advantage of easily available, rapid and robust thiol-ene chemistry to generate polysiloxane (PDMS and PMMS) networks containing 5-membered dioxaborolanes (Figure 1.8).[30] The resulting materials can self-heal without the addition of water and the authors reported a spontaneous hydrolysis process through water uptake from humidity on the surface. Indeed, from contact angle measurements of network droplets under atmospheric conditions, it was observed that these usually hydrophobic systems possess an increased water uptake most probably due to the opening of boronic esters resulting in uncontrolled creep. To avoid this loss of shape and in regard to the relatively poor mechanical properties of these systems, a non-dynamic crosslinking siloxane and 10-15 m% nanosilica had to be added. Resulting materials were less prone to creep by humidity uptake, but still were able to self-heal.

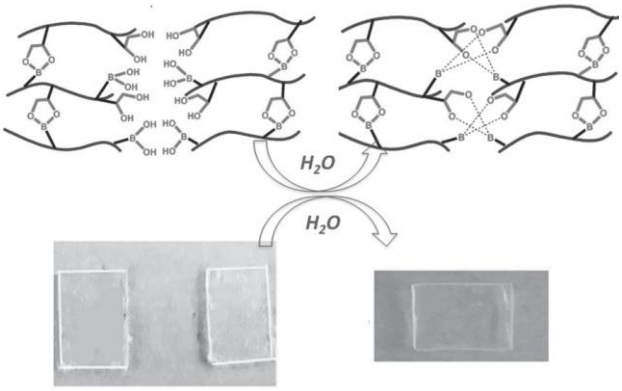

Figure 1.8. Boronic esters are hydrolyzed and re-formed upon addition of water allowing self-healing in a polysiloxane network.[30]

Boroxines, six-membered cycles obtained by condensation of three molecules of boronic acids are known to form upon water removal. Bao and co-workers designed a boronic acid containing PDMS material via amidification of pending amine groups.[31] The resulting chains were reversibly crosslinked through boroxine formation resulting in networks with a relatively high Young's modulus of up to 182 MPa which the authors attribute to the high concentration of boroxines. The addition of water was necessary to decrease the number of crosslinks and increase chain mobility for self-healing properties. Even though the systems resistance to creep was substantially increased compared to systems with boronic ester linkages, the necessity of water addition is limiting possible applications.

Although the exploitation of dissociative crosslinks has shown to be advantageous in respect to self-healing properties, this approach has some limitations. So far, most of these systems need external stimuli, *e.g.* water or heat, to become or maintain their reversible nature. In addition, reversible bond association/dissociation goes hand in hand with a decrease in the crosslink density of the networks, which can result in uncontrolled flow at elevated temperatures and dissolution. Additionally, the majority of reported dissociative systems were gels and possessed low mechanical strength and moduli. To generate dynamic bulk materials which can compete with classical thermosets' superior mechanical properties, especially at elevated temperatures, and to avoid uncontrolled flow at conditions where de-bonding of the dissociative systems is reported, the introduction of dynamic covalent bonds, *i.e.* exchange via an associative mechanism, is a strategy of choice.

1.2.3.2 Materials relying on associative exchange reactions of covalent bonds

Materials containing dissociative/associative reversible reactions were shown to be self-healing and processable under certain conditions and temperatures. However, they can lose their network integrity due to a decrease in crosslink density and become soluble. Materials which take advantage of dynamic covalent exchange reactions can be self-healing, (re-) processable and malleable while remaining insoluble thanks to the associative nature of the underlying exchange reaction.

A lot of research has been conducted on exchange reactions between thiols and disulfide compounds, as well as on disulfide exchange. Odriozola and co-workers described the generation of an poly(urea-uethane) elastomer containing aromatic disulfides as crosslinker.[44] The present hydrogen-bonding motifs prevent creep at room temperature while the dynamic nature of disulfide links allows processing at elevated temperatures (Figure 1.9). Indeed, the system showed remarkable recyclability in tensile testing experiments with almost no alteration of parameters such as stress at break. The material could easily be molded at 150 °C for 20 minutes under pressure and pristine as well as processed samples were reported as insoluble in a good organic solvent. As expected and due to the covalent exchange reaction the stress relaxation follows temperature with almost no relaxation at 25 °C (hydrogen-bonding) and full stress relaxation at 150 °C (few hydrogen bonding). Despite the highly crosslinked character of this material, its mechanical properties such as Young's modulus are rather weak. The nature of the un-catalyzed disulfide metathesis and the presence of monofunctional catalyzing thiol species remained un-discussed and could play a very significant role as exemplified and demonstrated by Goossens and co-workers.[45]

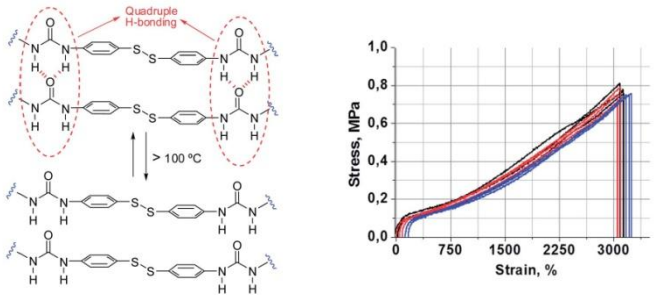

Figure 1.9. Left side: Disulfide "metathesis" in the presence of hydrogen bonding. Right side: tensile properties of self-healed disulfide containing materials.[44]

Indeed, Zhang and co-workers report the utilization of disulfide metathesis in the presence of a trialkylphosphine catalyst.[46] By epoxy-thiol polymerization, polysulfide networks were

generated. Rheological measurements of the dynamic material and fixed control networks revealed the dynamic nature of the polysulfide. Self-healing/recycling tests were performed and almost complete restoration of initial mechanical properties was achieved after 24 hours. Despite the impressive self-healing ability, the reported networks contained quite low molecular weight chains resulting in rather poor mechanical properties. Additionally, the stability of the exchange-enabling catalyst remains unclear at high temperatures, in the presence of humidity and at longer time periods.

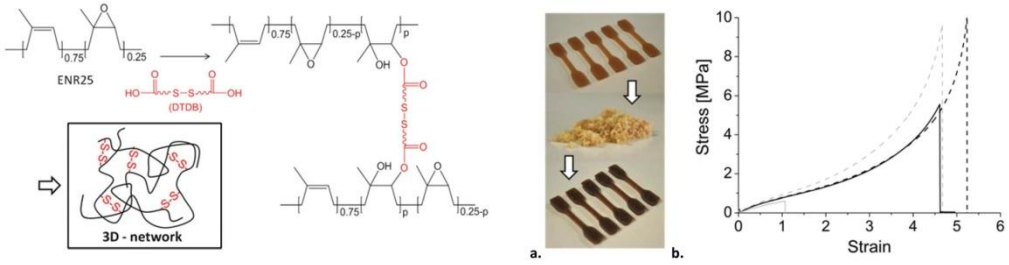

Figure 1.10. Left side: Crosslinking of epoxidized natural rubber. Right side: Reprocessing of materials containing disulfide crosslinks. Black: dynamic material, grey: control. Dashed lines: before re-processing, solid line: after re-processing.[47]

By using thermo-activated disulfide rearrangements in epoxidized natural rubber, Leibler and co-workers obtained chemically crosslinked yet reprocessable elastomers.[47] Crosslinking density was controlled by epoxy-ring-opening with disulfide-containing dicarboxylic acid crosslinkers, and to a low extent through unavoidable side reactions (Figure 1.10). Due to the presence of side reactions, the rubber networks did not achieve complete stress relaxation. However, sufficient creep was observed to reprocess the sample by compression molding and mechanical properties were recovered to *ca.* 50% (stress at break), 80% (strain at break) and 100% (Young's modulus). Additionally, adhesion tests at different temperatures confirmed that the dynamic rearrangements of crosslinks were sufficient to weld two specimens together resulting in an increased adhesion energy for the dynamic materials compared to their respective controls.

In early studies Grubb and co-workers concluded that rearrangements in polydimethylsiloxane elastomers can take place in pure networks resulting in an activation energy of 22.8 kcal/mol for the relaxation process.[48] Additionally, smalle traces of acids or bases and even water and carbon dioxide were reported to accelerate relaxation processes and a decreased activation energy of 5.1 kcal/mol was reported. McCarthy and co-workers extended the understanding of the underlying mechanism and reported an environmental

stable anionic type of re-equilibration.[49] In their material, reactive end groups, tetramethylammonium dimethylsilanolates, can restructure crosslinks through an associative mechanism or form cyclic oligomers (Figure 1.11). The reactive end groups were present from synthesis (anionic polymerization initiator), but other bases or acids were also able to catalyze the described exchange. The authors reported self-healing experiments by formation of objects, impregnation of patterns and fracture toughness measurements. In all cases, the healed material was not distinguishable from the pristine sample proving the excellent self-healing properties of this system. These systems can also be described as "living polymer network" and indeed, these materials can be degraded through evaporation of formed cyclic oligomers at elevated temperatures, shifting the equilibrium between inter – and intra molecular exchange reactions as studied and demonstrated in the PhD thesis of Fanny Angot.[50]

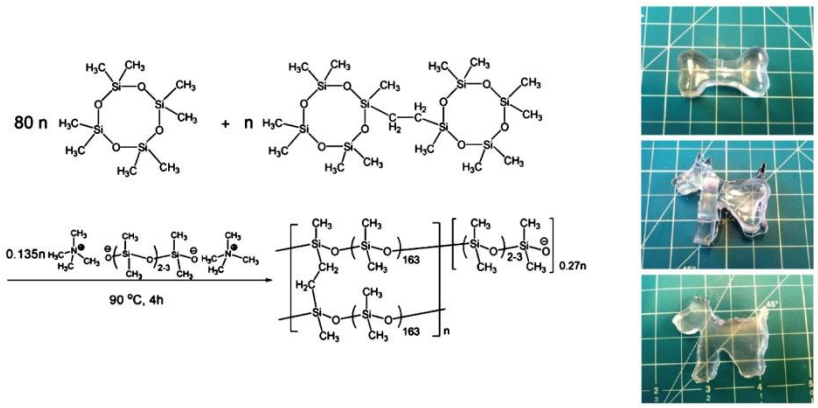

Figure 1.11. Left side: synthesis of a polysiloxane network. Right side: the material can be welded and re-formed into complex shapes.[49]

Dichtel and co-workers generated polyhydroxyurethanes via ring-opening of six-membered cyclic carbonates in the presence of amines (Figure 1.12).[51] The resulting networks possessed pending hydroxyl-groups which can, depending on temperature, react with carbamate linkages via nucleophilic attack. From stress relaxation experiments a rather high activation energy of 111 kJ/mol was determined which was different from the energy observed in small molecules kinetic studies (148 kJ/mol). The authors suggest that the exchange reaction is activated by stress, thus proceeds faster in stress relaxation experiments. DFT calculations seemed to confirm the twisting of N-lone electron pairs out of conjugation with the carbonyl pi-orbitals in the material. These systems could be (re-)processed recovering up to 75% of initial mechanical properties and were insoluble. It was not shown if these materials relax stress completely and indeed the authors report some degree of decomposition at elevated

temperatures detected by discoloration and thermogravimetric analysis. However, in the presence of an excess of network cleaving agents, the network could be de-crosslinked and completely solubilized.

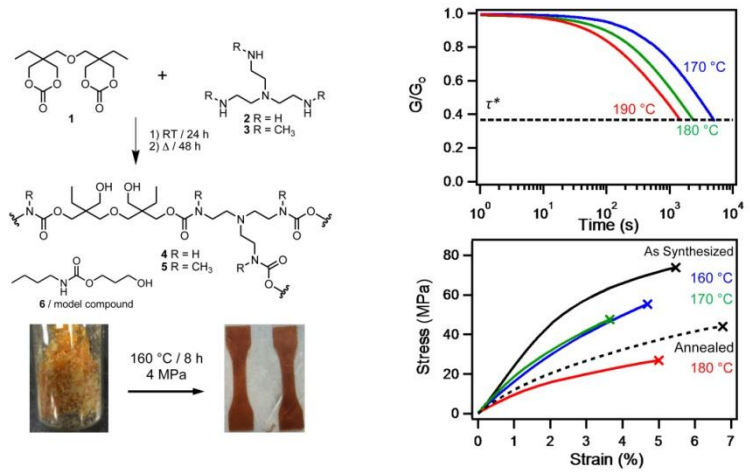

Figure 1.12. Left side: Synthesis and re-processing of polyhydroxyurethanes via ring opening polymerization. Top right side: Stress relaxation depending on temperature. Bottom right side: Tensile properties after different re-processing conditions.[51]

Schiff's base chemistry was applied to generate materials that possess associative reshuffling of network forming covalent bonds. By imine formation between an aromatic difunctional aldehyde (terephthalaldehyde) and di- and trivalent amines (diethylene triamine and triethylene tetramine) Zhang and co-workers formed crosslinked polymer films (Figure 1.13).[52] Monomers were mixed in the absence of any catalyst in a mixture of organic solvents and volatile compounds were allowed to evaporate at room temperature. Infrared spectroscopy was applied to monitor the conversion of aldehydes and generation of imines and the resulting material had a T_g of *ca.* 56 °C and a Young's modulus of *ca.* 1 GPa at room temperature. The so generated films were tested for stress relaxation at various temperatures and a temperature dependence was observed.

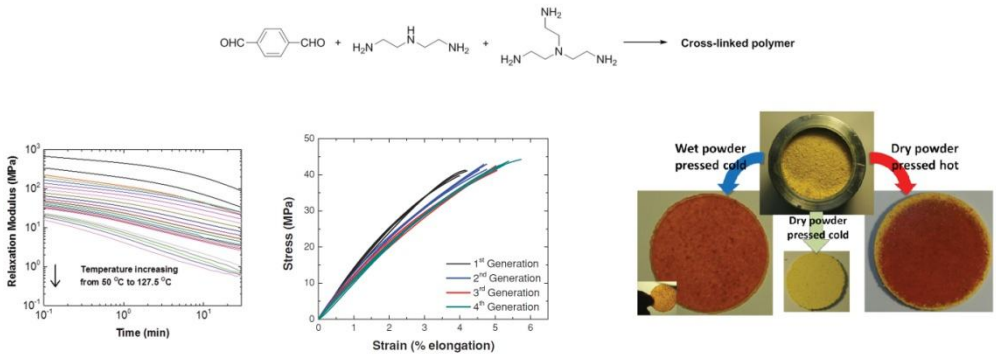

Figure 1.13. Top: Network forming imine-formation. Bottom from left to right: Stress relaxation curves with increasing temperature. Tensile properties after different cycles of re-processing. Different processing conditions and pictures of the respective specimens.[52]

The materials ability to be (re-)processed was investigated by changing conditions during compression molding of powder. At 80 °C and without the presence of purposely added water, the yellowish powder could partly be reprocessed: in the center of the disc-shaped specimen, the material was transparent and reddish whereas at the outer rim, the initial yellowish grains were still visible. By pressing at room temperature still without the presence of water the material could not be reprocessed at all. When adding water and pressing at 80 °C the entire specimen was transparent and reddish, proving the necessity of water. The so recycled specimens did not only recover initial mechanical properties in tensile testing experiments, but even enhanced stress and elongation at break after 4 cycles of re-processing. The reported system was proven to be (re)-processable and dynamic upon addition of water. However, in the absence of purposely added water, processing became more complicated and the nature of the underlying covalent exchange reaction was not further investigated. It can be assumed that the presence of water hydrolyzed network forming imines and de-crosslinked the system. Through heating and evaporation of water the material could be (re-)processed. However, even in the absence of water, the system showed stress relaxation which might be a hint for other exchange mechanisms, such as transimination with free amines remaining from synthesis or imine metathesis. Investigating further the idea of imine metathesis, Zhang and co-workers designed a polymer via conventional radical polymerization of a polyethylene glycol methacrylate ester benzaldehyde and *n*-butyl methacrylate which they subsequently crosslinked via the addition of an aromatic diamine (Figure 1.14).[53] To reveal the nature of the exchange reaction, a study on model molecules was performed. From the presence of imines in flame retardants and as antioxidants in rubber, taking advantage of the lone pair of the imine-bond's nitrogen, the authors draw the idea of a radical mediated exchange reaction. By adding a radical trap (2,2,6,6-tetramtheylpipperidin-1-yl)oxy (TEMPO) the presence of

radicals was monitored and detected by a decrease in the intensity in electron spin spectroscopy. As no radicals seem to be present at longer reaction times when the reaction is at equilibrium, a dual exchange mechanism between aromatic imines was proposed. In a first mechanism, the four respective exchange species might be generated from a four-membered transition state (Figure 1.14). Once at equilibrium, radicals were not detected anymore and the authors concluded that at this stage the mechanism proceeds by a direct metathesis pathway. The polyacrylate with pending aldehydes and imine crosslinks had a rather low T_g of *ca.* -33 °C, but was comparable to a generated control network without imine-functionality in the crosslinking molecules. Rheological comparison of both systems revealed the dynamic nature of the imine material with a cross-over even at room temperature (Figure 1.14). The control network did not show any relaxation under the same conditions. Self-healing and re-processing experiments at room temperature and under ambient atmosphere were performed and tensile testing data were promising.

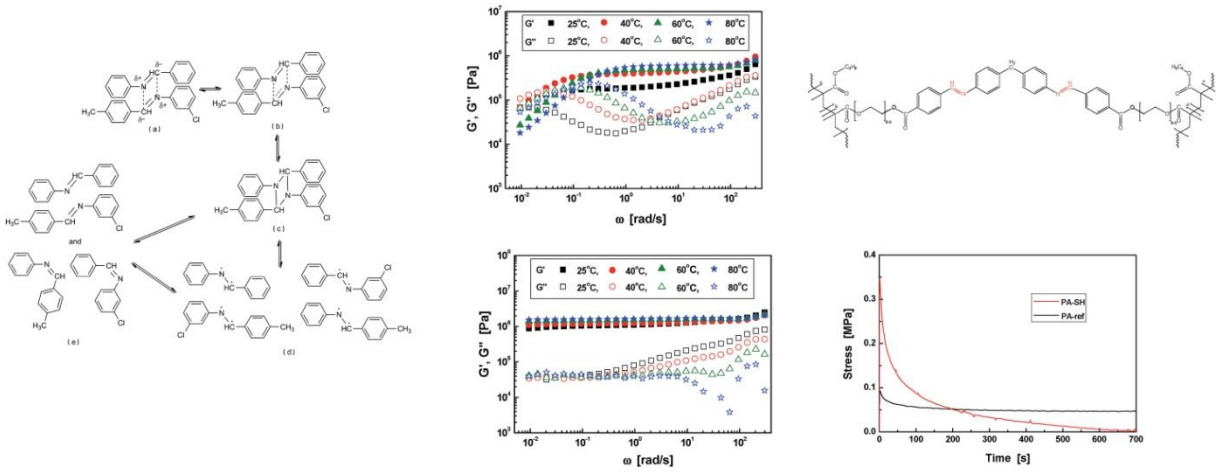

Figure 1.14. Left: Suggested pathway for imine metathesis. Middle: Frequency sweep measurements of the dynamic material and the control. Right: Structure of the crosslinked yet dynamic network and stress relaxation of the dynamic and the control material.[53]

Although the stress relaxation curve from the control network clearly showed that its relaxation was incomplete, the dynamic system seemed to relax stress to negative values. Indeed, the system seems to relax to less than "0" of remaining stress, possibly due to uncontrolled flow. The relatively low viscosity of the system is further supported by the low molecular weight of generated polymer chains (30 000 g/mol). An issue of possible side reactions and network defects might be the network forming procedure itself: to a chloroform solution of the polyaldehyde was added a chloroform solution of the crosslinker and after curing at 40 °C degree for 4 hours and evaporation at the same temperature for 10 additional

hours, the material was compression molded at 60 °C for 1-2 hours. Even though 40 °C might be sufficient to evaporate chloroform, the presence of remaining water cannot be excluded. The authors did not report the use of dry or anhydrous solvents. During processing, remaining water might create amines which, especially with acrylates, can undergo amide formation resulting in a less dynamic system. The presented works on imines show the potential of this type of bonds in dynamic materials, yet more work has to be performed to reveal underlying principles of the exchange mechanisms and to work in the absence of amine-releasing water.[52,53]

By transferring small molecule kinetics to dynamic properties of bulk materials, Guan and co-workers designed dynamic materials containing pending 1,2 diol functionalities and crosslinking diboronic esters (Figure 1.15).[54] The authors performed kinetic studies on the boronic ester transesterification of chemically different 6-membered boronic esters. Aryl boronic esters with an un-substituted aromatic radical exchanged slower than its tertiary-amine substituted counterpart. As possible explanation, the authors proposed that the nitrogen atom of the aminomethyl functionality acts as proximal base (protonated ammonium) facilitating the proton transfer during boronic ester transesterification. Thermoplastic 1,2 diol containing polycyclooctene polymers were generated by catalyst-mediated ring-opening metathesis polymerization with a functionality of ca 20 mol%. Studies on the respective toluene gels under similar conditions revealed the fast relaxation of the aminomethyl-containing crosslinker. The other system exchanged much slower (Figure 1.15).

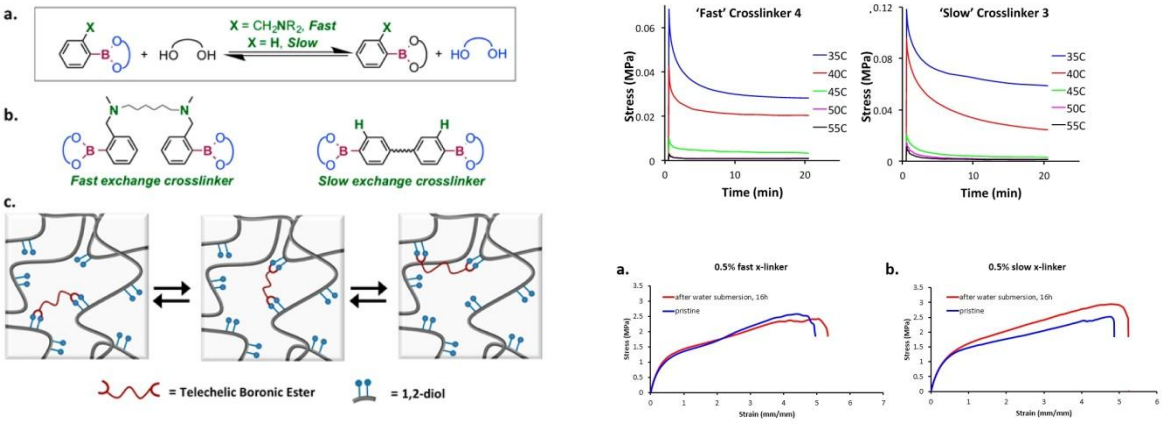

Figure 1.15. Top left: Chemical structure of studied crosslinkers. Bottom left: Schematic view of the material and the underlying reshuffling. Top right: Stress relaxation experiments at different temperatures for both materials. Bottom right: tensile properties after overnight immersion in water.[54]

After drying and compression molding, the two different materials were tested for self-healing properties. The "fast-exchanging" material was effectively healable with similar healing-properties for two different crosslink densities. The "slow-exchanging" system did not show any or very few restoration of initial mechanical properties. The authors assumed that the hydrophobic environment of the network forming chains was sufficient to protect boronic esters from hydrolysis, meaning de-crosslinking. Indeed, even after overnight immersion in water, none of the tested materials exhibited a decrease in mechanical properties confirming the above-made assumption. Recycling of the "fast-exchanging" system via compression molding of the powder resulted in almost full restoration of the initial mechanical properties. However, the tensile properties and Young's modulus of the reported materials were rather weak. Despite the reported low moduli, it seemed that complete stress relaxation could not be achieved, but no explanation was given. Also, the experiments were performed in a range of temperature where the thermal history and the exact moduli of the material were very complicated to control due to proximity of the melting temperature.

1.2.3.3 Vitrimers

It is known that thermoplastics lose their dimensional integrity at temperatures above their transition temperature (T_g, T_m) and start to flow. What is from utmost importance for easy processing, for example during injection molding, can be a drawback for mold-less welding, controlled shaping and assembling of objects with complex shapes. In Figure 1.16 is presented the viscosity as a function of the inverse temperature, normalized by the T_g, of different materials.[55] It can be seen that the viscosity of glass, in sharp contrast with common thermoplastics, *e.g.* polystyrene, changes gradually in an Arrhenius-like fashion, making it easily malleable over a wide range of temperatures. Insoluble yet dynamic polymer materials which take advantage of associative dynamic bond re-arrangements in the absence of permanent static crosslinks were coined vitrimers due to their glass-like (latin: "vitrum") behavior at elevated temperatures.[55] Instead of a sharp decrease of viscosity, these flow behavior of these systems can easily be controlled over a rather large range of temperature, enabling free shaping by local heating without the need of molds. The first systems reported by Leibler and co-workers applied a zinc catalyst to introduce dynamic covalent transesterification into classical and usually thermosetting epoxy/acid and epoxy/anhydride systems.[55-57] At room and service temperature, the materials behave like the classical

thermosets and do not flow. However, thanks to the catalyst-accelerated transesterification of β-hydroxy esters present in the network, the system can change its topology through bond reshuffling above a characteristic temperature. Solubility tests at high temperature were performed and confirmed the insolubility of these networks even after long periods of immersion in a good solvent, proving the associative nature of this exchange, *i.e.* the constant number of crosslinks (Figure 1.17).

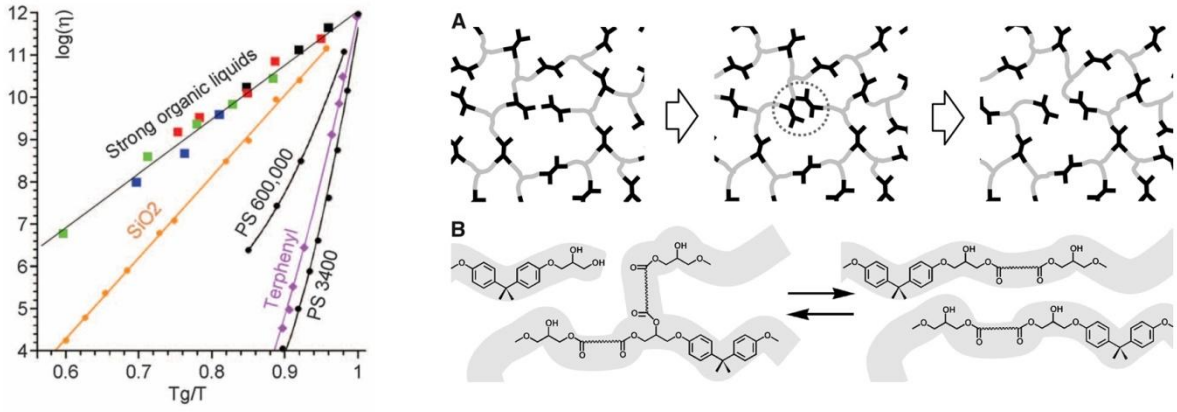

Figure 1.16. Left side: Angell fragility plot. The colored dots correspond to vitrimer data. Right side: Schematic view of the network reshuffling in a vitrimer matrix. The crosslink density remains constant at any time.[55]

These materials can flow above a second glass transition temperature, coined T_v, which can be seen as a topology freezing transition temperature. From creep-recovery and stress relaxation experiments, it can be concluded that these materials indeed show Arrhenius-like behavior in respect to their viscosity. This behavior is governed by the dynamic covalent exchange reaction and can be adjusted by changing the catalyst nature and loading.[56] These materials were easily mendable and could be twisted by local heating to adopt a new equilibrium shape if the time of twisting or stress application was longer than the relaxation time at the given temperature. By grinding and re-processing, using compression molding, the material recovered its initial tensile properties almost completely.[55]

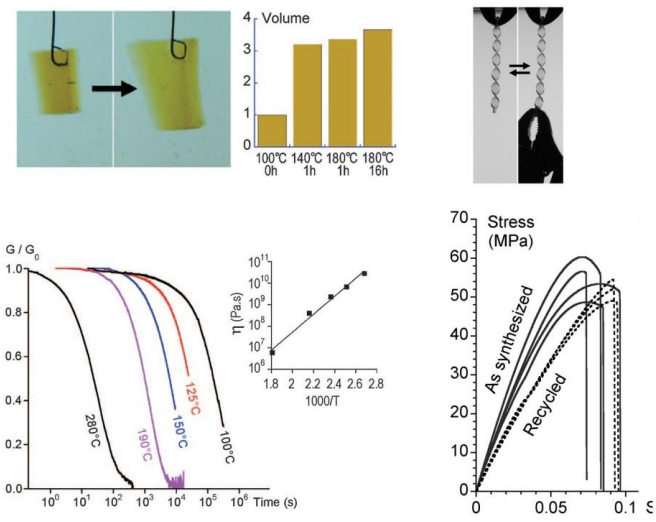

Figure 1.17. Top left: Swelling in trichlorobenzene at 180 °C for different durations. The material swells, but remains insoluble. Top right: At room temperature, the material does not creep. Bottom left: Stress relaxation at various temperatures and viscosity as a function of inversed temperature. Bottom right: Tensile properties before and after recycling of vitrimers.[55]

Further work on the covalent dynamic exchange of hydroxyl-groups with esters resulted in a deeper understanding of the role of the zinc-ion in the epoxy-based vitrimers and the performance of several other catalysts were studied.[58] Epoxy vitrimer composites with a glass fiber loading of more than 50 vol% were generated from a liquid formulation via a common resin-transfer molding technique.[58] Specimens of this composite did not only show superior mechanical properties, but also allowed adhesion to each other with a relative high force at break of 2800 N compared to 2500 – 5000 N for common structural adhesives under the same testing conditions. This welding approach is not only interesting for specimens which cannot easily be molded and welded due to their shape, but also because no adhesive layer is needed. Systems with unique properties due to a combination of supramolecular hydrogen-bonding and dynamic covalent exchanges via transesterification were presented by Michaud and co-workers.[60] Depending on the ratio of the hydrogen-bonding compounds to crosslinking tetraepoxy (vitrimer technology), these materials were self-healing yet possessed enhanced creep resistance (Figure 1.18, top). Hillmyer and co-workers applied transesterification catalyzed by a Sn-catalyst to a polylactide system resulting in remarkably fast relaxation times at a temperature as low as 120 °C (Figure 1.18, bottom).[61] Reinforced silica-epoxy vitrimer nanocomposites with a filler content up to 40 wt% were reported via a solvent-free and economical method.[62] The introduction of silica was observed to increase modulus in both glassy and rubbery region but seemed to slow down the covalent exchange reaction.

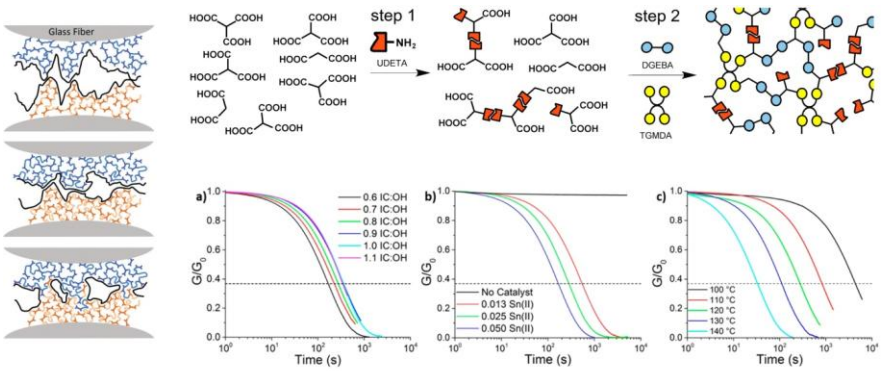

Figure 1.18. Left side: Schematic view of composite-vitrimer welding.[59] Top: Hybrid system with hydrogen-bonding and vitrimer technology.[60] Bottom: Stress relaxation curves of polylactide vitrimers. Speed of relaxation depends on catalyst loading, temperature and monomer ratio.[61]

Multi-responsive systems responding to 6 different triggers such as heat, light, pH, voltage, metal ions and redox chemicals were reported when adding an oligoaniline to epoxy vitrimer systems.[63] Transesterification was applied in other matrices, such as epoxidized soybean oil taking advantage of the esterification with citric acid.[64] Although self-healing was observed, the role of temperature and mending time remained unclear and the materials were not able to achieve complete stress relaxation. In the field of liquid crystalline elastomers, the macroscopic orientation of the crystals after processing is an issue due to fix permanent crosslinks. Ji and co-workers used the concept of vitrimers to generate moldable liquid crystalline elastomer actuators which were not only processable, but could also be remolded with different stress patterns to broaden the scope of applications.[65] By controlling the temperature and the change from polydomain isotactic to smectic phase, as well as the materials T_g, a triple shape-memory effect could efficiently be introduced (Figure 1.19).

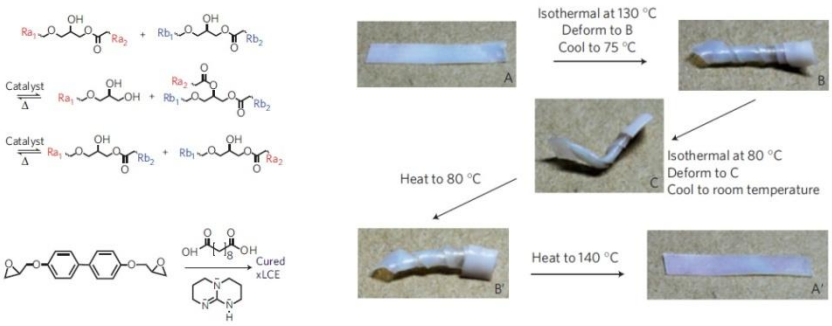

Figure 1.19. A liquid-crystalline vitrimer: The shape of the sample can be temporarily frozen by T_g and the respective transition from the polydomain isotactic to the smectic phase.[64]

Dynamic covalent transalkylation exchanges of C-N bonds were introduced by Drockenmuller and co-workers in high-value ion-conducting networks.[66] Via a solvent- and catalyst-free addition of an azide-alkyne monomer and a dibromo aliphatic species,

poly(1,2,3-triazole) containing networks were generated (Figure 1.20). The exchange between pending halide-functionalities and triazoles at elevated temperatures enabled the system to relax stress completely and to control viscosity as it can be done for glass. By a grinding compression molding procedure the authors demonstrated the re-processability of the materials without compromising the ion-conducting electrolyte nature of the systems.

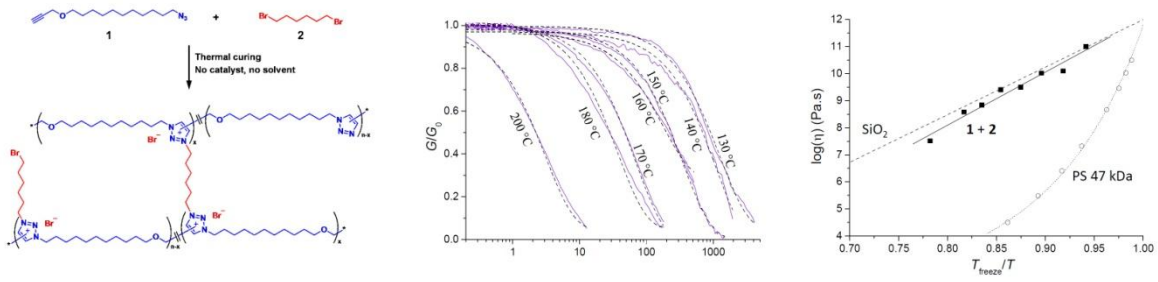

Figure 1.20. Left side: Synthesis of poly(1,2,3-triazole) containing networks. Center: Stress relaxation curves at different temperatures. Right side: Angell fragility plot revealing the glass-like behavior of the presented vitrimers.[66]

Crosslinked polybutadiene was turned into a material with vitrimer properties by addition of low percentages of Grubbs' second generation Ru-catalyst (Figure 1.21).[67] In the presence of 1 mol% of benzoyl peroxide in respect to the olefin, an insoluble network was generated by radical-induced crosslinking. Then, the material was swollen and all remaining small molecules were removed through washing. The dried materials were re-swollen in solution of Grubbs' catalyst to disperse it in a homogenous fashion. To obtain a control material the catalyst was deactivated through cross-metathesis with an excess of vinyl ether and both systems were investigated for their dynamic behavior. The authors showed that in the presence of the C-C metathesis catalyst, the alkylidene (catalyst) and the double bonds in the polymer backbone exchange and hence enable macroscopic flow. In cyclic creep-recovery experiments, it was observed that the material was able to creep continuously and a higher concentration of catalyst resulted in accelerated creep. Similar results were detected for increased temperatures and in stress relaxation experiments. The control sample, did not show any creep nor stress relaxation proving that the dynamic process was governed by the presence of C-C-metathesis enabling Grubbs' catalyst. Despite the fact that these materials are processable yet crosslinked, factors such as uncontrolled creep at room temperature and shelf-life of catalyst might cause some issues and should further be investigated.

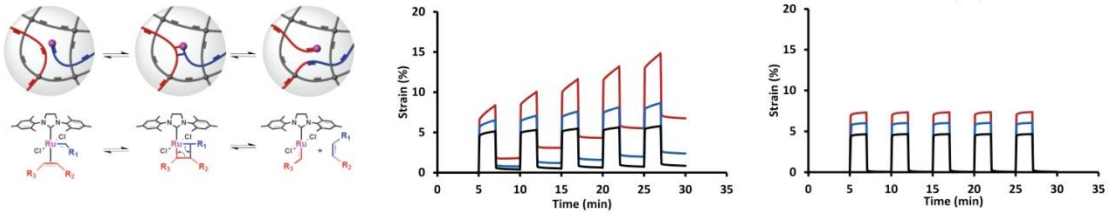

Figure 1.21. From left to right: Grubbs' catalyst mediated olefin-exchange in polybutadiene networks. Increasing creep with increasing catalyst loading for vitrimers. Control systems.[67]

Vitrimers with fast relaxation times at temperatures below 200 °C and a high modulus of ca 10 MPa on the rubbery plateau were reported by Leibler, Du Prez and co-workers (Figure 1.22).[67] This work took advantage of a catalyst-free dynamic covalent exchange reaction between vinylogous urethanes and amines. Kinetic studies on the underlying covalent exchange reaction in solution proved the fast rate of exchange and the thermal stability of the compounds. The materials were readily prepared from bulk polymerization of commercially available compounds and exhibit a rather high T_g of 80 °C. Swelling experiments and dynamic mechanical analysis measurements confirmed the materials insolubility and crosslinked nature. The rapid exchange of network forming bonds enabled fast stress relaxation (85 s at 170 °C) following an Arrhenius law, as reported for the first vitrimer systems using epoxy/acid or epoxy/anhydride systems (Figure 1.22). Comparison of the activation energies of transamination of vinylogous urethanes and transesterification confirms the accelerated rate of exchange in the here presented work, with *ca.* 60 kJ/mol to 80 kJ/mol, respectively. Creep-recovery and recycling by a compression molding/tensile testing method further proved the dynamic nature of the material. Interestingly, the networks could be de-crosslinked in the presence of an excess of benzyl amine under similar conditions as used for the swelling experiments. Although the presented exchange reaction seemed to be stable under the tested conditions, transfer into other polymeric matrices, especially species with electrophilic groups such as acrylates, might be an issue due to the presence of amines. Additionally, the relatively high modulus on the rubbery plateau might hinder processing via common techniques such as extrusion and injection molding.

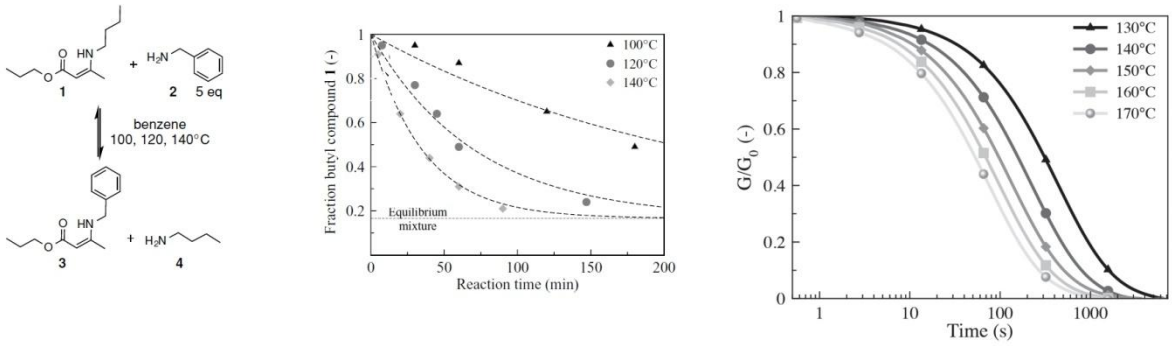

Figure 1.22. Left side: Transamination of vinylogous urethanes. Center: Kinetic plot of the exchange reaction with an initial ratio of 5/1. Right side: Temperature dependant stress relaxation of vinylogous vitrimers.[67]

1.3 Conclusion

Different approaches can be followed to render polymer networks repairable, processable and/or trigger-responsive. In the first chapter of this PhD thesis is shortly presented some of the reported work on healing in the presence of polymerizable substances in microcapsules as well as on responsive materials based on physical bonds. By using chemical (covalent) bonds, the mechanical properties of the responsive materials can be increased. Materials with interesting properties which function either via dissociative/associative crosslinking processes or via associative dynamic exchange reactions were discussed. Vitrimers, insoluble materials which in the absence of permanent static crosslinks take advantage of associative dynamic bond exchanges, were introduced. Vitrimers are processable, malleable and recyclable polymer networks that at all times and temperatures maintain their crosslink number. These materials are insoluble in organic solvents and exhibit rubbery plateaus at high temperatures. Different vitrimer systems were presented and discussed. So far almost all of these materials are made via step-growth processes and contain the dynamic covalently exchanging hetero-atoms in the polymer backbone. Additionally, the reported exchange reactions often need catalysts and are highly specific to the respective polymer matrix. To broaden the concept of vitrimers to other polymer families which contain C-C bond backbones only, dynamic covalent exchange reactions which are compatible with the respective polymer matrix, the polymerization and processing techniques must be investigated. To assure long shelf-life and repeatable processing cycles these chemistries should be as robust as possible and function without a catalyst. On the one hand, the introduced dynamic covalent bonds would crosslink the respective thermoplastic material and guarantee thermosetting properties such as insolubility and dimensional stability at elevated temperatures. On the other hand, efficient reshuffling of covalent bonds would guarantee processability, recyclability and malleability.

1.3 References

1. G. A. Stahl, ACS Symposium Series, **1981**, *175*, 25.
2. *American Chemical Society National Historic Chemical Landmarks*, "Bakelite: The World's First Synthetic Plastic", American Chemical Society, **2015**.
3. United States Patent Office, patent number 3633, "Improvement in India-rubber Fabrics", **1844**.
4. K. S. Whiteley, T. G. Heggs, H. Koch, R.Mawer, W. Immel, "Polyolefins" in Ullmann's Encyclopedia of Industrial Chemistry **2005**, Wiley-VCH, Weinheim.

5. *American Chemical Society National Historic Chemical Landmarks*, "Foundations of Polymer Science: Wallace Carothers and the Development of Nylon". *American Chemical Society*, **2015**.
6. *O. Bayer, Angewandte Chemie, **1947**, 59, 257.*
7. *P. C. Painter, M. M. Coleman, "Fundamentals of polymer science: an introductory text", Lancaster, Pa.: Technomic Pub. Co. **1997**.*
8. *J. Brandrup, E. H. Immergut, E. A. Grulke, „Polymer Handbook" (4 ed.). Wiley-Interscience, **1999**.*
9. *J. D. Hamilton, K. H. Reinert, J. V. Hagan, W. V. Lord, J. Air and Waste Man. Ass., **2012**, 247.*
10. C. P. MacDermott, A. V. Shenoy, "Selecting Thermoplastics for Engineering Applications", Marcel Dekker Inc., New York, **1997**.
11. O. Olabisi, K. Adewale, "Handbook of Thermoplastics, 2nd edition", CDC Press, **2015**.
12. S. R. White, N. R. Sottos, P. H. Geubelle, J. S. Moore, M. R. Kessler, S. R. Sriram, E. N. Brown, S. Viswanathan, *Nature*, **2001**, 794..
13. B. J. Blaiszik, M. M. Caruso, D. A. McIlroy, J. S. Moore, S. R. White, N. R. Sottos, *Polym.*, **2009**, *50*, 990.
14. T. Nesterova, K. Dam-Johanse, S. Kiil, *Prog. Org. Coat.*, **2011**, *70*, 342.
15. M. M. Caruso, B. J. Blaiszik, H. Jin, S. R. Scherkopf, D. S. Stradley, N. R. Sottos, S. R. White, J. S. Moore, *ACS Appl. Mater. Interf.*, **2010**, *2*, 1195.
16. R. J. Wojtecki, M. A. Meador, S. J. Rowan, *Nature Review Materials*, **2011**.
17. L. Yang, X. Tan, Z. Wang, X. Zhang, *Chem. Rev.*, **2015**, *115*, 7196.
18. L. Brunsveld, B. J. B. Folmer, E. W. Meijer, R. P. Sijbesma, *Chem. Rev.*, **2001**, *101*, 4071.
19. S. Zhang, A. M. Bellinger, D. L. Glettig, R. Barman, Y.-A. L. Lee, J. Zhu, C. Cleveland, V. A. Montgomery, L. Gu, L. D. Nash, D. J. Maitland, R. Langer, G. Traverso, *Nature Mater.*, **2015**.
20. P. Cordier, F. Tournilhac, C. Soulié-Ziakovic, L. Leibler, *Nature*, **2008**, 977.
21. C. J. Kloxin, T. F. Scott, B. J. Adzima, C. N. Bowman, *Macromolecules*, **2010**, *41*, 2643.
22. C. N. Bowman, C. J. Kloxin, *Angew. Chem. Int. Ed.*, **2012**, 4272..
23. C. J. Kloxin, C. N. Bowman, *Chem. Soc. Rev.*, **2013**, *42*, 7161.
24. J.-F. Lutz, J.-M. Lehn, E. W. Meijer, K. Matyjaszewski, *Nature Review Materials*, **2016**.
25. H. Ying, Y. Zhang, J. Cheng, *Nature Comm.*, **2014**.
26. G. Deng, C. Tang, F. Li, H. Jiang, Y. Chen, *Macromolecules*, **2010**, *43*, 1191.
27. G. Deng, F. Li, H. Yu, F. Liu, C. Liu, W. Sun, H. Jiang, Y. Cheng, *ACS Macro. Lett.*, **2012**, *1*, 275.
28. B. Yang, Y. Zhang, X. Zhang, L. Tao, S. Li, Y. Wei, *Polym. Chem.*, **2012**, *3*, 3235.
29. J. J. Cash, T. Kubo, A. P. Bapat, B. Sumerlin, *Macromolecules*, **2015**, *48*, 2098.
30. Y. Zuo, Z. Guo, C. Zhang, S. Feng, *Marcomol. Rapid Comm.*, **2016**.
31. J.-C. Lai, J.-F. Mei, X.-Y. Jia, C.-H. Li, X.-Z. You, Z. Bao, *Adv. Mater.*, **2016**.
32. X. Chen, M. A. Dam, K. Ono, A. Mal, H. Shen, S. R. Nutt, K. Sheran, F. Wudl, *Science*, **2002**.

33. X. Chen, F. Wudl, A. K. Mal, H. Shen, S. Nutt, *Macromolecules*, **2003**, *36*, 1802.
34. P. Reutenauer, E. Buhler, P. J. Boul, S. J. Candau, J.-M. Lehn, *Chem. Eur. J*., **2009**, *15*, 1893..
35. K. K. Oehlenschlaeger, J. O. Mueller, J. Brandt, S. Hilf, A. Lederer, M. Wilhelm, R. Graf, M. L. Coote, F. G. Schmidt, C. Barner-Kowollik, *Adv. Mater*., **2014**, *26*, 3561.
36. S. Yu, R. Zhang, Q. Wu, T. Chen, P. Sun, *Adv. Mater*., **2013**, *25*, 4912.
37. T. F. Scott, A. D. Schneider, W. D. Cook, C. N. Bowman, *Science*, **2005**.
38. R. Nicolaÿ, J. Kamada, A. Van Wassen, K. Matyjaszewski, *Macromolecules*, **2010**, *43*, 4355.
39. Y. Amamoto, J. Kamada, H. Otsuka, A. Takahara, K. Matyjaszewski, *Angew. Chem. Int. Ed*., **2011**, *50*, 1660..
40. Y. Amamoto, H. Otsuka, A. Takahara, K. Matyjaszewski, *Adv. Mater*., **2012**, *24*, 3975.
41. J. Kamada, K. Koynov, C. Corten, A. Juhari, J. Yoon, M. Urban, A. Balazs, K. Matyjaszewski, *Macromolecules*, **2010**, *43*, 4133.
42. J. Yoon, J. Kamada, K. Koynov, J. Mohin, R. Nicolaÿ, Y. Zhang, A. Balazs, T. Kowalewski, K. Matyjaszewski, *Macromolecules*, **2012**, *45*, 142.
43. B. T. Michal, C. A. Jaye, E. J. Spencer, S. J. Rowan, *ACS Macro Lett*., **2013**, *2*, 694.
44. R. Martin, A. Rekondo, A. R. de Luzuriaga, G. Cabanero, H. J. Grande, I. Odriozola, *J. Mater. Chem. A*, **2014**, *2*, 5710.
45. M. Pepels, I. Filot, B. Klumperman, H. Goossens, *Polym. Chem*., **2013**, *4*, 4955.
46. Z. Q. Lei, H. P. Xiang, Y. J. Yuan, M. Z. Rong, M. Q. Zhang, *Chem. Mater*., **2014**, *26*, 2038.
47. L. Imbernon, E. K. Oikonomou, S. Norvez, L. Leibler, *Polym. Chem*., **2015**, *6*, 4271.
48. R. C. Osthoff, A. M. Bueche, W. T. Grubb, *J. Am. Chem. Soc*., **1954**.
49. P. Zheng, T. J. McCarthy, *J. Am. Chem. Soc*., **2012**, *134*, 2024.
50. PhD thesis Fanny Angot, **2016**.
51. . J. Fortman, J. P. Brutman, C. J. Cramer, M. A. Hillmyer, W. R. Dichtel, *J. Am. Chem. Soc*., **2015**.
52. P. Taynton, K. Yu, R. K. Shoemaker, Y. Jin, H. J. Qi, W. Zhang, *Adv. Mater*., **2014**.
53. Z. Q. Lei, P. Xie, M. Z. Rong, M. Q. Zhang, *J. Mater. Chem*. A, **2015**.
54. O. R. Cromwell, J. Chung, Z. Guan, *J. Am. Chem. Soc*., **2015**, *137*, 6492.
55. D. Montarnal, M. Capelot, F. Tournilhac, L. Leibler, *Science*, **2011**.
56. M. Capelot, M. M. Unterlass, F. Tournilhac, L Leibler, *ACS Macro Lett*., **2012**, *1*, 789.
57. M. Capelot, D. Montarnal, F. Tournilhac, L. Leibler, *J. Am. Chem. Soc*., **2012**, *134*, 7664.
58. A. Demongeot, S. J. Mougnier, S. Okada, C. Soulié-Ziakovic, F. Tournilhac, *Polym. Chem*., **2016**, *7*, 4486.
59. E. Chabert, J. Vial, J.-P. Cauchois, M. Mihaluta, F. Tournilhac, *Soft Matter*, **2016**, *12*, 4838.
60. F. Sordo, S.-J. Mougnier, N. Loureiro, F. Tournilhac, V. Michaud, *Macromolecules*, **2015**, *48*, 4394.
61. J. P. Brutman, P. A. Delgado, M. A. Hillmyer, *ACS Macro Lett*., **2014**, *3*, 607.
62. A. Legrand, C. Soulié-Ziakovic, *Macromolecules*, **2016**, *49*, 5893.

63. Q. Chen, X. Yu, Z. Pei, Y. Yang, Y. Wei, Y. Ji, *Chem. Sci*., **2016**.
64. F. Altuna, V. Pettarin, R. J. J. Williams, *Green Chem*., **2013**, *15*, 3360.
65. Z. Pei, Y. Yang, Q. Chen, E. M. Terentjev, Y. Wei, Y. Ji, *Nature Mater*., **2014**.
66. M. M. Obadia, B. P. Mudraboyina, A. Serghei, D. Montarnal, E. Drockenmuller, *J. Am. Chem. Soc*., **2015**.
67. Y.-X. Lu, F. Tournilhac, L. Leibler, Z. Guan, *J. Am. Chem. Soc*., **2012**, *134*, 8424.
68. W. Denissen, G. Rivero, R. Nicolaÿ, L. Leibler, J. M. Winne, F. E. Du Prez, *Adv. Funct. Mater*., **2015**.

Chapter 2

Dynamic Exchange Reactions with Imines and Aldehydes

Table of Contents

Chapter 2 – Dynamic Exchange Reactions with Imines and Aldehydes

2.1 Introduction

Primary amines can react with aldehydes or ketones via reversible condensation resulting in water and species called Schiff' bases, azomethines or imines, which present a characteristic C=N bond (Scheme 2.1, (1)).[1] Since 1864, when Hugo Schiff first discovered this reaction, and thanks to a wide range of possible substitution patterns on the carbon and nitrogen atoms, such as aryl, alkyl or hydrogen atoms, these compounds have been studied thoroughly in biology, chemistry and material science.[2-12] The same holds for other structurally similar species. Hydrazones contain an additional nitrogen-atom adjacent to the nitrogen-atom of the C=N bond, acylhydrazones - hydrazones possess an additional keto functionality adjacent to the second nitrogen-atom, and oximes present a hydroxyl group attached to the nitrogen-atom of the C=N bond .[13-16] Another advantage of these compounds is the ubiquity of the bond forming amino functionality in organic chemistry, and more generally in nature.[12] The family of Schiff' base species can be generated by different synthetic methods, such as metal catalysis with TiO_2, $Cu(NO_3)_2$, Al_2O_3, $Mg(ClO_4)_2$ and others species.[17-25] Other approaches such as photo-, electro- and organocatalysis were reported.[26-31] Especially, simple yet efficient methods where the equilibrium is driven to the product side by trapping water, *e.g.* refluxing under azeotropic conditions or addition of molecular sieves or magnesium sulfate, are commonly used in research laboratories.[32]

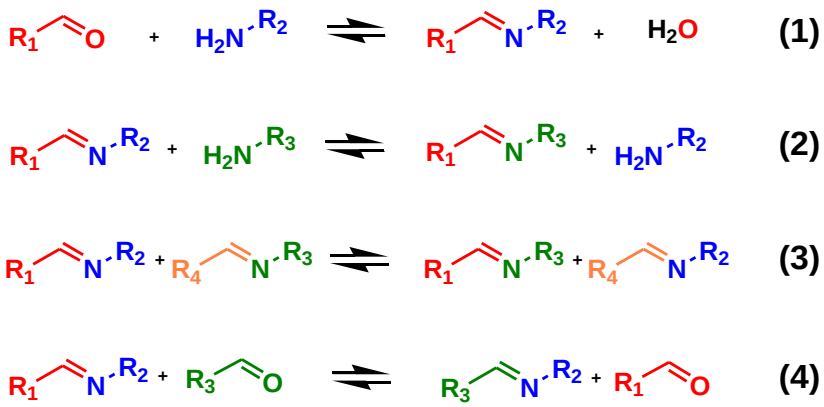

Scheme 2.1. Schiff'sche base reactions. Previously described reversible and/or dynamic reactions involving imines: (1) imine formation, (2) transimination and (3) imine metathesis,. Novel exchange reactions disclosed and studied in this PhD thesis: (4) imine aldehyde exchange and (3) imine metathesis catalyzed by aldehydes.

The equilibrium composition of starting compounds and imines in the absence of water trapping agents is governed by the thermodynamics of the system and can be modified by changing conditions such as solvent, pH and temperature. By addition of water, these compounds can be partially or completely hydrolyzed into their constituting carbonyl and amino compounds and studies have been conducted to determine the thermodynamic stabilities of imines in the presence of water and at different pH.[33-40] Imines can react with free amines via transimination to give another imine and amine (Scheme 2.1, (2)). Depending on the substitution pattern of the imine and amine, as well as other conditions such as solvent, temperature and pH, this exchange can be very fast even at room temperature.[41] Triflate salts of trivalent metals (Sc, Tb, Sm, La) were reported as catalysts that can accelerate the exchange up to five order of magnitudes.[42] It is reported that two imines can undergo a process called metathesis where, by definition, two similar chemical species exchange bonds to result in products with similar bond affiliations as the reactants (Scheme 2.1, (3)).[43] By mixing two imines with different R_i radicals, the final mixture will hence contain a total of four imines, the molar proportion of each imine at the thermodynamic equilibrium reflecting its stability. This exchange is often conducted in the presence of metal complex catalysts, such as Mo, Ta, Nb and Zr.[43-47] Additionally, organocatalysts, such as iminophosphoranes, secondary amines and others were reported.[48-49] In most cases, the reported systems show limitations and/or drawbacks such as high costs, high synthetic effort, short life cycles and toxicity (metal complexes). Also the speed of exchange is rather slow and even in the presence of metal catalysts high temperatures (<100 °C) were needed to drive the reaction.[41]

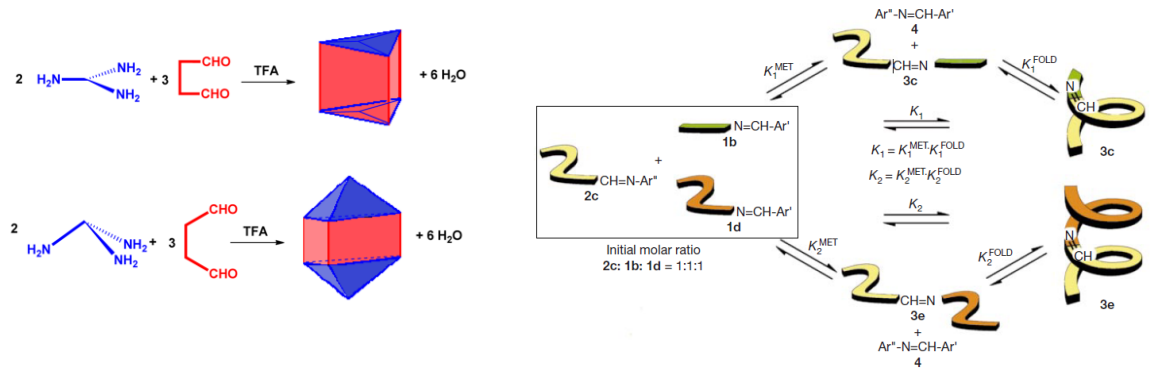

Figure 2.1. Left side: molecular cages made of imine bonds.[57] Right side: Foldable oligomers via imine metathesis.[58]

Thanks to their trigger responsiveness, their dynamic and tunable nature, imines have been reported in a variety of high added value applications. In biology, they have been used *e.g.* for

the synthesis of chitosan-based hydrogels and for the multi-responsive controlled release of bioactive molecules.[50] Taking advantage of differences in thermodynamic stability, a multitude of work has been reported on the use of imines in dynamic (covalent) combinatorial chemistry (DCC) for drug discovery and screening, receptor generation, phase separation studies and substrate binding.[51-56] In chemistry and material science, covalent organic frameworks (COF) were generated for molecular recognition, chemical sensing and gas separation and storage (Figure 2.1).[57] The reversibility of the imine bond has been used to selectively generate (folded) oligomers from small molecules by a folding driven, "error reading" procedure (Figure 2.1).[58] Single-chain polymer nanoparticles were shown to transform into hydrogels by a simple heating protocol via defolding. Additionally, deliberately degradable polymeric systems, *e.g.* core cross-linked star polymers have been reported.[60]

With the overall scope to introduce dynamic covalent crosslinkers based on exchanges of imines into high T_g polymeric matrices, we investigated the known above mentioned imine transimination and imine metathesis reaction by ^{1}H-NMR and gas chromatography (GC). Novel exchange reactions, namely imine-imine metathesis catalyzed by aldehydes and imine-aldehyde exchange were also studied. Different synthetic methods were tested for the generation of small molecules in rather high purity. Kinetic studies were performed in different solvents and in bulk on various imines, aldehydes and amines . Important parameters, such as the presence of water and air (humidity) were addressed by changing from air to protective atmosphere (dry argon).

2.2 Synthesis of model molecules and monomers

2.2.1 General synthesis of imines and overview of molecules

Chemicals, solvents and gases: Amines, aldehydes and other chemicals were purchased from Sigma Aldrich, Alfa Aesar, TCI, Acros and Fischer. Solvents and deuterated solvents were stored over fresh and dried 3Å molecular sieves. The respective ratio of molecular sieves to solvent (% mass/volume) and the minimum time to achieve maximum dryness for each solvent were taken from literature.[61]

NMR analysis: ^{1}H-NMR and ^{13}C-HNMR analyses were conducted on a Bruker Ultra Shield machine at 400 MHz or 100 MHz, respectively. NMR tubes were oven dried, and if not stated

otherwise, samples of 10 mg were analyzed and the obtained data were internally referred to the standard shift of the deuterated solvent.

GC-MS analysis:

GC-MS analyses were performed on a GCMS QP2010S device from Shimadzu.

The most straightforward route to synthesize imines is the condensation of an aldehyde and an amine in the presence of a water trapping agent (Scheme 2.2).[32] By using an excess of volatile amines in the presence of $MgSO_4$, the reaction is driven to completion and simple filtration and concentration are sufficient to yield high purity imines.

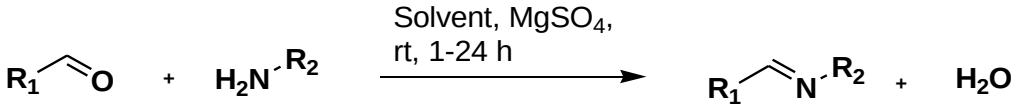

Scheme 2.2. Imine formation via condensation of an aldehyde with a primary amine.

Imines were synthesized according to the following general procedure: The amine (0.95 – 5 eq.) and the aldehyde (1 eq) were mixed in an anhydrous solvent (THF, DCM) and stirred at room temperature until full dissolution. Then, $MgSO_4$ (3 eq.) was added slowly and the mixture was stirred for 1-72 additional hours. The mixture was filtered and concentrated under reduced pressure to obtain the target compounds as oils or solids. In general, no or very small amounts of free amines and aldehydes were detected by ^{1}H-NMR analysis. As different molar ratios were used to synthesize the reported imines, the detailed ratio of amine (Am) and aldehyde (A) for each reaction is given in the analytical data separately (Am/A = eq/ eq).

Synthesis of monomer **A_1**:

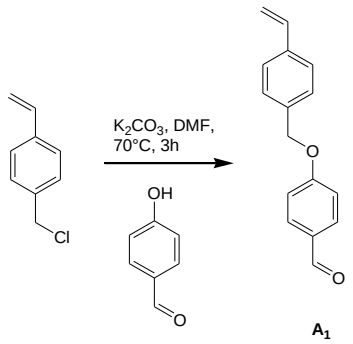

Scheme 2.3. Synthesis of monomer **A_1**.

Synthesis of monomer **A_1**: Chloromethylstyrene (6.63 g, 43.4 mmol), 4-hydroxybenzaldehyde (6.25 g, 51.1 mmol) and K_2CO_3 (17.7 g, 127.9 mmol) were introduced in a 250 mL round

bottom flask containing 75 mL of DMF. The mixture was left to react for 3 hours at 70 °C under nitrogen. The solution was poured into 500 mL of water, and the mixture was extracted with 3 × 100 mL of ethyl acetate. The organic layers were combined and washed with 150 mL of NaOH 0.5 M (3 × 150 mL), dried over $MgSO_4$, and the solvent was evaporated to obtain a yellowish solid. The solid was heated to 50 °C for 1 hour in 100 mL of heptane while stirring rapidly. Then, the solid was filtered and dried to give the target compound as a white solid (8.7 g, 36.3 mmol, 84%).

^{1}H NMR ($CDCl_3$, 400 MHz): δ 9.89 (s, 1H), 7.84 (d, J = 8.8 Hz, 2H), 7.42 (m, 4H), 7.07 (d, J = 8.8 Hz, 1H), 6.73 (dd, J = 17.6 Hz, 10.8 Hz, 1H), 5.77 (d, J = 17.6 Hz, 1H), 5.28 (d, J = 10.8 Hz, 1H), 5.14 (s, 2H). ^{13}C NMR ($CDCl_3$, 100 MHz): δ 190.8, 163.7, 137.7, 136.3, 135.4, 132.0, 130.2, 127.7, 126.6, 115.2, 114.5, 70.1. GCMS m/z (%): [M] calcd for $C_{16}H_{14}O_2$, 238.0944; found 238.20 (2), 117.2 (100), 115.15 (17), 91.15 (11).

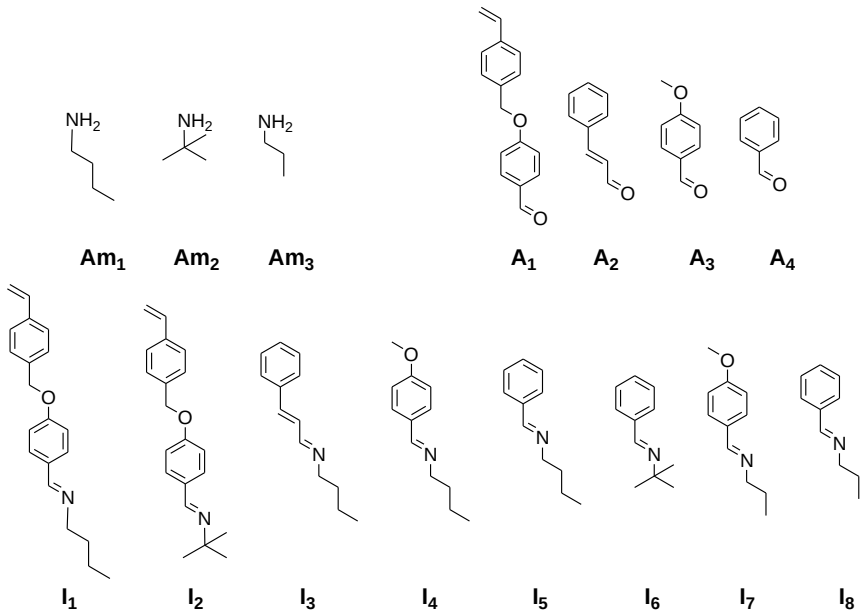

Scheme 2.4. Amines, aldehydes and imines used in the kinetic studies.

Imine **I_1**: Am/A = 5/1 and 1/1, white solid (95%). ^{1}H NMR ($CDCl_3$, 400 MHz): δ 8.20 (s, 1H), 7.66 (d, J = 8.8 Hz, 2H), 7.41 (m, 4H), 6.99 (d, J = 8.8 Hz, 2H), 6.73 (dd, J = 17.6 Hz, 10.8 Hz, 1H), 5.77 (d, J = 17.6 Hz, 1H), 5.27 (d, J = 10.8 Hz, 1H), 5.09 (s, 2H), 3.58 (t, J = 7.2 Hz, 2H), 1.67 (m, 2H), 1.38 (m, 2H), 0.95 (t, J = 7.2 Hz, 3H). ^{13}C NMR ($CDCl_3$, 100 MHz): δ 160.5, 160.0, 137.4, 136.4, 136.2, 129.6, 129.5, 127.8, 126.5, 114.9, 114.2, 69.8, 61.4, 33.2, 20.5, 14.0. GCMS m/z (%): [M] calcd for $C_{20}H_{30}$ NO, 293.4027; found 293.25 (1), 176.2 (8), 117.15 (100), 115.15 (11).

Imine **I_2**: Am/A = 5/1 and 1/1, white solid (95%). ^{1}H NMR ($CDCl_3$, 400 MHz): δ 8.22 (s, 1H), 7.69 (d, 2H, J = 8.8 Hz), 7.41 (m, 4H), 6.99 (d, J = 8.8 Hz, 2H), 6.73 (dd, J = 17.6 Hz, 10.8 Hz, 1H), 5.77 (d, J = 17.6 Hz, 1H), 5.27 (d, J = 10.8 Hz, 1H), 5.08 (s, 2H), 1.29 (s, 9H).

Imine **I_3**: Am/A = 2/1, yellowish oil (1.4 g, 7.3 mmol, 80%, ca 9.8 mol% free aldehyde). ^{1}H NMR ($CDCl_3$, 400 MHz): δ 8.19 (s, 1H), 7.70 (d, J = 9.6 Hz, 2H), 7.34 (m, 3H), 6.42 (m, 1H), 5.98 (m, 1H), 3.58 (t, J = 6.8 Hz, 2H), 1.71 (m, 2H), 1.50 (m, 2H), 0.98 (t, J = 7.2 Hz, 3H).

Imine **I_4**: Am/A = 5/1, yellow oil (2.0 g, 10.5 mmol, 81%, free aldehyde and amine < 1 mol%). ^{1}H NMR ($CDCl_3$, 400 MHz): δ 8.16 (s, 1H), 7.80 (d, J = 8.8 Hz, 2H), 6.85 (d, J = 8.8 Hz, 2H), 3.63 (t, J = 6.8 Hz, 2H), 3.43 (s, 3H), 1.78 (m, 2H), 1.54 (m, 2H), 1.05 (t, J = 7.2 Hz, 3H).

Imine **I_5**: Am/A = 5/1, yellowish oil (2.1 g, 12.9 mmol, 92%, free aldehyde < 0.2 mol%, free amine < 0.9 mol%). ^{1}H NMR ($CDCl_3$, 400 MHz): δ 8.28 (s, 1H), 7.73 (d, J = 9.6 Hz, 2H), 7.39 (m, 3H), 3.63 (t, J = 6.8 Hz, 2H), 1.74-1.66 (m, 2H), 1.45-1.36 (m, 2H), 0.96 (t, J = 7.2 Hz, 3H).

Imine **I_6**: Am/A = 5/1, yellowish oil (2.1 g, 13.0 mmol, 90%). ^{1}H NMR ($CDCl_3$, 400 MHz): δ 8.29 (s, 1H), 7.76 (d, J = 8.8 Hz, 2H), 7.40 (m, 3H), 1.30 (s, 9H).

Imine **I_7**: Am/A = 5/1, yellowish oil (2 g, 11.3 mmol, 70%, free aldehyde < 0.6 mol%, free amine < 2.8 mol%). ^{1}H NMR ($CDCl_3$, 400 MHz): δ 7.96 (s, 1H), 7.63 (d, J = 8.8 Hz, 2H), 6.68 (d, J = 8.8 Hz, 2H), 3.42 (t, J = 6.8 Hz, 2H), 3.28 (s, 3H), 1.73-1.64 (m, 2H), 0.93 (m, 3H).

Imine **I_8**: Am/A = 5/1, yellowish oil (1.5 g, 10.2 mmol, 73%, free aldehyde < 0.15 mol%, free amine < 0.5 mol%)). ^{1}H NMR ($CDCl_3$, 400 MHz): δ 7.95 (s, 1H), 7.69 (dd, J = 8.0, 2.4 Hz, 2H), 7.14-7.07 (m, 3H), 3.4 (t, J = 6.8 Hz, 2H), 1.72-1.63 (m, 2H), 0.92 (t, J = 6.8 Hz, 3H).

Preparation of dry aldehydes: Aldehydes utilized in the kinetic studies were dissolved in the selected anhydrous solvent (THF or DCM) and $MgSO_4$ (3.0 eq) was added. The mixture was stirred slowly for at least 24 hours, filtered and concentrated under reduced pressure to obtain the dry aldehyde.

Preparation of dry amines: Amines utilized in the kinetic studies as catalysts were mixed with dried molecular sieves and the mixture was kept for 24 hours. The amines were filtered to obtain dry amines.

2.3 Exchange reactions of Schiff bases

The studies of exchange reactions taking place in mixtures of imines or in mixtures of imines and aldehydes are presented in the following subchapters. Experiments were performed under various conditions, in the absence and in the presence of purposely added free amines and aldehydes, and were monitored via several techniques. Experiments were followed via ^{1}H-NMR spectroscopy (in dried $CDCl_3$ and in the presence of air) and via GC over molecular sieves in different dried solvents in the presence of air as well as under argon in bulk.

2.3.1 Kinetic studies followed by ^{1}H-NMR spectroscopy

Imines can be hydrolyzed by water to aldehydes and amines. It is known that free amines react with imines by transimination to generate another imine and another amine.[41-42] To address this issue and minimize contaminations by water, the kinetic studies of imine-imine exchange and imine-aldehyde exchange reactions were performed in anhydrous $CDCl_3$ (new bottle, septum). With the overall aim to introduce imine/aldehydes functionalized monomers in polymeric materials, we decided to perform some of the experiments on the later used monomers.

General mixing procedure: Stock solutions of all compounds were generated in closed vials (0.25 mM) in anhydrous $CDCl_3$ (new bottle). Via micro syringes, one of the compounds (0.1 mL of stock solution) was mixed with more $CDCl_3$ (0.5 mL) in the NMR-tube, before the second compound was added (0.1 mL, of stock solution). The tube was closed, sealed and shaken once before analysis was started. The time between mixing and acquisition of the first spectra was 3.5 minutes. For the analysis at elevated temperature, the NMR-machine was pre-heated. The temperature in the room of analysis was between 23.0-23.6 °C. Total concentration of the two reactants was 0.071 M (0.05 mmol/0.7 mL). The spectra at time t_x was treated with the de-convolution tool (Mestrenova, highest resolution, 20 fitting cycles).

Reaction	Reactant 1	Reactant 2	Products	Conditions	*$t_{30\ mol\%}$ (h)
1	**I_6**	**I_1**	**I_1, I_2, I_5, I_6**	23 °C	32.5
2	**I_6**	**I_1**	**I_1, I_2, I_5, I_6**	45 °C	23.0
3	**I_6**	**I_1**	**I_1, I_2, I_5, I_6**	23 °C, 10 mol% *n*-butylamine	10.0
4	**I_6**	**I_1**	**I_1, I_2, I_5, I_6**	23 °C, 10 mol% A_4	4.8
5	**I_6**	**I_1**	**I_1, I_2, I_5, I_6**	45 °C, 10 mol% A_4	0.8
6	**A_4**	**I_1**	**I_1, I_5, A_1, A_4**	23 °C	8.7

* time to generate 30 mol% of cross-products **I_2** and **I_5** or **I_5** and **A_1**.

Table 2.1. Exchanges of imines and aldehydes in $CDCl_3$ monitored via ^{1}H-NMR.

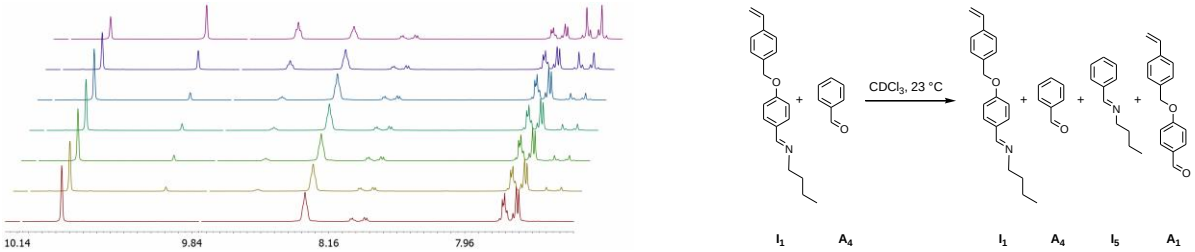

Scheme 2.5. Exchange reaction of imine **I_1** and aldehyde **A_4** in $CDCl_3$ under air.

Table 2.1 summarizes the investigated reactions between pure imines (purity >99 mol%), in the presence of 10 mol% free aldehyde or free amine and between an aldehyde and an imine. Additional reactions were conducted at higher temperature. The reactions of **I_1** and **I_6** were followed by the evolution of R-N=C*H*-R signals in the characteristic region between 8.29 ppm – 8.20 ppm. Imine **I_5** was monitored by its R-N-CH_2-R signal at 3.59 ppm due to partial overlapping with **I_6** at 8.28 ppm (Scheme 2.5). This integration value was then used to calculate the respective net integration value for imine **I_6** by subtraction from the overlap-sum of both imines at 8.28 ppm. The experiment with imine **I_1** and benzaldehyde **A_4** was monitored by the two aldehyde peaks at 10.05-9.90 ppm. In general, the concentration of substrates **I_1** and **I_6** (**I_1** and **A_4** for aldehyde-imine exchange**)** decreased, while the concentrations of cross-products **I_2** and **I_5** (**I_5** and **A_1** for aldehyde-imine exchange) increased in a proportional manner. The value at which the sum of cross-product species (**I_2** and **I_5** or **I_5** and **A_1**) equals 30 mol% in respect to the total amount of exchanging species was set as threshold to compare the different reactions (Figure 2.2).

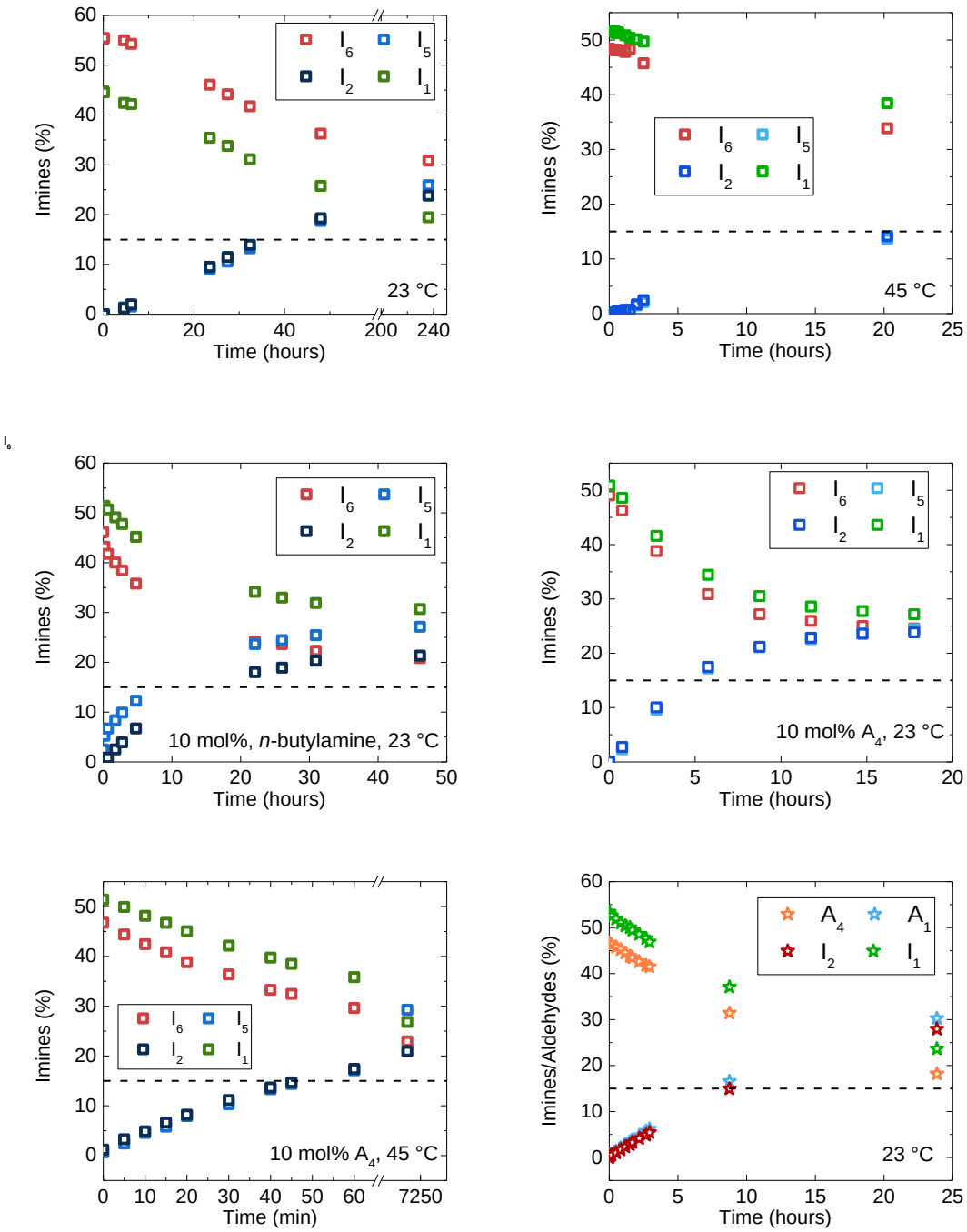

Figure 2.2. Kinetic plots of imine-imine and imine-aldehyde exchange reactions in $CDCl_3$ under air.

Exchange products were observed in all experiments. The reaction of two imines at room temperature proceeds very slowly ($t_{30\ mol\%}$ = 32.5 h) compared to the same reaction in the presence of 10 mol% **A4** ($t_{30\ mol\%}$ = 4.8 h). Free amines can catalyze the reaction ($t_{30\ mol\%}$ = 10.0 h), but seem to be less efficient than benzaldehyde. Heating accelerates the exchange reactions and the aldehyde-catalyzed reaction between two imines was found to be the fastest ($t_{30\ mol\%}$ = 0.8 h). The reaction between aldehydes and imines was tested under identical

conditions and observed to be faster than the reaction between imines ($t_{30\ mol\%}$ = 8.7 h), but slower as the experiments with two imines and 10 mol% aldehyde ($t_{30\ mol\%}$ = 4.8 h).

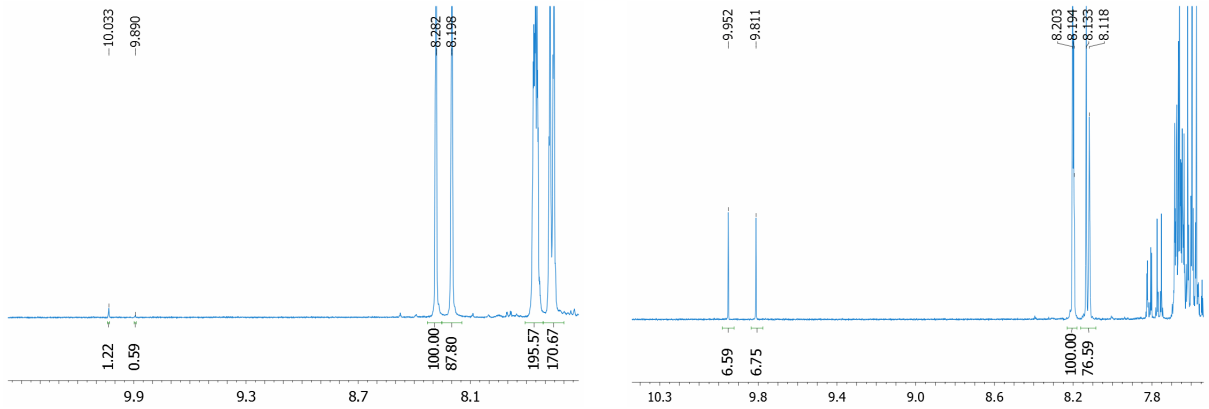

Figure 2.3. ^{1}H-NMR spectra of the exchange between imines $\mathbf{I_1}$ and $\mathbf{I_6}$ in $CDCl_3$ under air. Left side: Right after mixing (3.5 min). Right side: at equilibrium (240 min).

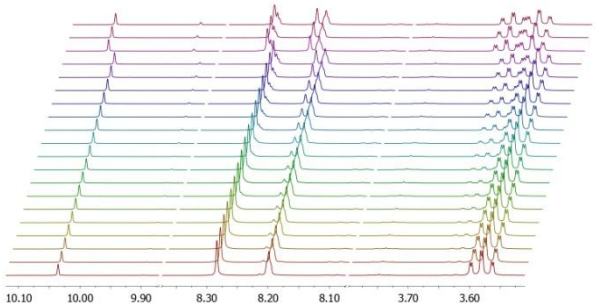

Figure 2.4. ^{1}H-NMR raw data of the exchange between imines $\mathbf{I_1}$ and $\mathbf{I_6}$ in $CDCl_3$ under air in the presence of 10 mol% $\mathbf{A_4}$.

Although anhydrous solvents and dry purified compounds were used, the formation of the corresponding aldehydes was observed during reaction 1 between imines $\mathbf{I_1}$ and $\mathbf{I_6}$ (from < 1 mol% right after mixing to 7 mol%) (Figure 2.3). Amine signals were in general more difficult to detect and quantify than the aldehyde signals at high ppm values. Figure 2.3 presents the spectrum after mixing and after equilibrium indicating the presence of a degradation process of imines. Possible explanations might be insufficient dryness of solvents or compounds and imine degradation via humidity uptake of the solvent. Both assumptions can be supported by the detection of small traces of water in the imine exchange at 45 °C and in the exchange with free amine. However, water was not detected in all experiments. Additionally, the reaction between two imines might have been catalyzed by traces of amines or aldehydes, instead of proceeding via the direct metathesis pathway. taking into account these difficulties and the rather important role that small traces of water and/or humidity seem to play, another experimental method was tested.

2.3.2 Kinetic studies followed by gas chromatography under air

GC analysis: GC analysis was conducted on a Shimadzu gas chromatograph GC-2014 equipped with a Zebron "inferno" or a Waxplus column and helium as carrier gas. Injection was done manually by injecting 1 μL sample volumes using a 10 μL syringe from Hamilton (gastight 1701). Before running analysis, the entire set-up was pre-heated to 350 °C and kept at constant carrier gas flow of 5 mL/min and split ratio of 2.0 for at least 30 minutes. The GC method (T_{inj}, T_{col}, T_{det}, gas flow, split ratio) was chosen according to the nature of the studied molecules and the respective exchange reaction. The column was reconstituted regularly by heating to 350 °C as described above.

Taking into account the encountered difficulties with the experimental set-up applied for ^{1}H-NMR spectroscopy, we decided to test the exchange reactions in less hydrophilic solvents (dried TCB and dried toluene) in the presence of a water trapping agent (molecular sieves). Kinetic studies of the possible exchange reactions between imines and between imines and aldehydes were followed by GC. Compounds were analyzed individually at different concentrations and external calibration curves with compound specific response factors (concentration – area relation) were generated. To further minimize the effect of humidity, a series of experiments was performed under protective atmosphere (argon) in bulk.

External calibration curves were generated as follow. A new bottle of the (anhydrous) solvent was opened and the solvent was then stored over molecular sieves.[61] Stock solutions of each compound with concentrations between 0.1 mM - 0.074 mM were generated over molecular sieves. The stock solutions were diluted subsequently by adding 10, 50 and 100 μL of the stock solution to 0.1 mL of the (anhydrous) dried solvent and characterized by GC using an injection volume of 1 μL. Concentrations were corrected for impurities observed by ^{1}H-NMR analysis if present. The slope of the linear fit of the four resulting points was used as external calibration reference to obtain the concentration - area dependence for each molecule.

The GC methods were adapted to solvent, reaction and column. For exchanges in TCB we tested the less polar Zebron "inferno" column and for exchanges in toluene and bulk the Waxplus with a higher polarity (Table 2.1).

Reactions	$T_{inj/det}$	T_{col}	Carrier gas flow	Split ratio	T program	Column
	(°C)		(mL)		Hold time (min)/ramp (°C/min)	
Reactions in TCB						
All	350/350	120	10	2.0	0.5/30	Zebron-5HT Inferno
Reactions in toluene under air or in bulk under argon						
All	350/350	150	10	2.0	0.5/30	ZB Waxplus

Table 2.2. Gas chromatography methods used to study exchange reactions of imines and aldehydes.

2.3.2.1 Exchanges in trichlorobenzene under air

The experiments were performed in a septum closed vial (1.5 mL) over molecular sieves. 50 □L of stock solutions of each compound (0.1 mM) were mixed in the preheated vial and samples of 1□□L were analyzed via GC at selected time interval. The time between sampling and injection was *ca.* 20 seconds and the time of sampling was noted as time of measurement. The exchange of Imine **I_6** and aldehydes **A_1** was analyzed at 6 different temperatures (Figure 2.5). To access the rate of reaction not only at moderate temperatures, but also at high temperatures, trichlorobenzene (TCB, boiling point = 214 °C) was chosen as reaction medium.

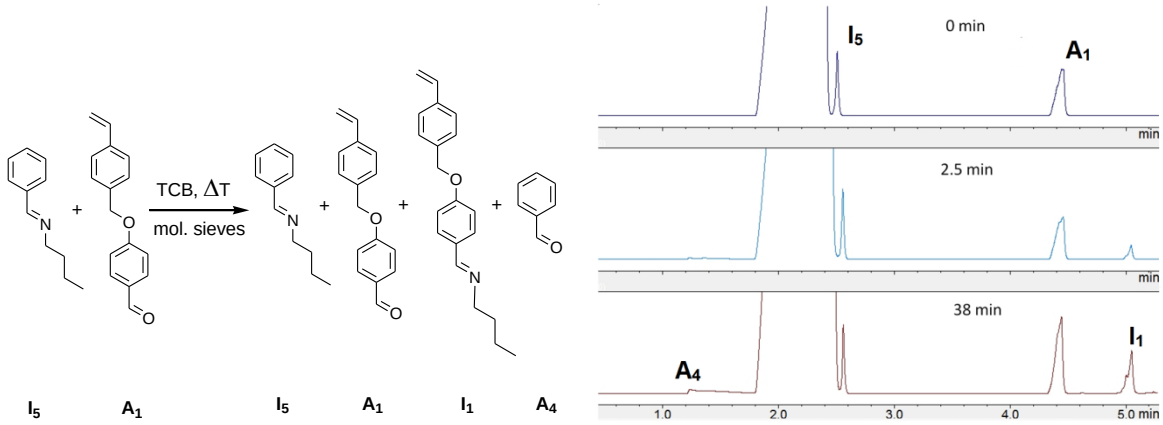

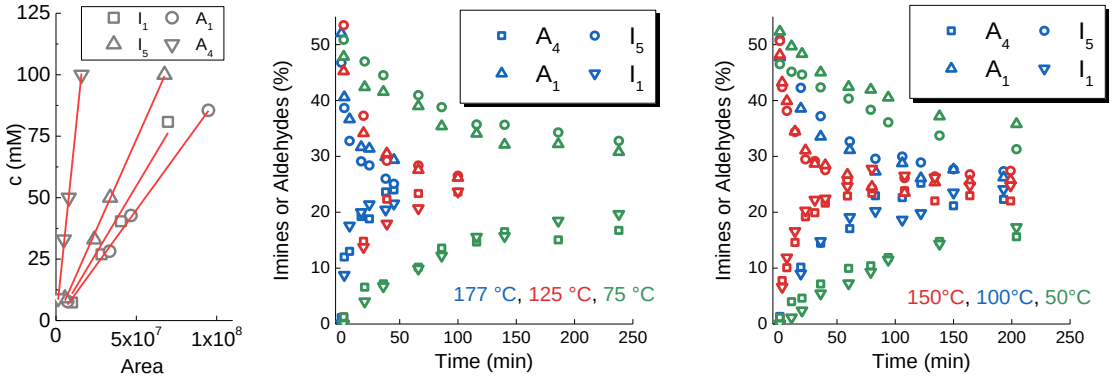

Figure 2.5. Top left: Exchange reaction of imine $\mathbf{I_5}$ with aldehyde $\mathbf{A_1}$ in TCB at various temperatures. Top right: GC raw data. Bottom row from left to right: GC external calibration curves for imines and aldehydes. Kinetic plots of the experiments at different temperatures.

As can be seen from the results in figure 2.5 several issues regarding the experimental methods were encountered. Although experiments could be performed at high temperatures (up to 177 °C), the solvent peak was very close to signal of imine $\mathbf{I_6}$ and even slightly overlapped. Another issue was that the benzaldehyde $\mathbf{A_4}$ had a smaller retention time than the solvent peak and an atypical shape which is most likely due to the low polarity of the column, *i.e.* mismatching polarities of the aldehyde and the stationary phase of the column.

Assuming the observed exchange follows second order reaction kinetics, the rate constant of the reaction can determined using the following relations:[62]

$$- d[\mathrm{A}]/dt = k[\mathrm{A}][\mathrm{B}]$$

With [A] = [B] integration results in

$$1/[\mathrm{A}] = 1/[\mathrm{A}]_0 + kt$$

Equation 2.1.

From this, the rate constant for a second order exchange reaction at a respective temperature can be derived from the slope of the plot of 1/[A] vs time. The inverse concentrations of both reactants at low conversion as a function of time are plotted in Figure 2.6.

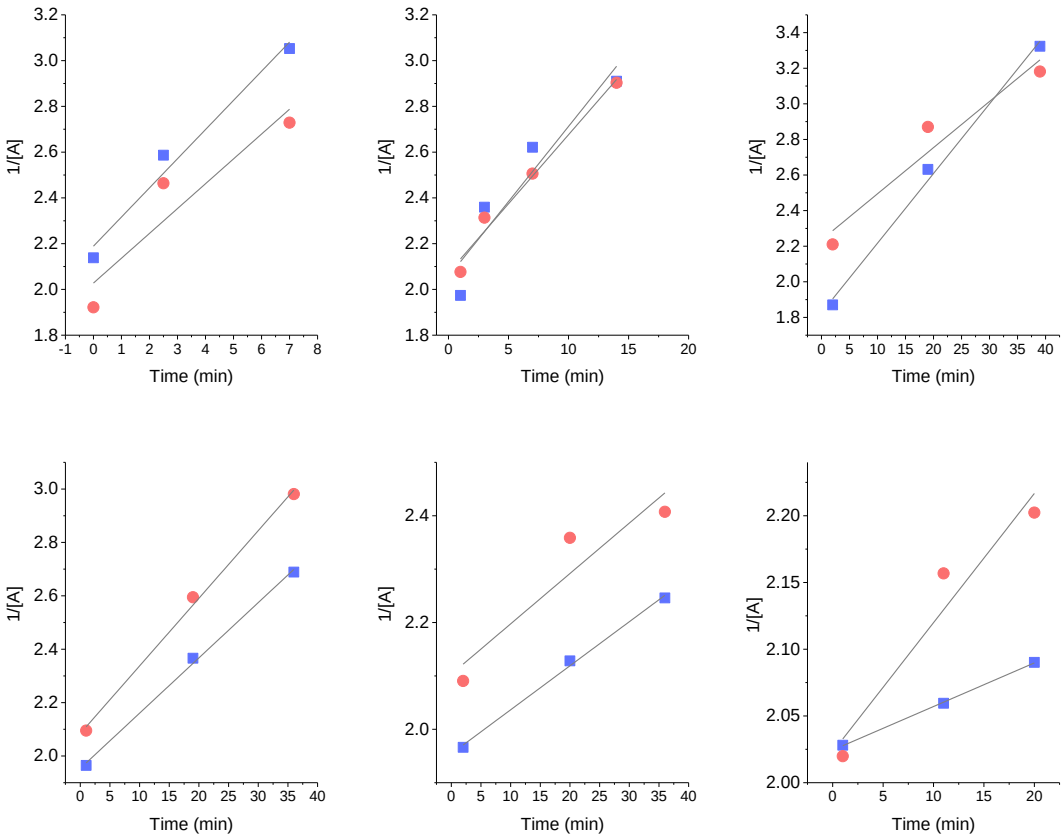

Figure 2.6. Kinetic plots to estimate the rate constants of the exchange of imine $\mathbf{I_5}$ with aldehyde $\mathbf{A_1}$ in TCB (red dots A1, blue squares: I5, from top left to bottom right: 177 °C, 150 °C, 125 °C, 100 °C, 75 °C, 50 °C).

The activation energy can be estimated by plotting the (average) logarithmic rate constants in dependence of the inverse temperature. Compared to transesterification (88 kJ/mol), the obtained activation energy of 28.2 kJ/mol is rather low (Figure 2.7).[64] To verify these results and address the above mentioned problems, *e.g.* broad and overlapping solvent peak, polarity issues, another series of exchanges was performed in toluene, using the more polar Waxplus column during GC analysis.

Assuming Arrhenius behavior:[62]

$$k = A \times \exp(-Ea/RT)$$

Equation 2.2

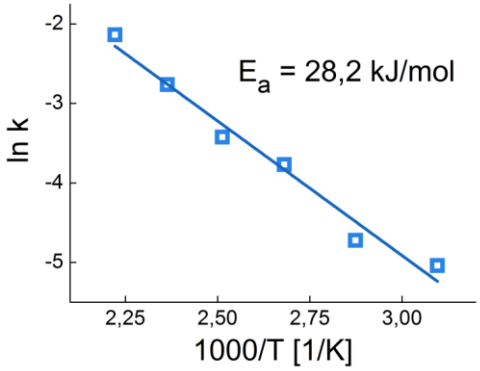

Figure 2.7. Activation energy of the exchange of imine $\mathbf{I_5}$ with aldehyde $\mathbf{A_1}$ in TCB.

2.3.2.2 Exchanges in toluene under air

Additionally to the external calibration (Figure 2.8), an internal calibration was done using dried tetradecane (over molecular sieves for 3 days in 30 vol%, *ca.* 0.3 mL/100 mL anhydrous toluene) as an inert internal standard (signal with smallest retention time in all spectra expect solvent peak).

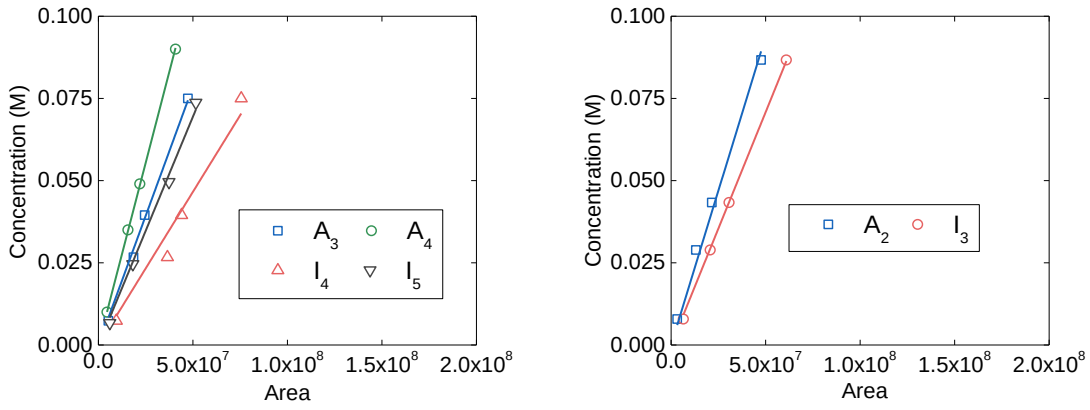

Figure 2.8. GC external calibration curves of imines ($\mathbf{I_4}$ and $\mathbf{I_5}$) and aldehydes ($\mathbf{A_3}$ and $\mathbf{A_4}$) studied in exchanges reactions in toluene .

The exchange reaction between $\mathbf{I_5}$ and $\mathbf{A_3}$ was studied in two different stoichiometric ratios (Figure 2.9). For the reaction in 5/1 ratio, at short reactions times the back reaction can be neglected and hence the reactions rate constants can be measured more precisely. Toluene solutions (over molecular sieves) of the imine (5.0 or 1.0 eq.) and the aldehyde (1.0 eq.) were mixed in preheated septum-closed glass vials (1.5 mL) under air (total initial concentration of compounds = 100 mM). The vial was then kept at the respective reaction temperature and samples were drawn by micro syringe and directly injected in the GC machine. Four

experiments with equimolar ratio (100 °C, 75 °C, 45 °C, 20 °C) and four with a five-fold excess of $\mathbf{I_5}$ were performed (100 °C, 75 °C, 50 °C, 25 °C) (Figure 2.9).

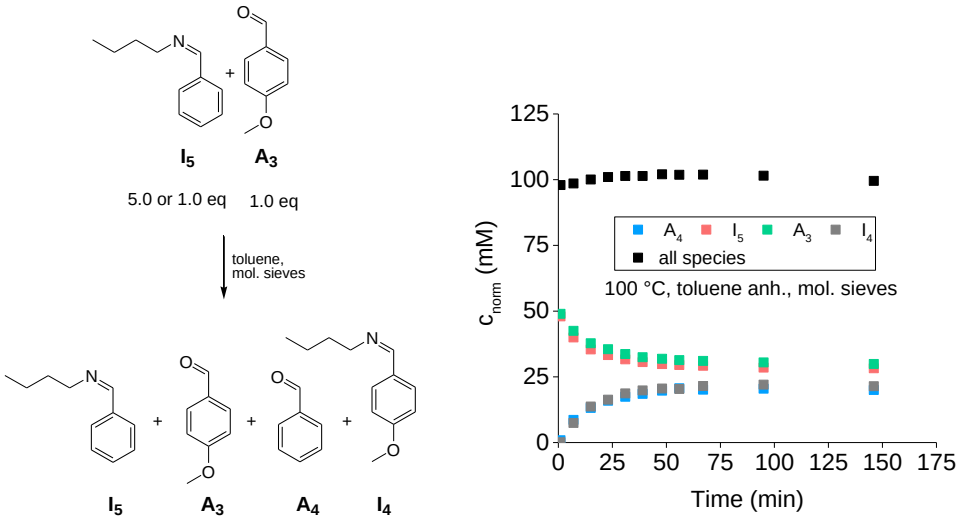

Figure 2.9. Left side: Exchange of imine $\mathbf{I_5}$ with aldehyde $\mathbf{A_3}$ in toluene over molecular sieves under air. Right side: Kinetic plot normalized to the internal standard tetradecane.

In Figure 2.9 is presented the stoichiometric reaction at 100 °C. From to the internal standard tetradecane normalized concentrations of exchanging species, it can be concluded that under these conditions no degradation can be detected via GC. For all four experiments the equilibrium distribution was not stoichiometric. Instead, the reactants show ca 5% of over expression. As by the here presented method no degradation of species could be observed, a possible explanation might be different thermodynamic stabilities and/or artifacts from the sampling method (insufficient column restitution during experiment - calibration issues). It is known that methoxy groups in *para*-position might exhibit mesomeric effects resulting in a thermodynamically more stable A_3. The reaction reaches its equilibrium after less than 100 min at 100 °C and more than 900 min at 20 °C (Figure 2.10).

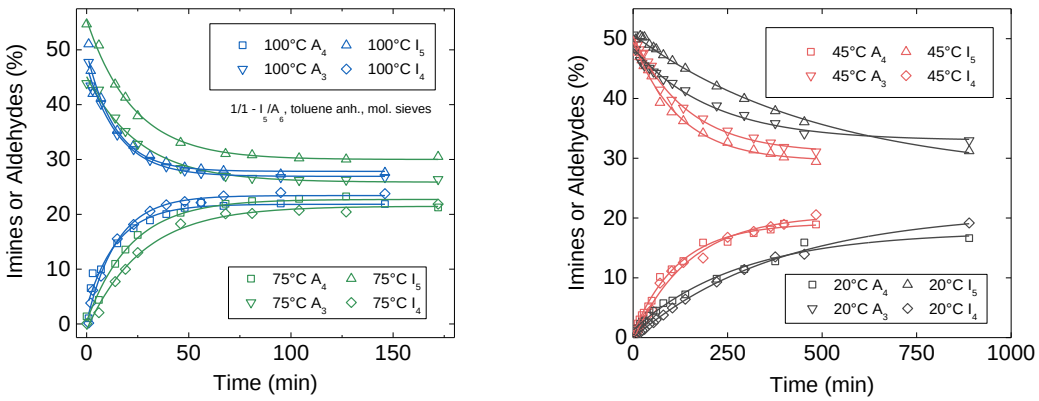

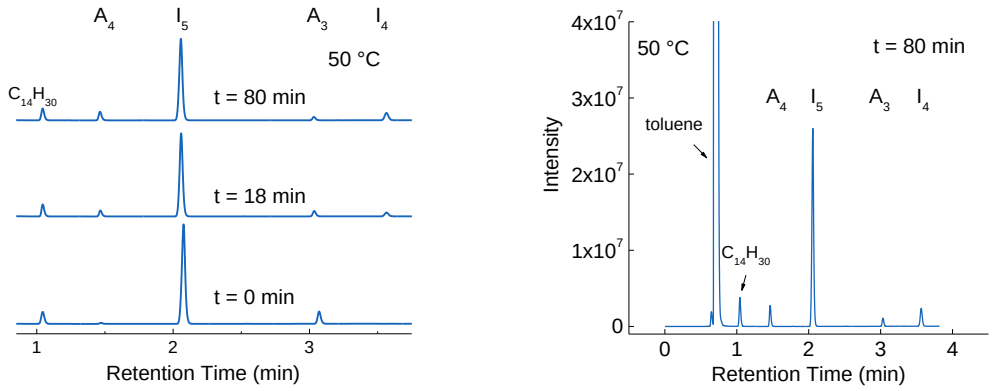

Figure 2.10. Top row: Kinetic plots of the exchange reaction between imine $\mathbf{I_5}$ and aldehyde $\mathbf{A_3}$ in toluene at different temperatures using a stoichiometric ratio of imine $\mathbf{I_5}$ and aldehyde $\mathbf{A_3}$. Bottom row: GC raw data of the exchange with a ratio of 5/1 between imine $\mathbf{I_5}$ and aldehyde $\mathbf{A_3}$.

Another method to study the exchange between the here presented species is to generate mixtures in uneven ratios (5/1 - $\mathbf{I_5/A_3}$, Figures 2.10, 2.11 and 2.12). This way, the back reaction can be neglected at short reaction times (low conversion) and the activation energy can be obtained from the measured rate constants (as above for the reactions in TCB).

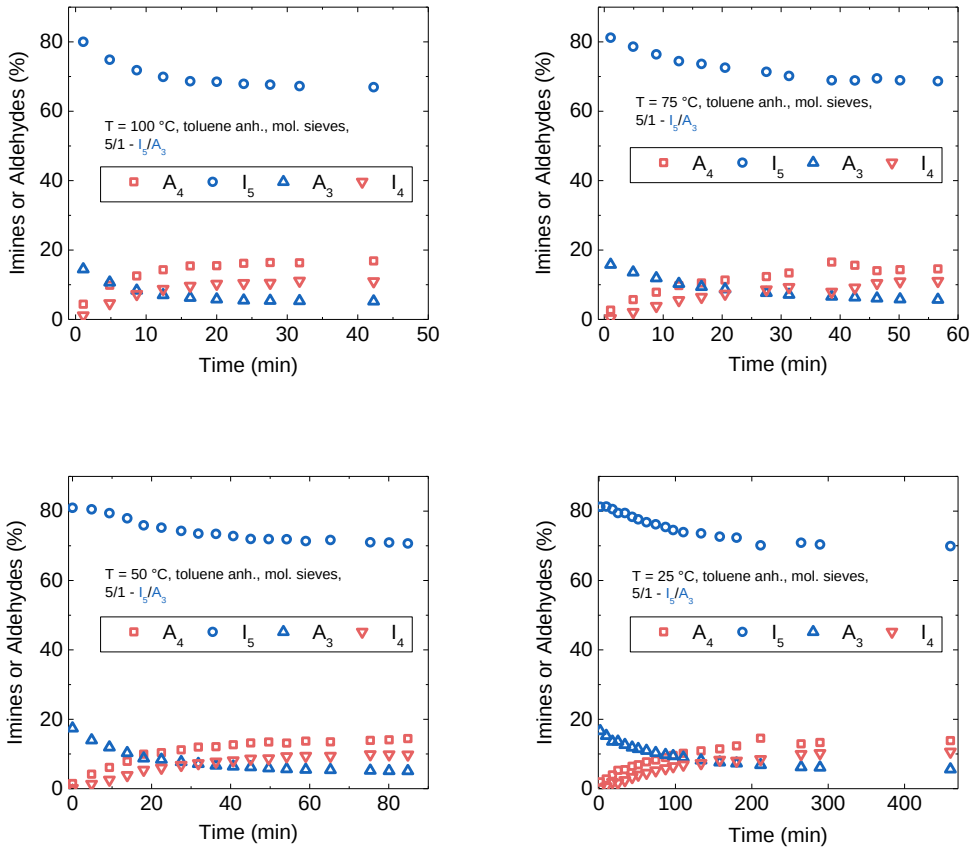

Figure 2.11. Kinetic plots of the exchange reaction between imine $\mathbf{I_5}$ and aldehyde $\mathbf{A_3}$ in toluene at different temperatures with a ratio 5/1 between imine $\mathbf{I_5}$ and aldehyde $\mathbf{A_3}$.

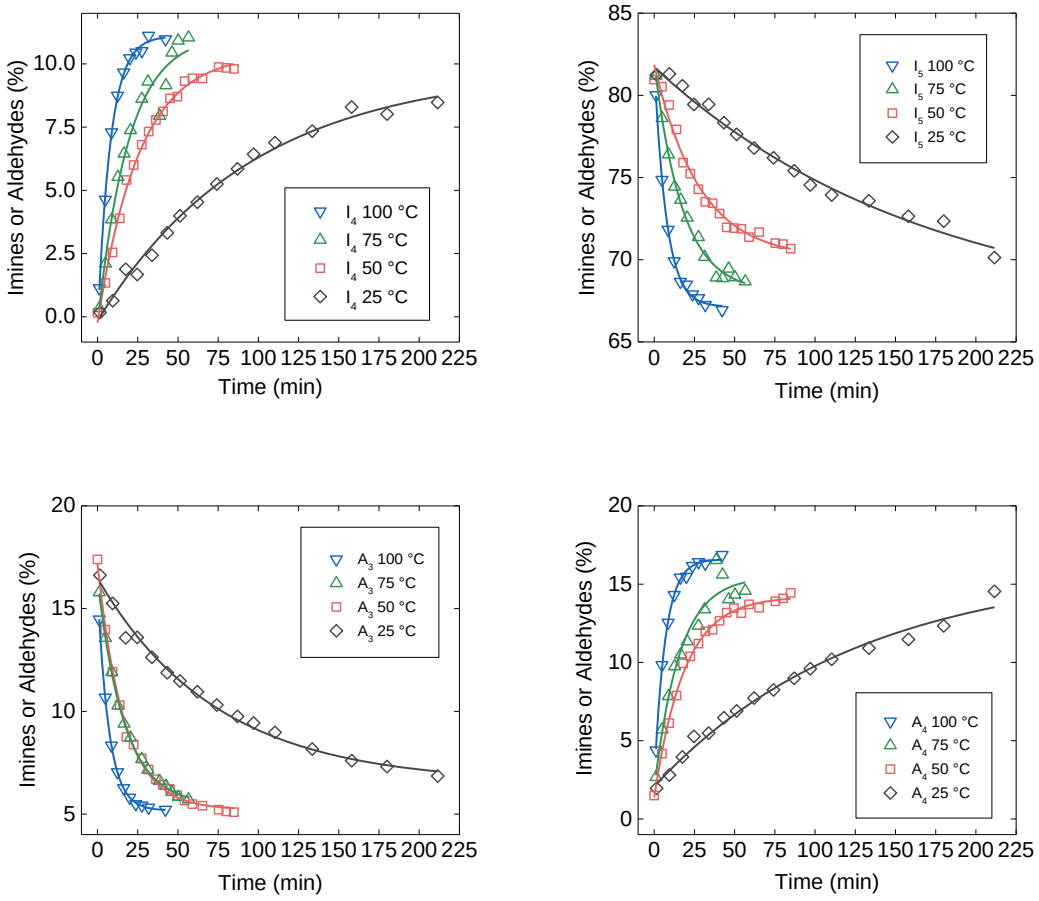

Figure 2.12. Kinetic plots of the exchange reaction between imine $\mathbf{I_5}$ and aldehyde $\mathbf{A_3}$ in toluene at different temperatures under air.

An activation energy of 33.3 kJ/mol was found (Figure 2.13), which is not significantly different from the activation energy of the exchange reaction of similar species in TCB (similar polarity, E_a = 28.2 kJ/mol).[63] Although a decrease in temperature slowed down the overall exchange, $\mathbf{A_3}$ was observed to be consumed with the same rate at 50 and 75 °C which might be due to above discussed insufficient column reconstitution. Compared to other dynamic exchange reactions, *e.g.* transesterification (88 kJ/mol),[64] the found activation energy (33.3 kJ/mol in toluene) of imine-aldehyde exchange reaction is quite low . In addition, the reaction does not necessitate catalyst, thus demonstrating a high potential for implementation not only in dynamic materials but also in molecular dynamics, *e.g.* screening techniques via library formation.

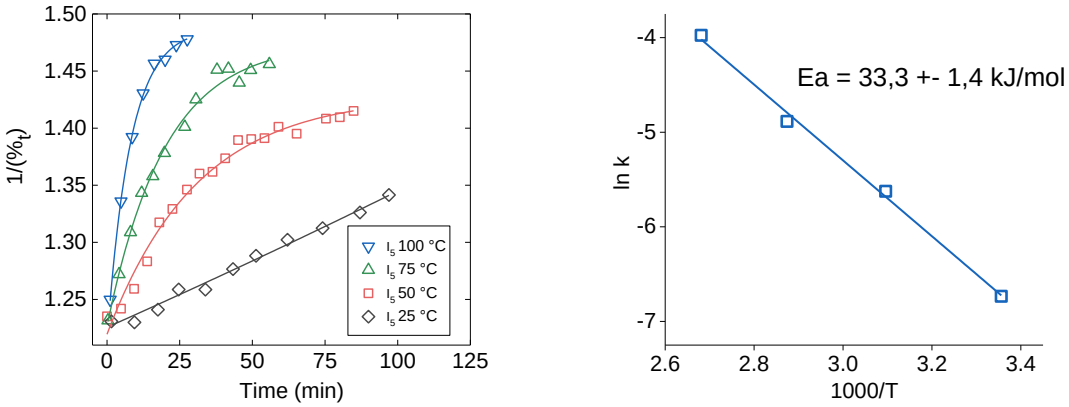

Figure 2.13. Left side: Kinetic plots to determine the rate constant of the exchange of imine **I$_5$** and aldehyde **A$_3$** in toluene under air. Right side: Activation energy of the exchange in toluene under air.

To check whether with other aldehydes of interest, *e.g.* terpenoid-like species, exchanges can be observed too, the reaction between imine **I$_5$** and aldehyde **A$_2$** was studied at 100 °C following the method described above with a five-fold excess of the imine (Figure 2.14).

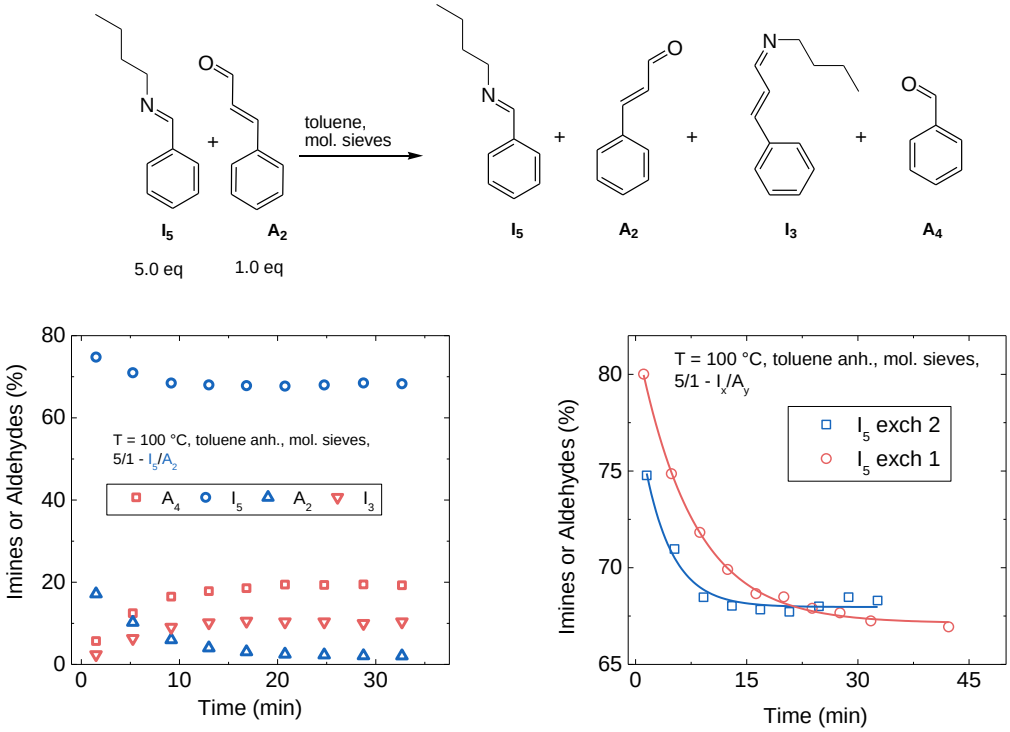

Figure 2.14. Top and bottom left: Imine-aldehyde (terpenoid-like) exchange and kinetic plot of in toluene under air. Bottom right: Comparison of the two exchanges in toluene under air in a ratio 5/1.

The exchange in figure 2.14 was slightly accelerated compared to the exchange in figure 2.9. Lower sterical hindrance of the $\mathbf{A_2}$ (alkene) compared to $\mathbf{A_3}$ (aromatic ring) and thus an increase in accessibility of the exchanging aldehyde functionality could be one of the reasons. However, the fact that $\mathbf{I_3}$ was generated in smaller quantity than the other product $\mathbf{A_4}$, likely indicates a degradation of the imine $\mathbf{I_5}$ and/or the corresponding aldehyde $\mathbf{A_2}$. Indeed, the molar % of $\mathbf{A_2}$ seems to approach 0 at longer experimental times, which is in agreement with reported observations that structurally similar terpenes can be rather instable even at room temperature.[65]

2.3.3 Kinetic studies followed by gas chromatography under argon

The obtained results seem to indicate that the exchange reactions between imines and aldehydes can be highly influenced by traces of water (humidity) or amines (from the synthesis). To further minimize contamination, we performed the exchange between two imines and between an imine and an aldehyde in bulk under protective atmosphere (dry argon) in oven-dried and purged Schlenk flasks. Compounds were synthesized and purified as described above, stored under argon and tested in high concentration (1.3 M) in ^{1}H-NMR to determine the exact amount of water, free amine and free aldehyde species (Scheme 2.6 and Figure 2.15). The dissociation constant K_{diss} of imine $\mathbf{I_5}$ was determined by adding a five-fold excess of water to its 25 mM THF-d_8 solution. The ^{1}H-NMR spectra after 2 h and 38 h of mixing at room temperature showed that only a very small amount of imines hydrolyzed under these conditions (Figure 2.16). Assuming a similar aldehyde and amine concentration and the thermodynamic dissociation constant was estimated according to equation 2.3 to be as small as 1.76×10^{-4} (Equation 2.3).

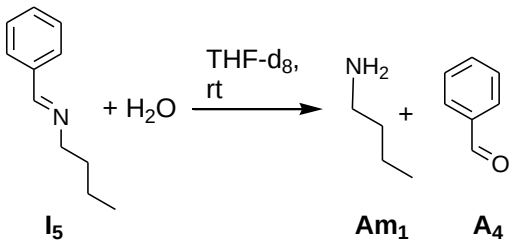

Scheme 2.6. Hydrolysis of imine $\mathbf{I_5}$ (25 mM) in THF-d_8 at room temperature.

$$K_{\text{diss}} = \frac{[amine][aldehyde]}{[imine][H2O]} = \frac{[0.4175][0.4175]}{[24.5821][124.5825]} = 1.76 \cdot 10^{-4}$$

Equation 2.3

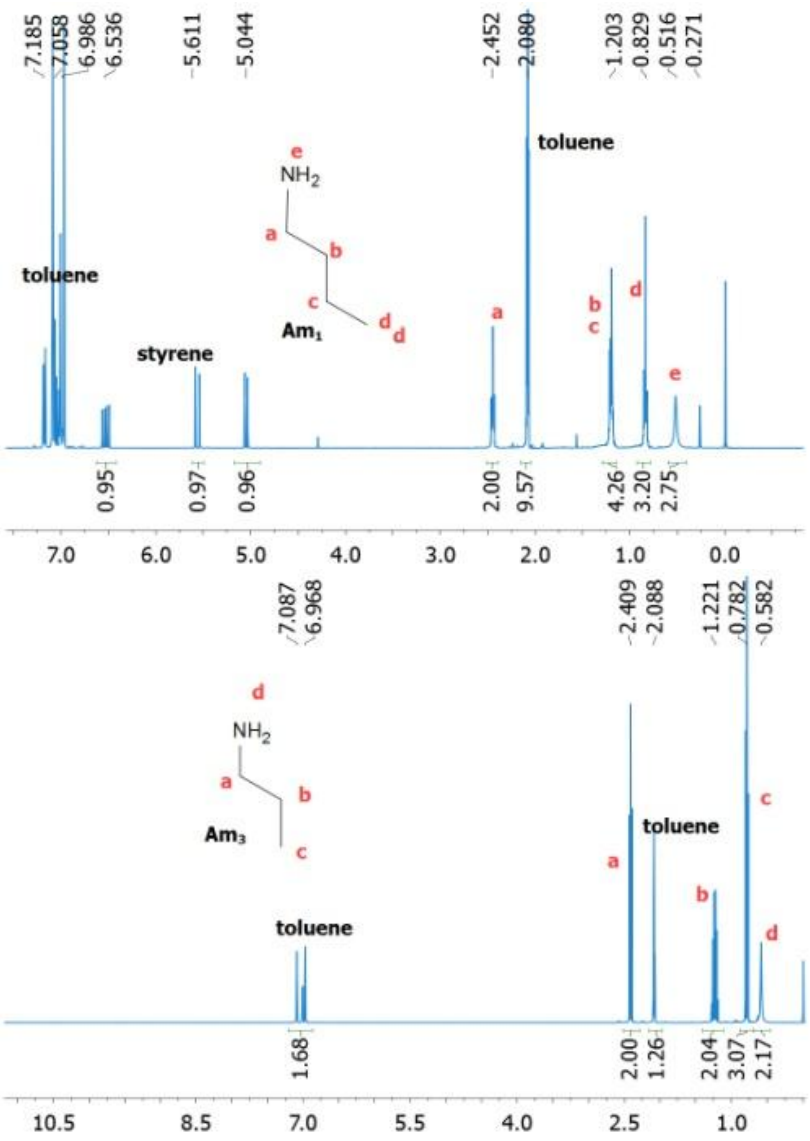

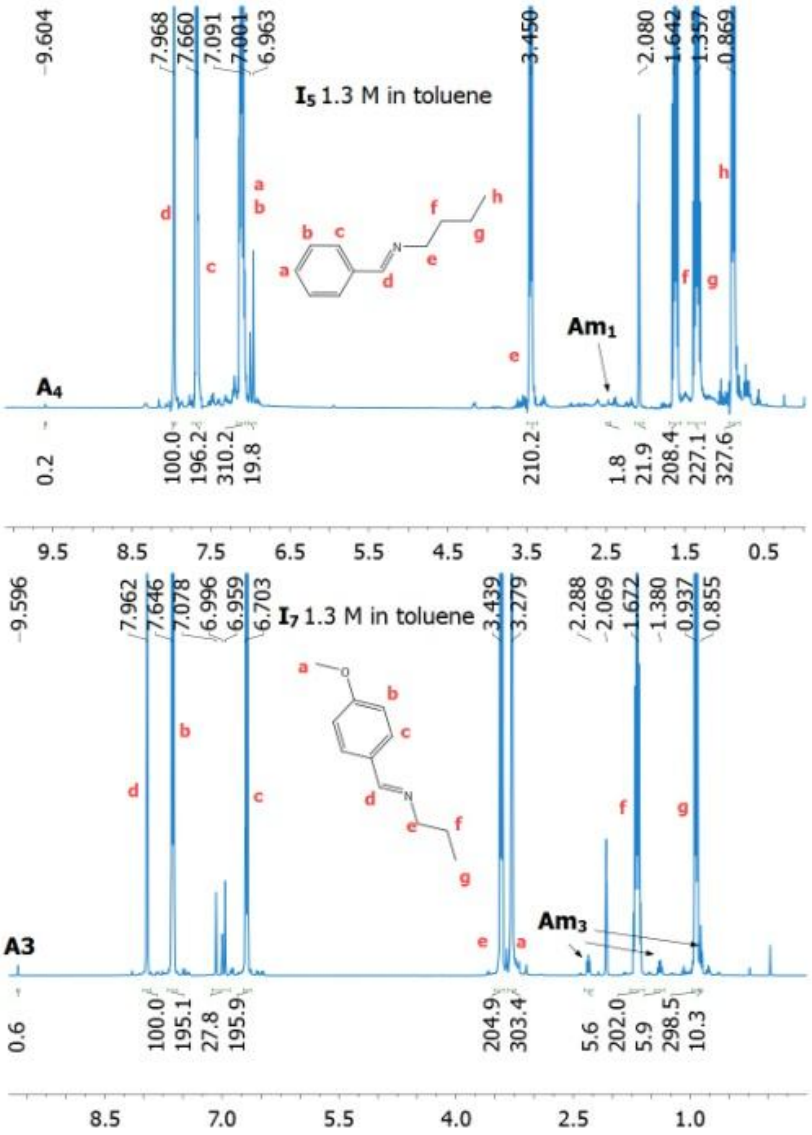

Figure 2.15. ^{1}H-NMR spectra of free amines and highly concentrated imines in toluene-d_8 (1.3 M) under argon. From top left clockwise: *n*-butylamine, *n*-propylamine, imine $\mathbf{I_7}$ (1.3 M) and imine $\mathbf{I_5}$ (1.3 M).

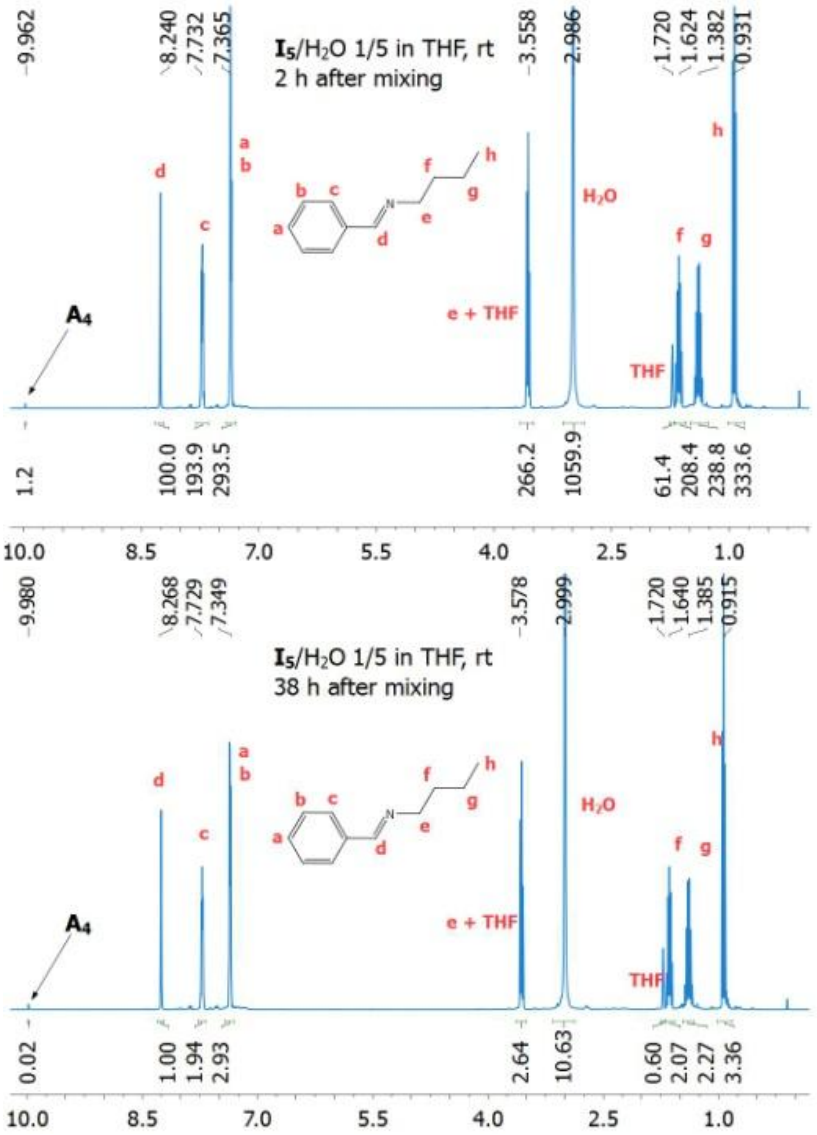

Figure 2.16. ^{1}H-NMR spectra of imine **I$_5$** in the presence of a five-fold excess of water in toluene-d$_8$ at room temperature. Left side: at 2 h after mixing. Right side: at 38 h after mixing.

By comparison of the ^{1}H-NMR spectra of the free amines and corresponding imines, we determined the free amine and aldehyde content to be <1 mol% (butylamine and aldehyde **A$_4$**) for **I$_5$** and <3 mol% (propylamine) and <1 mol% (aldehyde **A$_3$**) for **I$_7$**. The aldehyde **A$_3$** was treated as the imines and no water was detected in its ^{1}H-NMR spectrum. These compounds were used to perform exchange reactions in bulk under argon atmosphere according to the following procedure (Scheme 2.7). To an oven dried and argon purged Schlenk flask was added via an oven dried and argon purged syringe **I$_5$** (320 mg, 1.98 mM). Then, the dried tetradecane was added (1 eq.) and the Schlenk flask was heated to 60 °C. The other imine **I$_7$** was added (361 mg, 1.98 mM), which corresponds to t=0. Samples were taken with cleaned and oven-dried argon purged needles and samples were diluted in dried toluene. From this solution, 1 μL was injected into the GC apparatus. The exchange reaction in the mixture of **I$_5$**

and **A$_3$** was performed via the same method (Scheme 2.8). ^{1}H-NMR spectra were taken at the first point of measurements and at equilibrium to check whether any kind of imine degradation, *e.g.* hydrolysis took place during reaction. The time elapsed between sample collection and ^{1}H-NMR measurement was *ca.* 6 hours.

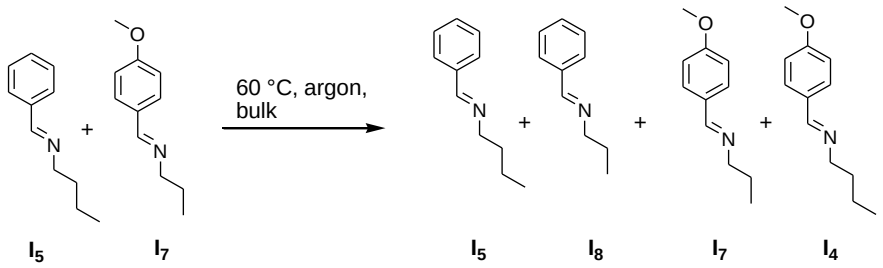

Scheme 2.7. Bulk reaction of imines **I$_5$** and **I$_7$** at 60 °C under protective atmosphere.

In both experiments, water could be detected neither at the beginning nor at the end of the reaction. The experimental data are shown in Figures 2.17 and 2.18 and for each reaction the tetradecane normalized data as well as the ratio (%) of exchanging species are presented. Assuming an initial bulk concentration of 5 M, the total amount of species did not decrease. However, as observed in other kinetic studies, the data are somewhat scattered which is most probably due to the analytical method. The exchange reaction in the mixture of the two imines (Scheme 2.7) was at equilibrium in less than 10 minutes and the composition at equilibrium was almost stoichiometric (Figure 2.17). In the initial mixture the signal of one aldehyde at 9.61 ppm could be detected in the expected small amount of ca 0.4 mol% as present in the starting compounds. At reaction equilibrium, another aldehyde peak at 9.58 ppm appeared. The relative integration value for both aldehydes was unchanged (0.4 mol%) compared to the initial value. The same holds for the free amine signals (1.3-1.6 mol%) proving thus the absence of hydrolysis via contamination from external sources.

However, the present traces of amines and aldehydes could form (undetectable) traces of water by imine formation. Nevertheless, the speed of equilibration was remarkably fast taking into account the very small amount of potentially reaction driving molecules such as free amines and the absence of hydrolysis through external processes. This result could further indicate that free aldehyde can act as very efficient catalyst of imine-imine exchange reaction and/or that the reaction is not a second order reaction in regards to imines.

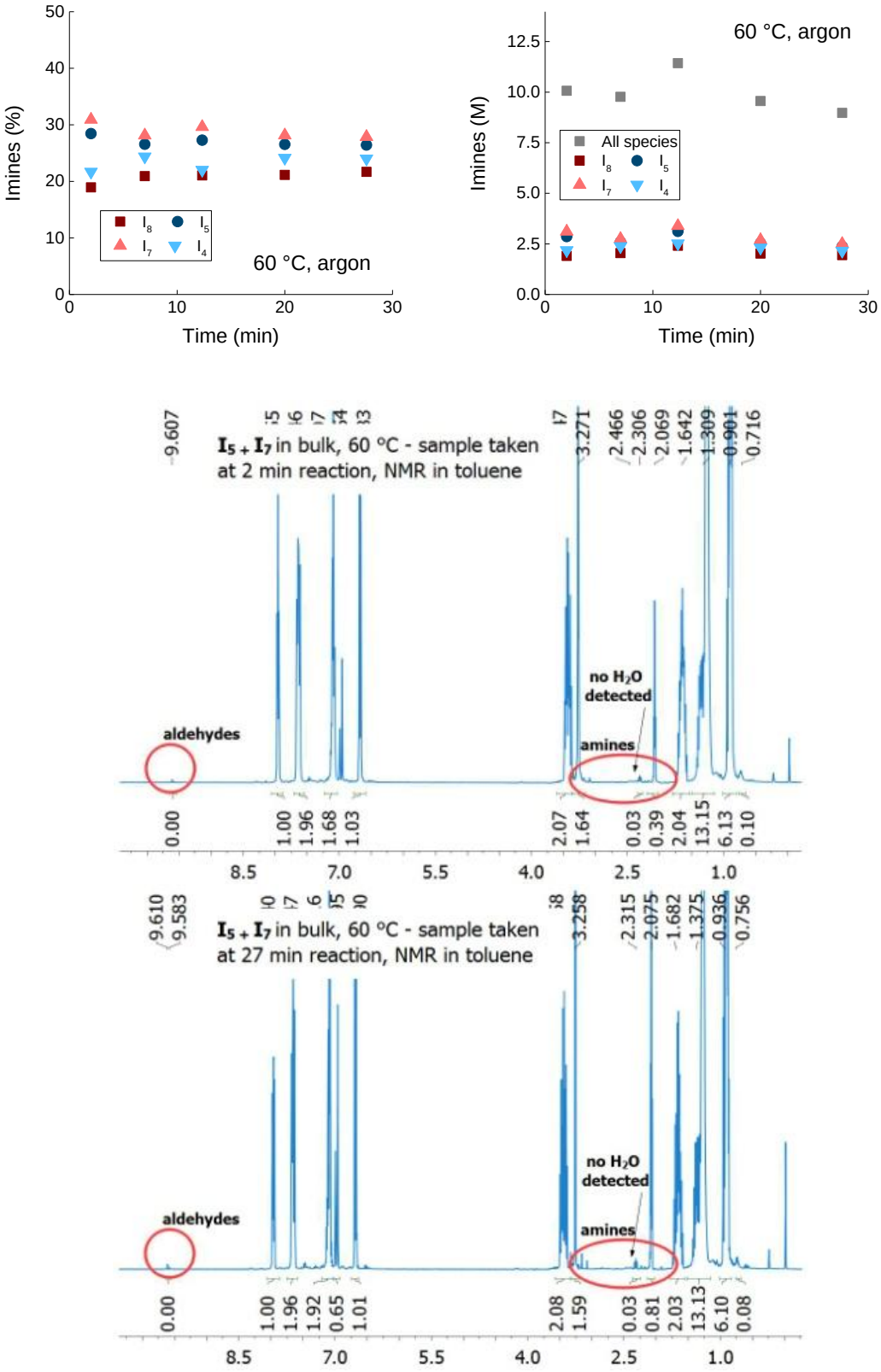

Figure 2.17. Kinetic plot in % and normalized to the internal standard tetradecane of the bulk reaction of imines $\mathbf{I_5}$ and $\mathbf{I_7}$ at 60 °C under protective atmosphere. ^{1}H-NMR spectra in toluene-d_8 of the mixture after addition of all species and after reaching equilibrium (27 min).

A similar experiment with imine **I$_5$** and an aldehyde **A$_3$** proceeded slower and reached its equilibrium state after more than 125 minutes (Scheme 2.8 and Figure 2.18). The total quantity of species was constant as for the imine-imine mixture, but as for the exchanges in TCB and in toluene it seems as if the composition at equilibrium is not stoichiometric. Indeed, as mentioned the mesomeric effect of the methoxy group in *para*-position might result in a higher stability of **A$_3$** compared to **A$_4$**. The same trend was confirmed in the ^{1}H-NMR analysis with an uneven (>1) ratio imine/aldehyde and the under-expression of benzaldehyde **A$_3$**.

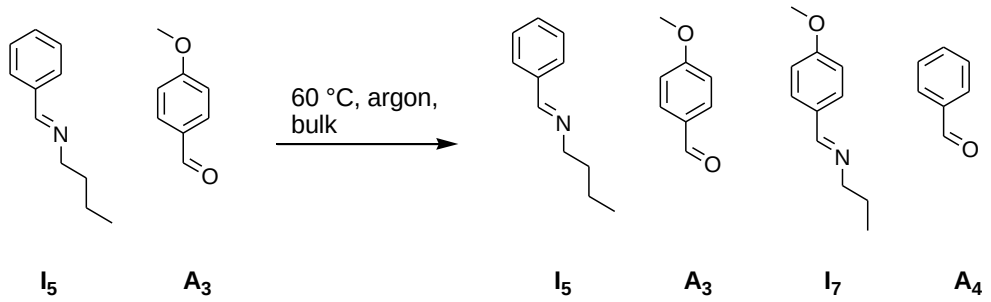

Scheme 2.8. Bulk reaction of imine **I$_5$** and aldehyde **A$_3$** at 60 °C under protective atmosphere.

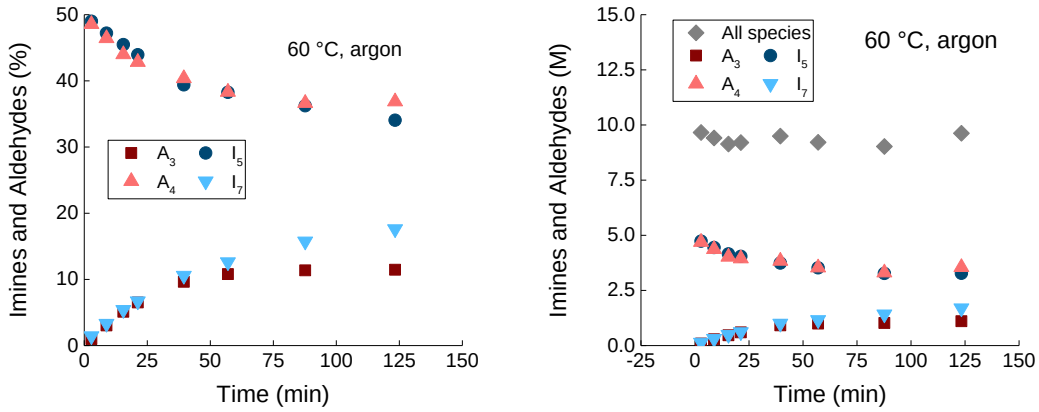

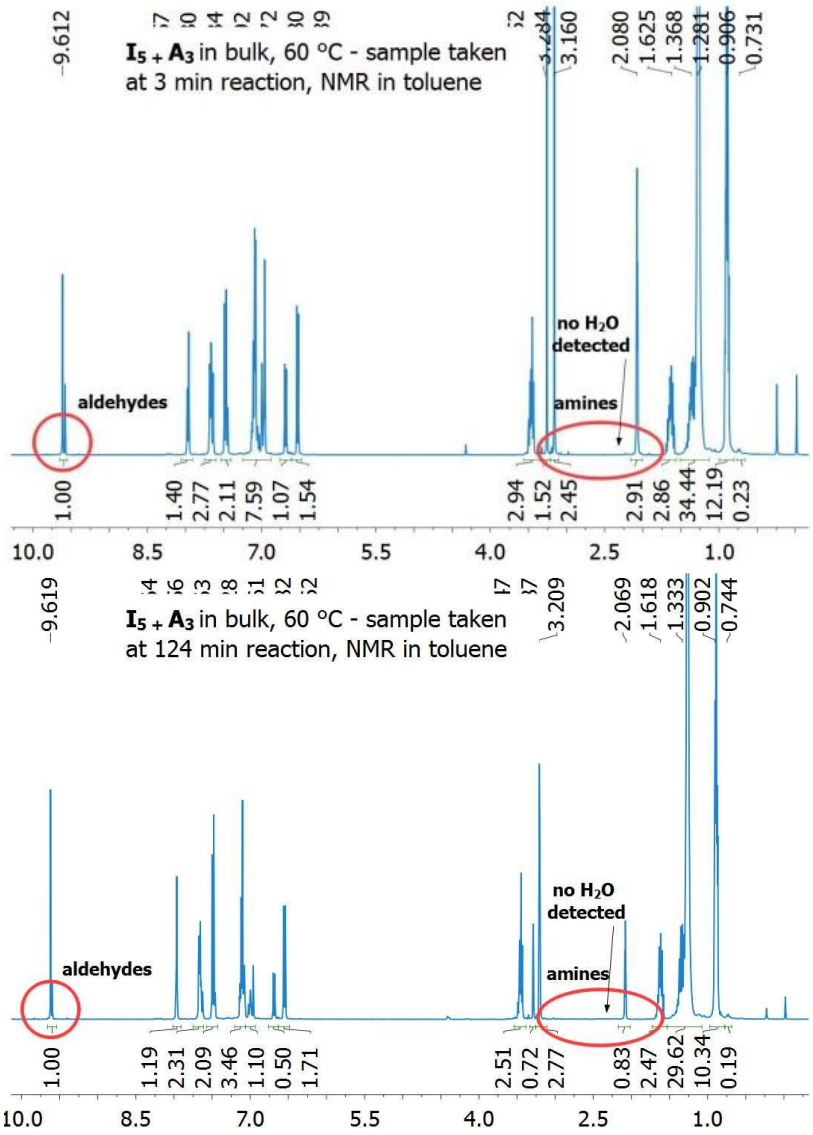

Figure 2.18. Kinetic plot in % and normalized to the internal standard tetradecane for the bulk reaction of imine $\mathbf{I_5}$ and aldehyde $\mathbf{A_3}$ at 60 °C under protective atmosphere. ^{1}H-NMR spectra in toluene-d_8 of the mixture after addition of all species and after reaching equilibrium (125 min).

2.4 Conclusion

In this chapter were presented the synthesis, purification and characterization of imines and aldehydes with the intention to study known transimination and imine metathesis exchange reactions as well as not reported imine-aldehyde exchange reaction. The degree of dissociation of an imine in the presence of an excess of water was estimated in THF and a rather small dissociation constant of 1.76×10^{-4} was obtained. Kinetic studies of mixtures of imines and imines/aldehydes were performed using ^{1}H-NMR spectroscopy and GC analysis. Exchange reactions were tested at different temperatures in the absence and in the presence of

other purposely added molecules, such as amines and aldehydes. Anhydrous solvents were dried over molecular sieves and in some experiments (toluene) molecular sieve was used during reaction to minimize the impact of possible water traces. Despite precautions, some degradation was observed in the first series of experiments using non-invasive ^{1}H-NMR spectroscopy in closed systems. Other difficulties were identified during GC analysis, *i.e.* an insufficient interaction between some compounds and the stationary phase of the GC column or the impossibility with some solvents to detect small quantities of hydrolyzed species. Eventually, an experimental set-up allowed us to perform experiments under protective (dry argon) atmosphere in bulk. Highly concentrated ^{1}H-NMRs analyses of imines and aldehydes allowed precise quantification of remaining traces of amines and aldehydes in the synthesized compounds. Comparison of ^{1}H-NMR spectra from the beginning and the end of the tested imine-imine and imine-aldehyde exchange reactions showed the absence of degradation or hydrolysis under these conditions. The exchange reaction between two imines resulted in very fast equilibration (<10 min at 60 °C) with stoichiometric distribution of the four imines. Such fast equilibration time was not anticipated for pure imines and potentially reflects the ability of aromatic aldehyde (present at traces level from the synthesis) to effectively catalyze imine-imine exchange, as indicated by other model reactions conducted. The same experiment with an imine and an aldehyde resulted in a non-stochiometric mixture in reasonbable reaction time (*ca.* 150 min), which might be explained by stability differences of aldehydes and corresponding imines. To refer the obtained results to the in literature reported imine metathesis and to fully understand the underlying mechanisms of the to our knowledge un-reported imine-aldehyde exchange, more work must be done both synthetically and analytically. Synthesis and purification of highly pure starting compounds must be achieved and GC monitoring adapted to the speed of exchange. Despite the mentioned difficulties in analysis and the necessity to precisely identify the different ways of action of traces of aldehydes and imines, it was shown that exchanges take place when rather pure imines are mixed with each other or with pure aldehydes. Especially, the fast exchanges (imine-imine catalyzed by aldehydes and imine-aldehyde) of molecules in bulk are promising in regard of their implementation into polymeric networks with the overall aim to generate vitrimers.

2.5 References

1. R. W. Layer, *Chem. Rev*., **1963**, 489.
2. H. Schiff, *Ann. Chem*., **1864**, *131*, 118.
3. P. A. Brady, R. P. Bonar-Law, S. J. Rowan, C. J. Suckling and J. K. M. Sanders, *Chem. Commun.*, **1996**, 319.
4. L. M. Greig and D. Philp, *Chem. Soc. Rev.*, **2001**, *30*, 287.
5. J.-M. Lehn, *Chem.–Eur. J.*, **1999**, *5*, 2455.
6. J. K. M. Sanders, *Pure Appl. Chem.*, **2000**, 2265.
7. R. L. E. Furlan, S. Otto and J. K. M. Sanders, *Proc. Natl. Acad. Sci.* U. S. A., **2002**, *99*, 4801.
8. S. J. Rowan, S. J. Cantrill, G. R. L. Cousins, J. K. M. Sanders and J. F. Stoddart, Angew. *Chem., Int. Ed*., **2002**, *41*, 898.
9. J.-M. Lehn, *Chem. Soc. Rev*., **2007**, *36*, 151.
10. Lehn, J.-M. *Prog. Polym. Sci*. **2005**, *30*, 814.
11. J.-M. Lehn, *Aust. J. Chem*. **2010**, *63*, 611.
12. T. Aida, E. W. Maije and S. I. Stupp, *Science* **2012**, *335*, 813.
13. S. J. Rowan, S. J. Cantrill, G. R. L. Cousins, J. K. M. Sanders and J. F. Stoddart, *Angew. Chem., Int. Ed*. **2002**, *41*, 898.
14. M. Belowich and J. F. Stoddart, *Chem. Soc. Rev*. **2012**, *41*, 2003.
15. R. A. R. Hunt and S. Otto, *Chem. Commun*. **2011**, *47*, 847.
16. J.-M. Lehn, *Chem.-Eur. J*. **1999**, *5*, 2455.
17. R.D. Patil and S. Adimaurthy, *Asian J. Org. Chem*. **2013**, *2*, 726.
18. L. Ravishankar, S. A. Patwe, N. Gosarani and A. Roy, *Synth.Commun*. **2010**, *40*, 3177.
19. A. Mobinikhaledi, P. J. Steel and M. Polson, *Synth. React. Inorg. Met*. **2009**, *39*, 189.
20. R. Dalpozzo, A. D. Nino, M. Nardi, B. Russo and A. Procopio, *Synthesis* **2006**, 1127.
21. H. Naeimi, F. Salimi and K. Rabiei, *J. Mol. Catal. A* **2006**, *260*, 100.
22. H. Naeimi, H. Shargi, F. Salimi and K. Rabiei, *Heteroat. Chem.* **2008**, *19*, 43.
23. M. Gopalakrishnan, P. Sureshkumar, V. Kanagarjan, J. Thanusu and R. Govindaraju, *J. Chem. Res*. **2005**, 299.
24. A. K. Chakraborti, S. Bhagat and S. Rudrawar, *Tetrahedron Lett*. **2004**, *45*, 7641.
25. J. Bennett, K. Meldi and C. Kimmell II., *J. Chem. Educ*. **2006**, *83*,1221.
26. A. Fujishima and K. Honda, *Nature* **1972**, *238*, 37.

27. X. Lang, W. Ma, Y. Zhao, C. Chen, H. Ji and J. Zhao, *Chem. Eur. J*. **2012**, *18*, 2624.
28. M. Largeron and M. B. Fleury, *J. Org. Chem*. **2000**, *65*, 8874.
29. M. Largeron, A. Chiaroni and M. B. Fleury, *Chem. Eur. J*. **2008**, *14*, 996.
30. M. Higuchi, I. Ikeda and T. Hirao, *J. Org. Chem*. **1997**, *62*, 1072.
31. K. C. Nicolaou, C. J. N. Mathison and T. Montagnon, *J. Am. Chem. Soc*. **2004**, *126*, 5192.
32. H. Schiff, *Annals* **1864**, *131*, 118.
33. Y. Xin and J. Yuan, *Polym. Chem*., **2012**, *3*, 3045.
34. A. K. Engel, T. Yoden, K. Sanui and N. Ogata, *J. Am. Chem. Soc*., **1985**, *107*, 8308.
35. 3 J. R. Anacona, V. E. Marquez and Y. Jimenez, *J. Coord. Chem*., **2009**, *62*, 1172.
36. L. Zhou, J. Yuan, W. Yuan, X. Sui, S. Wu, Z. Li and D. Shen, *J. Magn. Mater.*, **2009**, *321*, 2799.
37. J. B. Culbertson and L. Hines, *Proc. Iowa Acad. Sci*., **1934**, *41*, 172.
38. E. M. Langman, W. Healy and P. K. Dutt, Quart. *J. Indian Chem. Soc.*, **1927**, 175.
39. G. Reddelien and H. Danilof, *Ber*., **1921**, *54B*, 3132.
40. A. V. Willi, and R. E. Robertson, Can. *J. Chem*., **1953**, *31*, 363.
41. M. Ciaccia, R. Cacciapaglia, P. Mencarelli, L. Mandolini and S. Di Stefano, *Chem. Sci*., **2013**, *4*, 2253.
42. N. Giuseppone, J.-L. Schmitt, E. Schwartz and J.-M. Lehn, *J. Am. Chem. Soc*., **2005**, *127*, 5528.
43. G. K. Cantrell and T. Y. Meyer, *J. Am. Chem. Soc*., **1998**, *120*, 8035.
44. G. K. Cantrell and T. Y. Meyer, *Organometallics*, **1997**, *16*, 5381.
45. M. C. Burland, T. W. Pontz and T. Y. Meyer, *Organometallics*, **2002**, *21*, 1933.
46. J. W. Bruno and X. J. Li, *Organometallics*, **2000**, *19*, 4672.
47. R. L. Zuckerman, S. W. Krska and R. G. Bergman, *J. Am. Chem. Soc*., **2000**, *122*, 751.
48. M. C. Burland and T. Y. Meyer, *Inorg. Chem*., **2003**, *42*, 3438.
49. N. Wilhelms, S. Kulchat and J.-M. Lehn, *Helv. Ch. Acta*, **2012**, *95*, 2635.
50. Y. Zhang, L. Tao, S. Li and Y. Wei, *Biomacromolecules*, **2011**, *12*, 2894.
51. K. Osowska and O. S. Miljanic, *J. Am. Chem. Soc*., **2011**, *133*, 724.
52. J. F. Stoddart, *Angew. Chem., Int. Ed*. **2002**, *41*, 898.
53. N. Giuseppone, J.-M. Lehn, *Angew. Chem. Int. Ed* **2006**, *45*, 4619.
54. X. Chen, M. A. Dam, K. Ono, A. K. Mal, H. Shen, S. R. Nutt, K. Sheran and F. Wudl, *Science* **2002**, *295*, 1698.
55. J.-M. Lehn, *Aust. J. Chem*. **2010**, *63*, 611.

56. N. Hafezi and J.-M. Lehn, *J. Am. Chem. Soc*., **2012**, *134*, 12861.
57. Y. Jin, A. Jin, R. McCaffrey, H. Long and W. Zhang, *J. Org. Chem*., **2012**, *77*, 7392.
58. K. Oh, K.-S. Jeong and J. S. Moore, *Nature*, **2001**, *414*, 889.
59. D. E. Whitaker, C. S. Mahon and D. A. Fulton, *Angew. Chem. Int. Ed*., **2013**, *52*, 956.
60. A. W. Jackson, C. Stakes and D. A. Fulton, ***Polym. Chem.***, **2011**, ***2***, 2500.
61. D. Bradley, G. Williams and M. Lawton, *J. Org. Chem*. **2010**, 75, 8351.
62. P. Atkins and J. De Paula, "Physical chemistry", 9th edition, W. H. Freeman, **2009**.
63. P. A. Krieger, "High Purity Solvent Guide", Burdick and Jackson Laboratories, McGaw Park, IL, **1984**.
64. D. Montarnal, M. Capelot, F. Tournilhac, L. Leibler, *Science*, **2011**, *334*, 965.
65. S. A. Batterman, G.-Z. Zhang and M. Baumann, *Atm. Env*., **1998**, *32*, 1647.

Chapter 3

PBMA, PMMA and PS Vitrimers with Pending Aldehydes or Imines

Table of Contents

Chapter 3 – PMMA and PS Vitrimers with Pending Aldehydes or Imines

3.1 Introduction

This chapter describes the generation of vitrimers from monomers such as methyl methacrylate (MMA), n-butyl methacrylate (BMA) or styrene, based on the exchange reactions that can undergo pending aldehydes or imines with bis-imine crosslinkers. A styrene derivative with an aldehyde or imine or functionality was synthesized and used to prepare functional poly(methyl methacrylate), poly (n-butyl methacrylate) and polystyrene via radical polymerization. Two approaches were tested. Vitrimers were either generated from monomers directly, using a polymerizable bis-imine crosslinker or they were crosslinked in solution from synthesized functional thermoplastics. Vitrimers were processed via compression molding, but other techniques such as injection molding and extrusion were also tested. The materials were analyzed for their thermosetting properties (swelling tests, DMA) and thermoplastic properties (processing, rheology, recycling).

3.2 Synthesis of monomers, polymers and vitrimer formation

Chemical compounds: Chemical compounds and solvents were purchased from Sigma Aldrich, TCI Chemicals, Alfa Aesar or Acros. Solvents were used as purchased and dried over new and oven-dried molecular sieves (3 Å).[1] Oven dried glassware was usually used. Commercial monomers were passed over a basic alumina column to remove inhibitors or antioxidants. AIBN was recrystallized from hot methanol.

Gel permeation chromatography (GPC): GPC was performed on a Viscotek GPCmax/VE2001 connected to a Triple detection array (TDA 305) from Malvern. Obtained raw data were treated with the respective standard homopolymer calibration (PMMA or PS) in the presence of toluene which was added as internal standard to check the flow.

More detailed descriptions of the machines and methods used can be found in the respective sections.

Two approaches were tested to generate vitrimers with pending aldehydes and/or imines . We designed functionalized thermoplastics bearing aldehydes or imines pending from the

polymer backbone and performed crosslinking in solution or in extrusion by addition of a bis-imine molecule (Figure 3.1). Another approach consisted in mixing all compounds as monomers in the presence of a polymerizable bis-imine and generate the vitrimers in one-pot during polymerization. Both approaches were tested and the generation as well as the chemical characterization of the networks are described in the following subchapters.

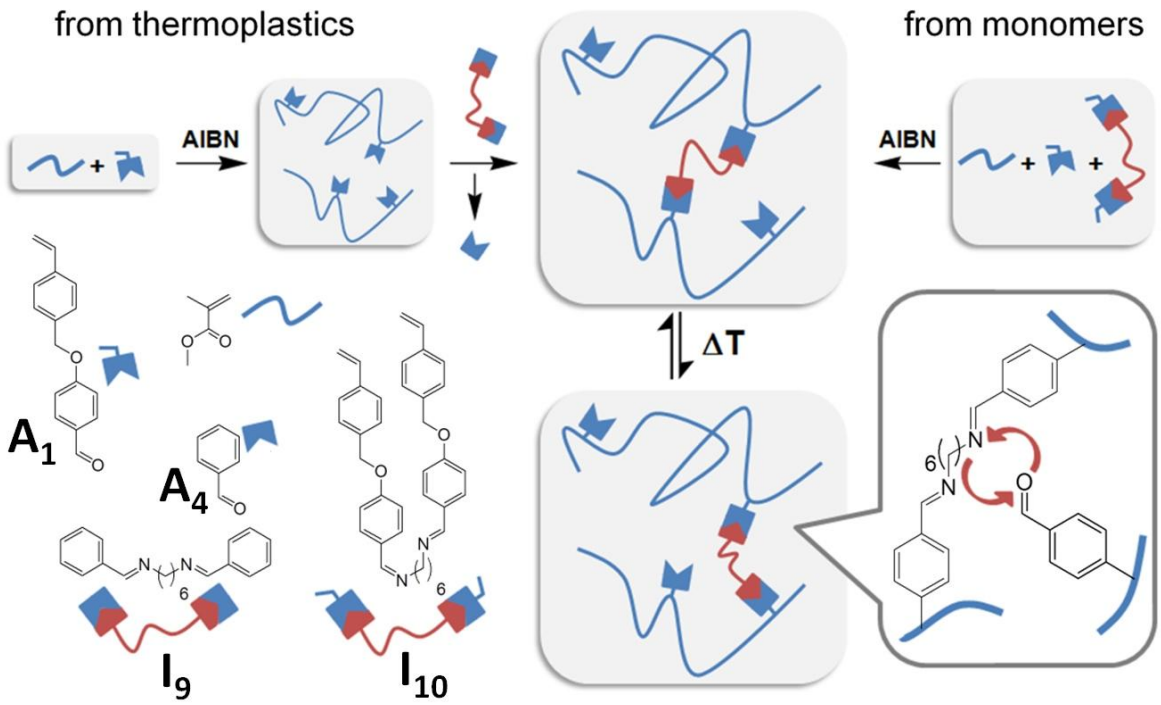

Figure 3.1. Two approaches to generate vitrimers with imine crosslinks and pending aldehydes. Left side: From functionalized thermoplastics. Right side: From monomers. The general concept can be broadened by using other comonomers or pending imines instead of aldehydes.

3.2.1 Monomer and crosslinker synthesis

The syntheses of monomers **A_1** and **I_1** are described in the chapter 2.

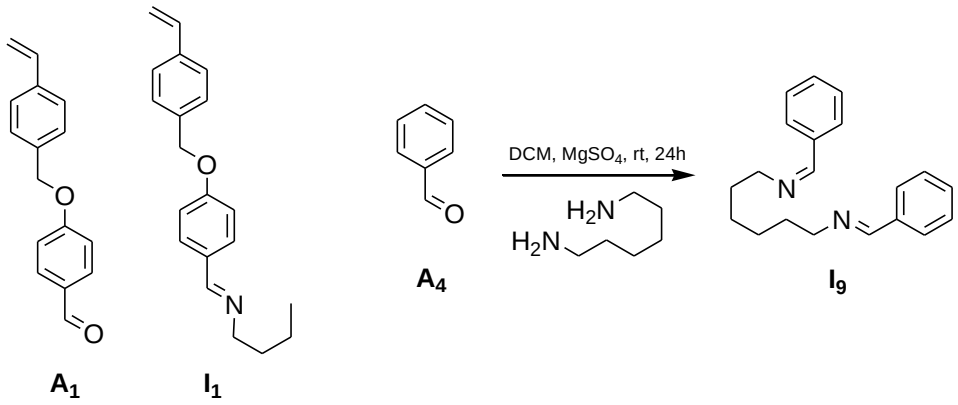

Scheme 3.1. Aldehyde monomer **A_1**and imine monomer **I_1**, and synthesis of bis-imine crosslinker **I_9**.

Synthesis of bis-imine crosslinker **I_9**: Benzaldehyde **A_4** (2.05 eq.) and 1,6-hexanediamine (1 eq.) were mixed in DCM (2 mL per mmol 1,6-hexanediamine) and $MgSO_4$ (3 eq.) was added. The mixture was stirred at room temperature for 24 hours, filtered and concentrated under reduced pressure to obtain a yellow oil (98%, 7 mol% free benzaldehyde).

^{1}H-NMR ($CDCl_3$, 400 MHz): δ 8.26 (s, 1H), 7.72 (m, 2H), 7.38 (m, 3H), 3.63 (t, J = 6.8 Hz, 2H), 1.74 (m, 2H), 1.42 (m, 2H). ^{13}C NMR ($CDCl_3$, 100 MHz): δ161.2, 136.2, 130.4, 128.6, 128.1, 62.0, 30.8, 27.2.

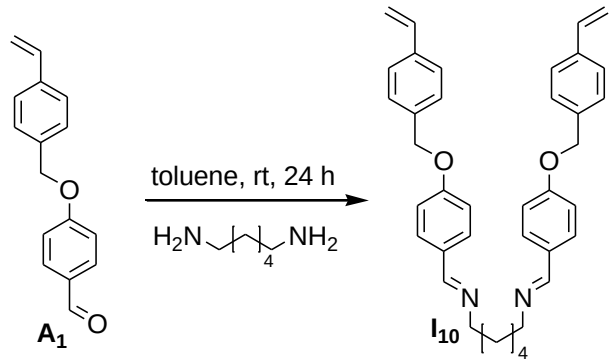

Scheme 3.2. Synthesis of polymerizable bis-imine crosslinker **I_{10}**.

Synthesis of bis-imine crosslinker **I_{10}**: The aldehyde monomer **A_1** (12.3 g, 51.46 mmol) and 1,6-hexanediamine (2.92 g, 25.17 mmol) were introduced in THF (150 mL) and $MgSO_4$ (9.1 g, 75.5 mmol) was added. The suspension was stirred at 50 °C for 24 hours. The reaction mixture was filtered and concentrated under reduced pressure to obtain the crude product. The whitish solid was immersed in heptane (150 mL), stirred at 50 °C for 1 hour, filtered and washed on the filter with pentane (3 x 150 mL) to yield the target compound as a white crystalline solid (9.8 g, 17.6 mmol, 70%).

^{1}H-NMR ($CDCl_3$, 400 MHz): δ 8.19 (s, 2H), 7.67-7.65 (m, 4H), 7.43-7.42 (m, 8H), 6.97 (d, J = 4.0 Hz, 4H), 6.73 (dd, J = 13.2 and 8.4 Hz, 2H), 5.76 (d, J = 13.2 Hz, 2H), 5.26 (d, J = 8.3 Hz, 2H), 5.08 (s, 4H), 3.56 (t, J = 4.5 Hz, 4H), 1.67-1.64 (m, 4H), 1.40-1.39 (m, 4H).

3.2.2 Vitrimers from monomers

PBMA, PMMA and PS vitrimers with pending aldehyde or imine functionalities and crosslinking imine bonds were synthesized by radical polymerization techniques via a "one-pot" approach (Scheme 3.3; Table 3.1).

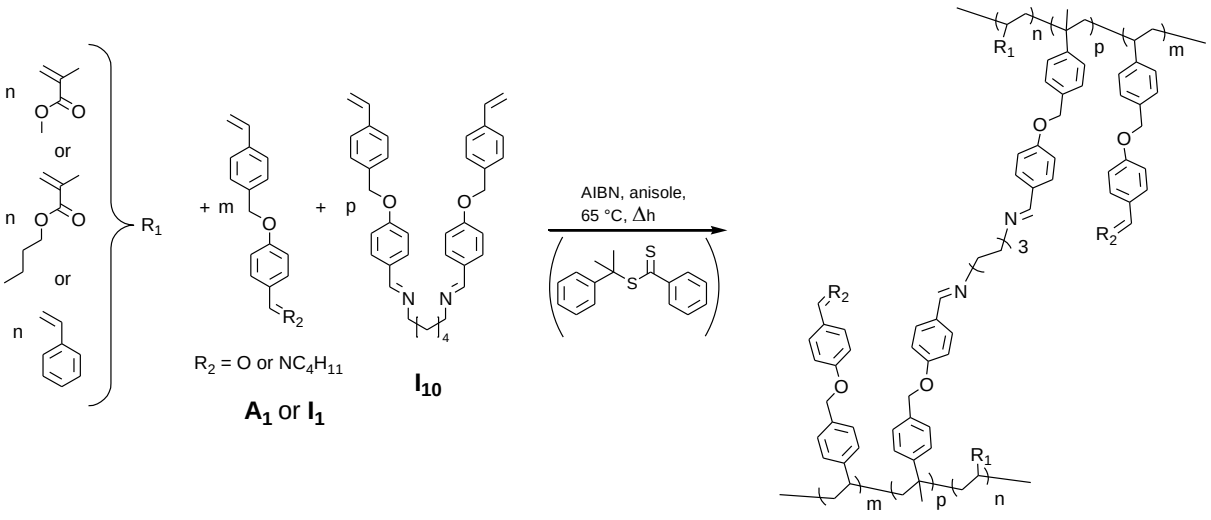

Scheme 3.3. General scheme for the generation of vitrimers from monomers via radical (conventional or controlled) polymerization techniques.

General synthesis: Monomer $\mathbf{A_1}$ or $\mathbf{I_1}$, crosslinker $\mathbf{I_{10}}$ and the comonomer (MMA or BMA or PS) were mixed in anisole in a septum sealed flask at 65 °C. The mixture was bubbled with nitrogen for 10 min at this temperature before cooling down to ca 35 °C. Then, anisole solutions of AIBN (1 mL) and of chain-transfer agent (1 mL) in the case of controlled radical polymerizations were added and the mixture was bubbled for 10 more min with nitrogen. After this time, the mixture was heated to 65 °C for 24 to 48 hours. The resulting gel was placed in anhydrous THF (350 mL) at room temperature for 6 hours to remove the anisole (solvent exchange). This procedure was repeated once more in anhydrous THF (350 mL) for 18 hours. The gel was then dried at 100 °C under high vacuum for 24 h.

System	Comonomer/functional monomer/$\mathbf{I_{10}}$/CTA/AIBN	Theoretical number of crosslinkers/ chain	Theoretical number of monomers between crosslinks	Theoretical ratio Comonomer/ functional monomer
Networks with pending imines ($\mathbf{I_1}$) by conventional radical polymerization at 65 °C				
^{M}PBMA I V1*	4/1/0.025/-/0.008	n/a	100	4/1
^{M}PBMA I V2*	4/1/0.075/-/0.008	n/a	33	4/1
^{M}PBMA A V1*	4/1/0.025/-/0.008	n/a	100	4/1
^{M}PS I V1*	4/1/0.025/-/0.008	n/a	100	4/1
Networks with pending aldehydes ($\mathbf{A_1}$) by RAFT polymerization at 65 °C				
^{M}PMMA A 1**	4/1/0/0.02/0.008	0	-	4/1
^{M}PMMA A V2**	4/1/0.016/0.02/0.008	1.6	156	4/1
^{M}PMMA A V3**	4/1/0.032/0.02/0.008	3.2	78	4/1
^{M}PMMA A V4**	4/1/0.064/0.02/0.008	6.4	39	4/1
^{M}PMMA A V5**	4/1/0.128/0.02/0.008	12.8	20	4/1
^{M}PMMA A N6 **,***	4/1/0.032/0.02/0.008	3.2	78	-

n/a = not applicable, *anisole 25 vol%, 48 h, ** anisole 50 vol%, 24 h, *** crosslinked with dimethacrylate hexanediol

Table 3.1 Vitrimers generated via the approach "from monomers".

As it is difficult to get precise information on the polymerization of functional monomers during gel forming polymerization, we synthesized a linear polymer (**^{M}PMMA A 1**) under identical starting conditions, but without crosslinker $\mathbf{I_{10}}$. Additionally, we compared the measured data to values obtained from theoretical considerations. Another approach to get information about the molecular weight was to de-crosslink the vitrimers with an excess of aldehyde (see swelling tests).

The conversion (ρ) was set to 100% (confirmed by 1H-NMR spectroscopy) and an efficiency of the initiator (f) = 0.5 was assumed. Hence the degree of polymerization (DP_n) of a controlled chain growth polymerization, can be expressed as:[2]

$$DP_n = \frac{\rho \times [M]_0}{[CTA]_0 + 2 \times f \times ([AIBN]_0 - [AIBN]_t)} = 198$$

Equation 3.1

Hence, the theoretical number average molar mass (M_n) is

$$M_n = DP_n \times (0.8 \times M_{MMA} + 0.2 \times M_{\mathbf{A1}}) + M_{CTA} = 25\,300 \text{ g/mol}$$

Equation 3.2

Comparison of the GPC results (PMMA calibration) of **^{M}PMMA A 1** (M_n = 25 300 g/mol, M_w = 30 300 g/mol, Đ = 1.20) shows an excellent match between experimental and theoretical

data. The narrow dispersity (1.19) is also characteristic for a good control during polymerization.

All these data confirm the compatibility of aldehyde monomer **A_1** with radical copolymerization of methacrylate monomers, at these moderate temperature at least. The compatibility of imine monomer **I_1** with radical polymerization of methacrylate was also studied and confirmed. The detailed results are presented and discussed in the following section.

3.2.3 Vitrimers from thermoplastics

PMMA and PBMA vitrimers with pending aldehyde or imine functionalities and imine crosslinking bonds were obtained by mixing functional thermoplastics synthesized by radical polymerization of functional monomers (Scheme 3.4) with the bis-imine crosslinker **I_9** (Figure 3.1 and Scheme 3.1).

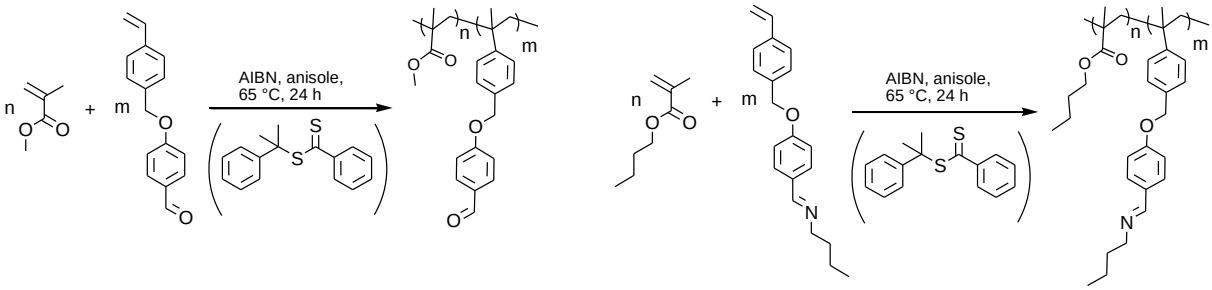

Scheme 3.4. Synthetic procedures to generate functional thermoplastic with pending aldehydes or imines .

3.2.3.1 Model polymerizations

Model polymerizations with 25 mol% of either imine monomer **I_1** or aldehyde monomer **A_1** were conducted by reversible addition-fragmentation chain transfer (RAFT) polymerization with methyl methacrylate (MMA) using 2-phenyl-2-propylbenzodithioate as chain transfer agent in anisole (Scheme 3.4 and Figure 3.2). During the model polymerizations, samples were taken from the reaction mixture at different time intervals and analyzed by ^{1}H-NMR spectroscopy and gel permeation chromatography (GPC). No inhibition period was observed during the model copolymerization of **A_1** with MMA. However, when the other monomer, **I_1** was used, the polymerization was retarded. After 12 hours at 65 °C in anisole, the reaction mixtures became very viscous and after a total of 24 hours the crude mixtures were poured

into dry diethyl ether to precipitate the polymers. Conversion of the monomers was followed over the course of polymerization and calculated by integration of the respective signals from the ^{1}H-NMR spectra using the anisole peak at 3.69 ppm as internal standard. The measured conversions of the functional monomers were similar for **I_1** and **A_1** with 99.4% and 92.3% (Figure 3.2). The MMA conversion was the lowest (<84% and 84.8%) in both experiments. Taking into account the reactivity ratios of MMA and styrene and an initial mixing ratio of 4/1 this drift to a polymer richer in **I_1** or **A_1** can be expected. As both polymerizations approached high conversions the overall copolymer composition was similar to the initial monomer composition. The evolution of molecular weight was observed to increase linearly with monomer conversion indicating a constant number of polymer chains. The elevated dispersity of 1.64 of the resulting polyimine in contrast to the narrow molecular distribution of 1.25 of the polyaldehyde likely indicates the presence of branching for materials containing imines. Additionally, the reason for the above mentioned inhibition period in the presence of the imine monomer **I_1** will have to be investigated further. After drying under reduced pressure, both polymers dissolved easily in common organic solvents such as acetone, chloroform, dichloromethane and THF.

System	Monomer M	MMA/M/CTA/AIBN vol% anisole	t (h)	Conversion (%)			M_n (kg/mol)	$Đ$
				MMA	Monomer	Total		
PMMA I 1	**I_1**	200/50/1/0.4 25%	65 °C, 24h	84.0	99.4	87.1	43	1.64
PMMA A 1	**A_1**	200/50/1/0.4 25%	65 °C, 24h	84.8	92.3	86.4	23	1.25

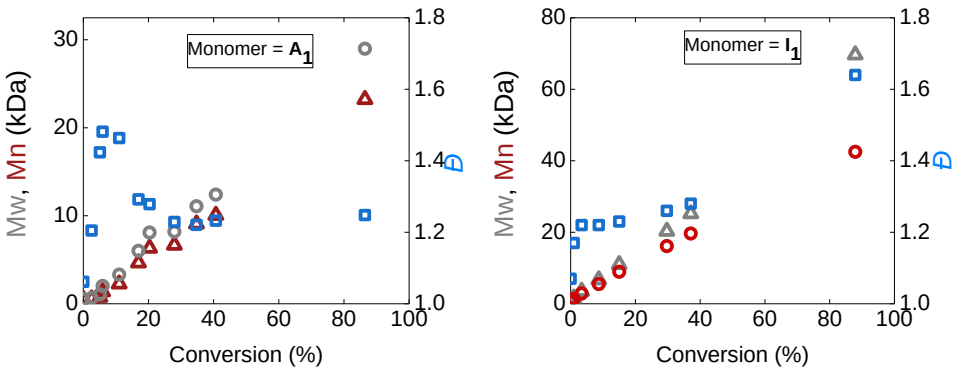

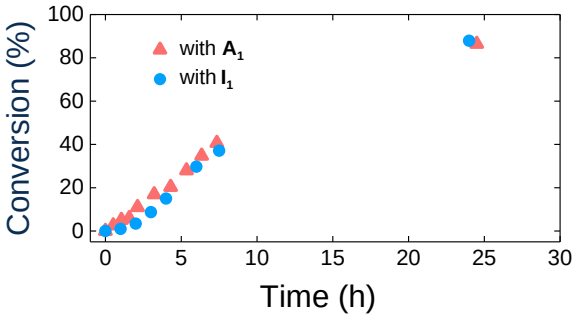

Figure 3.2. Top: Experimental conditions of the model polymerizations of imine and aldehyde monomers via RAFT. Center left: experiment with the aldehyde monomer $\mathbf{A_1}$. Center right: experiment with the imine monomer $\mathbf{I_1}$. Bottom: Conversion vs time for both model polymerizations.

3.2.3.2 Vitrimers from thermoplastics by radical polymerization

RAFT polymerizations:

Typical procedure: MMA, $\mathbf{A_1}$, 2-phenyl 2-propyl benzodithioate and AIBN were dissolved in anisole (50 vol%). The resulting mixture was bubbled with nitrogen at room temperature for 30 minutes before being heated up to 65 °C. The reaction mixture was kept under nitrogen while stirring at 65 °C for the time of reaction (Table 3.2). Then, a small amount of anhydrous THF was added and the polymer was precipitated into dry Et_2O. The pink polymer was dissolved in anhydrous THF, re-precipitated into dry Et_2O and dried under reduced pressure at 100 °C overnight.

Removal of the CTA chain-end of polymers prepared by RAFT polymerization

Typical procedure: The polymer (**PMMA A 4**, 8.0 g, 0.14 mmol chains, Table 3.2) was dissolved in THF (130 mL) and AIBN (216.5 mg, 1.3 mmol) was added. The pink solution was stirred for 6 hours at 60 °C and then cooled to room temperature and stirred for 10 additional hours. Triphenylphosphine (347.3 mg, 1.3 mmol) was added and the now colorless solution was stirred at 40 °C for one more hour before the colorless polymer was precipitated into methanol and dried at 100 °C under high vacuum for 24 hours (7.0 g colorless polymer).

Free radical polymerizations:

Typical procedure: MMA or *n*-butyl methacrylate (*n*BMA), $\mathbf{A_1}$ and AIBN were dissolved in anisole (50 vol%). The resulting mixture was bubbled with nitrogen at room temperature for

30 minutes before being heated up to 65 °C. The reaction mixture was kept under nitrogen while stirring at 65 °C for 7.5 hours. Then, a small amount of anhydrous THF was added and the polymer was precipitated into dry Et_2O. The colorless polymer was dissolved in anhydrous THF, re-precipitated in dry Et_2O and dried under reduced pressure at 100 °C overnight.

#	Comonomer/ $\mathbf{A_1}$/CTA/AIBN	Reaction time (h)	M_n (kg/mol)	M_w (kg/mol)	$Đ$	Ratio comonomer/$\mathbf{A_1}$	Average $\mathbf{A_1}$/chain
PBMA A 2	3.8/1/-/0.008 [a]	7.5	430	1097	2.55	2.9	661
PMMA A 2	20/1/-/0.034 [a]	7.5	164	340	2.07	14.0	100
PMMA A 3	3/1/-/0.008 [a]	7.5	356	926	2.6	2.0	822
PMMA A 4	800/200/1/0.4 [b]	16	57	67	1.17	4.4	84
PMMA A 5	800/200/1/0.4 [b]	20	57	74	1.29	3.4	99
PMMA A 6	2388/597/1/0.4 [b]	16	131	157	1.20	3.7	215
PMMA A 7	800/200/1/0.4 [b]	24	59	71	1.2	3.7	97
PMMA A 8	200/50/1/.04 [b]	24	25	29	1.16	2.6	50
PMMA A 9	4/-/-/0.002	16	43	78	1.82	-	-

[a]by free radical polymerization, [b]by RAFT

Table 3.2. Functionalized thermoplastics synthesized.

We designed functional thermoplastic copolymers of MMA or *n*BMA with pending aldehyde functionalities. The thermoplastics differed in molecular weight and monomer ratios. Copolymer compositions were determined by ^{1}H-NMR spectroscopy and molar mass were measured by GPC using THF as eluent and PMMA calibration.

Vitrimer (gel) formation and cleavage

Gel formation in anhydrous THF at room temperature and subsequent cleavage of the gel with an excess of benzaldehyde $\mathbf{A_4}$ were performed (Figure 3.3).

Typical procedure: 1 g of the functional thermoplastic polymer (**PMMA A 3**) was dissolved in anhydrous THF (5mL) and partitioned between two glass bottles. The bis-imine crosslinker $\mathbf{I_9}$ (0.01 mL, 0.03 mmol, 12.5 crosslinker/chain) was added to the right bottle, while no chemicals were added to the left control experiment (Figure 3.3 a). After 8 hours at room temperature, gel formation was observed (Figure 3.3 b). Both samples were kept for 72 more hours at room temperature. One half of the insoluble gel was immersed in 5 mL additional anhydrous THF (Figure 3.3 c top, picture after immersion for 24 hours at room temperature). To the other half of the gel was added $\mathbf{A_4}$ (1 mL, 9.8 mmol, 327 eq.) and more anhydrous

THF (5 mL). After 24 hours at room temperature complete dissolution was observed (Figure 3.3 c bottom).

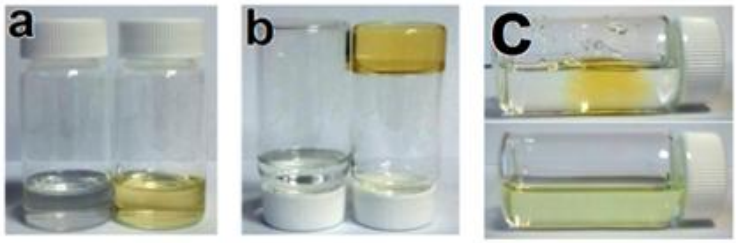

Figure 3.3. Left vial: Functional thermoplastic **PMMA A 3**. Right vial: functional thermoplastic **PMMA A 3** and bis-imine crosslinker $\mathbf{I_9}$. a) Right after mixing. b) 8 hours at room temperature after mixing. c) Top: The swollen gel in 5 additional mL of THF 24 hours after immersion. Bottom: De-crosslinked system 24 h at room temperature after the addition of 1 mL of $\mathbf{A_4}$.

Vitrimers were typically generated from functional thermoplastics via the following method: Networks were formed by adding the bis-imine crosslinker $\mathbf{I_9}$ to a solution of functional thermoplastic polymers in anhydrous THF at room temperature. After mixing, the solvent was evaporated under reduced pressure for 24 hours at T > 100 °C and the resulting solid was processed into the desired shape for characterization via compression molding at 150 °C.

Thermoplastics		Vitrimers		
System **PMMA A**		$\mathbf{I_9}$ (wt%)	$\mathbf{I_9}$/chain	Average number of monomers between crosslinks
1*	**V1****	0.7	8.1	159
2	**V2**	1.0	4.6	163
3	**V3**	1.2	8.6	142
4/4	**V4/V5**	0.9/4.5	1.9/9.3	119/24
5	**V6**	2.8	5.6	39
6	**V7**	0.5	2.2	230
7	**V8**	0.9	1.8	127
8	**V9**	3.5	3.2	28

***PBMA A 2, ****PBMA A V1**

Table 3.3. Vitrimers generated from functional PMMA thermoplastics.

Exchanges on linear polymers

Figure 3.4 depicts exchange-reactions between free small molecules (sharp peaks) and the linear polyimine **PMMA I 1** (broad peaks) in dry $CDCl_3$. The polyimine was separately

treated with equimolar amounts of free ethanolamine, **I_6** and **A_4**, and the resulting exchange products were monitored by ^{1}H-NMR spectroscopy after 24 hours of mixing. During transimination reaction with ethanolamine a second broad peak in the imine-characteristic R-N=C*H*-R region at 8.30 ppm was observed. Upon addition of **I_6**, the evolution of two additional imine-peaks (sharp and broad) at 8.35 – 8.15 ppm were observed. The exchange between polymeric imine species and free benzaldehyde **A_4** was observed by the evolution of a second aldehyde peak (broad) at 9.90 ppm and the respective second imine peak (sharp) at 8.25 ppm. These results indicate that the imine functionalities are sufficiently stable to survive polymerization conditions but stay dynamic to participate in the targeted exchange with small amine, imine and aldehyde molecules.

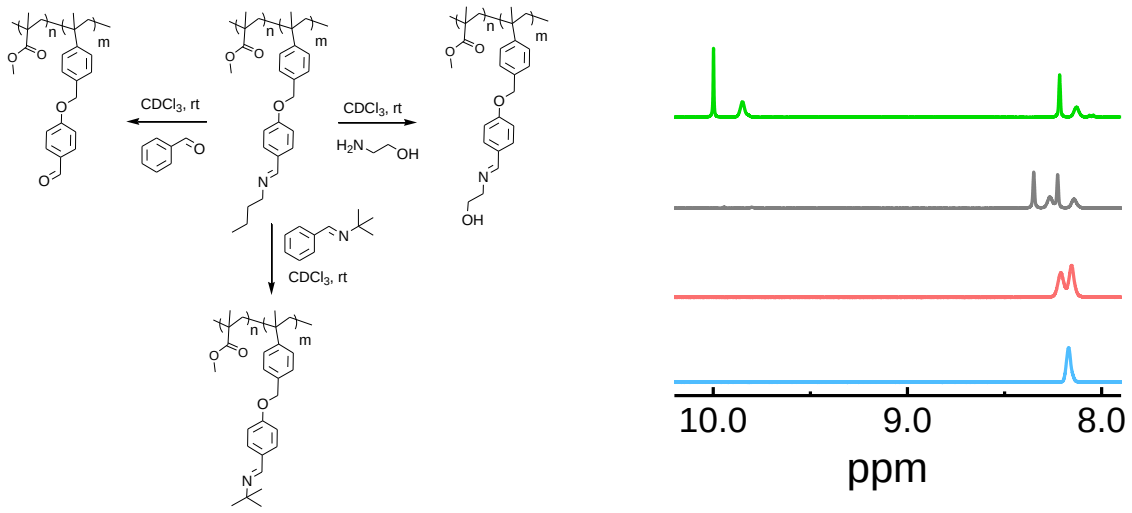

Figure 3.4. Left side: Qualitative exchanges of pending imine functionalities of **PMMA I 1** with aldehydes, amines and imines in $CDCl_3$ at room temperature under air. Right side: ^{1}H-NMR raw data of the exchanges after 24 hours at RT. From top to bottom: Aldehyde, imine, amine, control.

3.3 Processing and characterization of vinyl vitrimers with pending aldehydes or imines

Vitrimers with pending aldehydes or imines were processed by molding techniques such as compression and injection molding. Additionally, extrusion of samples was tested. For clarity, the results obtained for materials made via “vitrimers from monomers” and “vitrimers from thermoplastics” are presented together and are ordered by the experimental/analytical method.

3.3.1 Compression molding

Once dry, the vitrimers were ground into powder or cut into pieces and compression molded for 1-3 hours at 150 °C under a nominal pressure of 3-5 tons in a hot-press. Usually, both sides of the metal molds were covered with a Teflon layer to avoid direct contact with the plates of the hot-press. De-molding was done by hand, simply by pushing the cold specimen out of the mold (Figure 3.5).

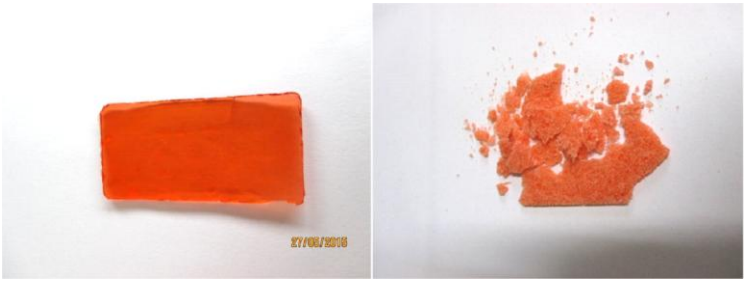

Figure 3.5. Left side: Vitrimer **^{M}PMMA A V3** (Table 3.1) from monomers compression molded for 1 h at 150 °C. Right side Thermoset **^{M}PMMA A N6** (Tale 3.1) compression molded for3 h at 150 °C.

As done for the vitrimer systems it was tried to process a permanently crosslinked PMMA network, namely **^{M}PMMA A N6** (Table 3.1). The dried polymer network was ground into powder and compression molded for 3 hours at 150 °C under a pressure of 3-6 tons. Via this procedure, a very crumbly and fragile material that broke immediately upon contact with hands was obtained. This material was not transparent and the grains of the powder initially introduced into the mold were still visible. Figure 3.5 illustrates that crosslinked poly(methyl methacrylate) networks containing pending aldehyde functionalities but no exchangeable imine functionalities in their crosslinks cannot be processed by compression molding techniques, unlike the vitrimers.

3.3.2 Injection molding

^{M}PMMA A V3 (3.0 g) and **^{M}PMMA A V4** (3.0 g and 2.4 g) (Table 3.1) were injection molded using a DSM Xplore micro 10 cc injection molding machine. The geometry of the hollow form in the mould was either a disc-shape (25 mm diameter) or a dog-bone shape (*ca.* 7 cm length) (Figure 3.6). The mold was preheated to 200 °C before the sample was added in powder form to the cold (ca 25-45 °C) injection barrel. The injection barrel was heated to 200 °C (5 minutes) and equilibrated at that temperature for 1 minute. The molding process consisted of 5 steps: 2 × 10 bar for each 30 seconds followed by 2 × 12 bar for 30 seconds and release of the pressure. After injection, the samples were kept in the mold at 200 °C for 1

additional minute before cooling of the mold with a water cooling system (*ca.* 3.5 minutes). The injected sample of **^{M}PMMA A V4** was tested for solubility. After 40 hours of immersion at 25 °C in anhydrous THF (100 mg in 10 mL) the sample was not dissolved, but swollen. An accurate number of the soluble fraction was not determined, because the sample fractured into several pieces. The injection molded sample was also tested for stress relaxation on DMA (3% deformation, 150 °C, 5 minutes equilibration at 150 °C). The plot of the normalized relaxation modulus showed that the vitrimer **^{M}PMMA A V4** was able to relax stress after the injection molding process at 200°C (Figure 3.6). However, relaxation slowed down as compared to the specimen compression molded at 150 °C (Figure 3.6). Additionally, it seemed as if the injection molded sample lost its ability to completely relax the stress with *ca.* 4% remaining stress. These observation might evidence the formation of few permanent crosslinks after processing by injection molding at 200 °C. Such permanent crosslinks could be generated by side reactions associated to imine and aldehyde functions and/or to instabilities of the methacrylate backbone under the injection conditions. Further tests to investigate the dynamic behavior of the presented systems and the impact high temperature might have on the reversibility of the systems are presented in the following subchapters.

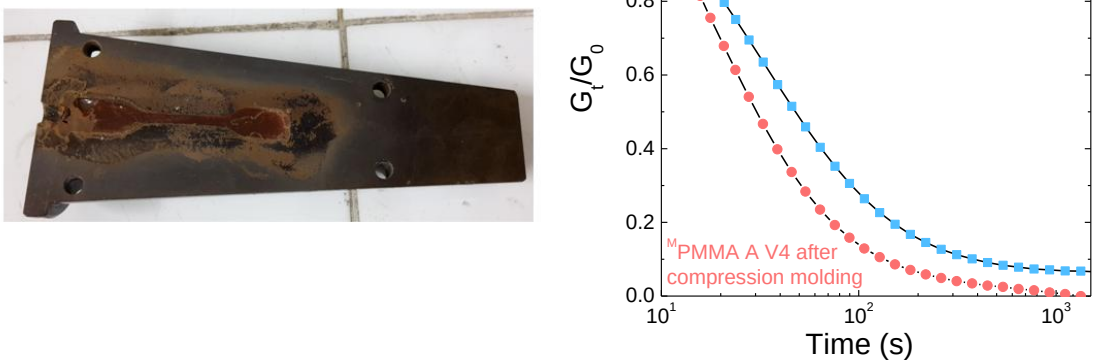

Figure 3.6. Injection molded **^{M}PMMA A V3**. Stress relaxation experiments in DMA at 150 °C of **PMMA A V4** after compression and injection molding.

3.3.3 Extrusion

3.2 g of the crosslinked polymer network **PMMA A V8** (Table 3.3) were added in the bivis DSM micro 5cc extrusion machine. Extrusion was performed at 200 °C with a rotational screw speed of 60 rounds per minute, a time of injection of 4 minutes and a time of circulation

of 11 minutes (Figure 3.7). After injection of the total amount of the crosslinked polymer network, the force measured by the screws reaches a plateau of 3200 N. In total, 2.5 g of the cross-linked polymer network were extruded.

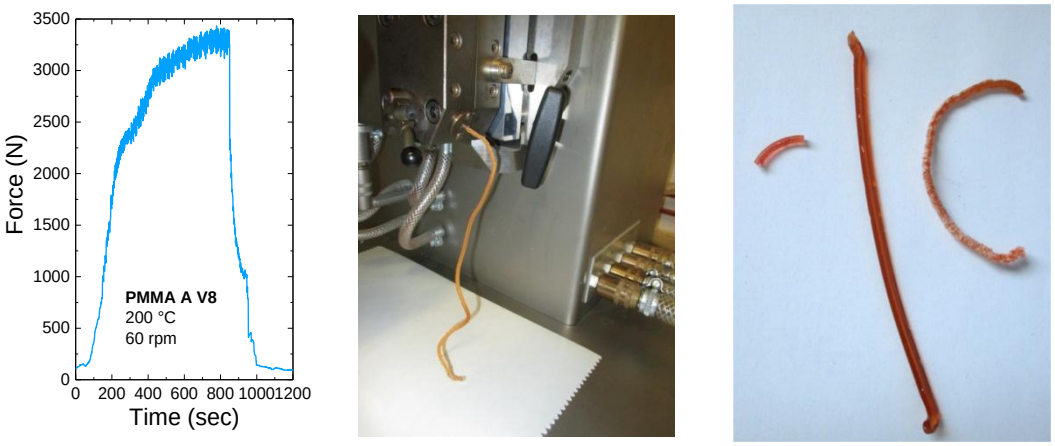

Figure 3.7. From left to right: Raw data from extrusion of **PMMA A V8**. Picture of the vitrimer **PMMA A V8** during and after extrusion.

Processing via extrusion of vitrimers which were generated by the other approach (from monomers) was tested on the system **^{M}PMMA A V3** (Table 3.1). Therefore 3,4 g of **^{M}PMMA A V3** were added in the bivis DSM micro 5cc extrusion machine. Extrusion was performed at 200 °C using a rotational screw speed of 60 rounds per minute, an injection time of 1 minute and a circulation time of 7 minutes. After injection of the total amount the crosslinked polymer network, the force measured by the screws reaches a plateau of 3000 N. In total, 3.0 g of the cross-linked polymer network were extruded.

In this subchapter, the processing of imine/aldehyde vitrimers via commonly used techniques was shown. Although systems can be compression/injection molded and extruded, some problems were encountered. First, the here tested systems possess low molecular weight network forming chains resulting in inferior mechanical properties. Additional tests with higher molecular weight vitrimers will have to be done to check if at higher viscosities these systems are still processable under these conditions. Injection molded samples lost their ability to completely relax stress after 1 cycle of injection (*ca.* 4% remaining stress). A possible explanation might be the presence of secondary reactions of crosslinking or pending imine functionalities at elevated temperatures (200 °C). Additionally, and especially for applications of PMMA systems, the ability to control the color is very important. Like the introduced imines, the generated vitrimers were colored. They were yellowish after crosslinking and turned orange/reddish the higher the processing temperature was.

3.3.4 Swelling tests

Crosslinked systems possess increased solvent resistance and by definition do not dissolve in good solvents of constituting polymer chains. To test the solvent resistance of the here presented systems, a series of swelling tests was performed on some of the imine/aldehyde vitrimers.

The swelling ratio and soluble fraction of the vitrimer materials were calculated as follow:

$$Swelling\ ratio = \frac{Mass\ swollen - Mass\ dried}{Mass\ dried}$$

Equation 3.3

$$Soluble\ fraction = 1 - (\frac{Mass\ dried}{Mass\ dry})$$

Equation 3.4

3.3.4.1 Swelling tests on vitrimers from monomers

The network **^{M}PBMA I V1** (Table 3.1) was immersed in neither dried nor anhydrous THF, acetone, dimethylformamide, chloroform, dichloromethane, trichlorobenzene, toluene, anisole (50 mg/5 mL) at room temperature for more than 48 hours. In all cases, the system did not dissolve, but swelling was observed.

A sample of 265 mg of **^{M}PBMA I V1** (pristine from synthesis) was immersed in 15 mL of anhydrous THF. The sample was immersed for 24 hours without stirring before the swollen gel was taken out of the flask and weighted. The gel was dried under high vacuum until constant weight (*ca.* 6 hours). This procedure was repeated twice more keeping the samples immersed for 12 hours in THF instead of 24 hours (Figure 3.8, left).

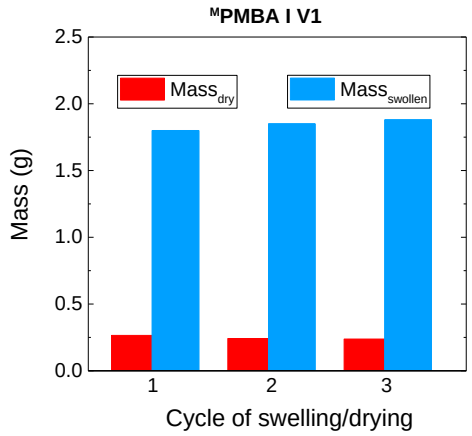

Swelling ratios				
	Processed samples			
Cycle	Pristine	1st sample	2nd sample	3rd sample
1st swelling	5.8	5.19	5.14	4.95
2nd swelling	6.64	5.37	5.40	5.51
Soluble fraction (%)				
1st swelling	9	4	4	4
2nd swelling	2	6	4	4

Figure 3.8. Swelling characteristics of **MPBMA I V1**.

These results prove the insolubility of vitrimers which are generated in one-pot from monomers. The determined soluble fractions were small and did not change significantly even after drying/swelling cycles. The same trend was observed for the swelling ratios indicating a constant degree of crosslinks.

Further swelling tests were performed with a pristine sample after synthesis and with three onetime processed samples of **MPBMA I V1** (Figure 3.8, right). Processing conditions: grinding into powder of the raw material after synthesis, pressing/compacting under a pressure of 10-11 tons at 150 °C for 5 hours. The swelling tests were performed in anhydrous THF. The mass of the respective sample was measured after 12 hours of swelling, which corresponds to the time at which the mass of the swollen samples was constant. All samples were then dried and re-tested for their swelling properties under the same conditions to check for reproducibility. The results of these experiments are reported in Figure 3.8 (right). These swelling tests show that the un-processed samples are highly insoluble, with a soluble fraction smaller than 10%. After recycling/processing the samples were still insoluble, displaying similar swelling characteristics, thus a similar cross-linking density, as the pristine material obtained right after synthesis. These observations not only to confirm the solvent resistance of vitrimers, but also the absence of side reactions during recycling/processing at150 °C.

Compression molded vitrimers **MPMMA A V2-V4** (disc shape, Figure 3.9) were immersed in anhydrous THF for 24 h at room temperature. Then, the solvent was carefully poured out of the vial and the swollen samples weight was determined.

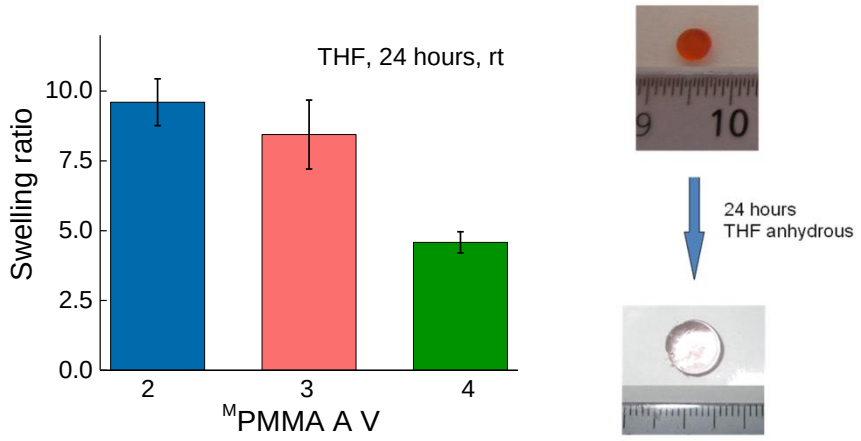

MPMMA A	*m* sample (mg)	*m* after swelling (mg)	Swelling ratio	*m* after drying (g)	Soluble fraction (%)
V2	66.4	685.5	10.32	0.06	13
	68.4	593.9	8.68	0.06	7
	71.7	702.2	9.79	0.07	8
V3	55.2	424.8	7.7	0.06	-2
	72.5	562.9	7.76	0.07	-2
	72	710.7	9.87	0.07	1
V4	91.2				-
	89.4	385.8	4.32	96.7	-8
	89.7	435.1	4.85	95.3	-6

Figure 3.9. Swelling characteristics of vitrimers from monomers.

It was observed that an increase in the concentration of crosslinker during polymerization resulted in a decrease of the swelling ratio of the respective system, *i.e.* a more crosslinked system, as should be expected. For systems **MPMMA A V2-V3** the soluble fractions follow the same trend: whereas for **MPMMA A V2** an average soluble fraction of 9.3% was observed, **MPMMA A V3** seemed to present almost no soluble fraction (average -1%). For **MPMMA A V4** even more negative soluble fractions of up to -8% were detected. The negative values for **MPMMA A V3** and **MPMMA A V4** might be due to drying problems (drying temperatuee < 120 °C) related to the higher crosslink density of these systems and drying under higher vacuum at temperatures > 120 °C should solve this problem.

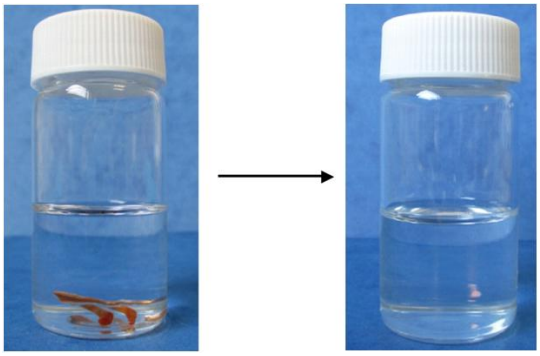

Figure 3.10. De-crosslinking of a processed vitrimer from monomers. Left side: right after immersion in THF. Right side: after dissolution (**A_4**, 3 days, RT).

To further characterize the vitrimers materials, *e.g.* to check the integrity of the dynamic covalent imine crosslinks after synthesis/processing (compression molding 150 °C, 1 h) and to characterize the polymer chains constituting the vitrimer, the imine crosslinks of the vitrimers were selectively cleaved, according to the following procedure: To processed vitrimers **^{M}PMMA A V2-V5** (50-100 mg) was added 0.1-0.8 mL of benzaldehyde **A_4** in anhydrous THF (10 mL) at room temperature. After 1-3 days without stirring, all vitrimers were completely dissolved. After filtration of the solution (no residue in filter) the polymers were precipitated into methanol and dried at 120 °C overnight under high vacuum. **^{M}PMMA A V2-V3** samples were directly analyzed by GPC (THF, PMMA calibration), but samples of **^{M}PMMA A V4-V5** did not dissolve in THF anymore. Assuming re-crosslinking during drying due to evaporation of mono-aldehydes, but remaining crosslinking diimines, the two systems were treated as above with **A_4** again and handed to GPC after full dissolution without precipitation.

System	*M_n (kg/mol)	*M_w (kg/mol)	*$Đ$
^{M}PMMA A 1	25.7	31.1	1.21
^{M}PMMA A V2	35.4	41.4	1.17
^{M}PMMA A V3	21.4	34.7	1.62
^{M}PMMA A V4	13.6	20.0	1.47
^{M}PMMA A V5	19.1	35.9	1.88

*after de-crosslinking with benzaldehyde **A_4**

Table 3.4. GPC analyses of de-crosslinked vitrimers from monomers.

The fact that all systems dissolved prove that the dynamic of the network forming bonds is maintained even after processing (150 °C, 1 h). The obtained molecular weight of the different systems seems to indicate that higher imine contents, *i.e.* a higher crosslinker concentration, result in smaller molecular weight polymers with few or no control.

3.3.4.2 Swelling tests on vitrimers from thermoplastics

A sample of the compression molded (150 °C, 1 h) cross-linked polymer network **PBMA A V1** with a mass of *ca.* 75 mg was placed in 10 mL of anhydrous THF and swollen for 16 hours at room temperature. This test was performed on two samples and small soluble fractions of 5 and 4% as well as equal swelling ratios of *ca.* 7.4 were measured. The same system was insoluble even after refluxing in anisole for 24 hours (Figure 3.11).

#	Swelling ratio	Soluble fraction (%)
1	7.4	5
2	7.4	4

Figure 3.11. Top: Swelling characteristics of **PBMA A V1** at room temperature. Bottom: Solubility tests on a processed (compression molding, 150 °C, 1 h) sample **PBMA A V1** (650 mg, 100 mL anisole). Left side: before heating, right side: after heating to 120 °C in anisole overnight.

Swelling tests on 4 generations of re-processed (150 °C, 1 h) **PMMA A V7** in anhydrous THF (50-150 mg, 10 mL, RT) confirmed the materials insolubility. Whereas one-time processed samples present an average soluble fraction of 13.9%, four-times processed samples did not lose any material anymore (-0.1% soluble fraction). As observed above, annealing might take place during the first processing and thus the swelling ratio decreased slightly from ca 13% to 9-10% after the first processing and then remained quite stable for the next recycled generations.

Generation	Mass initial (mg)	Mass swollen (mg)	Mass after drying (mg)	Swelling ratio	Soluble Fraction (%)	Average Soluble Fraction (%)
1	47.1	540.8	40	13.5	15.1	13.9
1	34.6	476.8	29.6	16.1	14.5	
1	57.6	550	51.4	10.7	13.4	
1	59.2	552	53.5	10.3	12.7	
2	106.4	1057.4	100.5	10.5	5.5	3.8
2	85.8	863.1	83.6	10.3	2.6	
2	77.7	845.3	75.1	11.3	3.3	
3	83.1	820.1	82.9	9.9	0.2	2.8
3	57.2	679.5	55.2	12.3	3.5	
3	31.5	403.9	30	13.5	4.8	
4	104.1	987.7	104.2	9.5	-0.1	-0.1
4	140.5	1335	142.4	9.4	-1.4	
4	111.8	1108.3	110.4	10.0	1.3	

Table 3.5. Swelling characteristics of **PMMA A V7**.

In this subchapter were presented swelling tests of vitrimers which were generated from both approaches, *i.e.* from monomers and from thermoplastics. All tested systems were insoluble in organic solvents which are known to be good solvents of the vitrimer-forming linear chains. In general, vitrimers from both approaches behave rather similarly. It was observed that the swelling ratio and the soluble fraction can be governed by the crosslink density (vitrimers from monomers), but also processing seemed to have an influence (tested for vitrimers from both approaches). The higher was the crosslink density, the smaller were the swelling ratio and the soluble fraction. In general, soluble fractions between 13%-0% (vitrimers from monomers, depending on crosslink density) and 13%-0% (one time to four times processed vitrimers from thermoplastics) were obtained. Similarly some materials presented an annealing effect during processing (150 °C, compression molding) with decreasing swelling ratio and soluble fraction the higher was the number of cycles of processing (vitrimers from monomers and thermoplastics). Consecutive swelling/drying cycles for both pristine from synthesis and one times processed samples (vitrimers from monomers) indicated the constant crosslink density. An experiment at elevated temperature (120 °C, anisole, overnight) further confirmed the insolubility of a vitrimer from thermoplastics. Eventually, all analyzed vitrimers from monomers (one time processed, 150 °C, 1 h) could be de-crosslinked with an excess of benzaldehyde proving that in these materials the network forming imines keep their dynamic character after polymerization and after processing at 150 °C for 1 h. De-crosslinking of vitrimers from thermoplastics was performed, too and is discussed in subchapter “3.3.8. Mechanical Testing”.

3.3.5 Dynamic mechanical analysis (DMA) and differential scanning calorimetry (DSC)

Important polymer properties such as modulus (E' and E") and glass transition temperature (T_g) can be measured via DMA and DSC.

3.3.5.1 DMA and DSC on vitrimers from monomers

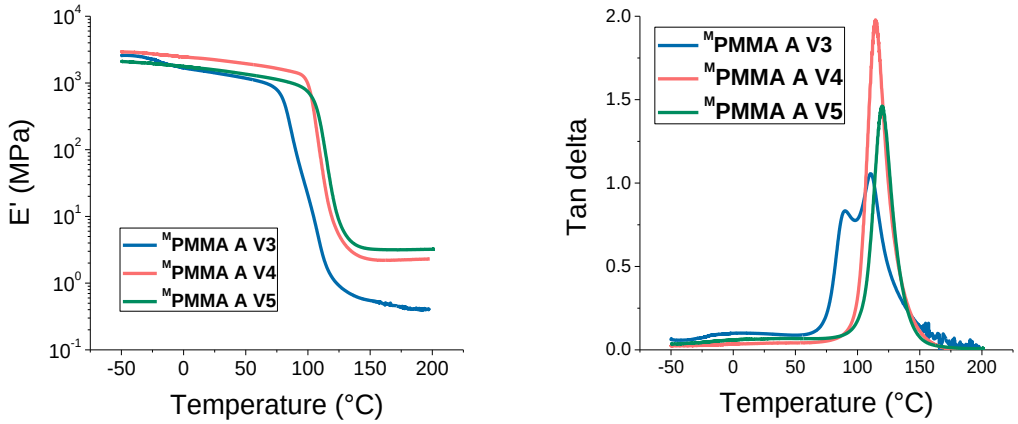

Figure 3.12. DMA experiments on vitrimers from monomers.

DMA was carried out on a TA Instruments Q800 in tension mode by ramping the temperature at 3 °C/min. **^{M}PMMA A V3-V5** (for characteristics of vitrimers see Table 3.1) were compression molded into rectangular shape and equilibrated at -50 °C in the DMA before starting the analysis. At temperatures far below T_g the systems possess high storage moduli between 1.8-2.5 GPa (Figure 3.12). Once the temperature is close to the transition temperature, the moduli decrease and at temperatures above T_g a rubbery plateau, characteristic for crosslinked systems was detected for all three vitrimers (Figure 3.12). In general, the nature of plateau is governed by several parameters such as crosslinking density and molecular weight of the network forming chains, *i.e.* entanglement. The modulus on the rubbery plateau followed qualitatively the concentration of the crosslinker and was the highest for the system with the highest crosslinker concentration (**^{M}PMMA A V5**). Similarly, the T_g of the materials increased with increased crosslinker concentration from 96 °C for **^{M}PMMA A V3** to 120 °C for **V5** (Figure 3.12). The tan delta of **^{M}PMMA A V3** had two peaks which might be explained by insufficient dryness (the evaporation of small molecules, *e.g.* solvent and monomers during the measurement). To compare with the corresponding thermoplastic, it was tried to test **^{M}PMMA A 1 (**M_n = 25 300 g/mol, M_w = 30 300 g/mol, Đ = 1.20**)** and also **^{M}PMMA A V2** (theoretically 1.6 crosslinkers per chain, see table 3.1) via the same procedure (for characteristics see table 3.1). Even after several attempts, no analysis could be performed due to the rupture of all samples either during de-molding or when placing the specimen into

the grips of the machine. Glass transition temperatures obtained by DSC experiments on films confirmed the observed trend of T_g increase with increasing concentration of bis-imine crosslinker $\mathbf{I_{10}}$ during polymerization (Figure 3.13). For the films, the glass transition temperatures obtained in DSC are shifted by about 11 °C-18 °C towards lower temperatures, but confirm the trends observed in DMA. In general, the DSC results on the un-processed powders are similar to those of the films (150 °C, compression molding, 1 h) with exception for **^{M}PMMA A V3** presenting values of 103 °C (powder) and 85 °C (film). For verification, the experiment on the powder of **^{M}PMMA A V3** should be repeated. .

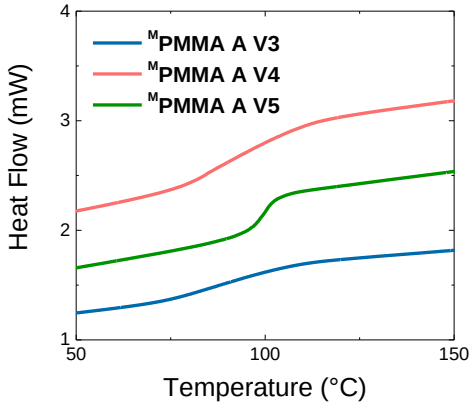

Vitrimers	Tg (°C)		
	DMA	DSC	
	Film	Powder	Film
^{M}PMMA A V2	-	106	-
^{M}PMMA A V3	96	103	85
^{M}PMMA A V4	114	101	100
^{M}PMMA A V5	120	105	102

Figure 3.13. Top: DSC experiments on vitrimers from monomers. Bottom: Glass transition temperatures of vitrimers from monomers obtained by DMA and DSC.

3.3.5.2 DMA and DSC on vitrimers from thermoplastics

The compression molded vitrimers **PMMA A V1-V7** and **V9** (for characteristics of the polymers see Table 3.2) were tested under similar conditions as described above (-50 °C to 200 °C at 3 °C/min) in tensile testing mode. All samples possess storage moduli superior to 2 GPa at temperatures below the glass transition temperature (Figure 3.14). Vitrimer **PMMA A V2** with few pending aldehyde functionalities exhibited the highest T_g (110 °C) whereas the *n*-butyl methacrylate system has the lowest (77 °C) (Figure 3.14 and Table 3.6). As seen above, a higher crosslink density increases the glass transition temperature from 107 °C for

PMMA A V4 to 113 °C for **PMMA A V5**. Interestingly, the T_g of system **PMMA A V7** increased from 98 °C after one cycle of processing via compression molding at 150 °C to 119 °C after 4 cycles of re-processing. As observed in the swelling tests, small plasticizing molecules might leave the system via evaporation during processing. Depending on the molecular weight and the crosslink density, more or less pronounced rubbery plateaus could be observed. For example, the storage modulus of **PMMA A V4** decreased rather fast after passing the T_g whereas a system with *ca*. 5 times more crosslinker, **PMMA A V5,** displayed a rather stable plateau modulus over a 50 °C window above its T_g. Additionally, the less crosslinked systems, *i.e.* **PMMA A V4** and **V7,** crept during the experiment, which affected the measurement of the storage modulus. Glass transition temperatures obtained in DSC are in general shifted to lower temperatures, but confirm the above mentioned trends (Table 3.6).

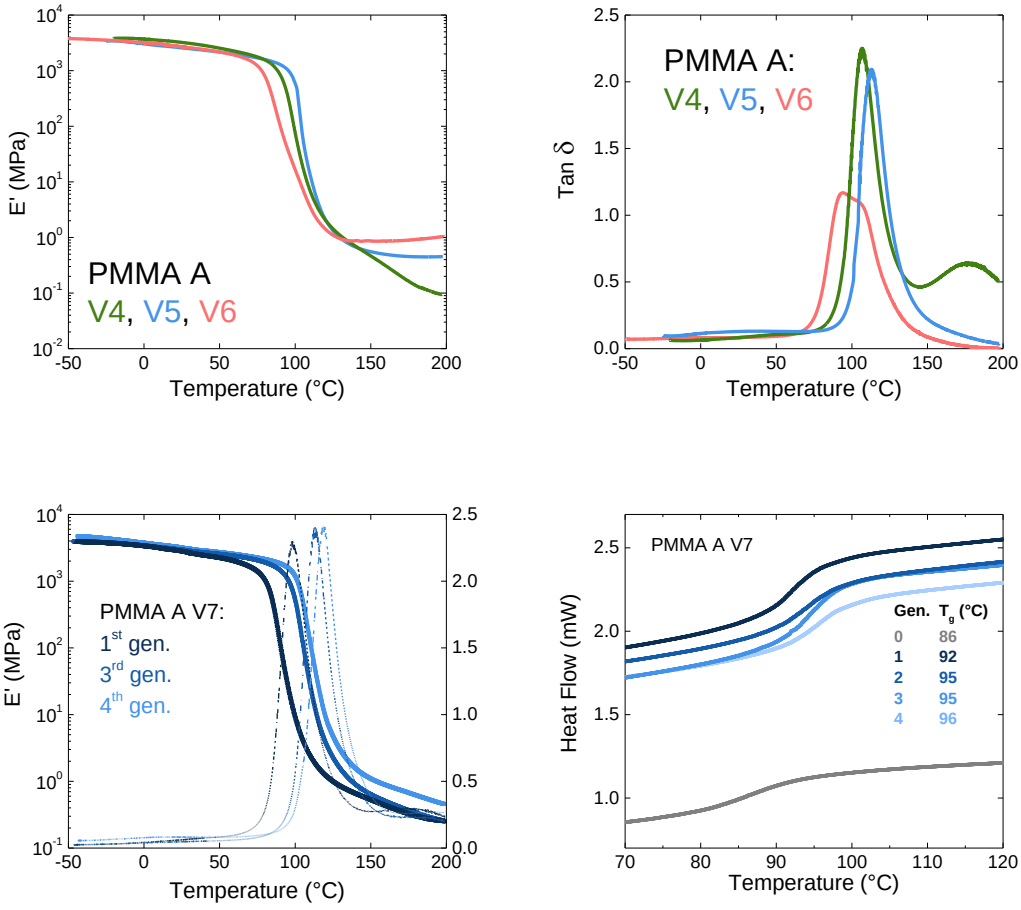

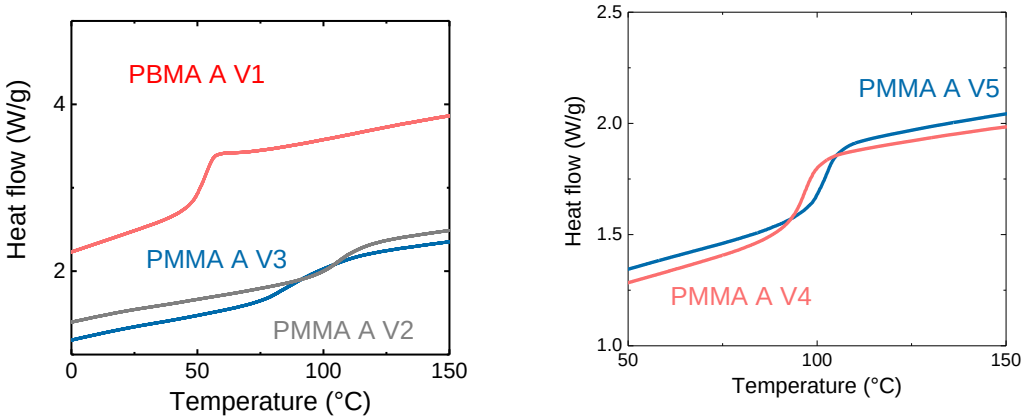

Figure 3.14. Vitrimers from thermoplastics were analyzed in DMA: 3 °C/min and in DSC: 10 °C/min.

System	T_g (°C)	
	DSC	DMA
PBMA A V1	50	77
PMMA A V2	107	110
PMMA A V3	88	100
PMMA A V4/V5	97/100	107/113
PMMA A V6	-	100
PMMA A V7*	86/92/95/95/96	-/98/-/113/119
PMMA A V8	-	-
PBMA A 2	-	-
PMMA A 8/PMMA A V9	-/-	-/109
*powder/1th/2nd/3rd/4th generation		

Table 3.6. Glass transition temperatures of vitrimers from thermoplastics.

DSC results showed that the T_g of the PMMA-based analyzed samples were close to those of the homopolymers (105 °C for PMMA). The system with BMA as comonomer exhibited the lowest T_g of 50 °C (DSC). DMA confirmed the existence of crosslinks in vitrimers synthesized via both approaches (from monomers and from thermoplastics) by the presence of rubbery plateaus. The plateau moduli of vitrimers from monomers was governed by the added amount of crosslinker during polymerization, *i.e.* the higher was the amount of added crosslinker during synthesis, the higher was the modulus (0.5 to 3 MPa for ^{M}**PMMA A V3** to **V5**, see Table 3.1). For low molecular weight systems, crosslinking increased stability: A thermoplastic polymer (M_n = 25 300 kg/mol, see Table 3.1) synthesized under identical starting conditions as the vitrimers could not be tested due to fracture in the DMA grips.

Crosslinking was observed to increase the T_g for materials made via both approaches (up to 24 °C for materials from monomers). For vitrimers from thermoplastics it was observed that the composition of the copolymer chain influenced the T_g of the material: the less pending aldehyde was present, the higher was the T_g (110 °C for **PMMA A V2** and 100 °C for **PMMA A V3** with MMA/$\mathbf{A_1}$ 14/1 and 2/1 respectively). Similarly, processing was shown to increase T_g, most likely via evaporation of remaining small volatile compounds (solvent and imines released during crosslinking). The higher was the crosslink density of higher molecular weight systems the more stable became the rubbery plateau (**PMMA A V4** and **PMMA A V5** with 1.9 and 9.3 crosslinks per chain respectively, see Table 3.3). The DSC results are shifted to lower temperatures compared to DMA results, but confirm the trends regarding the T_g.

3.3.6 Thermogravimetric analysis (TGA) on vitrimers from monomers and thermoplastics

To test whether the implemented imines and aldehydes are stable in the PMMA matrix, TGA measurements on a TG 209 F1 Libra from Netzsch were performed. Therefor, the temperature was either ramped at 10 °C/min or was hold in isothermal mode at 150 °C, 180 °C or 200 °C. Conditions were set to simulate air conditions with a ratio of nitrogen/oxygen 4/1.

The experiments performed with a temperature ramp of 10 °C/min on processed films revealed an increased heat stability of vitrimers with a higher crosslinking density as compared to the thermoplastic **^{M}PMMA A 1** and systems with lower crosslinking density, **^{M}PMMA A V2** and **V3** (Figure 3.15). Whereas **^{M}PMMA A V2** had thermal stability very similar to the thermoplastic control polymer, **^{M}PMMA A 1**, **^{M}PMMA A V3** seemed less stable than the thermoplastic control polymer while, **^{M}PMMA A V4** and **^{M}PMMA A V5** appeared more stable and decomposed at higher temperatures (Figure 3.15). The difference at temperatures <400 °C between powder and compression molded film is most likely due to annealing of the network during processing. **^{M}PMMA A V3** was tested for its mass loss under processing conditions (temperatures). A possible explanation for the surprisingly high mass loss (7-8%) at these temperatures (150 °C, 180 °C, 200 °C) might be the presence of solvent molecules and monomers from the synthesis. However, once these compounds are evaporated, the mass seems to reach a stable value (Figure 3.16). The different thermal analyses (DSC, DMA and TGA) performed **^{M}PMMA A V3** all tend to indicate that this

system might not be representative (problems during synthesis and/or purification) and experiment will have to be reproduced on it.

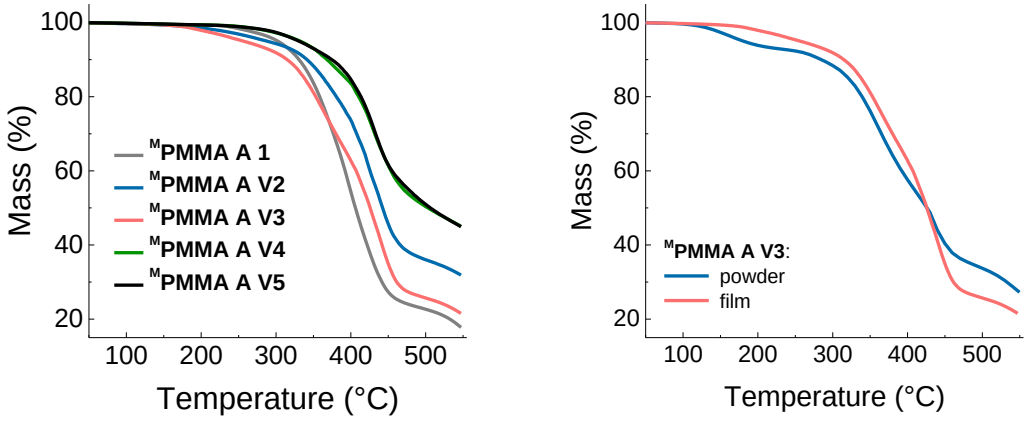

Network	T(-1% mass) (°C)	T(-5% mass) (°C)
^{M}PMMA A 1	230	301
^{M}PMMA A V2	168	286
^{M}PMMA A V3	170	255
^{M}PMMA A V4	246	331
^{M}PMMA A V5	238	331

Figure 3.15. Thermogravimetric analysis on vitrimers from monomers. Heating ramp: 10 °C/min. and N_2/O_2 = 4/1.

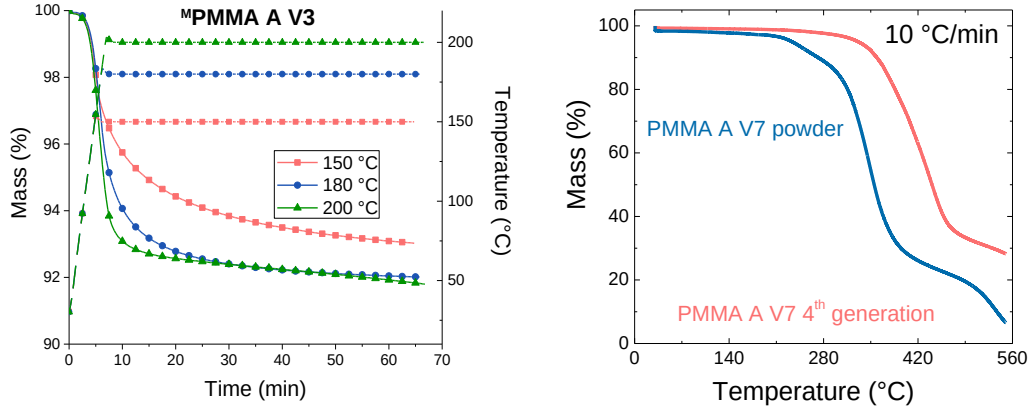

Figure 3.16. Thermogravimetric analyses on vitrimers (N_2/O_2 = 4/1). Left side: Vitrimers from monomers with a ramp of 25 °C/min followed by isothermal mode. Right side: Vitrimers from thermoplastics at 10 °C/min

The impact of processing was even more drastic for **PMMA A V7**. The un-processed powder lost 3% of its initial mass at ca 210 °C in contrast to 315 °C for the 4 times processed film. In contrast to the **^{M}PMMA A** V3 system from monomers the mass loss at processing temperatures was rather small (<3%, powder). This is because samples of vitrimers from thermoplastics can be generated almost entirely free of solvent or monomer molecules due to

repeated precipitation during synthesis. In contrast, vitrimers from monomers contain most likely a higher fraction of free monomers and solvent molecules that are more difficult to remove. During (repeated) processing these small molecules evaporate and the materials then become stable at processing temperatures

3.3.7 Rheology

The rheological properties of polymeric materials depend among others parameters on their molecular weight, structure (*e.g.* branching), interactions between molecules but also processing conditions can play an important role. Rheology can give detailed information about the structure and characteristics of materials and especially for thermoplastics interesting properties such as viscosity, creep-recovery behavior and relaxation times can be measured. By definition crosslinked systems can neither flow nor relax stress and thus have infinite viscosity. In the following section, vitrimer properties such as modulus, creep-recovery behavior, relaxation behavior, relaxation time and viscosity were investigated and compared to thermoplastics in rheological measurements. Vitrimers were analyzed on an ARES G2 from TA Instruments in parallel plate geometry using plates of 25 mm diameter in a convection oven in the presence of air. Samples were compression molded directly into disc shape and placed in the pre-heated geometry under air. After 5 minutes of equilibration, an initial normal force of 10-15 N was applied and the system equilibrated for at least 5 more minutes before the experiment was started.

3.3.7.1 Stress relaxation

Stress relaxation experiments were performed by applying a constant shear strain and monitoring the force to hold the sample at this constant strain. The time of 0.1 seconds after starting the experiment was chosen as t=0, because at this point the gap between th e upper and lower plates was observed to be constant. All of the tested vitrimers relaxed stress. Comparison of the vitrimers with similar molecular weight thermoplastic PMMA reveals that the relaxation process is modified (Figure 3.17). Additionally, the vitrimers **^{M}PMMA A V2** and **V3** relax via two modes whereas more crosslinked systems show a more monomodal behavior. Relaxation of vitrimers slows down for all systems compared to the thermoplastic and was the slowest of aldehyde systems for **^{M}PMMA A V4**. As expected for the weakly crosslinked **^{M}PMMA A V2,** it relaxed in a process more similar to the thermoplastic due to prior relaxation of dangling chain ends and a rather high number of monomers between

crosslinks. Surprisingly, **^{M}PMMA A V5** which is by synthesis more crosslinked than **^{M}PMMA A V4** presents a higher relaxation modulus and relaxes faster, while both vitrimers should have the same concentration .

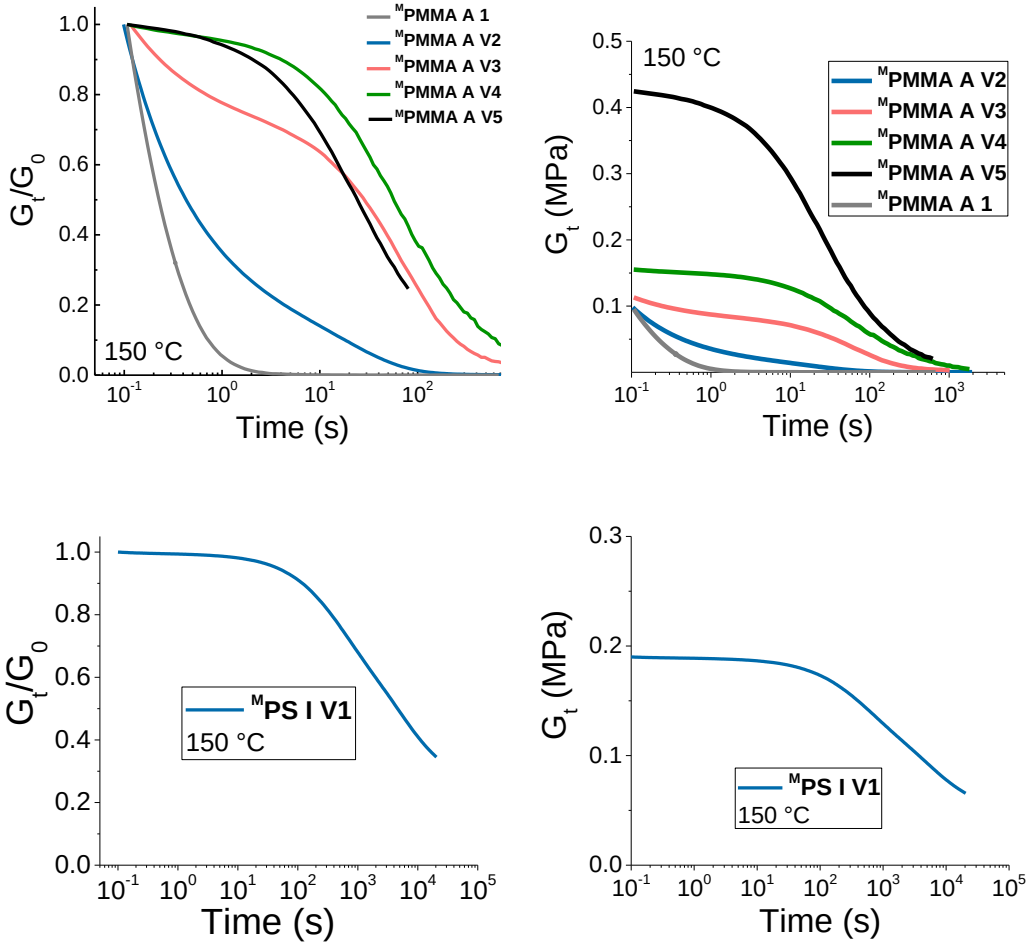

Figure 3.17. Normalized (G_0 at 0.1 s) and as measured stress relaxation curves of vitrimers from monomers (1% deformation). Top row: PMMA-based systems with pending aldehydes. Bottom row: PS-based system with pending imines.

Sample	$G_{0.1s}$ (10^3Pa)	τ (s)
^{M}PMMA A 1	95,2	0,3
^{M}PMMA A V2	98,1	0,9
^{M}PMMA A V3	113,1	57
^{M}PMMA A V4	155,2	102
^{M}PMMA A V5	424,5	42

Table 3.7. Initial relaxation moduli and stress relaxation times of vitrimers from monomers at 150 °C.

To compare to epoxy/acid and epoxy/anhydride vitrimers and assuming a Maxwell model the relaxation is exponential and a characteristic time can hence be defined as:[3]

$$G(\tau) = G_0 * (1/e) \text{ or } G(\tau) = G_0 * 37\%$$

Equation 3.5

The respective relaxation times are presented in Table 3.7 and were as small as 0.9 s for the weakly crosslinked system. The modulus at t = 0.1 s increased with crosslinking density as expected and previously confirmed by the DMA measurements (Figure 3.17). The relaxation times increased with increasing crosslink density except for **^{M}PMMA A V5** (Table 3.7). Figure 3.18 presents the normalized relaxation curves of **^{M}PMMA A V3** and **^{M}PMMA A V4** at different temperatures. All specimens relaxed to very small residual stresses or completely in the time of measurement. As expected and due to accelerated exchange reactions of crosslinks and pending groups the relaxation is faster at higher temperatures. For **^{M}PMMA A V3** a contribution of not-relaxed entanglements to the overall relaxation process was observed. For **^{M}PMMA A V4** this phenomenon was not observed due to a higher crosslink density. Other than the described PMMA-based vitrimers with pending aldehydes and relatively small molecular weight, the polystyrene-based system with pending imines **^{M}PS I V1** (for characteristics see table 3.1) shows a different behavior. At 150 °C the system relaxes much slower and it takes more than 4 hours to reach the characteristic value of 37% remaining stress. It also seemed as if the system would not relax completely. A possible explanation might be the choice of the commoner. It is known that MMA terminates by dismutation, while styrene terminates by recombination. As a consequence, the system based on styrene as comonomer will possess by synthesis a significant number of non exchangeable crosslinks which must slow down viscoelastic processes. In addition, as it was observed in the model studies (see Figure 3.2), the presence of imines under identical conditions (65 °C, 24 h, anisole) seems to decrease the control during RAFT polymerizations. This observation might be a hint for the presence of more branched structures and a reason for the slowing down of the stress relaxation due to permanent and static crosslinks. Another important parameter that must to be taken into account is the slower dynamics of imine-imine exchange as compared to imine-aldehyde and to imine-imine catalyzed by aldehydes exchanges. To verify these assumptions, cleavage tests with an excess of aldehydes or imines similar to those performed on some of the MMA-based vitrimers should be conducted, as well as relaxation experiments in the presence of small aldehyde catalysts.

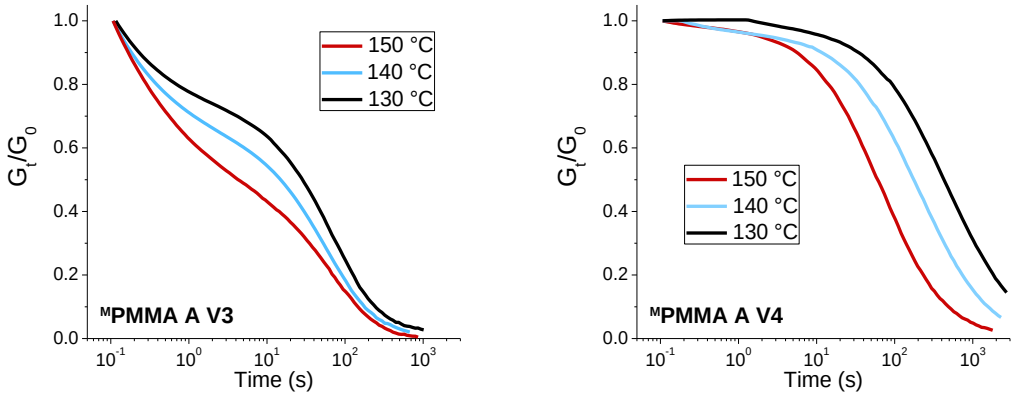

Figure 3.18. Normalized stress relaxation curves of PMMA vitrimers from monomers at different temperatures.

Similar observations were made for systems from functional thermoplastic precursors. The high molecular mass of system **PBMA A V1** (M_n = 430 kg/mol, BMA/**A**$_1$ 2.9/1, 8.1 crosslinks per chain, Table 3.2 and 3.3) has the longer relaxation time with a characteristic time > 4500 s (Figure 3.19). As seen for systems from monomers, vitrimers from polymers with similar molecular weight and pending aldehyde concentration **PMMA A V4/V5/V6** present different relaxation processes according to their crosslink density (Figure 3.19). High molecular weight vitrimer **PMMA A V7** relaxes very fast due to its low crosslink density. In general it was observed that systems which have both entanglements (sufficiently high molecular weight) and more than 2 crosslinks per chain (**PMMA A V5** and **PMMA A V6**) relax rather slowly (τ > 3 hours) under these conditions. As it was observed after the injection molding process, at higher temperatures the systems might lose some degree of their dynamic character and short relaxation times are thus desirable (Figure 3.6).

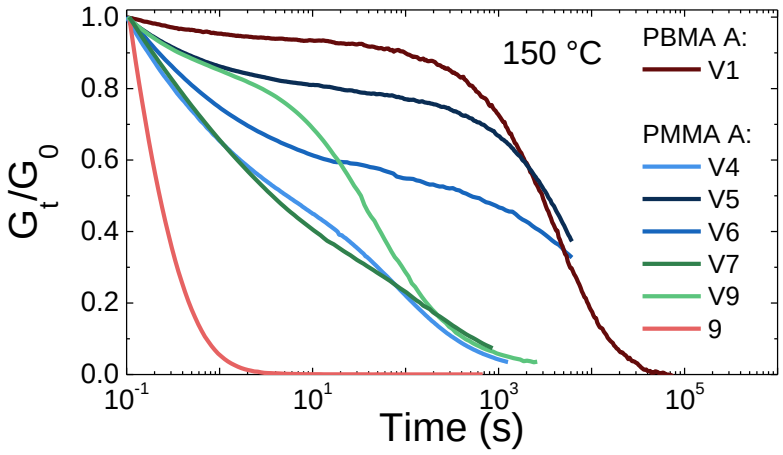

Figure 3.19. Normalized stress relaxation curves at 150 °C of vitrimers obtained from functional thermoplastics.

3.3.7.2 Creep recovery

Creep-recovery experiments were performed to analyze the flow behavior of the reported vitrimer systems at elevated temperature. A constant shear stress was applied to the sample and released after a certain time. The systems elongation under stress and after stress release was monitored and in some cases consecutive creep-recovery cycles were performed.

Figure 3.20 depicts creep-recovery experiments on **^{M}PMMA A V3-V5** at 150 °C under a constant shear stress of 5000 Pa and on the linear **^{M}PMMA A 1** under constant shear stress of 1000 Pa. The vitrimers showed creep and by release of the stress, almost only the initial elastic deformation was recovered. Compared to the thermoplastic, the vitrimers creep is slowed down. Assuming similar molecular weight, the density of dynamic exchanging crosslinks governs the creep and thus the observation that **^{M}PMMA A V5** deformed the least in the same time period under identical stress is coherent.

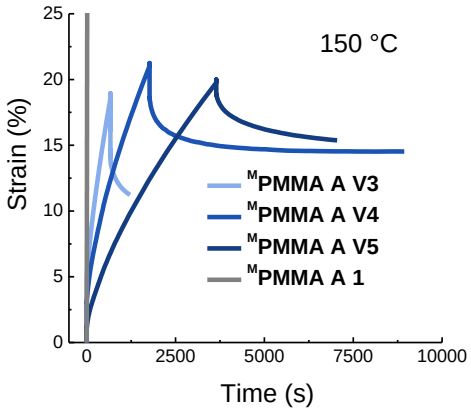

Figure 3.20. Creep-recovery curves of vitrimers from monomers at 150 °C with a shear stress of 5000 Pa.

From the slopes of the creep curves temperature dependent viscosities were determined to be as low as 2.7x10^{5} Pa s at 150 °C for **^{M}PMMA A V3**.[4]

$$\eta_{150\,°C}\,(\text{Pa s}) = \sigma/\text{slope}$$

Equation 3.6.

System	Elastic Modulus G (10^3Pa)	Viscosity (10^3 Pa.s)
^{M}PMMA A 1	not estimated	0,555
^{M}PMMA A V3	97,8	274
^{M}PMMA A V4	164,4	560
^{M}PMMA A V5	427,3	1222

Table 3.8. Estimated viscosities and elastic modulus of vitrimers from monomers from creep-recovery experiments at 150 °C.

Using the following expression, the initial elastic deformation can be converted to the elastic modulus. The determined values fit well with the corresponding moduli observed in the stress relaxation experiment at the same temperature (150 °C) proving the accuracy of the measurements.

$$\frac{\sigma}{\gamma} = G$$

Equation 3.7

Creep-recovery experiments were performed for vitrimers from thermoplastics too. For example when **PMMA A V4** was heated above its T_g and a stress of 4000 Pa was applied it started to creep (Figure 3.21). Depending on temperature, the creep was accelerated or slowed down. The initial elastic moduli at the respective temperatures were similar to those measured in DMA measurements (factor 3).[5] By changing the temperature from 140 °C to 160 °C, the systems viscosity obtained from the slope of the red marked parts of the curve decreased from $2.3x10^6$ Pa.s to $0.5x10^6$ Pa.s (Figure 3.21). Systems with higher molecular weight and/or higher crosslink density crept slower (e.g. **PBMA A V1**) and recovered more deformation (un-relaxed segments) (Figure 3.21). To show that the vitrimers can flow several times **PMMA A V9** was put under a relatively high stress of 10000 Pa (ca 8% initial elastic deformation) and after creep and recovery, the experiment was restarted (Figure 3.21). Although this cycle was repeated in total 5 times and up to a total deformation of almost 50% the material did not lose its ability to flow. Nevertheless and even under high shear stress, for some systems, *e.g.* high molecular weight **PBMA A V1**, rather small deformations and a high amount of recovery were observed.

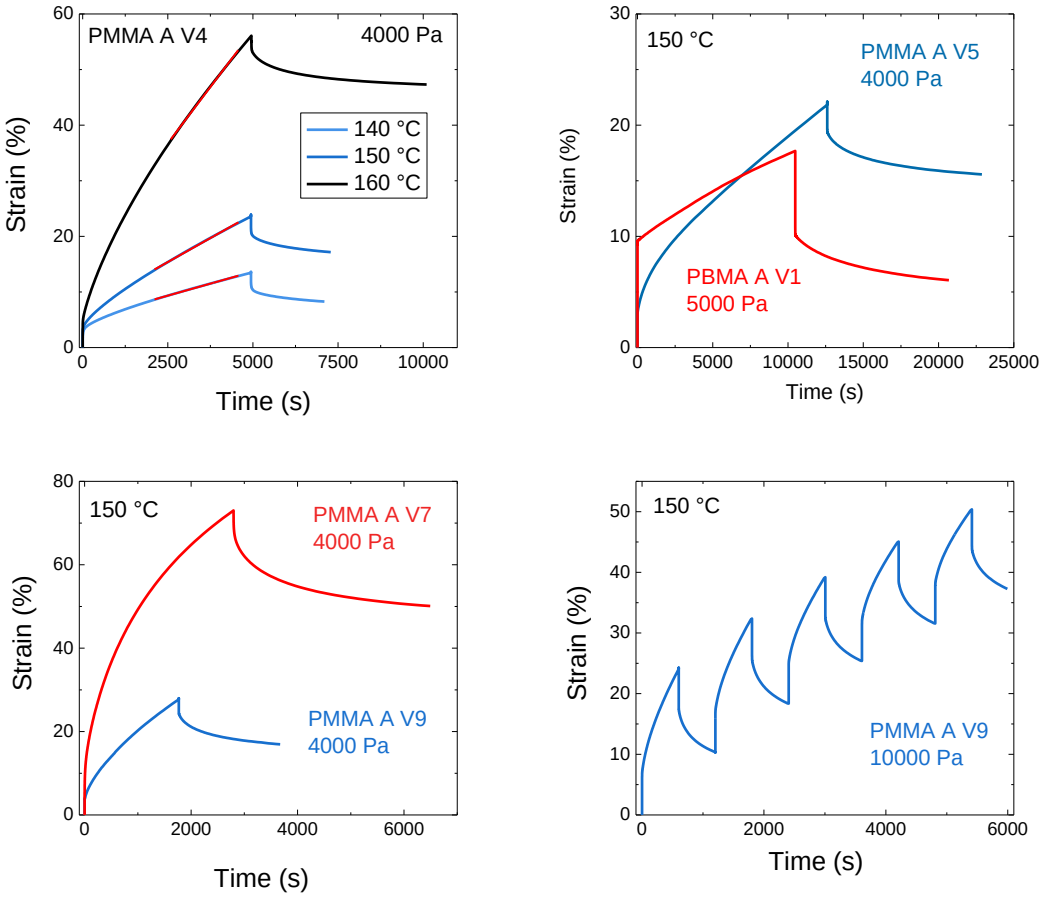

Figure 3.21. Creep-recovery experiments of vitrimers from thermoplastics. **PMMA A V4** was tested at different temperatures.

3.3.7.3 Frequency sweep

With the overall aim to further characterize and understand the vitrimers developed, we performed and compared frequency sweep measurements on a linear polyaldehyde and a vitrimer obtained from this polymer. As for stress relaxation and creep-recovery experiments, specimens of ^{M}**PMMA A 1** and ^{M}**PMMA A V4** were compression molded for 1 h at 150 °C into disc-shape specimens with a diameter of 25 mm. They were equilibrated for 5-10 minutes in the Ares G2 rheometer under an initial normal force of 10-15 N at 150 °C and the experiment was run at 1% deformation from 10^{2} s^{-1} to 10^{-2} s^{-1} radial frequency.

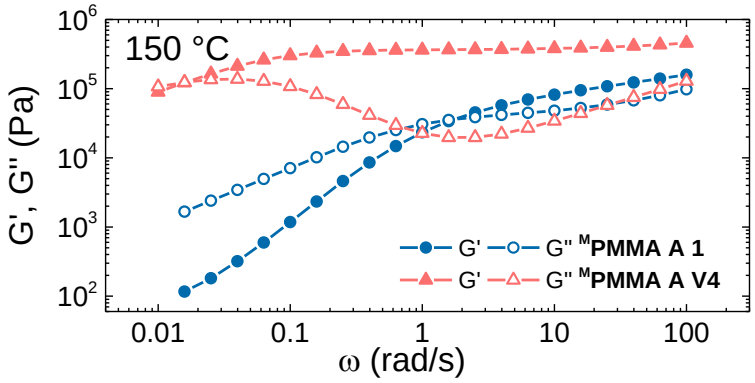

Figure 3.22. Frequency sweep at 1% deformation at 150 °C of a vitrimer from monomers and a similar molecular weight functionalized linear thermoplastic.

Characteristic relaxation times can be measured at G'(ω) = G"(ω) defining the longest relaxation time τ_d, the relaxation by reptation, and the shortest relaxation time τ_e, the relaxation time of chain fragments between entanglements. The following relaxation times, τ_d, were calculated: **^{M}PMMA A 1**: τ_d = 0.09 s and **^{M}PMMA A V4**: τ_d = 9.9 s. From the evolution of the shear modulus of the thermoplastic **^{M}PMMA A 1** (Figure 3.22) it can be concluded that the system is slightly entangled and considerations of the molecular weight of the polymer confirm this assumption (see cleavage experiments, Table 3.4). It is known that the mass of the polymer must be several times superior to the mass between entanglements M_e to exhibit a plateau between the two characteristic relaxation times. Indeed the mass of the tested thermoplastic (M = ca 25 000 Da) is superior than the reported mass between entanglements for a PMMA homopolymer of M_e = 12 500 Da but it is not high enough to result in a real plateau.[6] The vitrimer, by contrast, clearly exhibits a plateau and has an increased shear modulus G' at any chosen frequency. Its plateau can be attributed to the presence of crosslinks between chains. However, thanks to the dynamic nature of these crosslinks to exchange reversibly in the presence of pending monofunctional groups, the system relaxes eventually with an increased τ_d of *ca*. two orders of magnitudes.

3.3.8 Mechanical testing

Thanks to their ability to flow above a material characteristic temperature (T_g, T_m) thermoplastics are re-processable once synthesized and can be recycled. Thermosets on the other hand cannot be re-processed once cured and must be synthesized in their final shape. Mechanical testing and cyclic re-processing/recycling experiments were performed to test the vitrimers mechanical properties and their re-processability. Therefor, compression molded

dumbbell-shape specimen (150 °C, 1 h, l = 9.0 mm, w = 2.1 mm, h = 1.8 mm) were elongated to rupture at room temperature at 1.0-1.5 mm/min using an Instron 5564 tensile machine mounted with a 2 kN cell (Figure 3.23). Once tested, samples were cut into small pieces by hand and re-processed at 150 °C for 1 h and re-tested. Three different vitrimers from thermoplastics were analyzed.

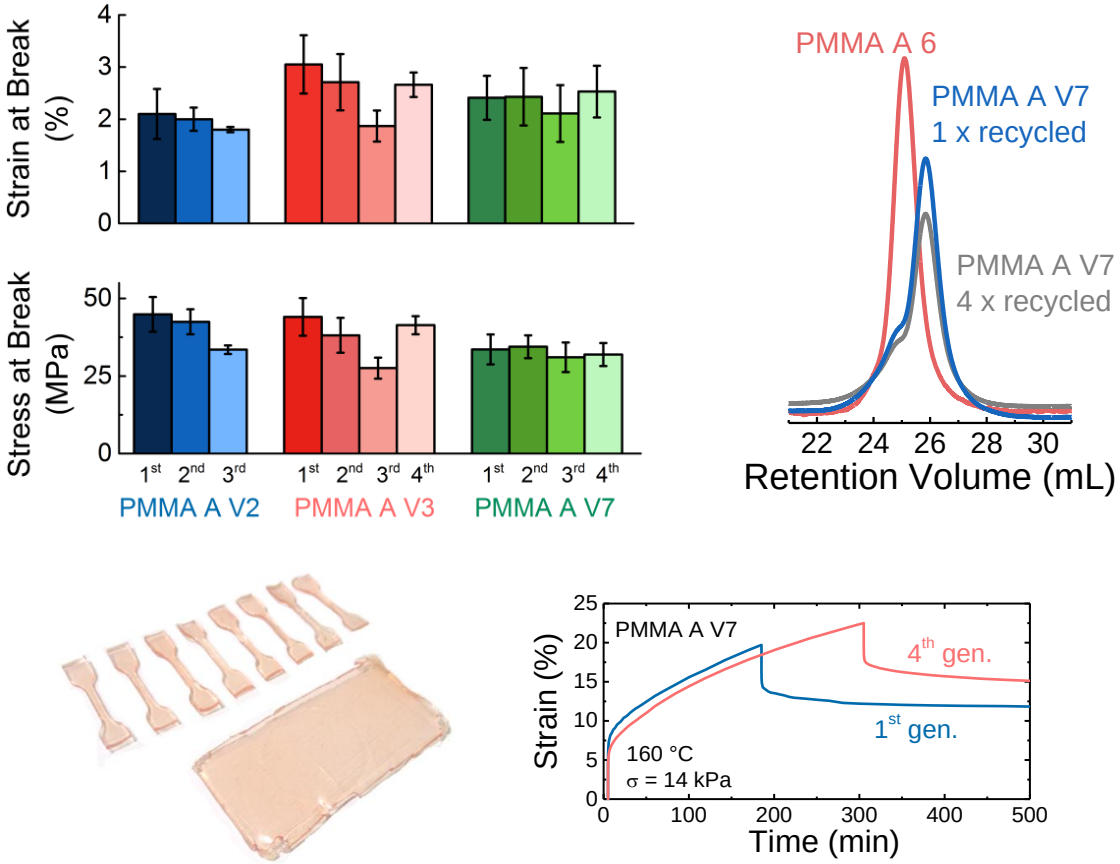

Figure 3.23. Top left: Mechanical properties of vitrimers prepared from functional thermoplastics. Top right: GPC raw data of the functional thermoplastic precursor and after de-crosslinking of one and four times processed samples. Bottom left: Tested dumbbell-shape specimen. Bottom right: Creep-recovery experiment with one and four times processed samples at 160 °C under a stress of 14 kPa in DMA.

All three tested systems could be re-processed by compression molding. The recycled specimes were transparent and nor cracks nor marks of the initial small pieces were visible. At room temperature stress and strain at break were mostly governed by molecular weight. In comparison to **PMMA A V7** with a stress at breakof 34 MPa, the materials **V2** and **V3** were composed of polydisperse and higher molecular weight backbone chains (M_n = 164 kg/mol and M_n = 356 kg/mol and $Đ$ = 2.07 and 2.60 respectively) and thus broke at higher load of 45 MPa and 44 MPa respectively (Figure 3.23). Recovery of initial stress at break in third generation for **V3** (63%) was observed to be inferior than in **V2** (75%) and might be

explained by the higher molecular mass and hence a possible higher viscosity (see table 3.2), which results in less efficient dynamic bond exchange. However, after compression molding of third generation **V3** for 3 hours instead of 1 hour, the system recovered up to 94% of the initial value. System **V7** with a lower crosslink density showed superior performance recovering up to 93% in third generation material and an identical value in its fourth generation due to lower viscosity (Figure 3.23). Elongation at rupture was observed to evolve silmilarly for all three systems **V2** (2.1%), **V3** (2.7%) and **V7** (2.4%). As found for the stress at break, **V7** recycles more effectively (86% in third generation) than **V3** (62% in third generation, but 87% in fourth generation). System **V7** elongates up to 2.4% and in its fourth generation the initial elongation was recovered completely (102%). Creep-recovery experiments on one time and four times recycled specimens proved that even after several cycles of re-processing the vitrimers keep their ability to flow. The films were fixed in a DMA machine and tested in tension mode at 160 °C under a stress of 14 kPa. A slight increase in initial elastic modulus (233 kPa to former 190 kPa) was observed for the four times recycled sample which is coherent with observations in other DMA experiments (annealing). Other than that, the viscosities (ca $4x10^7$ Pa s), *i.e.* the slope of the creep curves, were identical for the two specimens reaching ca 20% elongation after 3 hours under these conditions (Figure 3.23). To show that the crosslinks kept their dynamic behavior even after four re-processing steps, we performed de-crosslinking experiments as shown for gels and vitrimers from monomers. First and fourth generation samples of **PMMA A V7** (50 - 100 mg) were immersed in anhydrous THF (10 mL) and after addition of an excess of benzaldehyde $\mathbf{A_4}$ (0.5 mL) full dissolution was observed after 3 days at room temperature. GPC results indicated a small decrease in molecular weight between linear precursor and vitrimers. The molecular weight between one time recycled and four times recycled specimen were very similar (Figure 3.23, parent thermoplastic, de-crosslinked vitrimers of 1st and 4th generation: M_n = 131 kg/mol, M_n = 95 kg/mol and M_n = 91 kg/mol, $Đ$ = 1.20, 1.47 and 1.58). Comparing these results to the parent thermoplastic, a decrease in molecular weight, most likely caused by some chain scission, was observed. Taking into account these observations, it can be concluded that no or very few side reactions involving the dynamic covalent links occurred in the system during re-processing.

3.3.9 Malleability of vitrimers

Their ability to flow while keeping their crosslink density constant allows vitrimers to be welded like glass. Usually, the flow of thermoplastics follows the WLF equation once they are above a characteristic transition temperature. Vitrimers, thanks to their increased yet controllable viscosity, are easily malleable because their viscosity changes gradually and follows an Arrhenius law. By simple pressing a coin onto a compression molded **PMMA A V7** at 150 °C for 5 minutes the vitrimers surface adapts the coins pattern (Figure 3.24). When the system is re-heated without the coin, the pattern did not disappear. In a similar experiment, a rectangular specimen of the same system was kept by clamps in a fixed twist at 120 °C for 30 minutes. Upon removal of the clamps at room temperature, the system did not untwist. Even when re-heating to 120 °C for several minutes the system did not go back to its original shape meaning that the twist had become its new equilibrium state. When an identical sample was twisted for shorter times than the time of relaxation of the system at 120 °C (*ca.* 5 minutes) the system untwisted upon removal of the clamps at 120 °C (Figure 3.24).

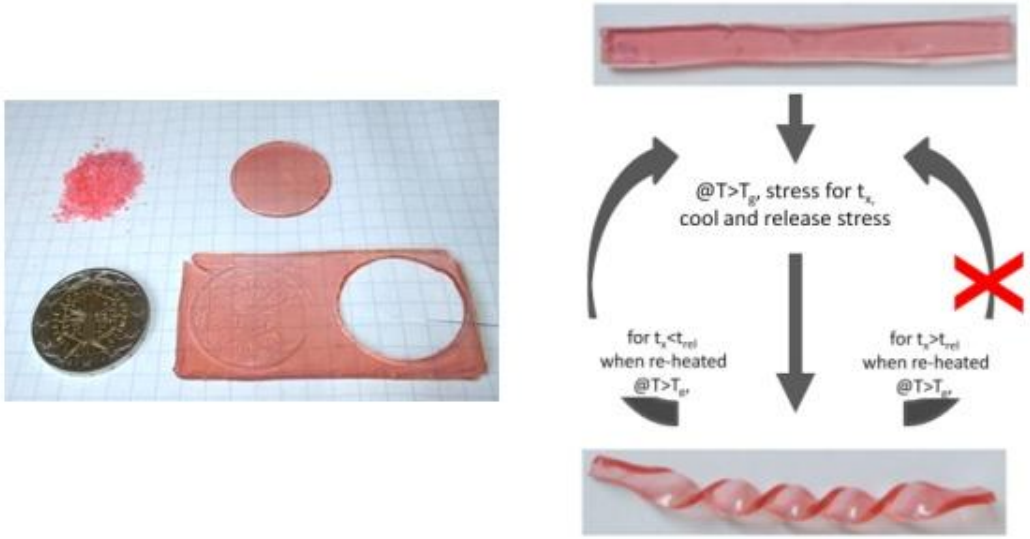

Figure 3.24. Malleability of vitrimers: “minting” and twisting and untwisting of vitrimers.

3.4 Conclusions

The generation and characterization of vitrimers from vinylic monomers, such as MMA, BMA and PS, containing pending aldehyde or imine functionalities and imine crosslinks are

presented in this chapter. In chapter 2, it was demonstrated that bulk exchange reactions between imines and aldehydes and between imines catalyzed by aldehydes can proceed with high rates (time to reach equilibrium for the imine-imine mixture ≤ 10 minutes) at relatively moderate temperatures (60 °C) in the presence of (very) small traces of amines/aldehydes. Taking advantage of these dynamic reactions, two synthetic approaches were tested: vitrimers were generated from monomers via a one-pot method in the presence of a polymerizable bis-imine crosslinker or by the addition of a non polymerizable bis-imine crosslinker to functional thermoplastics containing pendant aldehyde and/or imine functions. It was tested and verified that controlled radical polymerization of vinyl monomers containing pending aldehyde or imine functionalities is possible and that these functionalities keep their exchangeable character after polymerization and processing. Resulting materials were insoluble and showed other thermosetting properties such as rubbery plateaus in DMA experiments. The degree of crosslinking influences numerous properties such as the T_g, the modulus on the rubbery plateau, the relaxation time and the viscosities of the melt. Although crosslinked, these systems could be (re)-processed via compression molding, yielding recycled vitrimers with preserved mechanical properties even after several processing steps. For some systems, industrial processing techniques such as extrusion and injection molding were tested. In general, the presented vitrimers relax stress and creep so that viscosities between 10^5 and 10^7 Pa.s, depending on molecular weight, crosslink density, functionality and temperature, could be measured. It was even shown, using low molecular weight or systems with low crosslink density, that de-crosslinking after several cycles of (re)-processing can be achieved by addition of an excess of benzaldehyde. In these cases, the molecular weight of linear polymer chains did not change significantly during processing. Nevertheless, it was observed that for some systems, especially those with a high imine content, side reactions cannot be excluded. Assuming a given % of side reactions, systems with a high molecular weight would be affected differently (more) than systems based on small molecular weight polymers. For example, some PMMA systems (from thermoplastics) with molecular weights of ca M_n > 50 000 g/mol, which are required to obtain good mechanical properties, and crosslink densities of more than two functionalities per chain, exhibited rather slow and incomplete stress relaxation at 150 °C (more than 4 hours or 3 hours respectively). Similar results were obtained in creep-recovery experiments of the PMMA systems resulting in the need of long processing times. Additionally, already low molecular weight PMMA vitrimers showed secondary reactions in stress relaxation experiments after one injection molding cycle (200 °C, ca 4% remaining stress). In regard of applications and especially for PMMA

materials where the control of color is very important, imines might have an additional drawback. The generated vitrimers were yellow after removal of the RAFT chain-ends and changed their color to orange and reddish the higher the processing temperature and the longer the processing time. Although the high temperature and processing stabilities of imine based vitrimers need to be improved, and the dynamic of exchanged probably accelerated, depending on the polymer matrices and applications targeted, the reported systems show unique properties. They are crosslinked, yet (re)-processable and the concept of introducing pending dynamic bonds and crosslinks into thermoplastic can be expanded to other matrices and chemistries.

3.5 References

1. D. Bradley, G. Williams and M. Lawton, *J. Org. Chem.* **2010**, 75, 8351.
2. C. Barner-Kowollik, "Handbook of RAFT Polymerization", Wiley-VCH, **2008**.
3. D. Montarnal, M. Capelot, F. Tournilhac, L. Leibler, *Science*, **2011**, *334*, 965.
4. J. D. Ferry, "Viscoelastic Properties of Polymers" 3rd edition, John Wiley&Sons, **1980**.
5. M. T. Shaw, "Introduction to Polymer Rheology", Wiley, **2012**.
6. J. E. Mark, "Physical properties of polymer Handbook" 2nd edition, chap 25, 448, Springer, **2007**.

Chapter 4

Dynamic Exchange Reactions of Boronic Esters

Table of Contents

Chapter 4 – Dynamic Exchange Reactions of Boronic Esters

4.1 Introduction

Boronic acid containing substances have been utilized in a wide range of applications.[1-14] Small molecules and low molecular weight compounds are known to serve as protecting groups in organic chemistry and as intermediate structures in C-C coupling reactions such as Suzuki-Miyaura and others (*e.g.* Chan-Lam and Liebeskind-Srogl).[15-22] Additionally, they were used in conjugate addition, oxidation, homologation and C-H coupling reactions and molecular self-assembly.[23-26] Macromolecules containing boronic acids and their derivatives have found application in dynamic covalent materials, thermo- and chemo-responsive gels, drug carrying and releasing agents, biosensors, nanomaterials, separation, chromatography, cell capture and culture substrates, enzymatic inhibition, molecular hierarchical structures, cages and many others.[27-52] This chapter focuses on exchange reactions involving boronic esters.

The first reported synthesized organoboron compound was ethylboronic acid by Frankland in 1860.[53] The hydrolysis of dichlorophenyl borane was shown in the 1880s to yield phenylboronic acid, one of the most used building blocks in the field of boronic acids today.[54] Finally, the reaction of organometallic compounds based on lithium or magnesium (Grignards) with trialkyl borates and successive hydrolysis was established as the main synthetic route.[55] In the main synthetic route, one of the three carbon linked to the boron atom of trialkyl borates (trialkylborane) is hydrolyzed to yield the corresponding borinic acid which contains only a single hydroxyl group (Scheme 4.1). Borinic acids are more stable than their parent boranes but can easily be further hydrolyzed to boronic acids and eventually to boric acid with all alkyl groups replaced by hydroxyl groups. Boronic acids can form cyclic anhydride species, called boroxines, by the condensation reaction of three boronic acids and the release of water (Scheme 4.1). [1]

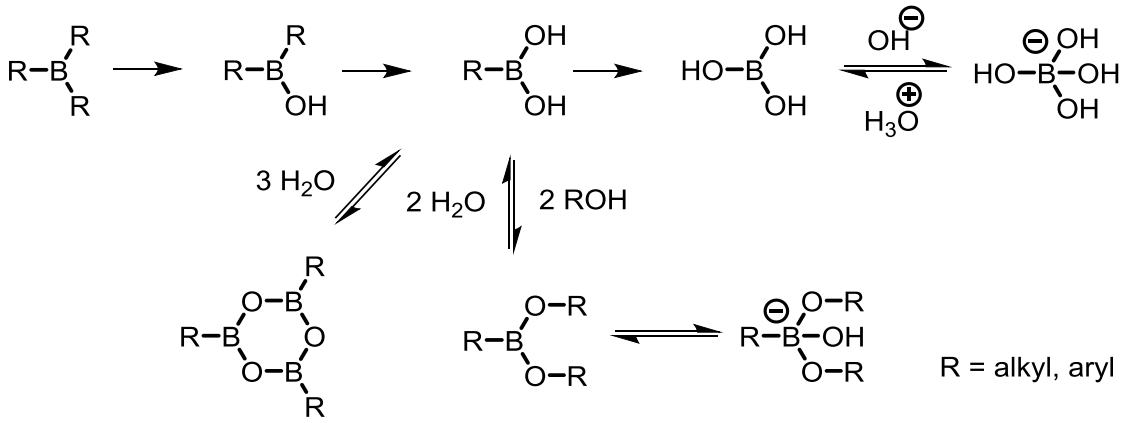

Scheme 4.1. General scheme of the main synthetic route of boronic acids and esters.

In the neutral form, the boron-atom of a boronic acid exists in a trigonal planar sp^2-hybridization with 6 valence electrons and a vacant *p*-orbital making it Lewis acidic. This and the easy accessibility favor the complexation with Lewis bases and the shift from sp^2 to tetrahedral sp^3 hybridization state. It was shown in aqueous media that at a boronic acid specific pH-value, hydroxyl-ions function as Lewis bases towards boronic acids. The pKa of boronic acids was then defined as the value where 50% of the boron centers exist as anionic boronate species. It was proven that the substitution pattern influences the pKa and values from 4.0 to 10.5 where reported for the most common boronic acids.[1] Addition of electron-donating substituents on the aromatic ring of the acid moiety can increase the pKa through inductive effects whereas electron-drawing functionalities can decrease the pKa.[56-63]

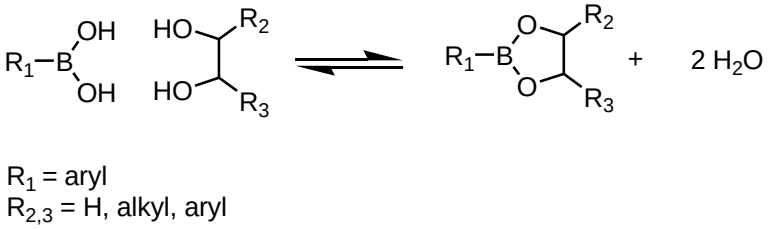

Scheme 4.2. General scheme of the condensation reaction between a boronic acid and a 1,2-diol to form a dioxaborolane.

The condensation reaction of boronic acids with diols results in the formation of boronic esters and water (Scheme 4.2). The characteristic equilibrium composition of boronic acid/diol and boronic ester/water was investigated in several studies and depends on the nature of the boronic acid, of the diol and on the reaction conditions. In water, boronic esters are formed above the pKa of the respective boronic acid either from the neutral planar or the anionic tetrahedral form.[1,64] Intramolecular complexation, *e.g.* in Wulff-type boronic acids, where a nitrogen-atom forms a dative (intramolecular) N-B bond or in the presence of

adjacent carbonyl functionalities, can change the pKa and the hydrolytic stability of boronic esters (Scheme 4.3).[1,64-67] Although exchange reactions of boronic acids and boronic esters in aqueous media were investigated thoroughly, there is rather few work reported in non-aqueous media.[68-76] In organic solvents, the spontaneous formation of *para*-substituted arylboronic esters with both diols and diamines was reported and supported by computational investigations. Interestingly, the influence of the substituent in *para*-position has a lower impact on the yield of formation of boronic esters than the choice of the donor, e.g. catechol typically gives product yields >90%. Other donors, such as dithiols, seem not to form stable products.[64]

It is known that boronic esters, depending on their stability towards hydrolysis, can degrade into boronic acid and the diol once they are in contact with water, or even when in contact with moisture (see subchapter 4.5). All other structural parameters kept aside, acyclic boronic esters and five membered cycle boronic esters, called dioxaborolanes, are more sensitive to hydrolysis than 6-membered boronic esters, known as dioxaborinanes. According to this, 1,3-diols form more stable boronic esters than their 1,2 analogues due to a higher stability of the resulting 6-membered rings (no ring strain). Boronic esters with 1,2-cyclohexanediol or related structures are more prone to hydrolysis than their linear aliphatic analogues due to an unfavorable conformation of the hydroxyl oxygens.[1] However, other species with B-O bond stabilizing intramolecular coordination, *e.g.* adjacent nitrogen atoms, or with bulky substituents on the diol moiety, *e.g.* pinacol containing boronic esters, are much less prone to hydrolysis.

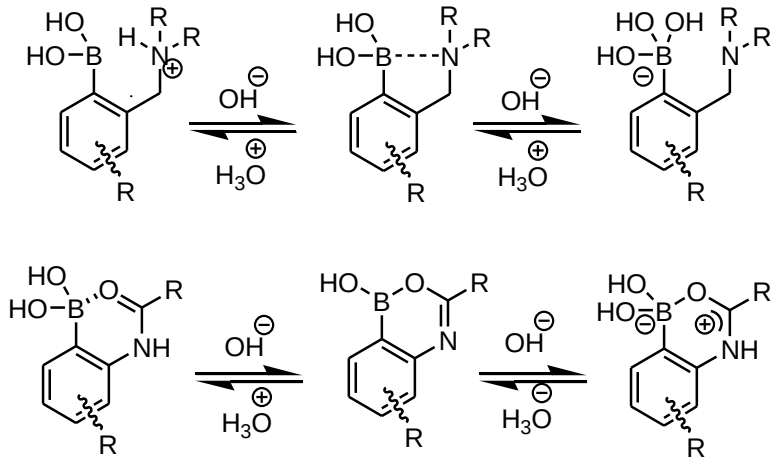

Scheme 4.3. Top: Wulff-type boronic acids. Bottom: Coordination in the presence of carbonyl functionalities.

Water removal during boronic ester synthesis drives the equilibrium to product side and the boronic ester can be obtained in good to very good yields. Different approaches exist such as

the addition of trapping agents (magnesium sulfate, molecular sieves) or azeotropic distillation with a Dean-Stark apparatus. Boronic esters can undergo transesterification in the presence of free diols to produce another boronic ester under release of the former bonded diol. The rate and efficiency of transesterification of a specific boronic ester with a specific diol depends on multiple parameters and is strongly related to the boronic acid substitution pattern, the diol donor ability and the boronic ester stability.[76] Boronic ester transesterification can be extremely fast in the presence of electron-withdrawing substituted dioxaborolanes containing an aliphatic diol functionality. Due to its bulkiness, pinacol containing boronic esters transesterify very slowly or not at all. Other parameters, such as ring-strain can play an important role, too. That is why, boronic esters containing 1,3-diols react slower, and form more stable boronic esters than their 1,2-diol counterparts. Other diols like the 1,5-diethanolamine forms stable bicyclic chelate boronic esters from 2-(phenyl)-1,3,2-dioxaborolane due to intramolecular coordination between the nitrogen and the boron-atom. Cyclic *trans*-1,2 diols were observed to be unreactive due to sterical effects whereas compounds in *cis*-conformation can exchange rapidly.

With the overall aim to introduce boronic ester exchanges into high T_g polymeric networks and to generate new dynamic covalent materials, a detailed kinetic study of the possible exchange reactions with boronic esters is reported. A procedure which allows the formation of highly pure boronic esters is presented and dissociation and association equilibrium constants of some relevant boronic esters are estimated. The influence of important factors such as the presence of moisture and protective atmosphere were investigated for mixtures of two dioxaborolanes and other boronic esters. Transesterification exchange kinetics between dioxaborolanes or dioxaborinanes with 1,2- or 1,3-aliphatic diols were studied. To estimate the rate constant and the activation energy for the transesterification of dioxaborolanes, two highly pure dioxaborolanes were mixed with known amounts of free diol at various temperatures under protective atmosphere. Eventually, the bulk reaction of two highly pure dioxaborolanes without the addition of any water or diol was observed and studied.

4.2 General experimental methods

Chemicals, solvents and gases: Boronic acids, diols and other chemicals were purchased from Sigma Aldrich, Alfa Aesar, TCI, Acros and Fischer. Solvents and deuterated solvents were stored under inert atmosphere over fresh and dried molecular sieves 3Å. The respective ratio

of molecular sieves to solvent (% mass/volume) and the minimum time to achieve dryness for each solvent were taken from literature.[77] The diols used as reactants and benzoic acid and triethylamine used as catalysts were dried over $MgSO_4$ and NaOH respectively (in DCM for benzoic acid and in bulk for triethylamine) and filtered. After concentration under reduced pressure at elevated temperature to remove any traces of water, they were stored under inert atmosphere. Argon in highest available purity (alphagaz 2, <0.5 ppm H_2O) was purchased from Air Liquide.

Glassware: Glassware was oven-dried and purged with nitrogen or argon while heating with a heat gun before addition of the chemicals.

NMR analysis: ^{1}H-NMR, ^{11}B-NMR and ^{13}C-HNMR analysis was conducted on a Bruker Ultra Shield machine at 400 MHz or 100 MHz, respectively. NMR tubes were oven dried and quartz tubes were used for ^{11}B-NMR studies. If not stated otherwise, samples of 10 mg were analyzed and the obtained data were internally referred to the standard shift of the respective deuterated solvent.

GC analysis: GC analysis was conducted on a Shimadzu gas chromatograph GC-2014 equipped with a Zebron-5HT "inferno" column and helium as carrier gas. Injection was done manually by injecting 1 µL sample volumes using a 10 µL syringe from Hamilton (gastight 1701). Before running analysis the entire set-up was pre-heated to 350 °C and kept at constant carrier gas flow of 5 mL/min and split ratio of 2.0 for at least 30 minutes. The GC method (T_{inj}, T_{col}, T_{det}, gas flow, split ratio) was chosen according to the nature of the studied molecules and the respective exchange reaction. The column was reconstituted regularly by heating to 350 °C as described above.

GC/MS analysis: Samples were analyzed either on a Trace-GC Ultra gas chromatograph coupled to an ITQ900 (Thermo Scientific) and performed by electronic impact ionization, or by infusion on an ion trap mass spectrometer ESQUIRE (Bruker) and performed by APCI.

More detailed descriptions of the machines and methods used can be found in the respective sections.

4.3 Synthesis, purification, storage and characterization of boronic esters

4.3.1 Synthesis, purification and storage of boronic esters

Boronic esters were synthesized by condensation between a boronic acid and a diol (Figure 4.1).[1]

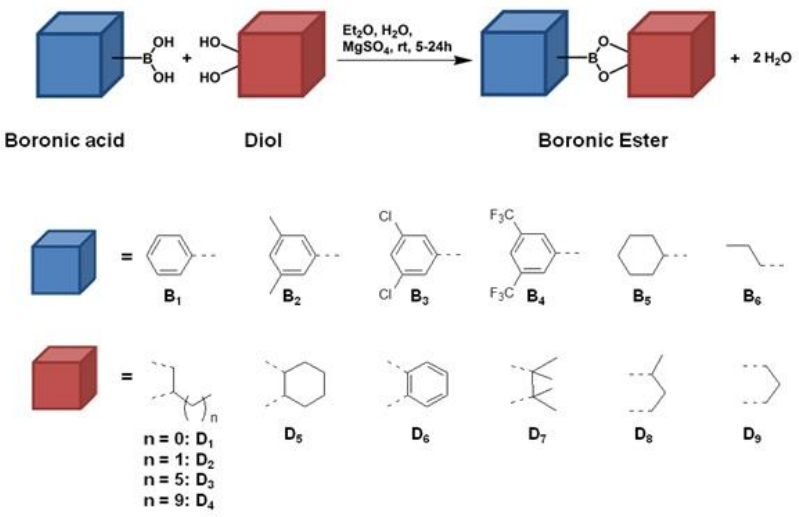

Figure 4.1. General scheme of boronic ester formation. Blue box: Rest attached to the boron atom, red box: Rest attached to diol functionality.

Three different strategies were used. Differences in the purification steps yielded compounds in very high purity, used as reactants in experiments under inert atmosphere (strategy 1), in high purity, used as reactants in experiments under air (strategy 2) and in decent purity for boronic esters used for external calibration (strategy 3).

Strategy 1: **B_1D_2**, **B_2D_1** and **B_1D_9**:

The diol (1.0 eq), the boronic acid (1.05 eq) and 0.1 vol% of water were mixed in Et_2O (2 mL/1 mmol boronic acid) at room temperature and stirred until complete dissolution of all compounds. $MgSO_4$ (3.0 eq) was added stepwise and the mixture was stirred at room temperature for 5-24 hours, filtered and concentrated under reduced pressure. The suspension was immersed in anhydrous heptane, stirred for 30 minutes at room temperature, filtered and the liquid phase was concentrated under reduced pressure. The resulting oil was distilled at

150 °C under high vacuum to yield the target compounds in very high purity as colorless oils (65-80%). The purified boronic esters were transferred directly to dried and purged Schlenk flasks and kept under inert atmosphere (argon).

Strategy 2: **B_1D_1**, **B_2D_5**, **B_2D_8**, **B_2D_9**, **B_3D_1**, **B_3D_3**, **B_4D_2**, **B_4D_4**, **B_5D_1**, **B_6D_4**

The diol (0.99-1.01 eq), the boronic acid (1.00 eq) and 0.1vol% of water were mixed in Et_2O (2 mL/1 mmol boronic acid) at room temperature and stirred until complete dissolution of all compounds. $MgSO_4$ (3.0 eq) was added stepwise and the mixture was stirred at room temperature for 5-24 hours, filtered and concentrated under reduced pressure. The suspension was immersed in anhydrous heptane, stirred for 30 minutes at room temperature, filtered and the liquid phase was concentrated under reduced pressure to yield the target compounds in high purity as colorless oils or white solids (30-80%). The purified boronic esters were transferred directly into small septum closed vials and tested.

Strategy 3: **B_1D_4**, **B_1D_6**, **B_1D_7**, **B_1D_8**, **B_2D_2**, **B_2D_3**, **B_2D_4**, **B_2D_6**, **B_3D_2**, **B_3D_4**, **B_3D_6**, **B_4D_1**, **B_4D_3**, **B_4D_6**, **B_4D_8**, **B_5D_4**, **B_5D_5**, **B_5D_8**, **B_6D_1**, **B_6D_6**, **B_6D_8**

The diol (0.99-1.01 eq), the boronic acid (1.00 eq) and 0.1vol% of water were mixed in Et_2O (2 mL/1 mmol boronic acid) at room temperature and stirred until complete dissolution of all compounds. $MgSO_4$ (3.0 eq) was added stepwise and the mixture was stirred at room temperature for 5-24 hours. The suspension was filtered and concentrated under reduced pressure to yield the target compounds as colorless oils or white solids (30-78%). The boronic esters were transferred directly into small septum closed vials.

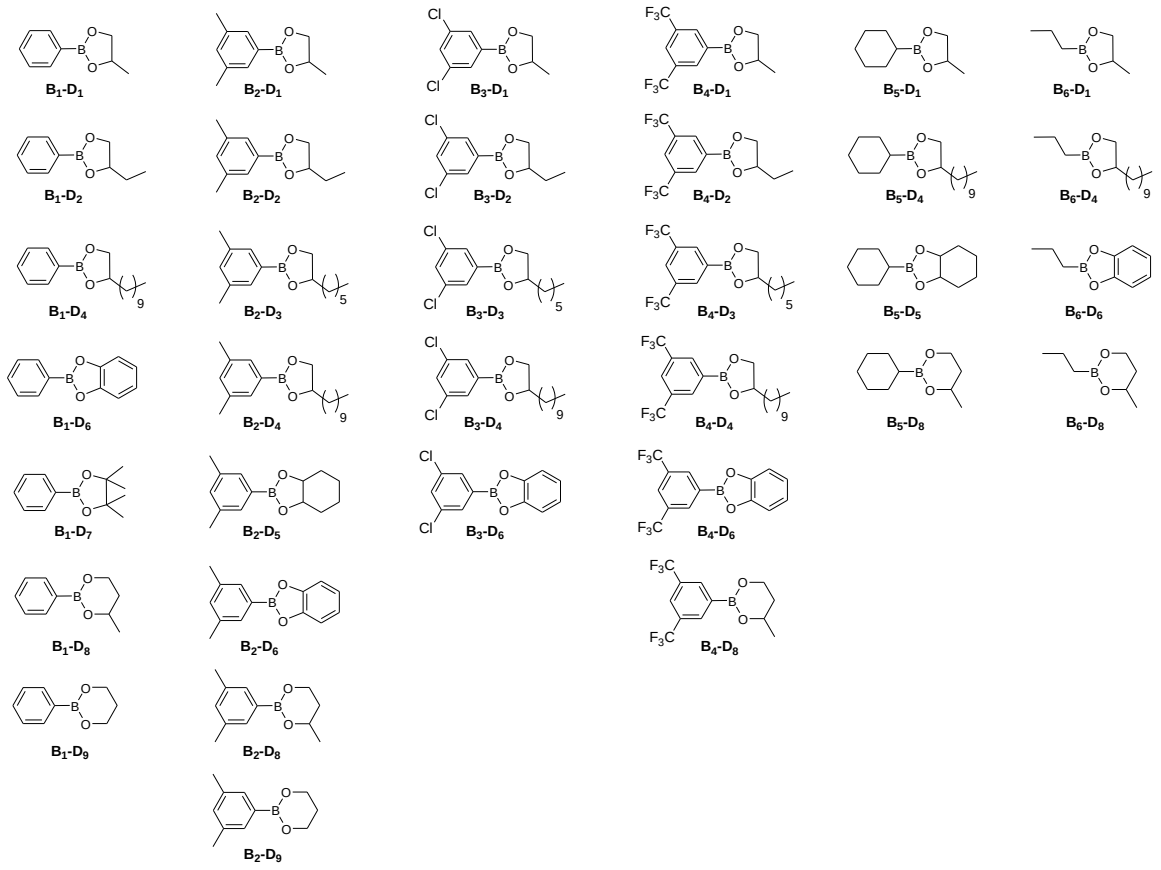

Figure 4.2. Boronic esters synthesized and studied in model experiments, organized according to the boronic acid radical.

4.3.2 Detection limit of 1, 2-butanediol in ^{1}H-NMR spectroscopy

To determine the purity of boronic esters generated via strategy 1, the detection limit for free diol compounds in ^{1}H-NMR analysis was estimated by deliberately decreasing the concentration of 1,2 butanediol (**D_2**) in $CDCl_3$ (Table 4.1). A stock solution of **D_2** at a concentration of 25.5 mM was generated and further diluted with the deuterated solvent. Styrene was added as internal standard (at a concentration of 25.0 mM) to the deuterated chloroform before it was dried with molecular sieves and the stock solution was prepared.

Stock Solution $\mathbf{D_2}$				
m (mg)	**M (g/mol)**	**n (mmol)**	**V_{CDCL3} (L)**	**c (mM)**
11,5	90.12	0.128	0,005	25,5

#	c_{D2} (mM)	Chemical shift (ppm)						
		Styrene		$\mathbf{D_2}$				
		6,72	5,75	3,67 (CH_2)	3,44 (CH)	1,99 (CH)	1,81 (CH)	0,97 (CH_3)
F1	25,52	1	1,03	2,31	1,21	1,1	1,12	3,51
F2	10	1	1,02	0,79	0,42	0,38	0,37	1,15
F3	5	1	1,03	0,39	0,21	0,19	0,19	0,55
F4	1	1	1,03	0,13	0,07	0,06	0,06	0,15
F5	0,5	1	1,03	0,1	0,06	0,05	0,05	0,09
F6	0,1	1	1,03	nd*	nd*	nd*	nd*	0,03
*nd = not detectable								

Table 4.1. Determination of the detection limit of 1,2-butanediol ($\mathbf{D_2}$) in ^{1}H-NMR spectroscopy: Concentration and integration values of 1,2-butanediol in $CDCl_3$.

In total six solutions were analyzed. In the ^{1}H-NMR spectrum of the 0.5 mM solution, $\mathbf{D_2}$ can still be detected and the integration values of the different signals match rather well. At a concentration of 0.1 mM the signals of $\mathbf{D_2}$ cannot be detected anymore with exception of the CH_3-signal at 0.98 ppm. At a concentration below 1 mM the correlation to the internal standard styrene becomes rather imprecise.

Assuming a detection limit of 0.1 mM, the maximum free diol content in the synthesized boronic esters $\mathbf{B_1D_2}$, $\mathbf{B_2D_1}$ and $\mathbf{B_1D_9}$ was estimated by analyzing highly concentrated boronic ester solutions in ^{1}H-NMR spectroscopy (Figures 4.3, 4.4 and 4.5).

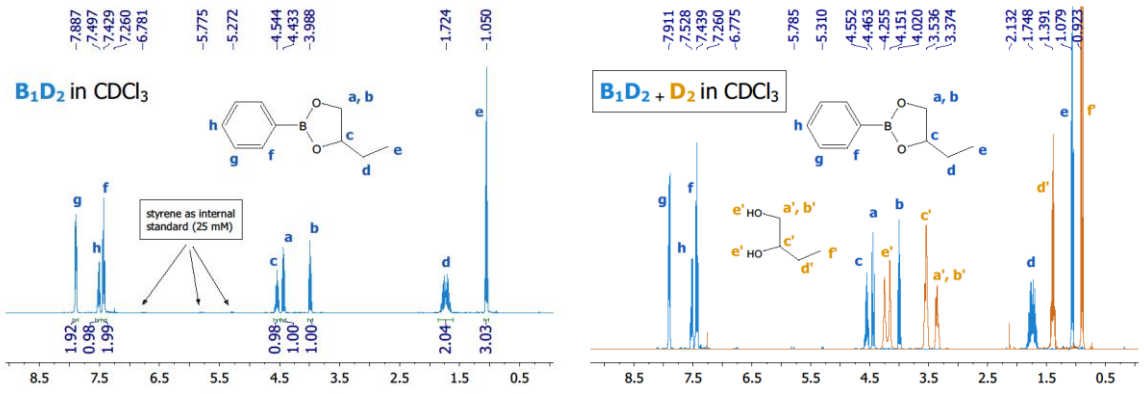

Figure 4.3. ^{1}H-NMR analysis in $CDCl_3$of $\mathbf{B_1D_2}$ (1 M, left) and the overlap with free $\mathbf{D_2}$ (right).

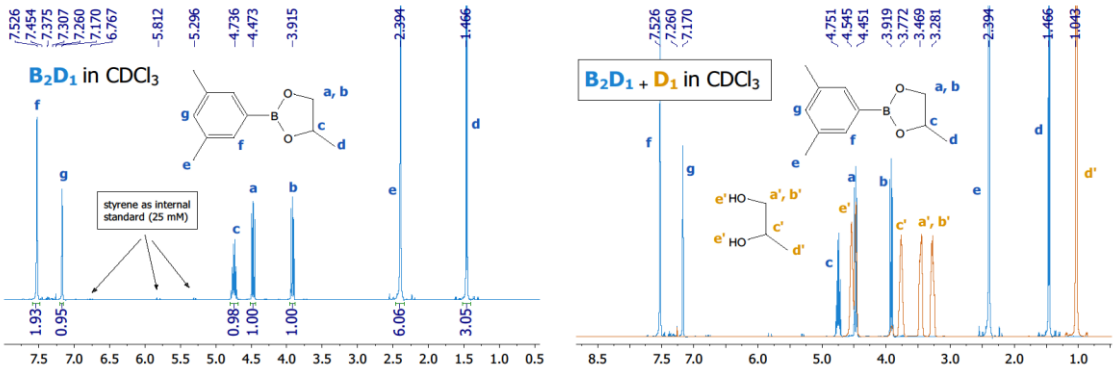

Figure 4.4. ^{1}H-NMR analysis in $CDCl_3$ of $\mathbf{B_2D_1}$ (1 M, left) and the overlap with free $\mathbf{D_1}$ (right).

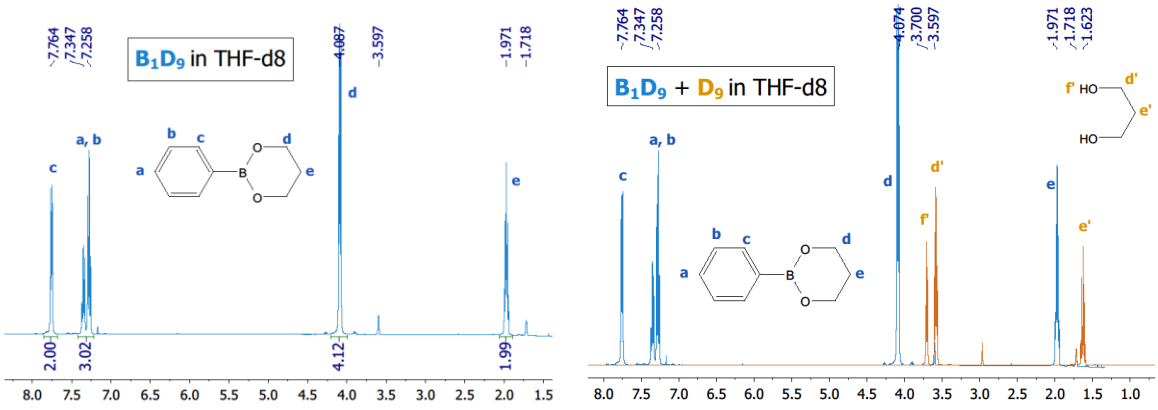

Figure 4.5. ^{1}H-NMR analysis in $CDCl_3$ of $\mathbf{B_1D_9}$ (1 M, left) and the overlap with free $\mathbf{D_9}$ (right).

In all three cases, the respective diol signals in the ^{1}H-NMR spectra are undetectable. The maximum diol content in the boronic esters can be calculated by using the above estimated detection limit via the following relation:

$$diol_{max}[\%] = \frac{[diol]_{max}}{\langle [diol]_{max} + [boronic\ ester] \rangle}$$

$$= \frac{0.1\ mM}{\langle 0.1\ mM + 1000\ mM \rangle}$$

$$= 0.01\%$$

Equation 4.1.

The boronic esters $\mathbf{B_1D_2}$, $\mathbf{B_2D_1}$ and $\mathbf{B_1D_9}$ possess thus a minimum purity of 99.99 mol% in respect to the corresponding diols.

Similarly, in the ^{1}H-NMR spectra of the boronic esters synthesized via strategy 2 no free diol signals were detected. The maximum free diol content was calculated via the same procedure as above by using the general concentration in the ^{1}H-NMR samples (m_{sample} = 10 mg, V = 0.5 mL, see general methods). The concentration depends on the molecular weight of the respective boronic ester and was estimated to be between 0.08 mol% for **B_1D_1** (smallest molecular weight) and 0.22 mol% for **B_4D_4** (highest molecular weight). The boronic esters synthesized via strategy 2 possess thus a minimum purity of 99.78 mol% in respect to their corresponding diols.

4.4 Association and dissociation equilibrium constants of dioxaborolanes and a dioxaborinane

4.4.1 Formation of a dioxaborolane and assessment of its association equilibrium constant

In an attempt to get information about the equilibrium composition of boronic acids, diols and boronic esters in the absence of a water trapping agent, the association constant of **B_1D_2** was determined. Phenylboronic acid (**B_1**) was mixed with 1,2 butanediol (**D_2**) in equimolar amounts (50 mM each) in dried THF-d_8 at 20 °C and handed to ^{1}H-NMR spectroscopy (Scheme 4.4). The oven-dried NMR tube was purged with argon before, during and after the addition of the solution to minimize the presence of humidity.

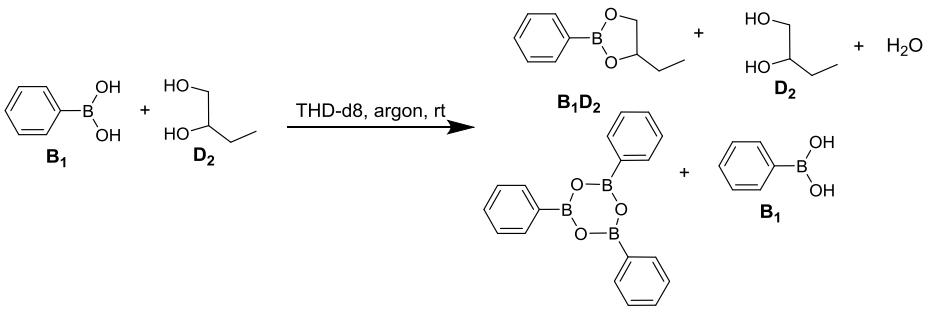

Scheme 4.4. General scheme of the formation of boronic ester **B_2D_1**.

The sample was analyzed via ^{1}H-NMR spectroscopy after 16 hours of mixing and boronic ester (**B_1D_2**) signals at 0.99 ppm (-CH_3) and the remaining free diol signals at 1.31 (-CH_2) and 0.91 ppm (-CH_3) were compared (Figure 4.6). Via the following equation, the association

equilibrium constant was calculated assuming no or little boroxine in the starting boronic acid as well as no or little boroxine formation during the course of the reaction:

$$K_{ass} = \frac{[B_1D_2] * [H_2O]^2}{\langle [B_1] * [D_2] \rangle}$$

$$= \frac{48.1\ mM * 96.2\ mM * 96.2\ mM}{\langle 1.9\ mM * 1.9\ mM \rangle}$$

$$= 123\ \text{M}$$

Equation 4.2.

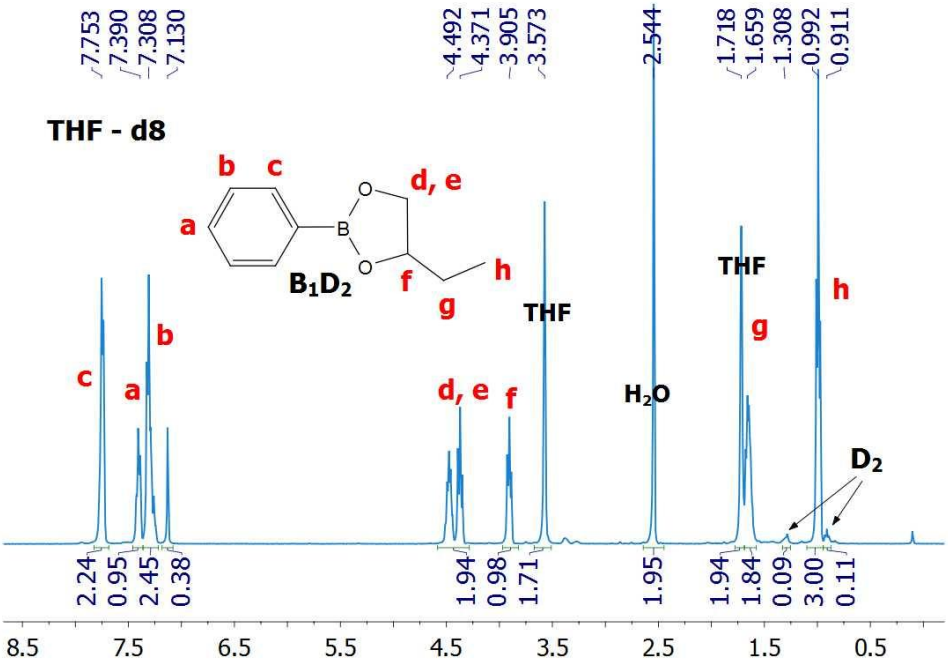

Figure 4.6. ^{1}H-NMR spectrum of the formation of boronic ester $\mathbf{B_2D_1}$ after 16h at room temperature.

The value was estimated to be K_{ass} = 123 M. As mentioned above, several assumptions had to be made and detection of relevant species was difficult. The exact initial ratio of boronic acid/diol could not be guaranteed due to unknown amounts of boroxines in the starting boronic acid. In addition, the apparent ratio water/boronic ester (^{1}H-NMR: 1/1) is doubtful as one would expect the release of two molecules of water during the formation of one boronic esters. The formation of boroxines would displace the equilibrium towards the free boronic acid and the diol, whereas the degradation of (initially present) boroxines by water consumption would result in a shifted equilibrium towards a higher amount of boronic esters. Finally, the concentrations of diols and free boronic acids might be imprecise, due to rather high variation (*ca* 30%) of the ^{1}H-NMR signals (diols). Interestingly, this experiment showed

that under these conditions, water does not have to be trapped to reach high conversion of aromatic boronic acids and aliphatic 1,2-diols into boronic esters.

4.4.2 Hydrolysis of dioxaborolanes and dioxaborinanes formed with aliphatic diols and their dissociation equilibrium constants

At room temperature and in closed systems, boronic esters are formed by a reversible and equilibrated condensation of boronic acids and free diols that releases two equivalents of water. That is why, in the presence of water, pure boronic esters can undergo partial to complete hydrolysis. Hydrolysis is governed by different parameters such as the experimental conditions (pH, solvent, concentration of water and boronic esters, temperature) and the structural characteristics of the boronic esters, as discussed above. With the aim to obtain more detailed information about the water stabilities of boronic esters, hydrolysis experiments were performed on **B_1D_2**, **B_2D_1** and **B_1D_9** in THF (Scheme 4.5, Table 4.2 and Figure 4.7). To access the rate of hydrolysis and the dissociation equilibrium constant ($1/K_{ass}$), water (millipore) was added in different ratios to THF-d_8 stock solutions with a known concentration of boronic esters (100 mM) and the samples were analyzed by ^{1}H- and ^{11}B-NMR spectroscopy. All tubes were oven-dried and purged with argon using a small needle before, during and after addition of the solution. Once added, the needle which was used to keep the tube under argon was slowly removed and the tube was sealed with a cap and a Teflon stripe. The dissociation was followed in detail for four different ratios of **B_1D_2**/H_2O by ^{1}H-NMR spectroscopy and for one of **B_1D_9**/H_2O at 23 °C (Table 4.2). The dissociation equilibrium constant of **B_2D_1** was determined after the reaction was completed (Table 4.4). To verify the equilibrium compositions ^{11}B-NMR spectra were taken after complete reaction (Figure 4.10).

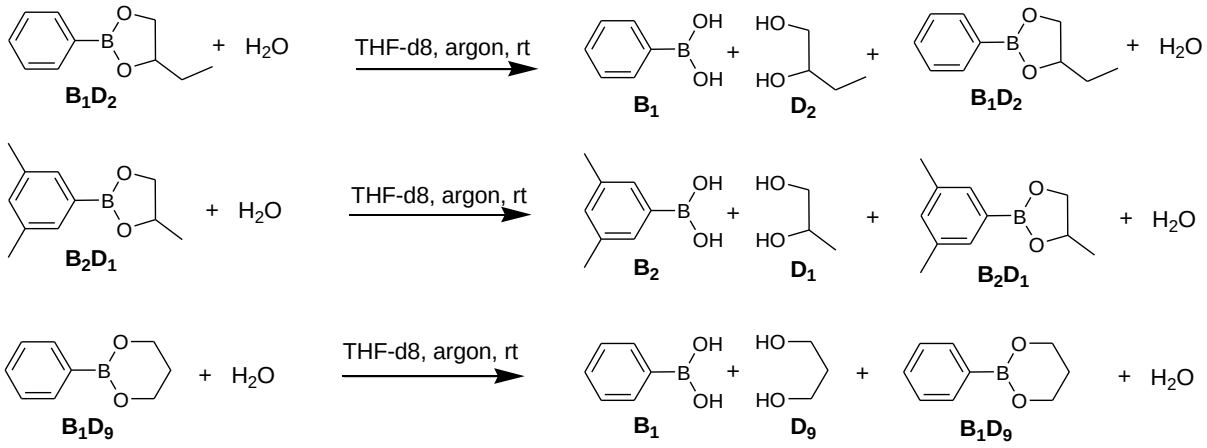

Scheme 4.5. Hydrolysis reactions of boronic esters $\mathbf{B_1D_2}$, $\mathbf{B_2D_1}$ and $\mathbf{B_1D_9}$.

#	Compound	*M*	*m*	*n*	*V*	c_{t0}	r_{t0}
		g/mol	mg	mmol	µL	mol/L	$\mathbf{B_nD_m}/H_20$
Tube solution	$\mathbf{B_1D_2}$	176	12,3	0,07	700	0,1	
F1	H_2O	18	8,82	0,49	8,82	0,7	1/7
F2			6,17	0,34	6,17	0,49	1/4,9
F3			3,53	0,20	3,53	3,53	1/2,8
F4			0,88	0,05	0,88	0,88	1/0,7
Tube solution	$\mathbf{B_2D_1}$	190	9,5	0,05	500	0,1	
F5	H_2O	18	7,2	0,4	7,2	0,8	1/8
Tube solution	$\mathbf{B_1D_9}$	176	12,3	0,07	700	0,1	
F6	H_2O	18	8,82	0,49	8,82	0,7	1/7

Table 4.2. Reactants quantities used to study the hydrolysis reactions of boronic esters $\mathbf{B_1D_2}$, $\mathbf{B_2D_1}$ and $\mathbf{B_1D_9}$.

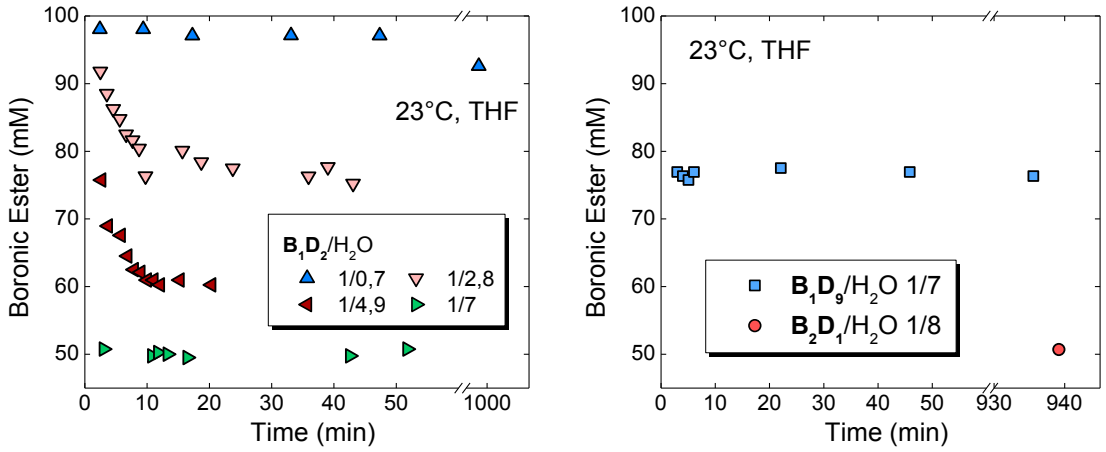

Figure 4.7. Kinetics of the analyzed hydrolysis reactions of boronic esters **B_1D_2**, **B_2D_1** and **B_1D_9**.

As known in literature and already mentioned, boronic esters are prone to hydrolysis and their water stability is dependent on their substitution pattern.[1,78-89] When adding a 7-fold excess of water to **B_1D_2**, the hydrolysis is almost instantaneous (< 3 min) and the kinetics cannot be followed by ^{1}H-NMR spectroscopy (Figure 4.7). The process at a ratio boronic ester/water of 0.7 is very slow and reaches equilibrium only after several hours (> 15 hours). The experiments at ratios of 4.9 and 2.8 show that hydrolysis follows an exponential behavior and equilibration after 20 and 45 min respectively were observed. Accordingly the data showed that the more water is added, the more boronic ester is decomposed. The dissociation constants of the boronic esters can be calculated by the following expression:

$$K_{diss} = \frac{[B_1] * [D_2]}{\langle [B_1D_2] * [H_2O]^2 \rangle}$$

This can be expressed as:

$$[H_2O]^2 = \frac{[B_1] * [D_2]}{\langle [B_1D_2] * K_{diss} \rangle}$$

Equation 4.3.

Under the assumption that boronic ester decomposition proceeds by the consumption of two water molecules and the generation of a free boronic acid and diol species, the equilibrium composition changes from ca 50/50 to 93/7 (boronic esters/diols or boronic acids) for experiments with high water content to low water content. From the plot of $[H_20]^2$ vs [**B_1**]*[**D_2**]/[**B_1D_2**] a dissociation constant of 0.131 M^{-1} was obtained for **B_1D_2** (Table 4.3 and

Figure 4.8 and 4.9). This value corresponds to K_{ass} = 7.6 M which is in contradiction with the measured 123 M (Figure 4.6). As mentioned above, uneven mixing ratios due to boroxines and imprecise determination of final concentrations, especially of water, might be responsible for significant errors when estimating K_{ass}.

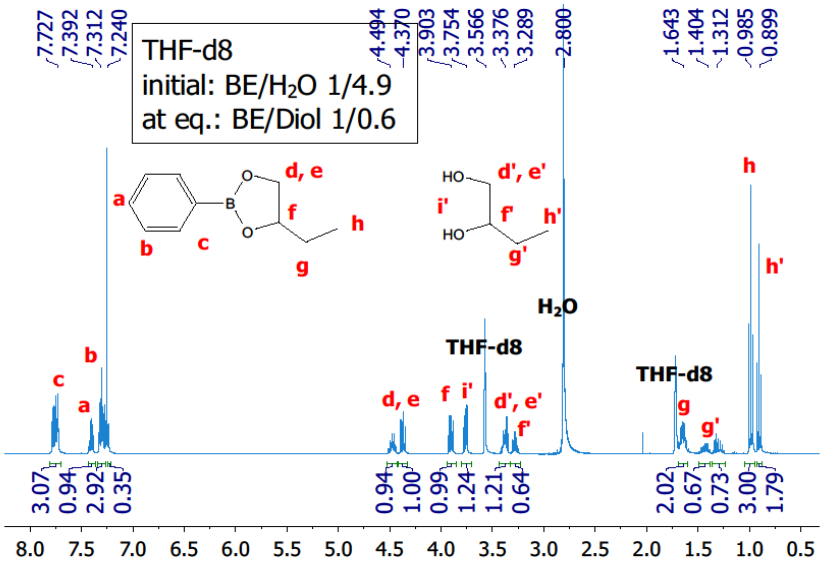

Figure 4.8. ^{1}H-NMR of $\mathbf{B_1D_2}$ and $\mathbf{D_2}$ after hydrolysis reaction (initial ratio: 4.9/1).

#	Integration of relevant NMR signals (a.u)		Concentration (mol/L)				K_{diss}. (L mol^{-1})
B_1D_2							
	B_1D_2 –CH_3 0,99 ppm	**D_2** –CH_3 0,90 ppm	**B_1D_2**	H_2O	**D_2**	**B_1**	
F1	3,1	3,0	0,05	0,60	0,05	0,05	0,13
F2	4,5	3,0	0,06	0,41	0,04	0,04	0,16
F3	8,7	3,0	0,07	0,23	0,03	0,03	0,17
F4	37,5	3,0	92,6	685,2	7,4	7,4	0,19
B_2D_1							
	B_2D_1 –CH_3 1.33 ppm	**D_1** –CH_3 1.03 ppm	**B_2D_1**	H_2O	**D_1**	**B_2**	
F5	3.09	3.0	0,05	0,70	0,05	0,05	0,10
B_1D_9							
	B_1D_9 –CH_2 1.98 ppm	**D_9** –CH_2 1.63 ppm	**B_1D_9**	H_2O	**D_9**	**B_1**	
F6	6.4	2	0,07	0,65	0,02	0,02	0,02

Table 4.3. Determination of the dissociation equilibrium constant K_{diss} via ^{1}H-NMR spectroscopy.

For the structurally similar boronic ester **B_2D_1** a dissociation constant of 0.097 M^{-1} was calculated proving the two boronic esters comparable stability. At a comparable 7-fold excess of water, the hydrolysis of **B_1D_9** is instantaneous as for **B_1D_2**. However, due to its stability increasing 6-membered ring structure, the boronic ester is less prone to hydrolysis resulting in a smaller dissociation constant of 0.017 M^{-1} (Table 4.3). The data obtained from ^{11}B-NMR spectroscopy prove the equilibrium compositions (Figure 4.10). In general, it was observed that the process of hydrolysis of dioxaborolanes proceeds very fast even at moderate excess of water at room temperature, hence the rate of hydrolysis could not be determined via NMR techniques.

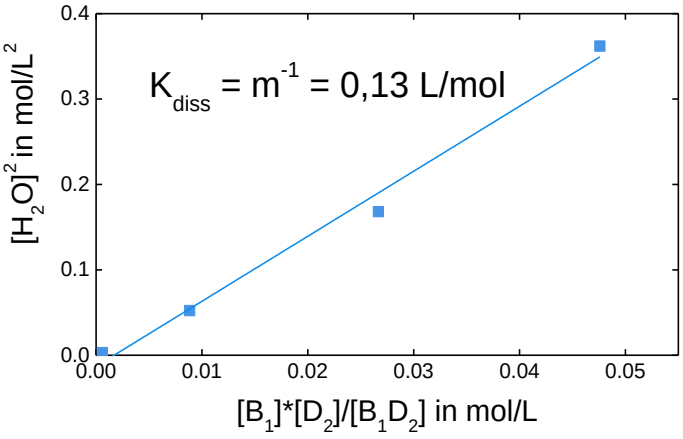

Figure 4.9. Graphical determination if the dissociation constant of $\mathbf{B_1D_2}$ in THF at 23°C.

The dissociation constants calculated from the equilibrium composition depend on the concentration of all species. To prove one of the underlying assumptions that two molecules of water decompose one boronic ester and thus that no "half-open" species with only one ester bond exist, the ^{1}H-NMR data of the hydrolysis experiments for $\mathbf{B_1D_2}$ and $\mathbf{B_1D_9}$ were investigated (Figure 4.8) in depth. In both experiments, signals corresponding to the free diol species were observed. Additionally, the compounds hydroxyl-group protons which are detectable due to strong hydrogen bonding between diols were detected with matching integration values. Thus, no "half-open" species were detected in these systems.

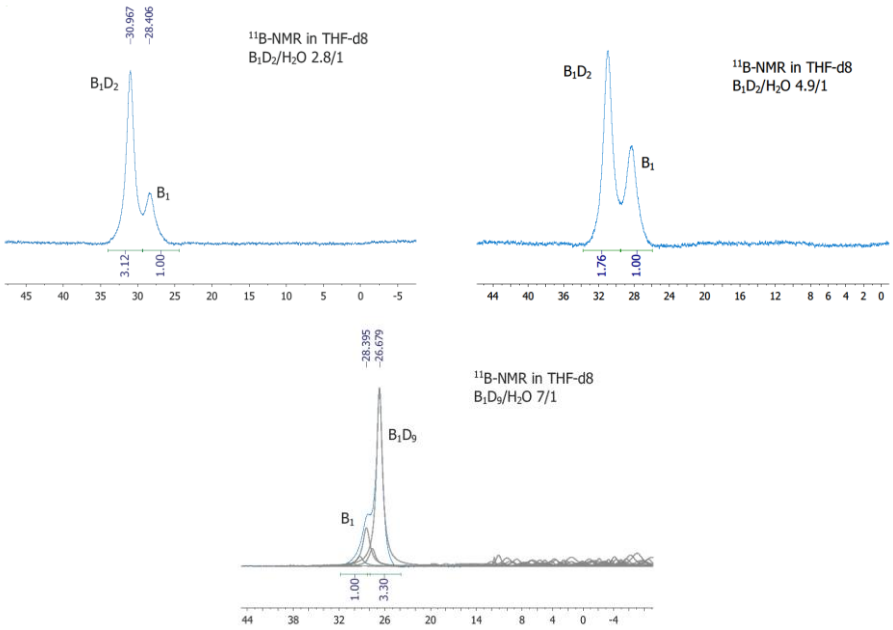

Figure 4.10. Top left: ^{11}B-NMR of $\mathbf{B_1D_2}$ and generated $\mathbf{B_1}$ (initial ratio: 2.8/1). Top right: ^{11}B-NMR of $\mathbf{B_1D_2}$ and generated $\mathbf{B_1}$ (initial ratio: 4.9/1). Bottom: ^{11}B-NMR of $\mathbf{B_1D_9}$ and generated $\mathbf{B_1}$ (initial ratio: 7/1).

In this subchapter is presented the estimation of associative and dissociative equilibrium constants (K_{ass} and K_{diss}) of different boronic esters under protective atmosphere in dry solvents (THF). Untreated boronic acid (**B_1** phenylboronic acid) was mixed with 1,2 butanediol (1/1) and the equilibrium composition in THF was measured to be 123 M. The undefined content of initially present boroxines in the boronic acid as well as boroxine formation/degradation during reaction were not taken into account. In the final NMR spectrum the expected 1/2 ratio between generated boronic esters and water was not observed and diol/boronic acid signals were not precisely detectable. Interestingly, it was shown that even in the absence of a water trapping agent (*e.g.* $MgSO_4$) most of the boronic acid and diol molecules are converted into the respective boronic ester. Thermodynamic dissociation equilibrium constants (K_{diss}) of three different highly pure boronic esters were estimated (**B_1D_2**, **B_2D_1** and **B_1D_9**) under identical conditions and did not match with the above estimated association equilibrium constant ($K_{diss} = K_{ass}^{-1}$). Depending on the boronic ester ring strain, the constants range from 0.13 M^{-1} (**B_1D_2**) and 0.097 M^{-1} (**B_2D_1**) for dioxaborolanes (5 membered species, ring strain) to more stable dioxaborinanes (6 membered cycles, no ring strain) with 0.017 M^{-1} (**B_1D_9**). Due to the very high purity of the starting boronic esters, the higher precision of the measures, and the reproducibility of the results, the thermodynamic dissociation equilibrium constants (K_{diss}) found seem quite reliable. Hydrolysis proceeded fast and the equilibrium composition was reached in less than an hour in most cases. ^{11}B-NMR spectroscopy confirmed the estimated equilibrium compositions. To study the influence that moisture can have on mixtures of pure two or more boronic esters in organic solvents, the following experiments were performed.

4.5 Exchange reactions under air without addition of free diol or water

To further deepen our understanding of the influence of water on boronic esters exchange and to check whether mixtures of two or more pure boronic esters can undergo exchange reactions in the presence of moisture, the following series of experiments was performed. Kinetic experiments were performed with boronic esters under air via GC analysis and ^{1}H-NMR was used to detect possible degradation products such as diols.

4.5.1 GC methods: internal and external calibration

The kinetics of boronic esters exchange were followed via gas chromatography (GC). To correlate GC raw data to the molar quantity of the different boronic esters studied, internal and external calibration methods were used.

For internal calibration, an inert standard was added and the reactants signals were referred to the standards signal. The standard was chosen according to its column compatibility, retention time, temperature stability and its inert character in respect to boronic esters. Dodecane and tetradecane were used as internal standards. These molecules were dried and stored over molecular sieves (3 days) under inert atmosphere before use.

External calibration curves were generated for each boronic ester. Therefor, each boronic ester was analyzed at four different concentrations at a constant sample volume of 1 µL (Figure 4.11) and compound specific response factors were obtained from the slope of the concentration vs area plot (Figure 4.12).

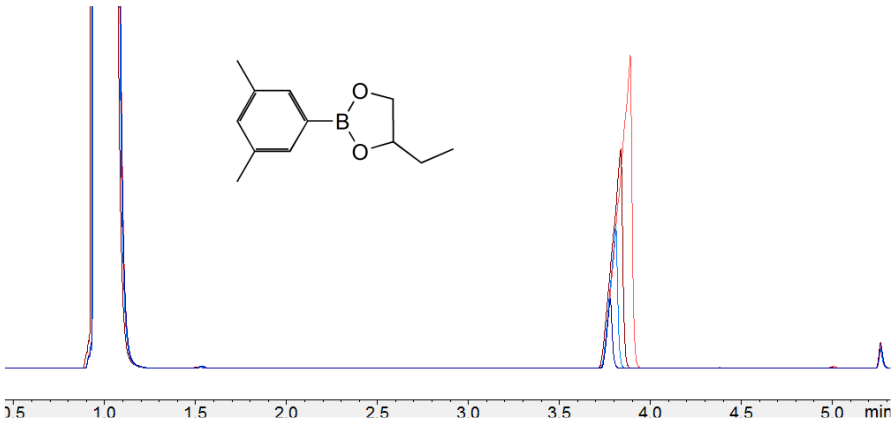

Figure 4.11. Example of the raw data used for the external calibration curve of boronic ester $\mathbf{B_2D_2}$.

Stock solutions of each boronic ester were prepared the following way: 0.1 mmol of the boronic ester was added to 1 g of the respective solvent and 100, 50 and 10 µL of this solution were further diluted with 0.1 mL of the solvent. The concentrations and the GC methods were chosen such that they were comparable to those used in the studied exchange reaction kinetics. For boronic esters generated via strategy 3, the concentrations were adjusted to boronic acid and diol impurities quantified by ^{1}H-NMR analysis. Figure 4.12 depicts the totality of the external calibration curves generated.

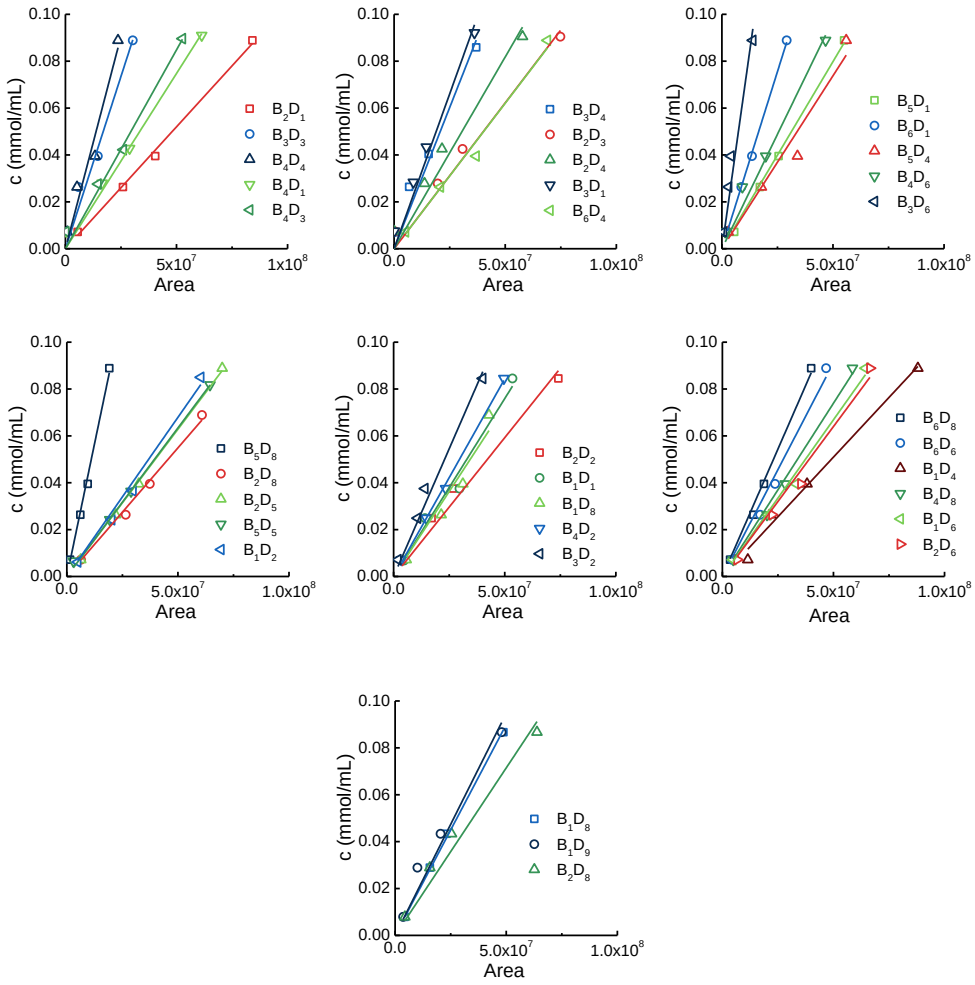

Figure 4.12. External calibration curves of boronic esters studied in model exchange reactions.

GC methods were adapted to the nature of the studied boronic esters (polarity, molecular weight) and the speed of the exchange reaction (Table 4.4). The methods varied in detection/injection temperature, starting temperature of the column and the temperature program. Additionally, the carrier gas flow was adapted if necessary. The parameters were chosen as a compromise between a short retention time (to maximize the number of measures in a given time) and good separation between the reactants (to improve the precision and reproducibility of the results). Table 4.4 depicts the totality of applied GC methods.

Reactions	$T_{inj/det}$	T_{col}	Carrier gas flow	Split ratio	T program
	(°C)		(mL)		Hold time (min)/ramp (°C/min)
Reactions under air: 4.5.					
1-10	300	100	5.0	2.0	2/30
11	300	150	4.0	2.0	1/60
12, 14, 21, 22	300	150	4.5	2.0	3/20
13	300	100	8.0	2.0	3/20
15, 16	300	100	5.0	2.0	3/20
17	300	100	5.0	2.0	3/30
18-20	270	120	2.0	2.0	3/15
Reactions under inert atmosphere: 4.6.					
All	350	120	5.0	4.0	0/30

Table 4.4. GC methods used for kinetic studies of boronic ester exchanges.

4.5.2 Changing the conditions from protective atmosphere to air

To check if the experimental conditions, *i.e.* the presence of moisture can be sufficient to trigger the exchange of boronic esters instead of adding water or diols deliberately, the following experiments were designed. Two highly pure boronic esters $\mathbf{B_1D_2}$ and $\mathbf{B_2D_1}$ were mixed in equimolar ratio under argon in THF and the evolution of the reaction was monitored (Scheme 4.6 and Figure 4.13). After 200 minutes, the Schlenk flask was opened for 30 seconds and the argon was exchanged with air via a weak flux of air at the top of the flask.

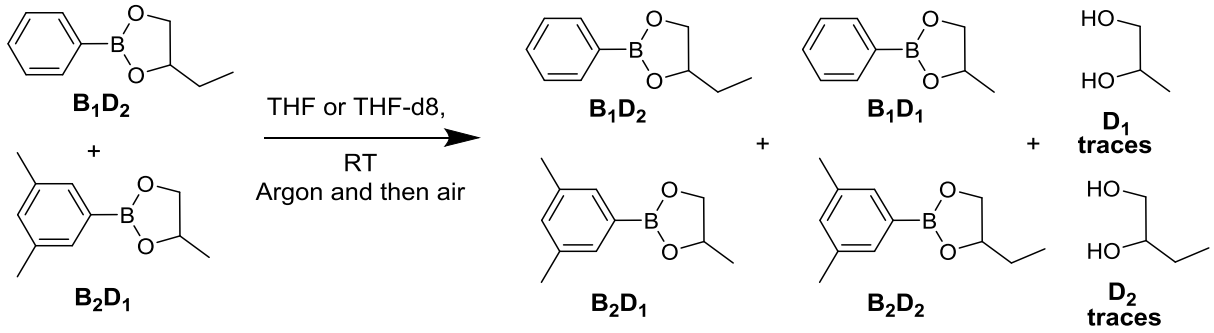

Scheme 4.6. The exchange of two highly pure 5-membered boronic $\mathbf{B_1D_2}$ and $\mathbf{B_2D_1}$ esters in THF at 20 °C under air results in a mixture of four boronic esters and the two respective free diols.

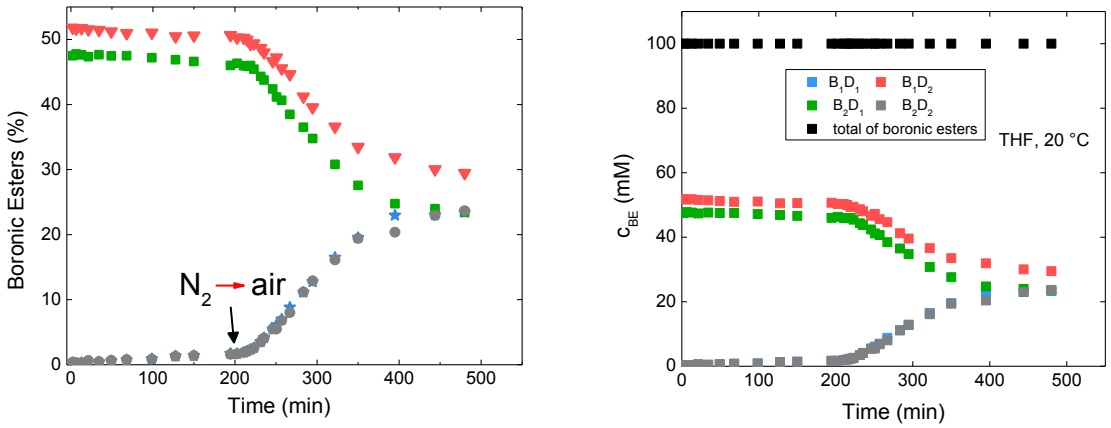

Figure 4.3. Exchange of highly pure boronic esters $\mathbf{B_2D_1}$ and $\mathbf{B_1D_2}$ in THF with changing experimental conditions. At 200 minutes the protective argon atmosphere was exchanged with air. Left side: in mol%, right side: in concentrations (from internal standard).

Under inert atmosphere and without any added water, almost no reaction was detected. Upon exchange of the argon protective atmosphere with air, *i.e.* introduction of moisture at 200 min, the reaction accelerated and reached equilibrium in *ca.* 300 minutes as from thi spoint. These results show that in an hydrophilic solvent the contact with moisture in the air is sufficient to drive an exchange reaction between boronic esters via in-situ generated diols. A more detailed study of the amount of water and the diol content which can be present during and after such a reaction can be found below (4.5.4).

4.5.3 Influence of experimental conditions on a mixture of two dioxaborolanes

With the aim to further deepen the effect that moisture in the air might have on the exchange of highly pure boronic esters, and to examine the role of a possible "in-situ" generation of diols by humidity uptake of the solvent, the following series of experiments was designed.

$\mathbf{B_1D_2}$ and $\mathbf{B_2D_1}$ were mixed in a stoichiometric ratio (c_{total} = 100 mM) in 1.5 mL vials under air. **Vial #1** was not closed with a septum, **vial #2** was closed with a septum in which were punched holes with a 10 micro L syringe (the syringe which was used for sampling) and **vial #3** was closed with an intact septum and holes occurred through sampling with the syringe only.

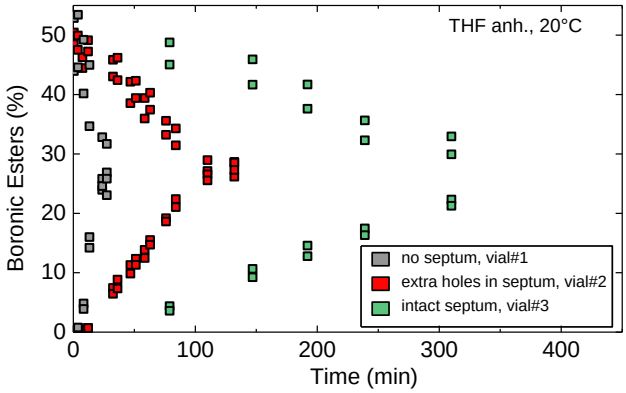

Figure 4.14. Exchange of two pure boronic esters $\mathbf{B_1D_2}$ and $\mathbf{B_2D_1}$ under closed and open conditions.

As expected from the experiment in 4.5.2. the kinetic data for the three experiments are drastically different (Figure 4.14). The reaction in **vial #1** was complete after 24 minutes, while **vial #2** proceeded 115 minutes and **vial #3** more than 300 minutes. Additionally an inhibition period for **vials #2** and **#3** was observed which can be related to the process of humidity entering the solvent/subsequent hydrolysis and creation of diols/acids. The reaction is thus highly susceptible to humidity and even with an intact septum (green points, only very small hole after 1-2 samples, figure 4.14) sufficient humidity has entered the reaction mixture to function as trigger to generate diols.

4.5.4 Determination of the free diol content in mixtures of two dioxaborolanes under air

To accurately determine the diol content during experiments under air, the same exchange reaction as in 4.5.2 was performed in THF-d_8 and analyzed via ^{1}H-NMR. The two highly pure boronic esters were mixed in THF-d_8 in a small 1.5 mL vial with a septum under air (c_{BE} = 50 mM) and ^{1}H-NMR spectra were taken after mixing at t=0 and at equilibrium at t=350 min (Figure 4.16). The NMR tubes were purged with argon before, during and after addition of samples and sealed as above for the determination of K_{diss}. The resulting kinetic data show that in the beginning no reaction occurred (Figure 4.15). The concentration of boronic esters $\mathbf{B_1D_2}$ and $\mathbf{B_2D_1}$ stayed constant until ca 35 minutes where the two product species can be detected. The reaction proceeded and reached an equilibrium state after ca 300 min total experiment time with a stoichiometric distribution of all four boronic esters.

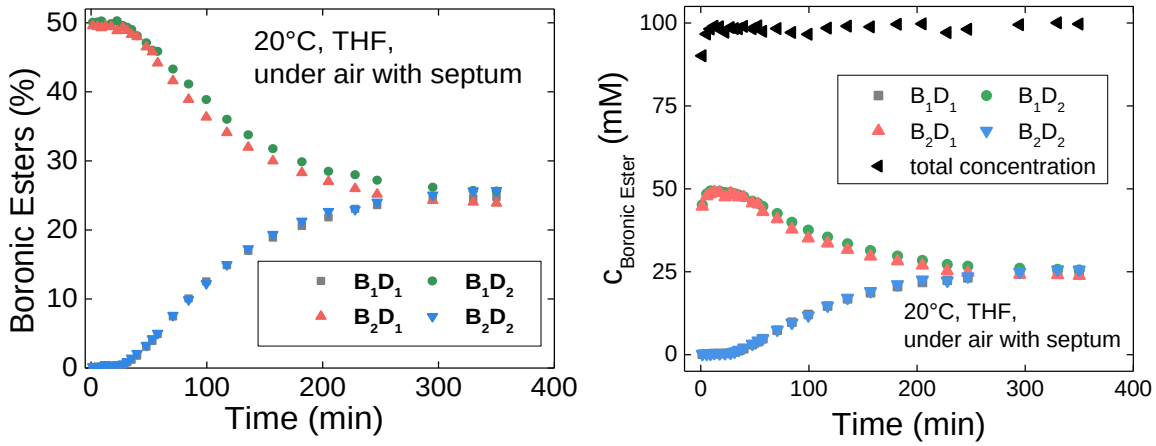

Figure 4.15. Reaction kinetics of the exchange between two highly pure 5-membered boronic esters $\mathbf{B_1D_2}$ and $\mathbf{B_2D_1}$ in THF at 20 °C under air. The overall initial concentration of boronic esters was c = 100 mM (internal standard).

As can be seen from the ^{1}H-NMR spectrum at t=0 (Figure 4.16), in the beginning of the experiments diols were not detectable and thus an exchange was not happening or happening extremely slow (Figure 4.15). With time, and probably due to /hole generation caused by sampling with a syringe, additional humidity entered the vial and the solvent, resulting in diol generation through boronic ester hydrolysis. The diols catalyze the exchange and function as a sort of "in situ-generated" catalysts. The measured ^{1}H-NMR spectrum at 350 min reveals that at the point of measurement, ≤ 6 mol% free diols were present and thus proves that boronic esters hydrolyze through humidity uptake (in THF) and that the hydrolysis is sufficient to drive the reaction (see Appendix, Table 4.6). The fact that additional diols could have been generated during NMR measurement through absorbed, but yet un-reacted water in the solvent was neglected. Figure 4.15 depicts the concentrations of exchanging boronic ester species measured via GC analysis. Although the total concentration seems to be rather constant, the data points are rather scattered (5%) preventing an accurate determination of the expected small changes in total concentration of boronic esters through hydrolysis (not more than 6 mol% from ^{1}H-NMR). In general, hydrolysis of boronic esters could not be accurately analyzed via GC analysis and thus the following results are plotted in % referring to the relative total amount of boronic esters.

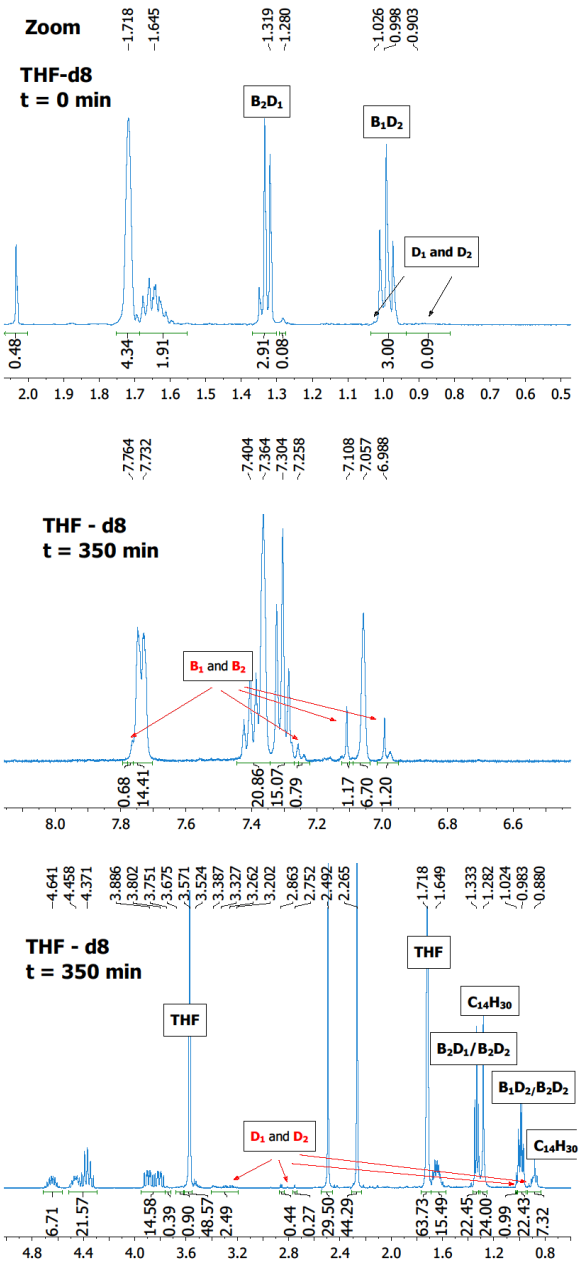

Figure 4.16. [1]H-NMR spectra of the exchange of two highly pure 5-membered boronic esters $\mathbf{B_1D_2}$ and $\mathbf{B_2D_1}$ in THF at 20 °C under air at t = 0 min (top, left) and t = 350 min (top right and bottom, at equilibrium).

4.5.5 Exchange reactions of dioxaborolanes under various conditions

To test the reproducibility of the observed humidity-triggered exchange reaction in mixtures of two pure boronic esters, the experiment was repeated (Figure 4.17, left side). Although important parameters, such as humidity and the transfer of air from the outside to the inside of the vial were not controlled, the total equilibrium times were comparable (around 350 minutes). However, the initial inhibition period varied between experiments due to the

uncontrolled sampling process. To further investigate the impact of solvent, solvent dryness and catalysts, more experiments were performed using the same method.

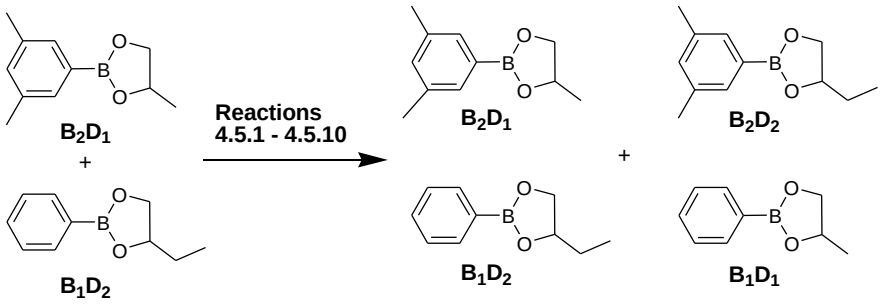

Scheme 4.7. The exchange between two highly pure 5-membered boronic esters was studied under air. The influence of parameters such as solvent, temperature and the presence of small catalyzing molecules was investigated.

For example, when changing the reaction solvent from dried anhydrous THF to THF (not dried, new bottle, <0.002% H_2O) no significant changes were observed (Appendix, Figure 4.32). Small traces of water in the not-dried solvent might hence be neglected compared to the water uptake of the solvent during sampling. Changing the solvent from THF to acetone (new bottle) did not result in significantly different reaction kinetics either (Figure 4.17, right side). With less than 200 minutes at 60 °C it was observed that increasing temperature resulted in decreased equilibrium times (Appendix, Figure 4.8). However, the effect is rather small pointing to a low activation energy of the underlying process of transesterification of dioxaborolanes. The addition of 1 mol% of vacuum dried benzoic acid or dried triethylamine (NaOH) as catalyst accelerated the exchange by a factor of 6-7 comparable to the experiment in the presence of 1 mol% of water (Appendix, Figure 4.32).

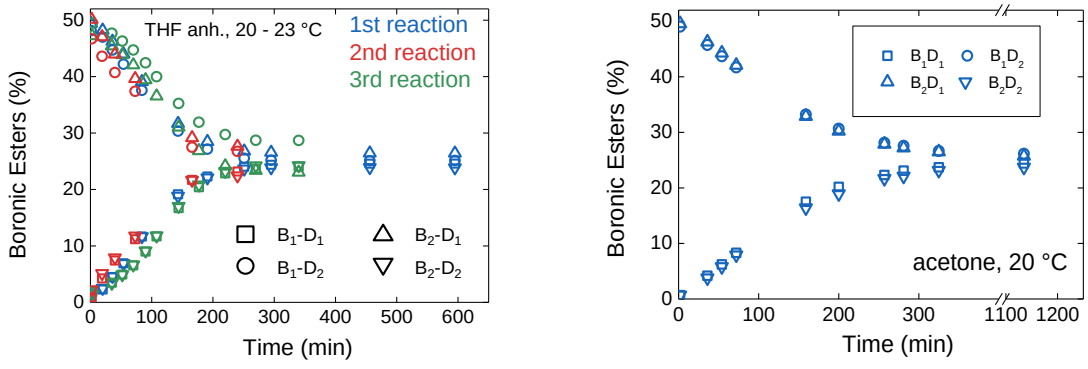

Figure 4.17. The exchange of two pure boronic esters (**B_1D_2** and **B_2D_1**) in solution in the presence of humidity results in the stoichiometric mixture of four different boronic esters. Left: reproductibility of the results in THF at RT. Right: exchange in acteone at 20°C..

4.5.6 Influence of substitution pattern on mixtures of two or more boronic esters in the presence of air

To check how different substitution patterns can influence the exchange kinetics of boronic esters under similar experimental conditions as where applied in 4.5.5, the following series of tests was performed (Table 4.5, reactions 4.5.11-22 and Figure 4.2 for boronic esters structures).

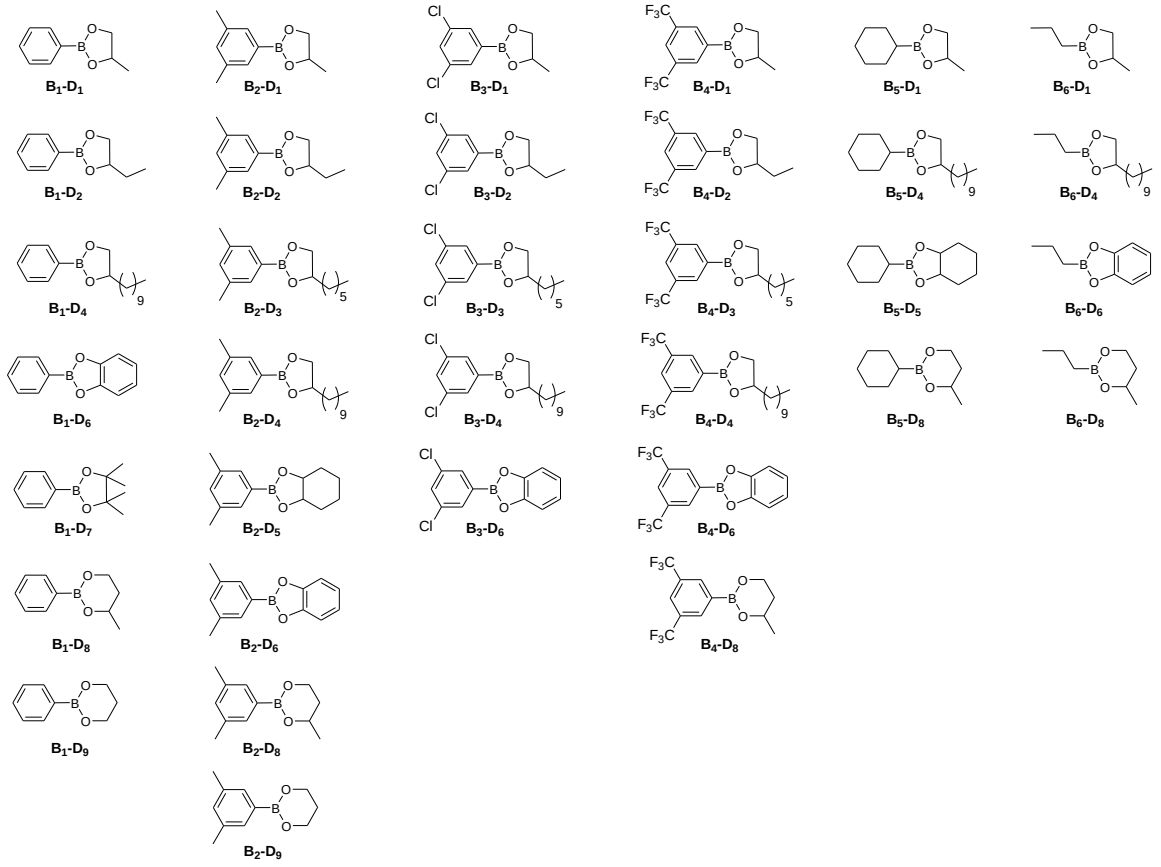

Figure 4.2. Boronic esters synthesized and studied in model experiments, organized according to the boronic acid radical.

Results such as time to reach equilibrium and equilibrium composition were tried to be related to the pKa values of boronic esters as well as to the structure and substitution degree of diol moieties. For example when mixing the two halogen-substituted dioxaborolanes **B_3D_1** and **B_4D_2** in THF, the exchange proceeds very fast compared to not halogen-substituted boronic esters counterparts (*ca*. 300 min, Appendix Figure 4.33) and equilibrium was reached in less than 7 minutes.

Reaction 4.5.	Boronic ester 1	Boronic ester 2	T (°C)	Solvent	$t_{eq.}$(min)
1-3	B_1D_2	B_2D_1	20-23	THF anh.	*ca.* 350
4			20	THF	*ca.* 350
5*			20	THF anh.	*ca.* 25
6,7			40/60		250/180
8,9****			20		<50/<50
10			20	Acetone	*ca.* 350
11***	B_3D_1	B_4D_2	20-23	THF anh.	<7
12	$B_2D_1 + B_3D_3 + B_4D_4$				<10
13	B_3D_3	B_4D_6			50
14	B_5D_1	B_6D_4			350
15	B_5D_1	B_2D_5			>1000
16	B_5D_1	B_2D_8			>4500
17	B_1D_1	B_2D_8	100 °C	Toluene	<1500
18-20	B_1D_9	B_2D_8	35/70/100 °C		<1500/>1500/>1500
21	B_1D_7	B_4D_4	60 °C	THF	No exchange
22	B_1D_7	B_4D_6			
*1 mol% water, **1 mol% benzoic acid or NEt_3 ***N_2, molecular sieves					

Table 4.5. Overview table of boronic ester exchange reactions in the presence of humidity.

Both chloro- and trifluoromethyl-substituents are electron withdrawing substituents and thus decrease the boronic esters pKa value, which results in increased hydrolysis and an accelerated transesterification of boronic esters. The equilibrium distribution was stoichiometric proving that both boronic esters exhibit comparable stability towards hydrolysis. The mixture of the two tested electron withdrawing substituted boronic esters and boronic ester **B_2D_1** resulted in a 9-compound library with rather similar distribution of compounds (Figure 4.18). The time to reach equilibrium was as expected for these fast reacting compounds very short, but still longer than for the 2-compound mixture and most probably controlled by the less acidic not-halogen substituted **B_2D_1**.

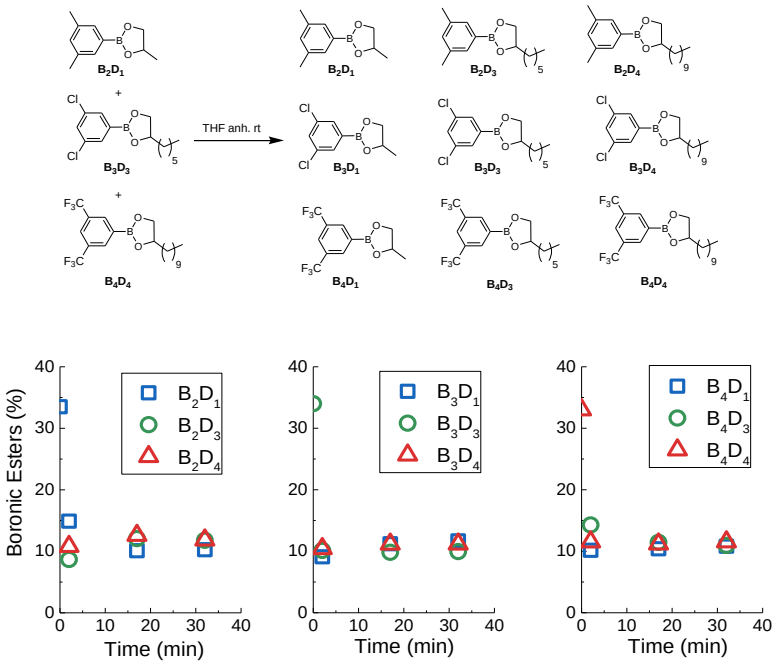

Figure 4.18. Reaction 4.5.12. in anhydrous THF at room temperature.

By changing the linear 1,2 aliphatic diol functionality to an aromatic cyclic structure (catechol), the transesterification between two halogen-substituted boronic esters **B_3D_3** and **B_4D_6** slows down ($t_{eq.}$=ca 50 min) compared to all aliphatic diol containing boronic esters (<7 min) (Appendix, Figure 4.34). In contrast to 1,2-propane or butanediol and in agreement with the results catechol is a disubstitued 1,2-diol which can form more stable boronic esters. However, the fact that catechol boronic esters might suffer from decreased stability due to the opposing conjugation between the phenolic oxygens and the benzene ring, should be considered, too. The exchange between **B_3D_3** and **B_4D_6** reached equilibrium considerably faster than the exchange of compounds without electron withdrawing substituents (**B_1D_2** and **B_2D_1**). In Figure 4.35 (Appendix) it can be observed that boronic esters **B_5D_1** and **B_6D_4** with linear aliphatic diol moieties and aliphatic boronic acid moieties exchanged in a similarly fashion as their aromatic boronic ester counterparts (without electron withdrawing substituents, **B_1D_2** and **B_2D_1**, *ca*. 350 min, Figure 4.17). Interestingly, the reaction with a sterically more hindered boronic ester made with 1,2-cyclohexyldiol remarkably slowed down the exchange with equilibration times of more than 1000 minutes (Appendix, Figure 4.36). Taking into account reported results from literature where aromatic boronic esters from 1,2 cyclohexyl diols were observed to be less stable than aliphatic diols due to conformation issues, these results have to be further investigated.[89] Exchanges between boronic esters made with 1,2- and 1,3- aliphatic diols are very slow due to the increased stability of the 6-membered boronic ester rings (no ring strain). For example, the exchange between

dioxaborolane **B_5D_1** and dioxaborinane **B_2D_8** was significantly slower, as compared to exchange reactions between two dioxaborolanes, with an equilibration time >4500 minutes in THF at room temperature (Appendix, Figure 4.37). Even at increased temperatures (100 °C, toluene) a similar reaction mixture of boronic esters dioxaborolane **B_1D_1** and dioxaborinane **B_2D_8** was not at its equilibrium before 1300 minutes. Additionally, the resulting equilibrium distribution was not stoichiometric anymore, instead it displayed an over-expression of the more stable dioxaborinanes **B_1D_8** and **B_2D_8**. The exchange between two dioxaborinanes, namely **B_1D_9** and **B_2D_8**, in toluene at 35 °C was very slow too and did not reached equilibration even after more than 1500 minutes (Figure 4.19).

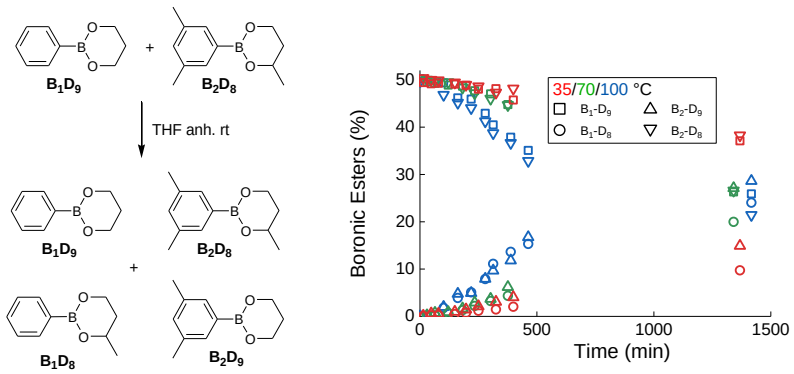

Figure 4.19. Reaction of dioxaborinanes. in toluene at 35/70/100 °C.

By increasing the temperature to 70 °C and 100 °C the reaction was accelerated, but still slower than reactions of dioxaborolanes, 5-membered boronic esters. The initial period of hydrolysis and diol generation is clearly visible for all three experiments and was shorter the higher was the temperature. The equilibrium distribution of compounds at 100 °C seemed to be not fully stoichiometric, but differs to what was observed in the two other experiments at different temperatures (during reaction). Exchanges with boronic esters that contained pinacol diols were not observed under the tested conditions (room temperature and 60 °C, Appendix, Figure 4.39). The bulky nature of the diol resulted in high stability towards hydrolysis of the respective boronic esters and hindered free diols to attack and exchange through transesterification.

The influence of moisture/humidity towards boronic esters in solution was analyzed. In the absence of added water or diol the exchange in a mixture of two highly pure dioxaborolanes under protective atmosphere in solution is very slow. As soon as air gets in contact with the solvent (THF, hydrophilic) water is dissolved and diols are generated resulting in an accelerated exchange of boronic esters. Chemically different boronic esters were tested for

moisture mediated exchange reactions in solution. It was tried to relate the kinetic results to the respective substitution pattern. Electron withdrawing groups attached to the aromatic boronic acid moiety increased the speed of exchange due to more acidic boronic esters. By changing the aliphatic diols to cyclic aromatic diols, the exchange slowed down. Boronic esters made of 1,3-aliphatic diols were more stable and exchanged slower than their 1,2 aliphatic diol counterparts. Pinacol, although a 1,2 aliphatic diol, generates boronic esters that did not undergo sufficient hydrolysis and transesterification to detect an exchange under the here presented testing conditions. To obtain more information, such as the rate constant, *k*, and the activation energy, E_a, of the transesterification of dioxaborolanes and dioxaborinanes, a series of experiments was performed with highly pure compounds under protective atmosphere.

4.6 Exchange reactions under inert atmosphere

To even better understand the role of water in solutions of two boronic esters, controlled amounts of water where added to two compound mixtures and the reactions were followed by GC. Additionally, direct transesterification of dioxaborolanes and dioxaborinanes was investigated. Under protective atmosphere, hydrolysis can be neglected and parameters such as the rate constant *k* and the activation energy E_a of the transesterification of dioxaborolanes could be estimated by mixing controlled amounts of diols with mixtures of two highly pure boronic esters. Eventually, the bulk reaction of highly pure boronic esters was investigated and very interesting results were obtained.

4.6.1 Variation of water content

The hydrolysis of the boronic esters $\mathbf{B_1D_2}$, $\mathbf{B_2D_1}$ and $\mathbf{B_1D_9}$ was studied above. The more water was added, the more boronic esters were decomposed resulting in free acid and diol. In 4.5 the effect of moisture was analyzed. Here, the effect of controlled added amounts of water in mixtures of highly pure boronic esters was studied. In the presence of water and without the addition of any free diol the exchange of the two boronic esters $\mathbf{B_1D_2}$ and $\mathbf{B_2D_1}$ was studied (Figure 4.20).

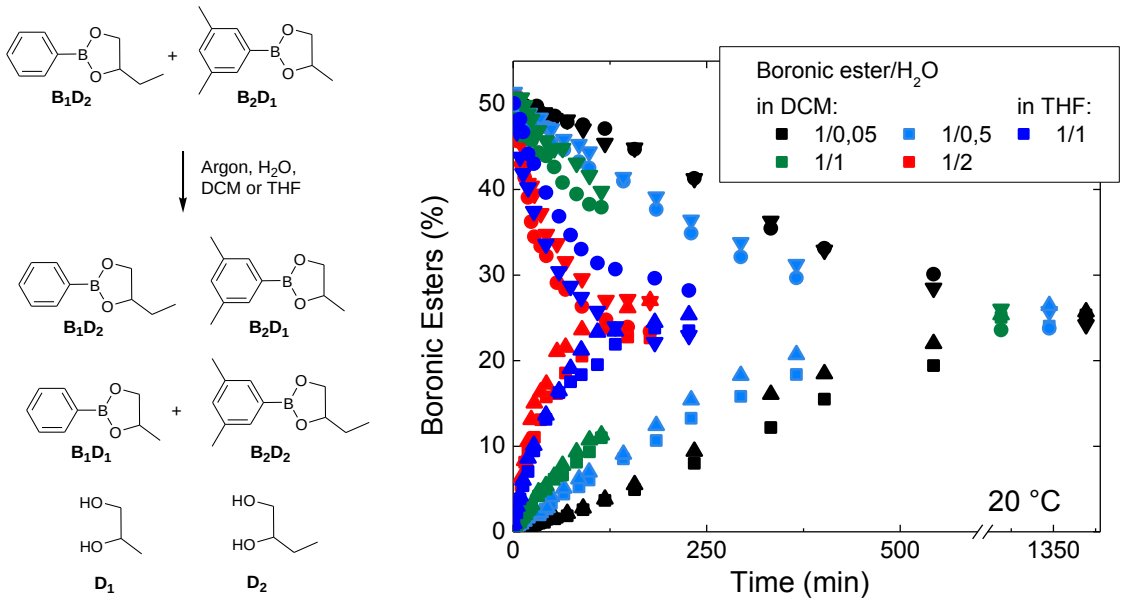

Figure 4.20. Exchange of highly pure boronic esters $\mathbf{B_2D_1}$ and $\mathbf{B_1D_2}$ in THF or DCM at room temperature and in the presence of different amounts of water.

To an equimolar mixture of the two boronic esters (c_{tot} = 100 mM, 4 mL) kept under argon at room temperature, was added the desired molarity of water in 0.4 mL of the respective solvent. In DCM, the ratio boronic esters/water was changed, whereas in THF only one ratio was studied (Figure 4.20). At all ratios, and in both solvents, the addition of the respective amount of water was enough to drive the reaction between two highly pure boronic esters (strategy 1) to form two additional boronic esters by the generation of free diols and boronic acids. The more water was added, the faster the reaction proceeded. In DCM the exchange with *ca.* 5 mol% of water was rather slow ($t_{eq.}$ > 10 hours) and showed a sigmoidal form. In the beginning no diols are present and as seen above, the hydrolysis, *i.e.* the diol generation, can be rather slow at low water concentrations. As hydrolysis progressed more diols were present in the system accelerating the exchange reaction. At higher water concentrations, the reaction kinetics were mono-exponential and at a ratio of 1/2 boronic esters/water the reaction reached equilibrium already after *ca.* 200 min. The reaction in THF was faster than in DCM keeping other parameters similar. Several factors may play a role, such as the solvent influence of the dissociation constant which would influence the diol concentration. Other parameters, *e.g.* the tendency of generated boronic acids to precipitate as boroxines resulting in a changed water and boronic acid concentrations might be important, too.

4.6.2 Transesterification of dioxaborolanes with 1, 2 butanediol

In an attempt to verify the fast rate of the direct transesterification reaction of a boronic ester made of a phenylboronic acid and an aliphatic 1,2-diol with a structurally similar 1,2-diol, the following experiment was performed (Figure 4.21). Stock solutions with a concentration of 100 mM of $\mathbf{B_2D_1}$ and 100 mM of dried $\mathbf{D_2}$ were generated and equimolar amounts of $\mathbf{D_2}$ (2 mL) were added to $\mathbf{B_1D_2}$ (2 mL) in DCM under inert atmosphere at 20 °C.

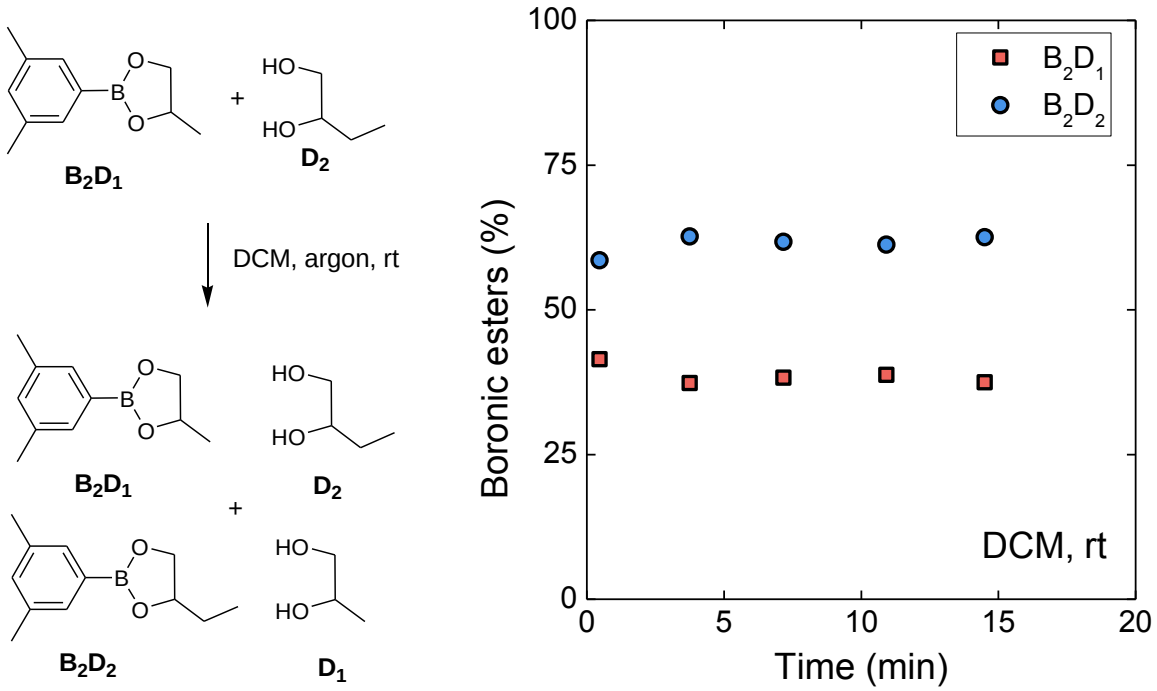

Figure 4.21. Transesterification of $\mathbf{B_2D_1}$ and $\mathbf{D_2}$ in DCM at an initial ratio of 1/1.

The data from GC analysis show the consumption of $\mathbf{B_2D_1}$ and the proportional generation of $\mathbf{B_2D_2}$. Free diols could not be detected by GC due to their very short retention in GC analysis. The exchange is almost instantaneous and the system reaches its equilibrium composition in less than 5 minutes. The equilibrium distribution is not stoichiometric meaning that boronic ester $\mathbf{B_2D_2}$ is slightly more stable under these conditions. It was thus proven that the transesterification of dioxaborolanes with a 1,2-aliphatic diol moiety proceeds very fast even at room temperature. Characteristic parameters such as the rate constant and the activation energy could not be obtained under these conditions. An alternative to working at drastically decreased temperatures was found by reacting two structurally similar dioxaborolanes in the presence of controlled small amounts of free diols. Using this procedure the exchange reaction kinetics slow down and become measurable (vide infra, subchapter 4.6.5).

4.6.3 Transesterification of dioxaborinanes with 1, 3 butanediol

4.6.3.1 Variation of added diol content

Similar to the transesterification of dioxaborolanes, 5-membered cyclic boronic esters, the transesterification of dioxaborinanes, 6-membered cycled boronic esters, with a 1,3-aliphatic diol was studied (Figure 4.22). Stock solutions with a concentration of 100 mM of **B_1D_9** were generated and different amounts of **D_8** (in 2 mL) were added to **B_1D_9** (2 mL) in DCM under inert atmosphere at 20°C.

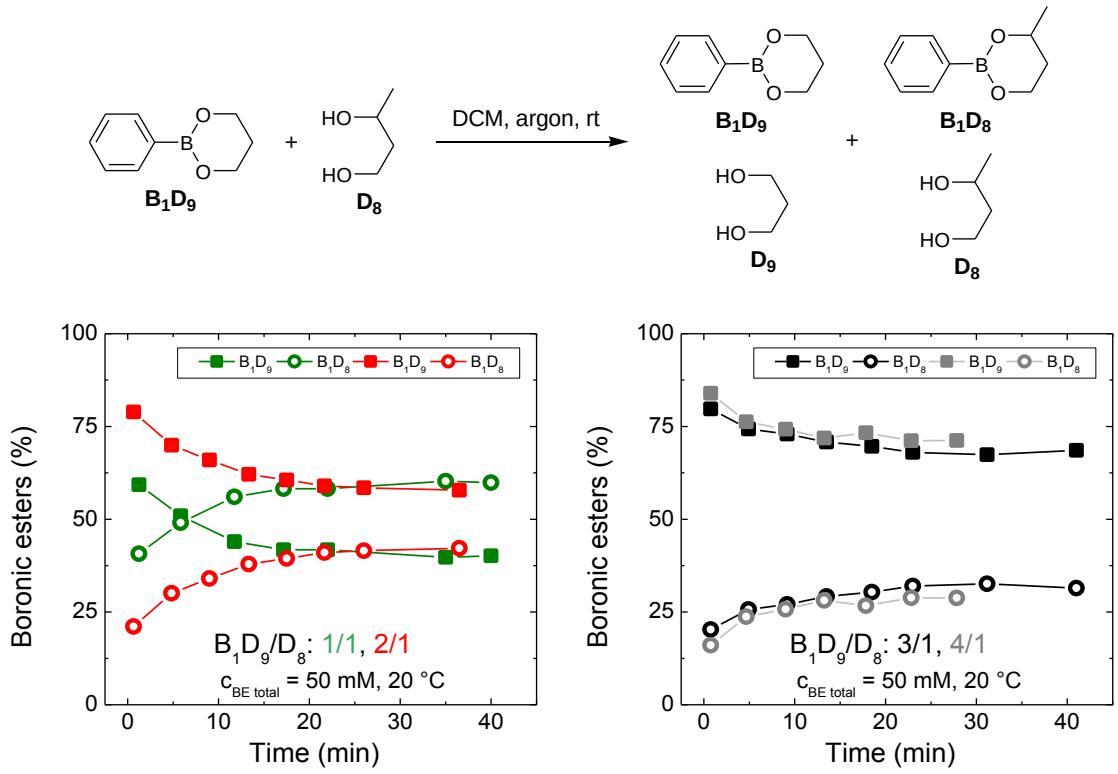

Figure 4.22. Exchange of a highly pure dioxaborinane **B_1D_9** with a 1,3-aliphatic diol **D_8** at 20 °C with changing boronic ester/diol ratio.

In contrast to the reaction of 5-membered cyclic boronic esters, the transesterification of 6-membered cyclic boronic esters was slower due to the higher stability of the 6-membered rings. In all experiments the reaction reached equilibrium after *ca.* 30 min. and the product distribution depended on the initial ratio of **B_1D_9** and **D_8** (Figure 4.22). For example, the reaction with an equimolar initial ratio resulted in an equilibrium composition of ca 3/2 **B_1D_8**/**B_1D_9**. An explanation for the over-expression of **B_1D_8** is the reported higher stability of this ester due to the additional methyl group of **D_8** as compared to D_9.Increasing the ratio in favor of **B_1D_9** led to the respective equilibrium compositions.

4.6.3.2 Variation of total reactant concentration with constant boronic ester/diol ratio and variation of both parameters

Tests with a constant ratio of **B_1D_9/D_8** (2/1) but different overall concentrations of compounds were performed. In Figure 4.23 are plotted the respective kinetic curves of the three experiments with varying total compound concentration (67/50/29 mM). The curves overlap almost perfectly, proving that the reaction is not concentration dependent at constant boronic ester/diol ratio. Experiments where both the boronic ester/diol ratio and overall compound concentrations were changed further validate both assumptions. The equilibrium distribution shifts, independently of the global compound concentration, in favor of **B_1D_8**. The higher is the initial concentration of **D_8** compared to the initial concentration of **B_1D_9** the more **B_1D_8** is over expressed.

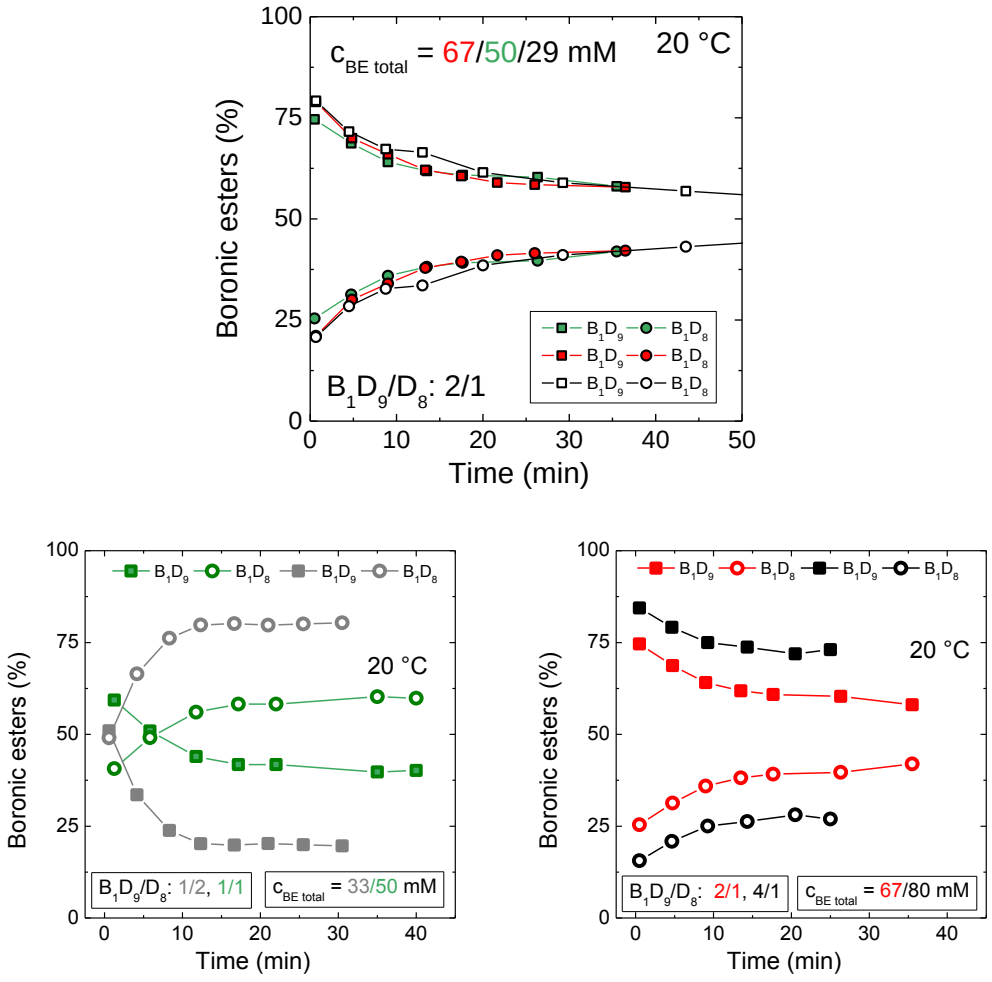

Figure 4.23. Exchange of a highly pure dioxaborinane **B_1D_9**, with a 1,3-aliphatic diol, **D_8**, at 20 °C with varying total concentration and boronic ester/diol ratio.

4.6.4 Transesterification of dioxaborolanes with 1,3-butanediol

After testing the transesterification of dioxaborolanes with 1,2-diols and dioxaborinanes with 1,3-diols, the exchange of the highly pure dioxaborolane **B_2D_1** with a 1,3-diol, namely 1,3-butanediol, was performed. Compounds were mixed in stoichiometric amounts in DCM under protective atmosphere at room temperature and the exchange was followed by GC.

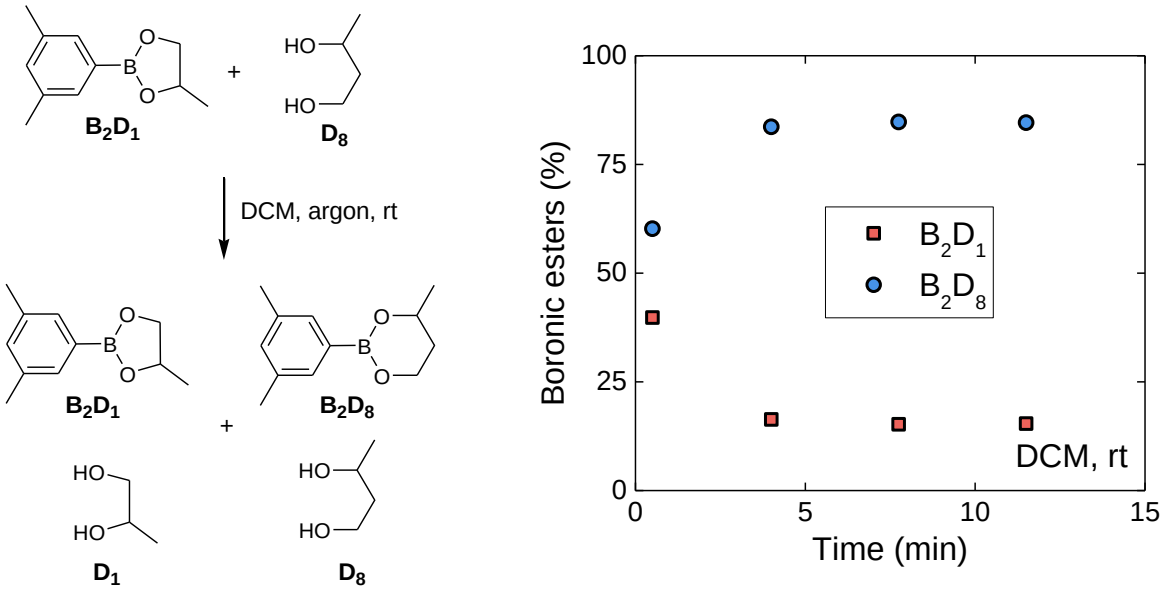

Figure 4.24. Exchange of a highly pure dioxaborolane **B_2D_1** with a 1,3-aliphatic diol **D_8** at 20 °C.

The exchange was extremely fast (t_{eq} < 4 min) and the equilibrium composition reflects the different stabilities of the two boronic esters: more than 80% of the 5-membered boronic ester (less stable) was converted into the more stable 6-membered boronic ester (Figure 4.24). In general, all of the analyzed transesterification reactions were too fast to be studied. With the aim to obtain characteristic parameters such as the rate constant of reaction and the activation energy, another method was designed.

4.6.5 Transesterification in mixtures of two dioxaborolanes in the presence of 1,2-butanediol

All of the studied boronic ester transesterification reactions were too fast to be measurable. To extend the time required to reach equilibrium, another experimental method was designed.

4.6.5.1 Variation of the free diol content

To make transesterification of dioxaborolanes made from 1,2-aliphatic diols measurable, the following experimental method was used. Boronic ester transesterification was studied by the

addition of different amounts of dried free diol to equimolar amounts of **B_1D_2** and **B_2D_1** in DCM under inert atmosphere at 20 °C (Scheme 4.8).

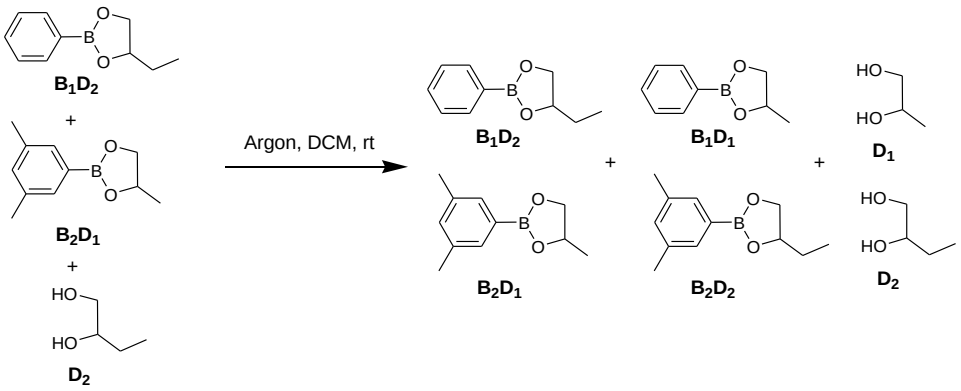

Scheme 4.8. Transesterification of **B_2D_1**, **B_1D_2** and **D_2** at room temperature under protective atmosphere.

Stock solutions with a concentration of 50 mM of **B_1D_2** and 50 mM of **B_2D_1** were generated in DCM and kept in Schlenk flasks under inert atmosphere. Stock solutions of dried **D_2** with different concentrations were generated and also stocked in Schlenk flasks under inert atmosphere. **B_1D_2** (2 mL) and **D_2** (0.1 mL) were mixed in the respective ratio of **B_1D_2** to **D_2** and stirred. As soon as **B_2D_1** (2 mL) was added the reaction was followed by GC analysis (Figure 4.25). Each sample was taken with a cleaned, oven dried and purged needle and injected into a small septum closed vial containing dried DCM before injection of 1 µL into the GC machine with a 10 µL syringe to avoid any contamination of the reaction mixture. For a total amount of 100 mmol boronic esters the following amounts of **D_2** were added: 0.6/1.24/1.9/4.19/7.25/10 mmol.

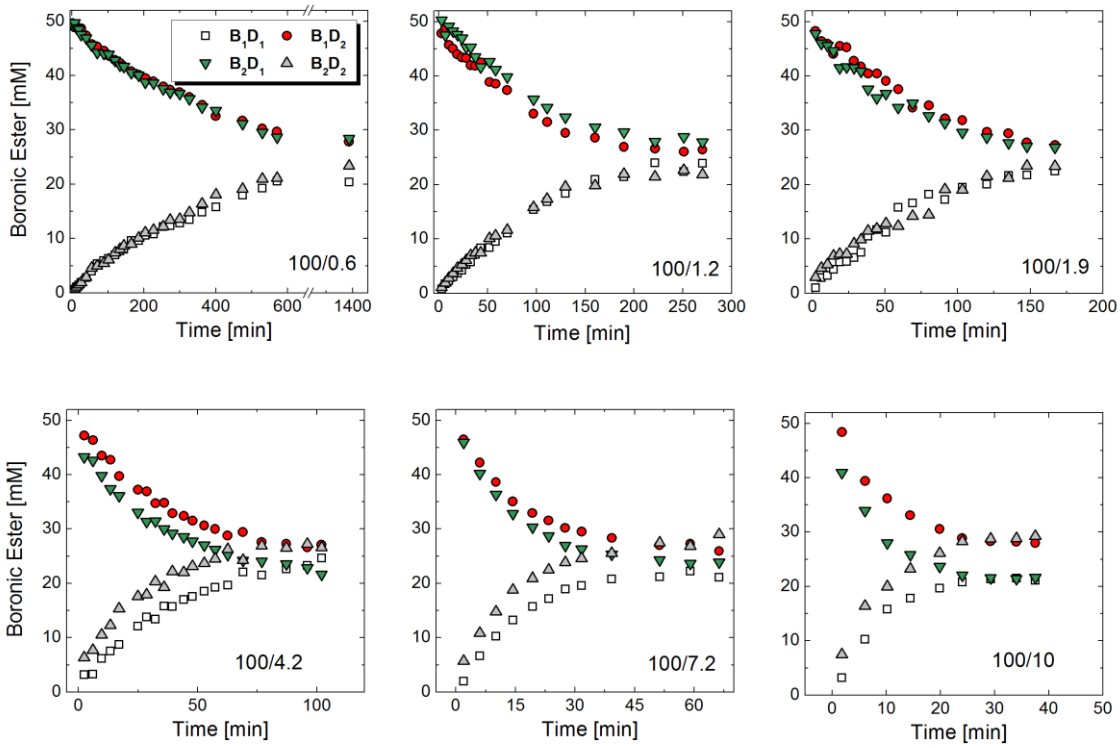

Figure 4.25. Kinetic data of the exchange reaction between two highly pure dioxaborolanes, $\mathbf{B_2D_1}$ and $\mathbf{B_1D_2}$, at room temperature in dry DCM, under protective atmosphere and in the presence of different amounts of added free diol $\mathbf{D_2}$.

The higher the amount of added free diol, the faster the reaction reached the equilibrium (Figure 4.25). At low concentrations of $\mathbf{D_2}$ the reaction was very slow $t_{eq.}$ > 20 h. At higher $\mathbf{D_2}$ content the reaction accelerated to reach equilibrium in less than 45 minutes when 10% of D2 was added in respect to $\mathbf{B_1D_2}$ and $\mathbf{B_2D_1}$. The same trend was followed for the over-expression of $\mathbf{D_2}$ containing boronic esters $\mathbf{B_1D_2}$ and $\mathbf{B_2D_2}$: the more $\mathbf{D_2}$ was added, the more pronounced their over-expression and the under-expression of the other two boronic esters containing $\mathbf{D_1}$, respectively.

Using the relation below the rate constant k was determined (for details see Appendix):

$$\sum_t [B_1D_2 + B_2D_1] = [B_1D_2]_0\,[1 - exp(-kt[D_1] + [D_2])]$$

$$[B_1D_2]_0 = 0.05\ M$$

$$[D_2] = 0.6/1.2/1.9/4.2/7.2/10.0\ \text{mM and}\ [D_1] = 5\text{x}10^{-3}\ \text{mM}$$

Equation 4.4

The experimental data fit the equations (Figure 4.26). The least suitable fit is obtained for [$\mathbf{D_2}$] = 1.24 mM with r^2 = 97.8. The obtained average rate constant k_{trans} was calculated to be:

$$k_{average} = {(k_{0.6} + k_{1.2} + k_{1.9} + k_{4.2} + k_{7.2} + k_{10})}/{6}$$

$$k_{average} = 0.145\ M^{-1}s^{-1}$$

Equation 4.5

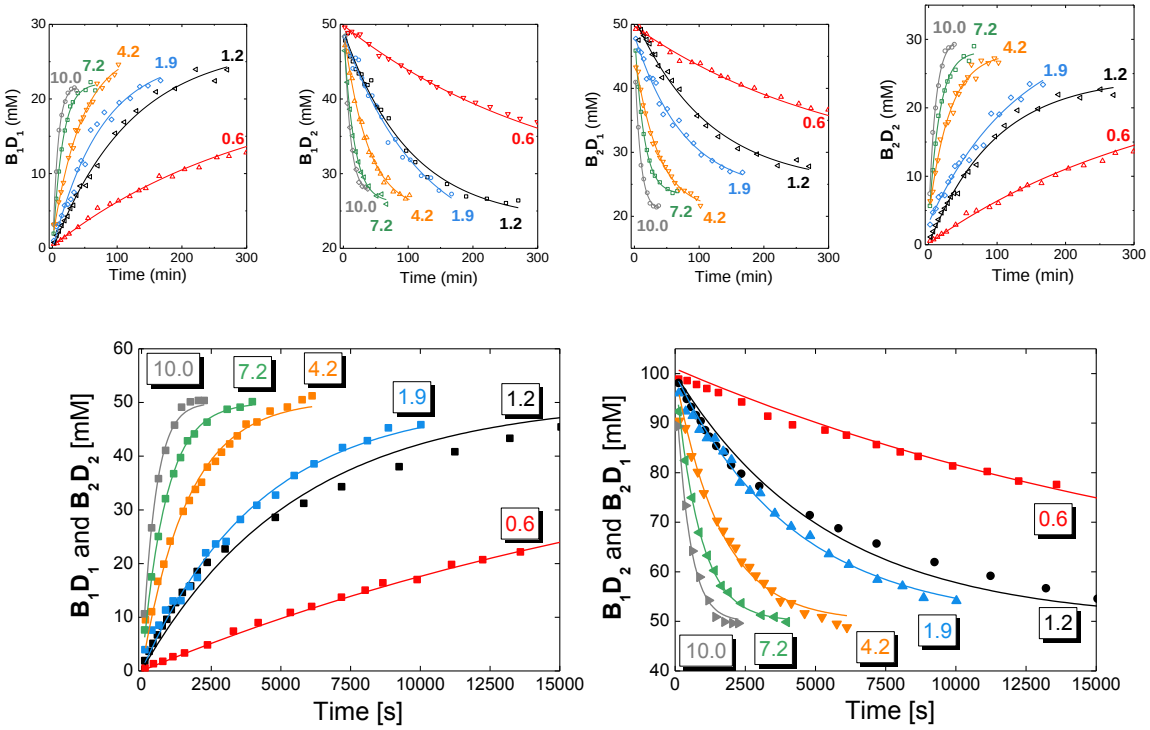

Figure 4.26. Kinetic data of the exchange reaction between highly pure dioxaborolanes $\mathbf{B_2D_1}$ and $\mathbf{B_1D_2}$ in the presence of different amounts of free diol $\mathbf{D_2}$. Top row: the data are organized by the different boronic esters. Bottom row: The data are organized by the sum of reactants and products.

In this section is presented the estimation of the rate constant of the transesterification of dioxaborolanes with 1,2 aliphatic diols (*k*). Due to the very short equilibrium time of dioxaborolane transesterification with monosubstitued 1,2-diol (mixture of $\mathbf{B_2D_1}$ and $\mathbf{D_2}$), the experiment was performed in the following set-up. To the equimolar mixture of two highly pure dioxaborolanes ($\mathbf{B_2D_1}$ and $\mathbf{B_1D_2}$) under argon in dry solvents were purposely added controlled amounts of 1,2-butanediol. This way the exchange slowed down and became measurable via GC. The more diol was added, the faster proceeded the reaction and for the highest amount of free diol (10 mol% of free diol) the equilibrium was reached in less than 40 minutes at room temperature. The rate constant was estimated to be $k_{average}$ = 0.145 M^{-1} s^{-1}. This value implicates that the exchange of a highly pure boronic ester with a 1,2 aliphatic

diol, *e.g.* $\mathbf{B_2D_1}$ with $\mathbf{D_2}$, would require around 70 s (at 100 mM) which is comparable to results presented in 4.6.2., where the equilibrium is reached in ≤ 220 s.

4.6.5.2 Variation of temperature

The temperature dependency of boronic ester transesterification was determined by exchanging $\mathbf{B_1D_2}$ and $\mathbf{B_2D_1}$ in the presence of a fixed amount of $\mathbf{D_2}$ at different temperatures under inert atmosphere. Stock solutions of $\mathbf{B_1D_2}$, $\mathbf{B_2D_1}$ and $\mathbf{D_2}$ were generated in toluene/MeCN 10/1 in Schlenk flasks under inert atmosphere (100 mM each boronic ester and 10 mM for $\mathbf{D_2}$). After addition of the reactants (2 mL of each stock solution of the boronic esters and 0.4 mL of the stock solution of $\mathbf{D_2}$) to a pre-heated Schlenk flask (overall concentrations of boronic esters after mixing = 45 mM) the reaction was monitored as described above for the experiments in DCM at the respective temperature of 20/35/50 and 75 °C (Figure 4.27).

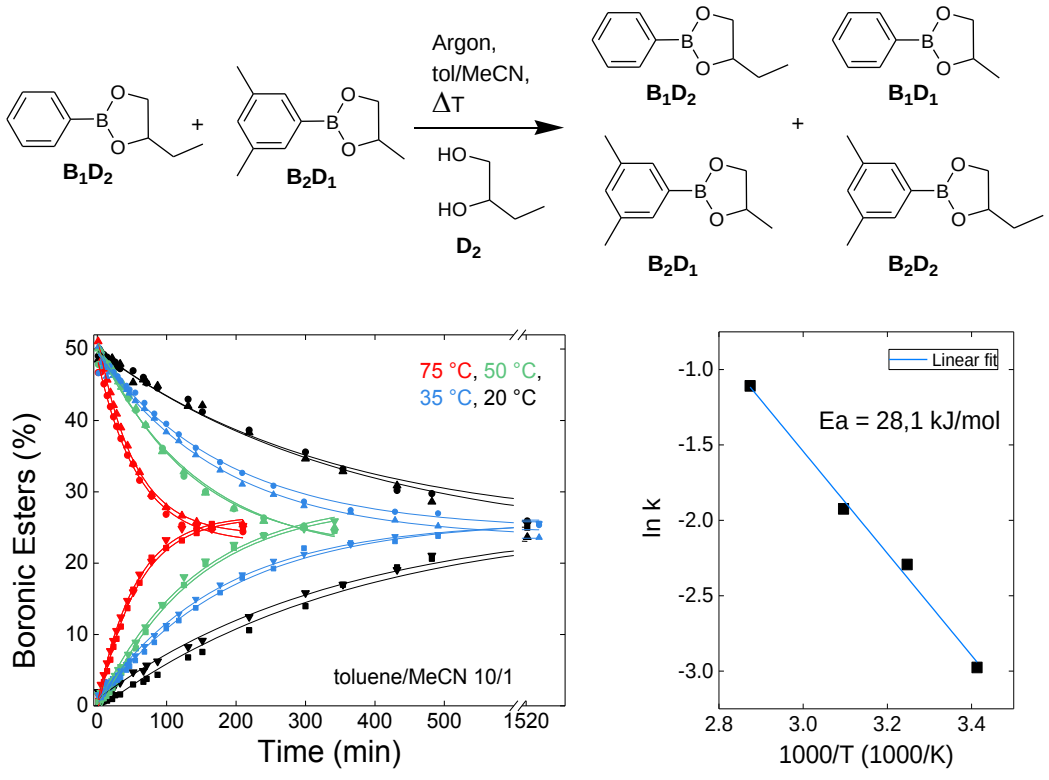

Figure 4.27. Left: The exchange of highly pure boronic esters $\mathbf{B_2D_1}$ and $\mathbf{B_1D_2}$ in the presence of 1 mol% of free diol $\mathbf{D_2}$ in toluene/MeCN at different temperatures. Right: Activation energy of boronic ester transesterification.

Increasing the temperature accelerated the exchange reaction. The reaction at 20 °C reached equilibrium in more than 8 hours whereas the reaction at 75 °C was already terminated after *ca.* 3 hours. Interestingly, these results differ from the characteristic equilibration time

observed in DCM at room temperature with a comparable amount of free diol. The exchange in toluene/MeCN was slowed down by a factor of almost three (k_{trans} = 0.051 M^{-1} s^{-1}) at room temperature) which might be due to solvent polarity. Assuming Arrhenius behavior, the four experiments in toluene/MeCN with 1%free diol were fitted with the above used equations and the resulting average rate constants were plotted against the inverse of the respective temperature to obtain an activation energy of 28.1 kJ/mol from the slope.[90,91]

$$k = A*\exp(-Ea/RT)$$

Equation 4.6.

Compared to other covalent exchange reactions, *e.g.* transesterification (*ca.* 88 kJ/mol) or vinylogous urethanes (*ca.* 59 kJ/mol) the determined activation energy for boronic ester transesterification is low, indicating that this reaction is less thermoactivated. The pre-factor A can give information about the number of collisions of molecules that are in a favorable orientation for reaction. The pre-factor A was calculated with the activation energy (28.1 kJ/mol) and the transesterification rate constant (k_{trans} = 0.051 M^{-1} s^{-1}) to be 5210 M^{-1} s^{-1} at room temperature.[17,18]

4.6.6 Exchange of dioxaborolanes in bulk without the addition of free diols or water

4.6.6.1 Variation of temperature

Humidity in the atmosphere was enough to trigger the reaction between highly pure boronic esters through water uptake of the solvent (THF) and diol generation. The observed process is most certainly strongly influenced by the capacity of the respective solvent to dissolve water from air and other solvents might result in slower or faster reaction kinetics. Boronic ester transesterification in solution was studied by the addition of controlled amounts of free diol to equimolar mixtures of highly pure boronic esters. At a fixed amount of diol, the temperature dependency of the exchange reaction was analyzed. When water was added instead of diol, the exchange takes place by boronic ester decomposition and diol generation. Without addition of diol or water and under inert atmosphere, the reaction is extremely slow at room temperature and at these concentrations of boronic esters(100 mM overall). Under these conditions, *i.e.* without any detectable diol or water, the reaction could proceed through a direct exchange between boronic esters or through successive transesterifications made possible by non detectable traces of diols. In the following section is presented the study of

the exchange of highly pure dioxaborolanes **B_1D_2** and **B_2D_1** in bulk at different temperatures without the addition of neither diol nor water and under inert atmosphere (Figure 4.28).

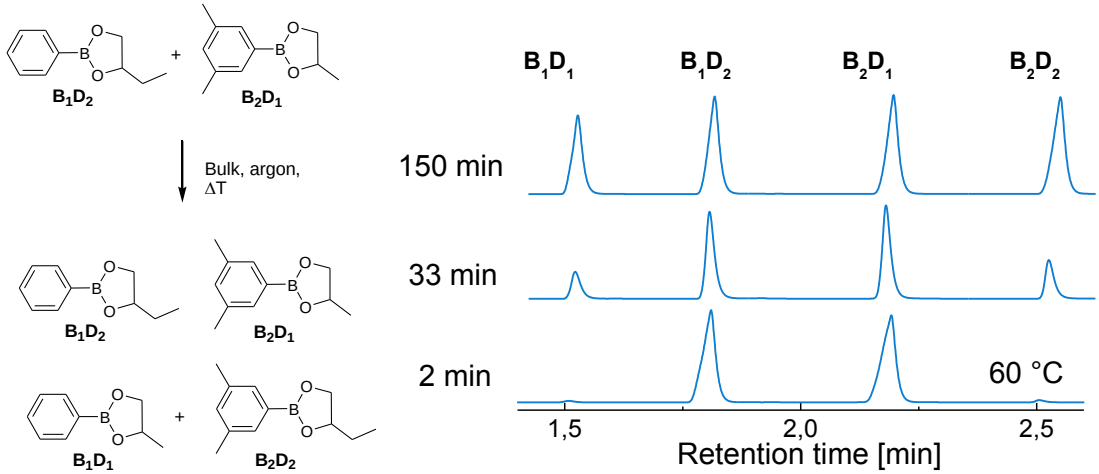

Figure 4.28. Exchange of highly pure boronic esters **B_2D_1** and **B_1D_2** in bulk at different temperatures under protective atmosphere. Right side: GC raw data of the exchange at 60 °C.

The boronic esters were mixed in equimolar amounts under argon in preheated flasks at six different temperatures. At 60 °C the reaction is finished after less than 3 hours while at 150 °C the equilibrium is reached in *ca*. 1 hour. At 180 °C, evaporation/condensation of the lightest boronic ester **B_1D_1** on the flasks walls was observed. Before sampling at this temperature the walls were "rinced" three times with the reaction mixture to minimize unequal compound composition.

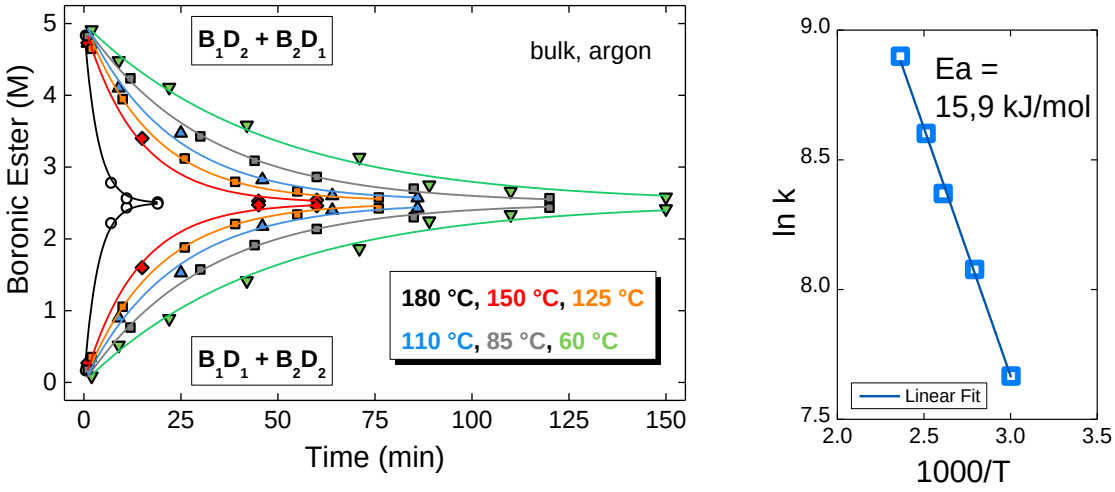

Figure 4.29. Exchange of highly pure boronic esters **B_2D_1** and **B_1D_2** in bulk at different temperatures and under protective atmosphere. Right side: Activation energy of the bulk reaction.

Other than for the experiment in solution, in the here presented experiments the exchange between two dioxaborolanes was observed without the addition of any diol or water. Assuming bulk concentrations of $[\mathbf{B_1D_2}]_0 = [\mathbf{B_2D_1}]_0$ = 5 M and $[\mathbf{D_2}]$ = 10^{-3} M (maximal amount of free diols, see Equation 4.1) rate constants of 21-73 M^{-1} s^{-1} were found by fitting with the above derived equations (see Equation 4.4). From the plot of ln k vs 1000/T the activation energy was calculated to be 15.9 kJ/mol. The pre-factor A was calculated according equation 4.6 to be 6600 M^{-1} s^{-1}. Samples of the reaction mixture were analyzed by ^{1}H-NMR spectroscopy right after mixing at the respective temperature and after the reaction reached equilibrium. In all cases, the content of free diols was too small to be detected. Below an example of the experiment at 150 °C, t = 1 min and t = 60 min.

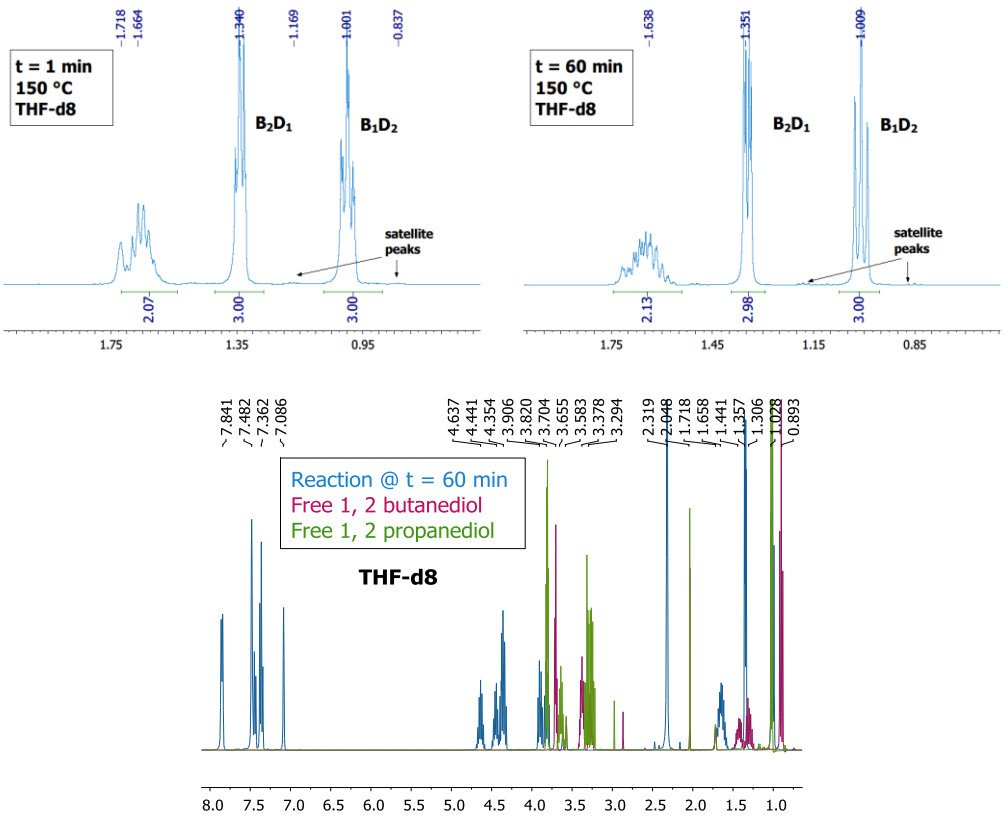

Figure 4.30. Top row from left to right: ^{1}H-NMR spectra in THF-d_8 of the bulk exchange reaction between highly pure boronic esters $\mathbf{B_2D_1}$ and $\mathbf{B_1D_2}$ at 150 °C at t=1 min and t=60 min. Bottom: overlay with the free diols in the same solvent.

By taking into account the difference (factor 2) between the estimated activation energies of the in this section presented reaction in bulk (15.9 kJ/mol) and of the reaction in solution (28.1 kJ/mol), the estimated rate constants can be compared. Surprisingly, the data vary by a factor of *ca.* 100 as compared to the rate constant found at room temperature. It was confirmed by ^{1}H-NMR that this very high difference cannot be explained by potential

hydrolysis and presence of diols. Furthermore, the pre-factors A, which give information about the successful collision of molecules in the reaction, are very similar for the reaction in bulk (6600 M^{-1} s^{-1}) and in solution (5210 M^{-1} s^{-1}). Whereas in solution, at low concentration of all species, almost no exchange was observed (Figure 4.13), in bulk at high concentration, the role that play undetectable traces of diols in respect to the exchange process might be altered. Additionally, the absence of a direct exchange process between the boronic esters cannot be excluded. More work has to be done on other boronic ester systems, *e.g.* on mixtures of two dioxaborinanes, to compare to kinetic studies which were performed in solution. Additionally, the exchange in bulk could be performed at lower temperatures to allow the sampling of more data points at the beginning of reaction. To check the role that the presence of purposely added diols can have on the above presented bulk reaction, the following experiments were performed.

4.6.6.2 Addition of free diol

It was observed that highly pure boronic esters $\mathbf{B_1D_2}$ and $\mathbf{B_2D_1}$ can undergo an exchange reaction without the addition of any diol or water in bulk. In regard of the increased rate constant of this reaction compared to the value found for the exchange in solution (factor 100), the role of free diols was investigated by deliberately adding small amounts of diol $\mathbf{D_2}$ to the bulk reaction mixture (Figure 4.31). The diol was added in 2 mol% [0.2 M] and 0.2 mol% [0.02 M] at 60 °C under argon following the same protocol as for the experiments without purposely added diol.

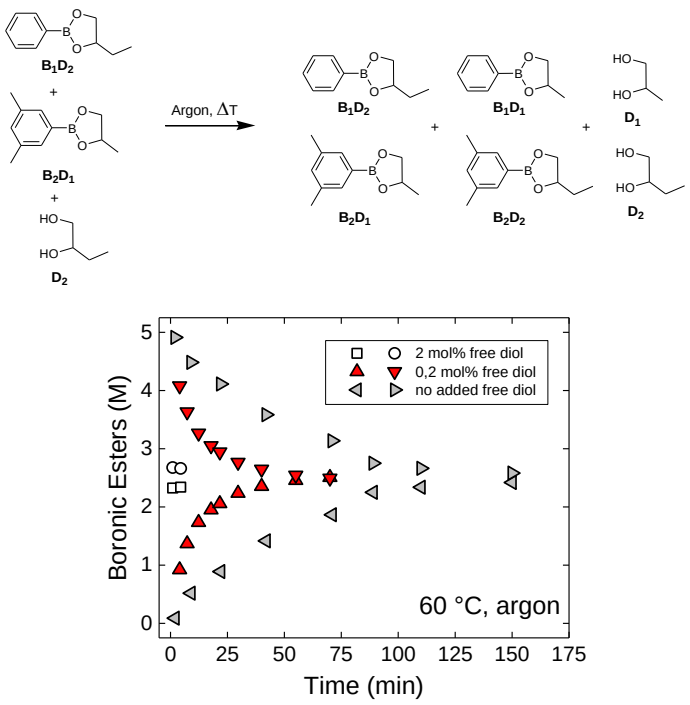

Figure 4.31. Exchange of highly pure boronic esters $\mathbf{B_1D_2}$ and $\mathbf{B_2D_1}$ in bulk in the presence of different amounts of free diol $\mathbf{D_2}$ under protective atmosphere.

The more diol was added, the faster the reaction reached the equilibrium. With 2 mol% added diol the reaction is terminated instantaneously. By decreasing the added diol concentration by a factor of 10, the reaction slowed down to reach equilibrium at *ca.* 75 min. Whereas the addition of 1.9 mol% of $\mathbf{D_2}$ resulted in an equilibrium time of ca 150-200 minutes for the experiments in solution, the influence of free diol seems to be much more important in bulk (equilibrium time <1 min at 2 mol%). This comparison further confirms the idea of an altered process in exchange reactions of boronic esters at high concentrations (in bulk).

4.7 Conclusion

In this chapter we reported a method to analyze dynamic covalent exchange reactions between diols and boronic esters. Compounds were synthesized in high to very high (free diol content ≤ 0.01 mol%) purities depending on the synthetic strategy. The association and disassociation of some boronic esters was studied in the presence of controlled amounts of water under protective atmosphere via ^{1}H-NMR. The stability of boronic esters under air, *i.e.* in solutions in the presence of humidity, and subsequent "in-situ" generation of exchange enabling diols was studied for 5-membered boronic esters under various conditions. The substitution pattern of boronic esters influenced their hydrolytic stability in solvent and thus resulted in different reaction kinetics under the tested conditions. The tested electron withdrawing groups attached to the aromatic boronic acid moiety increased the speed of exchange due to more acidic

boronic ester. By changing the linear aliphatic diols to cyclic diols, the exchange slows down due to the bulkiness of the diol moiety. Boronic esters made of 1,3-aliphatic diols are more stable due to the absence of ring strain and exchange slower than their 1,2-aliphatic diol counterparts. Pinacol, although a 1,2-aliphatic diol, generates boronic esters that do not undergo sufficient hydrolysis and transesterification to detect an exchange under the here presented testing conditions. Due to their liability towards water, a series of experiments was conducted under controlled conditions (argon, dried and purged glass ware, etc) using GC. According to literature, it was proven that boronic ester transesterification can be very fast, *e.g.* for 5-membered boronic esters, but also for 6-membered species. Via a special set-up, the mixing of two highly pure boronic esters and controlled amounts of diols or water, important parameters such as rate constants (k = 0.145 M^{-1} s^{-1}, at room temperature) and activation energy (E_a = 28.9 kJ/mol) were determined for the boronic ester transesterification of 5-membered species with an aromatic boronic acid and an aliphatic 1,2-diol moiety. Although in a dry solution of two highly pure boronic esters no exchange was observed without addition of free diol or water, the same reaction in bulk proceeded rapidly. The absence of (detectable) traces of diols and water before and after bulk reactions was verified via ^{1}H-HMR spectroscopy and a rate constant k = 21 M^{-1} s^{-1}, at 60 °C, and an activation energy of E_a = 15.9 kJ/mol were estimated. In conclusion, the exchange of highly pure boronic esters in solution was very slow under the here presented testing conditions. However in high concentration, *i.e.* in bulk, the exchange proceeded rapidly without compound degradation even at high temperatures. Bulk reactions will need to be further investigated, *e.g.* by testing the bulk reaction of two dioxaborinanes for comparison. Additionally, exchange reactions could be studied at lower temperatures to allow sampling of more data points at low conversions. Overall, the exchange in bulk is very promising for incorporation in polymer matrices due to the stability (temperature) and compatibility of boronic esters with a wide range of polymer backbones. Next and with the overall aim to generate vitrimers, boronic ester functionalities were introduced into different polymer systems.

4.8 Appendix

4.8.1 Characterization of boronic esters

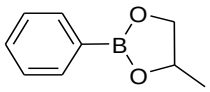

B_1D_1

^{1}H-NMR (400 MHz, $CDCl_3$): δ 7.84 p.p.m. (d, J = 5.6 Hz, 2H), 7.52-7.38 (m, 3H), 4.78-4.68 (m, 1H), 4.64 (dd, J = 1.2 Hz, 8.8 Hz, 1H), 3.90 (dd, J = 1.6 Hz, 8.8 Hz, 1H), 1.43 (d, J = 6.4 Hz, 3H). ^{13}C-NMR (100 MHz, $CDCl_3$): δ 134.7, 131.5, 127.9, 73.7, 72.4, 21.8. Carbon adjacent to boron not detected. Purity of **B_1D_1**: GC (FID) no impurities detected. ^{1}H-NMR: no diol detected.

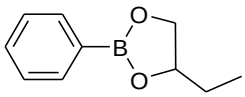

B_1D_2

^{1}H-NMR (400 MHz, $CDCl_3$): δ 7.84 p.p.m. (d, J = 6.4 Hz, 2H), 7.51-7.48 (m, 3H), 4.55 (m, 1H), 4.43 (dd, J = 8.8 Hz, 1.2 Hz 1H), 3.98 (dd, J = 2.0 Hz, 8.8 Hz, 1H), 1.82-1.63 (m, 2H), 1.04 (t, J = 7.6 Hz, 3H). ^{13}C-NMR (100 MHz, $CDCl_3$): δ 134.9, 131.4, 127.8, 78.6, 70.8, 29.0, 9.0. Carbon adjacent to boron not detected. Purity of **B_1D_2**: GC (FID) no impurities detected. ^{1}H-NMR: no diol detected.

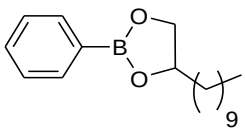

B_1D_4

^{1}H-NMR (400 MHz, $CDCl_3$): δ 7.83 p.p.m. (dd, J = 8.0, 2.8 Hz, 2H), 7.51-7.46 (m, 1H), 7.42-7.37 (m, 2H), 4.61-4.54 (m, 1H), 4.40 (dd, J = 8.8, 1.2 Hz, 1H), 3.96 (dd, J = 8.8 Hz, 1.2 Hz,

1H), 1.80-1.29 (m, 18H), 0.91 (t, J = 6.8 Hz, 3H). ^{13}C-NMR (100 MHz, $CDCl_3$): δ 134.6, 131.2, 127.8, 71.2, 36.2, 32.0, 29.2, 25.0, 22.7, 14.0. Carbon adjacent to boron not detected.

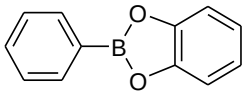

B_1D_6

^{1}H-NMR (400 MHz, $CDCl_3$): δ 8.12 p.p.m. (dd, J = 8.0, 1.6 Hz, 2H), 7.63-7.58 (m, 1H), 7.58-7.53 (m, 2H), 7.37-7.32 (m, 2H), 7.18-7.13 (m, 2H). ^{13}C-NMR (100 MHz, $CDCl_3$): δ 148.6, 134.9, 132.4, 128.4, 122.8, 113.0. Carbon adjacent to boron not detected.

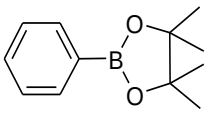

B_1D_7

^{1}H-NMR (400 MHz, $CDCl_3$): δ 7.85 p.p.m. (m, 2H), 7.45 (m, 3H), 1.38 (s, 12H). ^{13}C-NMR (100 MHz, $CDCl_3$): δ 134.8, 131.2, 127.8, 83.7, 25.0. Carbon adjacent to boron not detected.

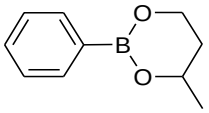

B_1D_8

^{1}H-NMR (400 MHz, $CDCl_3$): δ 7.83 p.p.m. (d, J = 8.0 Hz, 2H), 7.48-7.35 (m, 3H), 4.35-4.10 (m, 3H), 2.04-1.97 (m, 1H), 1.84-1.76 (m, 1H), 1.40 (d, J = 6.4 Hz, 3H). ^{13}C-NMR (100 MHz, $CDCl_3$): δ 133.7, 130.4, 127.6, 67.3, 61.4, 34.2, 23.0. Carbon adjacent to boron not detected.

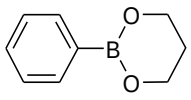

B_1D_9

^{1}H-NMR (400 MHz, $CDCl_3$): δ 7.78 p.p.m. (dd, J = 8.4 Hz, 1.2 Hz, 2H), 7.45-7.40 (m, 1H), 7.35 (t, J = 7.2 Hz, 2H), 4.17 (t, J = 5.6 Hz, 4H), 2.09-2.03 (m, 2H). ^{13}C-NMR (100 MHz, $CDCl_3$): δ 133.5, 130.3, 127.5, 61.9, 27.6. Carbon adjacent to boron not detected. Purity of **B_1D_9**: GC (FID) no impurities detected. ^{1}H-NMR: no diol detected.

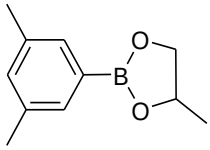

B_2D_1

^{1}H-NMR (400 MHz, $CDCl_3$): δ 7.46 p.p.m. (s, 2H), 7.13 (s, 1H), 4.73 (m, 1H), 4.46 (dd, J = 8.8 Hz, 1.2 Hz, 1H), 3.90 (dd, J = 8.8 Hz, 1.2 Hz, 1H), 2.34 (s, 6H), 1.43 (d, J = 6.0 Hz, 3H). ^{13}C-NMR (100 MHz, $CDCl_3$): δ 137.2, 133.2, 132.5, 73.72, 72.5, 21.8, 21.2. Carbon adjacent to boron not detected. Purity of **B_2D_1**: GC (FID) no impurities detected. ^{1}H-NMR: no diol detected. MS (m/z): [M] calcd for $C_{11}H_{15}BO_2$, 190.1165; found, 190.07.

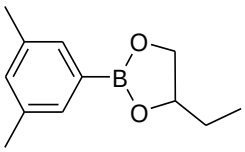

B_2D_2

^{1}H-NMR (400 MHz, $CDCl_3$): δ 7.45 p.p.m. (s, 2H), 7.12 (s, 1H), 4.56-4.94 (m, 1H), 4.42 (dd, J = 0.8 Hz, 8.8 Hz, 1H), 3.96 (dd, J = 2.0 Hz, 8.8 Hz, 1H), 2.35 (s, 6H), 1.80-1.62 (m, 2H), 1.02 (t, J = 7.6 Hz, 3H). ^{13}C-NMR (100 MHz, $CDCl_3$): δ 137.4, 133.2, 132.9, 78.5, 70.7, 28.8, 20.9, 8.7. Carbon adjacent to boron not detected.

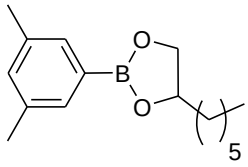

B_2D_3

^{1}H-NMR (400 MHz, $CDCl_3$): δ 7.43 p.p.m. (s, 2H), 7.12 (s, 1H), 4.56 (m, 1H), 4.41 (dd, J = 8.8 Hz, 1.2 Hz), 3.94 (dd, J = 8.8 Hz, 1.2 Hz, 1H), 2.33 (s, 6H), 1.76-1.27 (m, 10H), 0.89 (t, J = 6.8 Hz, 3H). ^{13}C-NMR (100 MHz, $CDCl_3$): δ 137.2, 133.0, 132.5, 77.5, 71.0, 36.2, 31.9, 28.9, 25.1, 22.5, 21.2, 14.0. Carbon adjacent to boron not detected.

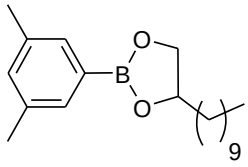

B_2D_4

^{1}H-NMR (400 MHz, $CDCl_3$): δ 7.45 p.p.m. (s, 2H), 7.12 (s, 1H), 4.57 (m, 1H), 4.42 (dd, J = 8.8 Hz, 1.2 Hz, 1H), 3.94 (dd, J = 8.8 Hz, 1.2 Hz, 1H), 2.34 (s, 6H), 1.73-1.28 (m, 18H), 0.90 (t, J = 6.8 Hz, 3H). ^{13}C-NMR (100 MHz, $CDCl_3$): δ 137.2, 133.1, 132.5, 77.5, 71.7, 36.2, 31.9, 29.7, 29.6, 29.5, 29.4, 24.9, 22.7, 21.2, 14.1. Carbon adjacent to boron not detected.

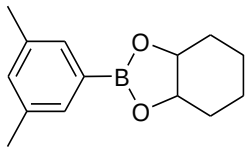

B_2D_5

^{1}H-NMR (400 MHz, $CDCl_3$): δ 7.48 p.p.m. (s, 2H), 7.13 (s, 1H), 4.53 (m, 2H), 2.34 (s, 6H), 1.94-1.78 (m, 4H), !1.65-1.55 (m, 2H), 1.45-1.35 (m, 2H). ^{13}C-NMR (100 MHz, $CDCl_3$): δ 137.2, 133.2, 132.5, 75.6, 28.7, 21.2, 19.4. Carbon adjacent to boron not detected. Purity of **B_2D_5**: ^{1}H-NMR: no diol detected. MS (m/z): [M] calcd for $C_{14}H_{19}BO_2$, 230.1478; found, 230.2.

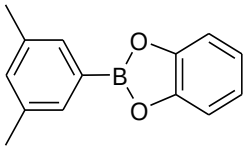

B_2D_6

^{1}H-NMR (400 MHz, $CDCl_3$): δ 7.71 p.p.m. (s, 2H), 7.32-7.29 (m, 2H), 7.22 (s, 1H), 7.15-7.09 (m, 2H), 2.40 (s, 6H). ^{13}C-NMR (100 MHz, $CDCl_3$): δ 148.6, 137.4, 134.3, 132.6, 122.5, 112.4, 21.3. Carbon adjacent to boron not detected.

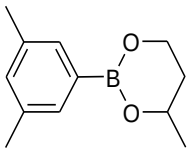

B_2D_8

^{1}H-NMR (400 MHz, $CDCl_3$): δ 7.41 p.p.m. (s, 2H), 7.05 (s, 1H), 4.28 (m, 1H), 4.19 (m, 1H), 4.10 (m, 1H), 2.3 (s, 6H), 2.02 (m, 1H), 1.81 (m, 1H), 1.37 (d, J = 6.4 Hz, 3H). ^{13}C-NMR (100 MHz, $CDCl_3$): δ 136.8, 132.2, 131.3, 67.6, 61.1, 34.3, 22.9, 21.3. Carbon adjacent to boron not detected. Purity of **B_2D_8**: ^{1}H-NMR: no diol detected. MS (m/z): [M] calcd for $C_{12}H_{17}BO_2$, 204.1322; found, 204.10.

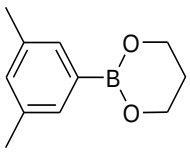

B_2D_9

^{1}H-NMR (400 MHz, $CDCl_3$): δ 7.39 p.p.m. (s, 2H), 7.06 (s, 1H), 4.16 (t, J = 5.6 Hz, 4H), 2.31 (s, 6H), 2.07-2.02 (m, 2H). ^{13}C-NMR (100 MHz, $CDCl_3$): δ 136.9, 132.3, 131.3, 61.9, 27.4, 21.3. Carbon adjacent to boron not detected. Purity of **B_2D_9**: GC (FID) no impurities detected. ^{1}H-NMR: no diol detected.

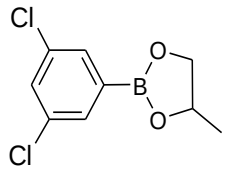

B_3D_1

^{1}H-NMR (400 MHz, $CDCl_3$): δ 7.64 p.p.m. (s, 2H), 7.43 (s, 1H), 4.71 (m, 1H), 4.46 (dd, J = 8.8 Hz, 1.2 Hz, 1H), 3.88 (dd, J = 8.8 Hz, 1.2 Hz, 1H), 1.42 (t, J = 6.8 Hz, 3H). ^{13}C-NMR (100 MHz, $CDCl_3$): δ 134.8, 132.9, 131.2, 74.0, 72.3, 21.3. Carbon adjacent to boron not detected. Purity of **B_3D_1**: GC (FID) no impurities detected. ^{1}H-NMR: no diol detected.

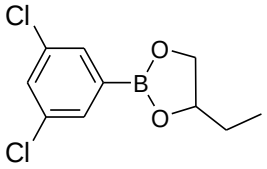

B_3D_2

^{1}H-NMR (400 MHz, DMSO): δ .7.77 p.p.m. (t, J = 2.0 Hz, 1H), 7.58 (d, J = 2.0 Hz, 2H), 4.59-4.52 (m, 1H), 4.44-4.40 (dd, J = 8.8, 0.8 Hz, 1H), 3.95 (dd, J = 8.8, 2.0 Hz, 1H), 1.67-1.60 (m, 2H), 0.93 (t, J = 7.2 Hz, 3H). ^{13}C-NMR (100 MHz, DMSO): δ 134.1, 133.7, 132.3, 78.7, 70.5, 28.3, 8.7. Carbon adjacent to boron not detected.

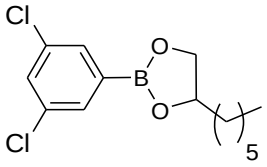

B_3D_3

^{1}H-NMR (400 MHz, $CDCl_3$): δ 7.65 p.p.m. (d, J = 2 Hz, 1H), 7.43 (t, J = 2 Hz, 1H), 4.61-4.54 (m, 1H), 4.43 (dd, J = 8.8, 1.2 Hz, 1H), 3.95 (dd, J = 8.8 Hz, 1.2 Hz), 1.76-1.26 (m, 10H), 0.89 (t, J = 6.8 Hz, 3H). ^{13}C-NMR (100 MHz, $CDCl_3$): δ 134.8, 132.8, 131.2, 78.0, 71.5, 36.1, 31.7, 29.2, 25.0, 22.6, 14.1. Carbon adjacent to boron not detected. Purity of **B_3D_3**: ^{1}H-NMR: no diol detected.

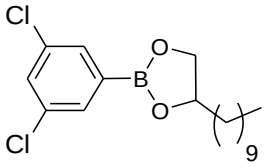

B_3D_4

^{1}H-NMR (400 MHz, $CDCl_3$): δ 7.65 p.p.m. (d, J = 2 Hz, 1H), 7.45 (t, J = 2 Hz, 1H), 4.61-4.54 (m, 1H), 4.43 (dd, J = 8.8, 1.2 Hz, 1H), 3.95 (dd, J = 8.8 Hz, 1.2 Hz), 1.76-1.27 (m, 18H), 0.88 (t, J = 6.8 Hz, 3H). ^{13}C-NMR (100 MHz, $CDCl_3$): δ 134.8, 132.8, 131.2, 78.1, 71.5, 36.1, 31.9, 29.6, 29.5, 29.4, 29.3, 29.2, 24.9, 22.7, 14.1. Carbon adjacent to boron not detected.

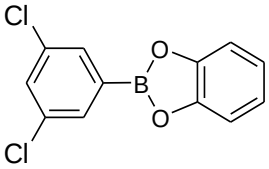

B_3D_6

^{1}H-NMR (400 MHz, $CDCl_3$): δ 7.93 p.p.m. (s, 2H), 7.56 (s, 1H), 7.33 (m, 2H), 7.16 (m, 2H). ^{13}C-NMR (100 MHz, $CDCl_3$): δ 143.4, 132.9, 132.3, 123.3, 121.4, 115.3, 112.9. Carbon adjacent to boron not detected.

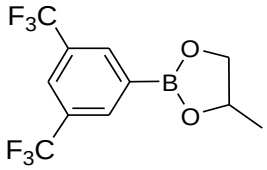

B_4D_1

^{1}H-NMR (400 MHz, $CDCl_3$): δ 8.24 p.p.m. (s, 2H), 7.96 (s, 1H), 4.79 (m, 1H), 4.54 (dd, J = 8.8 Hz, 1.2 Hz, 1H), 3.95 (dd, J = 8.8 Hz, 1.2 Hz, 1H), 1.46 (d, J = 6.0 Hz, 3H). ^{13}C-NMR (100 MHz, $CDCl_3$): δ 134.7, 124.9, 124.8, 122.1, 74.3, 72.8, 21.6. Carbon adjacent to boron not detected.

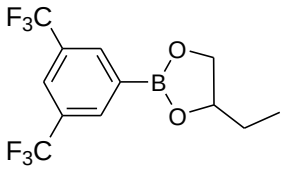

B_4D_2

^{1}H-NMR (400 MHz, $CDCl_3$): δ 8.25 p.p.m. (s, 2H), 7.96 (s, 1H), 4.64-4.57 (m, 1H), 4.89 (dd, J = 8.8, 0.8 Hz, 1H), 4.03 (dd, J = 8.8, 1.6 Hz, 1H), 1.78-1.67 (m, 2H), 1.04 (t, J = 7.2 Hz, 3H). ^{13}C-NMR (100 MHz, $CDCl_3$): δ 134.4, 127.5, 124.7, 122.1, 79.3, 70.5, 28.5, 8.8. Carbon adjacent to boron not detected. Purity of **B_4D_2**: GC (FID) no impurities detected. ^{1}H-NMR: no diol detected.

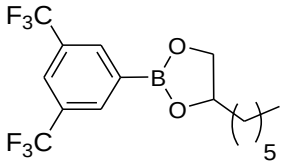

B_4D_3

^{1}H-NMR (400 MHz, $CDCl_3$): δ 8.25 p.p.m. (s, 2H), 7.96 (s, 1H), 4.68-4.61 (m, 1H), 4.49 (dd, J = 8.8 Hz, 1.2 Hz, 1H), 4.01 (dd, J = 8.8 Hz, 1.2 Hz, 1H), 1.81-1.32 (m, 10H), 0.90 (t, J = 6.8 Hz, 3H). ^{13}C-NMR (100 MHz, $CDCl_3$): δ 134.7, 131.1, 130.8, 124.8, 78.3, 71.6, 36.1, 31.7, 29.0, 25.0, 22.5, 13.9. Carbon adjacent to boron not detected.

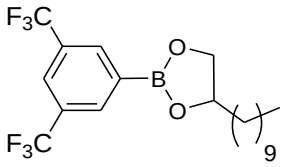

B_4D_4

^{1}H-NMR (400 MHz, $CDCl_3$): δ 8.24 p.p.m. (s, 2H), 7.96 (s, 1H), 4.67-4.60 (m, 1H), 4.49 (dd, J = 8.8 Hz, 1.2 Hz, 1H), 4.01 (dd, J = 8.8 Hz, 1.2 Hz, 1H), 1.80-1.27 (m, 18H), 0.88 (t, J = 6.8 Hz, 3H). ^{13}C-NMR (100 MHz, $CDCl_3$): δ 134.7, 131.2, 130.8, 124.8, 78.3, 71.6, 36.1, 31.9, 29.6, 29.5, 29.4, 29.3, 29.1, 24.9, 22.7, 14.1. Carbon adjacent to boron not detected. Purity of **B_4D_4**: ^{1}H-NMR: no diol detected.

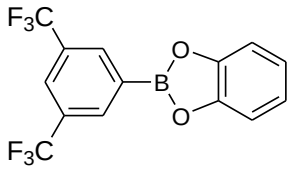

B_4D_6

^{1}H-NMR (400 MHz, $CDCl_3$): δ 8.52 p.p.m. (s, 2H), 8.01 (s, 1H), 7.38 (m, 2H), 7.19 (m, 2H). ^{13}C-NMR (100 MHz, $CDCl_3$): δ 148.0, 134.8, 125.8, 124.4, 123.5, 121.9, 113.0. MS (m/z): [M] calcd for $C_{14}H_7BF_6O_2$, 332.0443; found, 332.03.

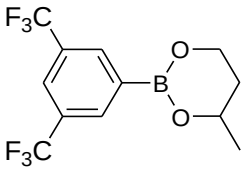

B_4D_8

^{1}H-NMR (400 MHz, $CDCl_3$): δ 8.21 p.p.m. (s, 2H), 7.89 (s, 1H), 4.37-4.30 (m, 1H), 4.26-4.21 (m, 1H), 4.18-4.12 (m, 1H), 2.10-2.04 (m, 1H), 1.83-1.78 (m, 1H), 1.40 (d, J = 6.4 Hz, 3H). ^{13}C-NMR (100 MHz, $CDCl_3$): δ 133.7, 68.1, 67.4, 61.3, 34.0, 30.2, 25.4, 22.6. Carbon adjacent to boron not detected.

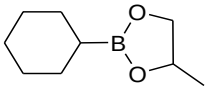

B_5D_1

^{1}H-NMR (400 MHz, $CDCl_3$): δ 4.48 p.p.m. (m, 1H), 4.23 (m, 1H), 3.66 (m, 1H), 1.69-1.01 (m, 14H). ^{13}C-NMR (100 MHz, $CDCl_3$): δ 73.0, 72.0, 28.1, 27.2, 26.7, 21.6. Carbon adjacent to boron not detected. Purity of **B_5D_1**: GC (FID) no impurities detected. ^{1}H-NMR: no diol detected. MS (m/z): m/z: [M] calcd for $C_9H_{17}BO_2$, 168.1322; found, 169.0.

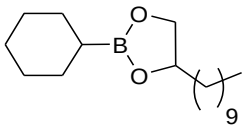

B_5D_4

^{1}H-NMR (400 MHz, $CDCl_3$): δ 4.32 p.p.m. (m, 1H), 4.18 (t, J = 8.4 Hz, 1H), 3.71 (t, J = 8.4 Hz, 1H), 1.87-0.98 (m, 29H), 0.85 (t, J = 6.8 Hz, 3H). ^{13}C-NMR (100 MHz, $CDCl_3$): δ 76.7, 70.5, 65.8, 36.2, 31.9, 29.6, 29.5, 29.3, 28.0, 27.1, 26.7, 24.9, 22.7, 14.1. Carbon adjacent to boron not detected.

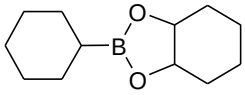

B_5D_5

^{1}H-NMR (400 MHz, $CDCl_3$): δ 4.32 p.p.m. (m, 2H), 1.83-1.46 (m, 10H), 1.43-1.25 (m, 8H), 1.07-0.98 (m, 1H). ^{13}C-NMR (100 MHz, $CDCl_3$): δ 74.9, 28.5, 28.0, 27.2, 26.8, 19.0. Carbon adjacent to boron not detected.

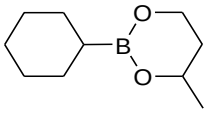

B_5D_8

^{1}H-NMR (400 MHz, $CDCl_3$): δ 4.17-3.87 p.p.m. (m, 3H), 1.98-1.49 (m, 7H), 1.37-1.14 (m, 8H), 0.78 (t, J = 8.8 Hz, 1H). ^{13}C-NMR (100 MHz, $CDCl_3$): δ 67.0, 61.8, 60.9, 28.2, 27.4, 26.9, 23.0. Carbon adjacent to boron not detected.

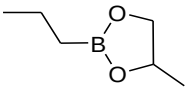

B_6D_1

^{1}H-NMR (400 MHz, $CDCl_3$): δ 4.48 p.p.m. (m, 1H), 4.22 (t, J = 8.4 Hz, 1H), 3.66 (t, J = 8.4 Hz, 1H), 1.47-1.16 (m, 4H), 0.91 (t, J = 7.2 Hz, 3H), 0.79 (t, J = 7.2 Hz, 3H). ^{13}C-NMR (100 MHz, $CDCl_3$): δ 72.9, 72.0, 21.9, 17.5, 16.8. Carbon adjacent to boron not detected.

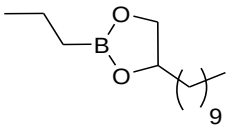

B_6D_4

^{1}H-NMR (400 MHz, $CDCl_3$): δ 4.34 (m, 1H), 4.21 (m, 1H), 3.74 (m, 1H), 1.68-1.25 (m, 22H), 0.95-0.79 (m, 6H). ^{13}C-NMR (100 MHz, $CDCl_3$): δ 76.8, 70.7, 36.2, 32.0, 29.6, 29.6, 29.5, 29.3, 25.0, 22.6, 17.5, 16.9, 14.0. Purity of **B_6D_4**: ^{1}H-NMR: no diol detected. MS (m/z): [M] calcd for $C_{15}H_{31}BO_2$, 254.2417; found, 254.05.

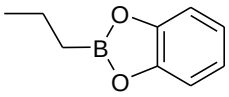

B_6D_6

^{1}H-NMR (400 MHz, $CDCl_3$): δ 7.25-7.21 p.p.m. (m, 2H), 7.10-7.04 (m, 2H), 1.78-1.64 (m, 2H), 1.34-1.30 (m, 2H), 1.07 (t, J = 7.2 H, 3H). ^{13}C-NMR (100 MHz, $CDCl_3$): δ 148.3, 123.0, 112.0, 24.7, 9.8. Carbon adjacent to boron not detected.

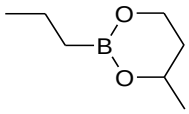

B_6D_8

^{1}H-NMR (400 MHz, $CDCl_3$): δ 4.12-3.86 p.p.m. (m, 3H), 1.92-1.81 (m, 1H), 1.67-1.57 (m, 1H), 1.39-1.30 (m, 2H), 1.23 (d, J = 8.8 Hz, 3H), 0.87 (t, J = 7.2 Hz, 3H), 0.63 (t, J = 7.6 Hz, 2H). ^{13}C-NMR (100 MHz, $CDCl_3$): δ 67.0, 60.8, 34.2, 22.8, 17.4, 16.9. Carbon adjacent to boron not detected.

4.8.2 Determination of free diols after reaction in THF-d8

Shift [ppm]	Integration	Protons (theory)	Integration per proton	Average integration per proton
Boronic esters				
Aromatics	14.41 + 20.86 + 15.07 + 6.7 = 57.04	16	3.57	28x3.57 + 12x3.69 + 4x3.87 + 12x3.74 = 204.6 204.6/56 = **3.65**
4.64 - 3.75	6.71 + 21.57 + 14.58 = 42.86	12	3.57	
2.27	44.29	12	3.69	
1.649	15.49	4	3.87	
1.33 + 0.983	22.45 + 22.43 = 44.88	12	3.74	
Free acids and diols				
7.76 + 7.25 + 7.10 + 6.98	0.68 + 0.79 + 1.17 + 1.2 = 3.84	16	0.24	32*0.24 + 12*0.19 = 9.96 9.96/44 = **0.226**
3.8 – 3.2	0.39 + 0.9 + 2.49 = 3.78	16	0.24	
1.20 + 0.88	0.99 + 1.32 = 2.31	12	0.19	
% free diols (acids)				
0.226/(0.226 + 3.65) = 0.0583 ca 6% of free diols (acids) in respect to boronic esters				

Table 4.6. To determine the overall fee diol content in the sample at 350 minutes, the average values of all detectable relevant integration values were taken.

4.8.3 Exchange reactions under air

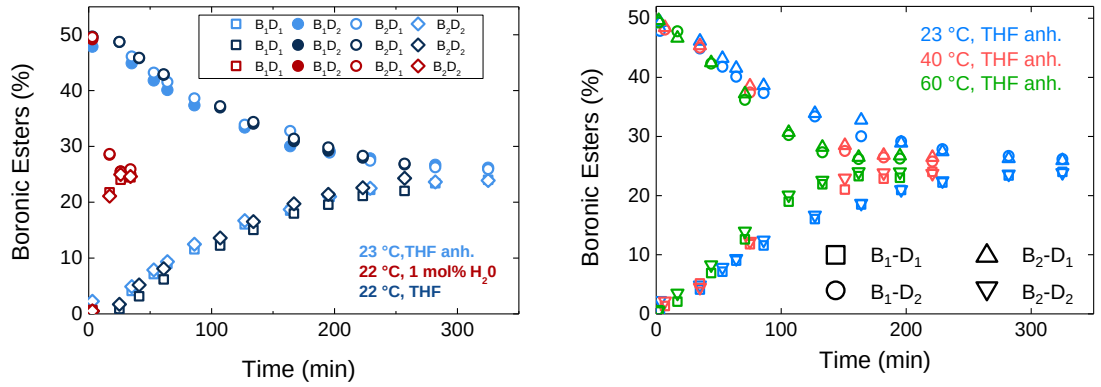

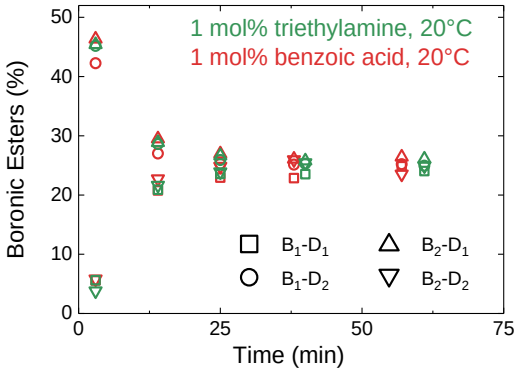

Figure 4.32. The exchange of two pure dioxaborolanes (**B_1D_2** and **B_2D_1**) in solution in the presence of humidity results in a stoichiometric mixture of four different boronic esters. From top to bottom and left to right: Reactions 4.5.1 – 4.5.10.

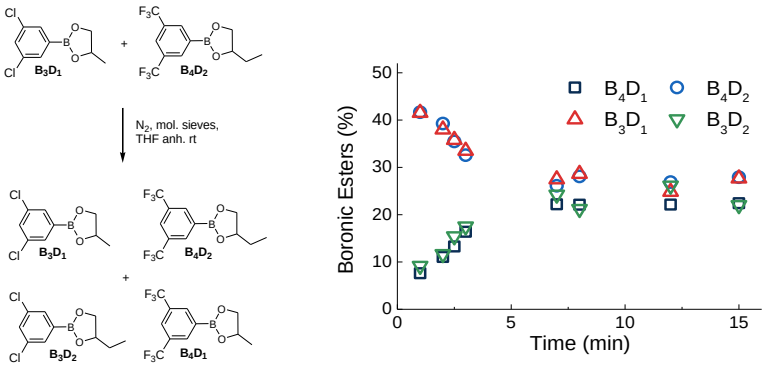

Figure 4.33. Reaction 4.5.11. in anhydrous THF at room temperature.

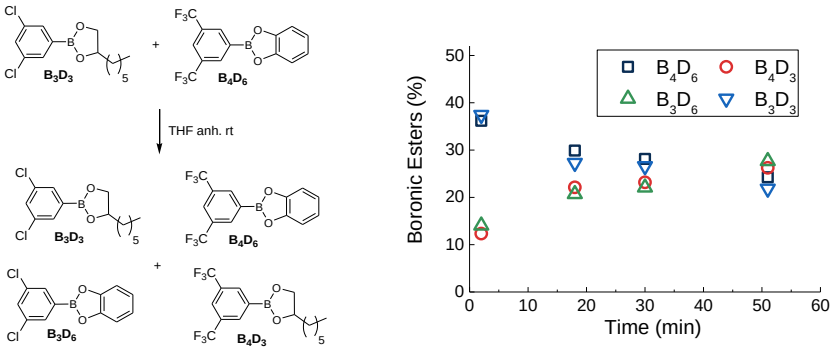

Figure 4.34. Reaction 4.5.13. in anhydrous THF at room temperature.

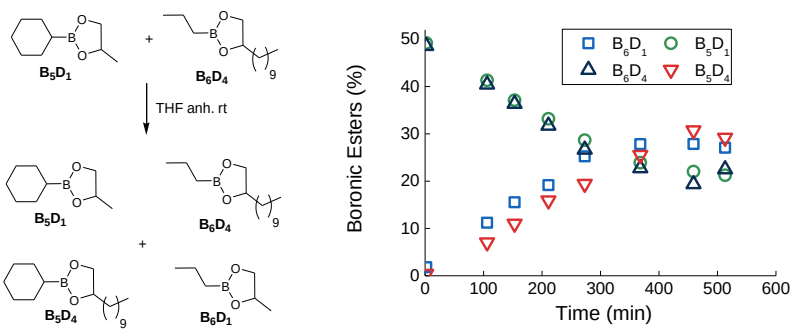

Figure 4.35. Reaction 4.5.14. in anhydrous THF at room temperature.

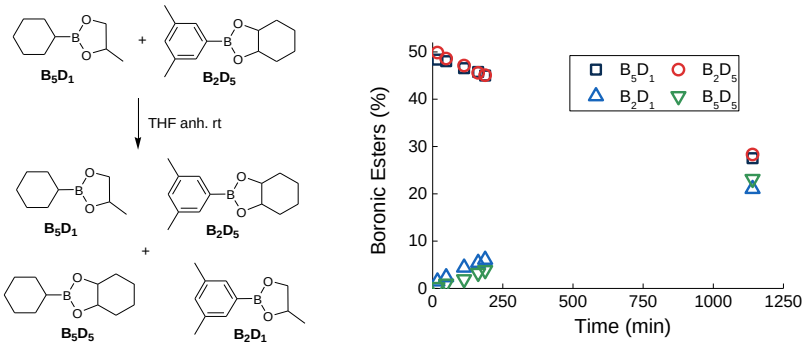

Figure 4.36. Reaction 4.5.15. in anhydrous THF at room temperature.

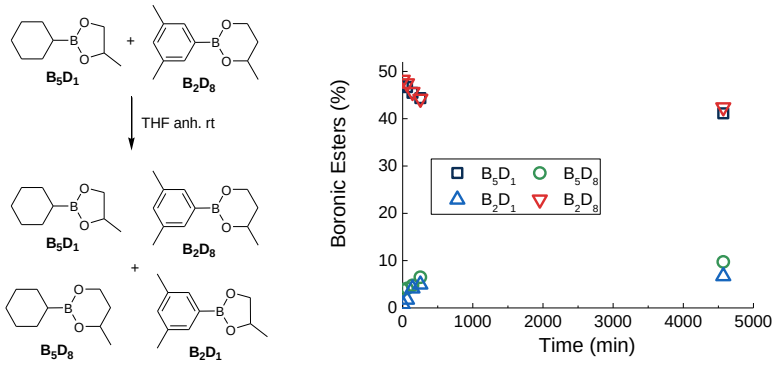

Figure 4.37. Reaction 4.5.16. in anhydrous THF at room temperature.

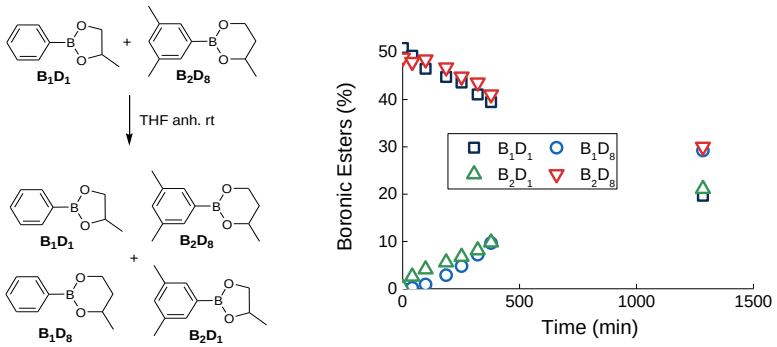

Figure 4.38. Reaction 4.5.17. in toluene at 100 °C.

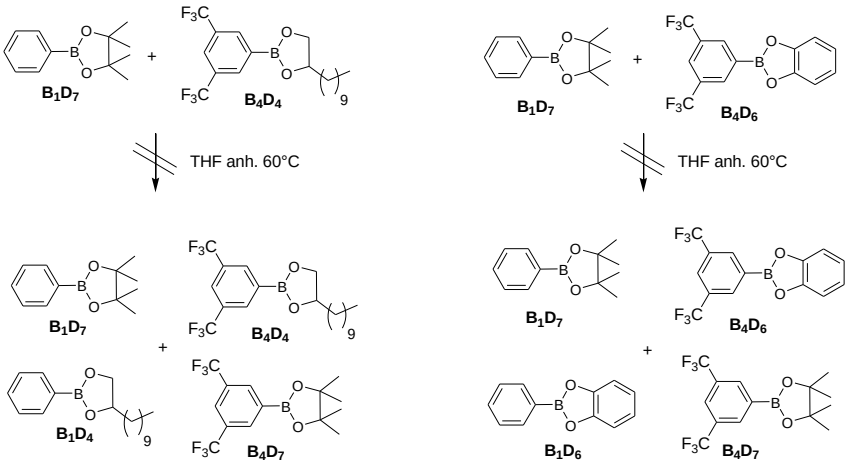

Figure 4.39. Reactions 4.5.21. and 4.5.22. in anhydrous THF at 60 °C.

4.8.4 Equations for the estimation of the rate constants

Equations for the estimation of rate constants of boronic ester exchanges in bulk, developed from Ludwik Leibler:

If transesterification only

$$[D_1] + [D_2] + [B_1D_2] + [B_2D_1] \longrightarrow [D_1] + [D_2] + [B_1D_2] + [B_2D_1] + [B_1D_1] + [B_2D_2]$$

and

$$\dot{[D_1]} = -k[D_1][B_1D_2] - k[D_1][B_2D_2] + k[D_2][B_2D_1] + k[D_2][B_1D_1] = \dot{[B_2D_2]} - \dot{[B_1D_1]}$$

$$\dot{[D_2]} = -k[D_2][B_2D_1] - k[D_2][B_1D_1] + k[D_1][B_1D_2] + k[D_1][B_2D_2] = -\dot{[B_2D_2]} + \dot{[B_1D_1]}$$

$$\dot{[B_1D_2]} = -k[D_1][B_1D_2] + k[D_2][B_1D_1]$$

$$\dot{[B_2D_1]} = -k[D_2][B_2D_1] + k[D_1][B_2D_2]$$

$$\dot{[B_1D_1]} = -k[D_2][B_1D_1] + k[D_1][B_1D_2] = -\dot{[B_1D_2]}$$

$$[B_2D_2] = - k[D_1][B_2D_2] + k[D_2][B_2D_1] = - [B_2D_1]$$

We suppose

$$[B_1D_2]_0 = [B_2D_1]_0 = c_{BE}/2 = c_0 \quad \text{and} \quad [B_2D_2]_0 = [B_1D_1]_0 = 0$$

$$[\dot{B_1}D_2] = - [\dot{B_1}D_1] \Rightarrow [B_1D_2] = [B_1D_2]_0 - [B_1D_1] = c_0 - [B_1D_1]$$

$$[\dot{B_2}D_1] = - [\dot{B_2}D_2] \Rightarrow [B_2D_1] = [B_2D_1]_0 - [B_2D_2] = c_0 - [B_2D_2]$$

$$[\dot{D_1}] = [\dot{B_2}D_2] - [\dot{B_1}D_1] = - [\dot{D_2}]$$

$$[D_1]_t = [D_1]_0 + [B_2D_2]_t - [B_1D_1]_t \quad \text{and} \quad [D_2]_t = [D_2]_0 - [B_2D_2]_t + [B_1D_1]_t$$

To solve:

$$[\dot{B_1}D_1] + [\dot{B_2}D_2] = - [D_2]\,([B_1D_1] + [B_2D_1]) + [D_1]\,([B_1D_2] - [B_2D_2])$$

$$= - [D_2]\,([B_1D_1] - c_0 + [B_2D_2]) + [D_1]\,(c_0 - [B_1D_1] - [B_2D_2])$$

$$= - [D_2]\,([B_1D_1] + [B_2D_2]) + c_0[D_2] + c_0[D_1] - [D_1]\,([B_1D_1] + [B_2D_2])$$

$$= - ([D_1] + [D_2])\,([B_1D_1] + [B_2D_2]) + c_0\,([D_1] + [D_2])$$

$$= ([D_1] + [D_2])\,(c_0 - ([B_1D_1] + [B_2D_2]))$$

$$= d_0\,(c_0 - ([B_1D_1] + [B_2D_2]))$$

With $[D_1] + [D_2] = [D_1]_0 + [B_2D_2] - [B_1D_1] + [D_2]_0 - [B_2D_2] - [B_1D_1] = [D_1]_0 + [D_2]_0 = d_0$

We define a characteristic time

$$\tau = 1/(k([D_1]_0 + [D_2]_0))$$

and a fraction of boronic esters χ

$\chi = ([B_1D_1] + [B_2D_2])/[B_1D_2]$ (we supposed $[B_1D_2]_0 = [B_2D_1]_0$)

Solving

$$\tau\,\dot{\chi} = 1 - \chi$$

for χ gives (t = 0, χ = 0)

$$\chi = 1 - \exp(-t/\tau)$$

Hence, the sum of products (starting compounds) is

$$\Sigma_t = c_0 (1 - \exp(-tk/\tau)$$

$$= [B_1D_1] + [B_2D_2] = [B_1D_2]_0 (1 - \exp(-tk([D_1]_0 + [D_2]_0)))$$

With

$[B_1D_2]_0 = 0.05$ M and $[D_2]_0$ = 0.6/1.2/1.9/4.2/7.2/10.0 mM and $[D_1]_0 = 5 \times 10^{-3}$ mM

4.9 References

1. D. G. Hall, "Boronic Acids", Wiley-VCH Verlag GmbH & Co. KGaA, **2005**.
2. B. F. Spielvogel, Phosphorus Sulfur Silicon Relat. Elem., **1994**, *87*, 267.
3. A.-K. Azab, M. Srebnik, V. Doviner, A. Rubinstein, *J. Contr. Release*, **2005**, *106*, 14.
4. P. F. Bross, R. Kane, A. T. Farrell, S. Abraham, K. Benson, M. E. Brower, *Clin. Canc. Res.*, **2004**, *10*, 3954.
5. Z. M. O, Rzayev, O. Beskardes, Collect. Czech. *Chem. Commun*., **2007**, *72*, 1591.
6. N. A. Petasis, *Aust. J. Chem*., **2007**, *60*, 795.
7. P. C. Trippier, C. McGuigan, Med. *Chem. Commun*., **2010**, *1*, 183.
8. W.-D. Jang, K. M. K. Selim, C.-H. Lee, I. K. Kang, *Prog. Polym. Sci*., **2009**, *34*, 1.
9. C. Baldock, Y. D. Deene, S. Doran, G. Ibbott, A. Jirase, M. Lepage, *Phys. Med. Biol.* **2010**, 55.
10. A. Goy, F. Gilles, *Clin. Lymphoma*, **2004**, 230.
11. R. J. Weir, R. S. Fisher, *Toxicol. Appl. Pharmacol*., **1972**, *23*, 351.
12. S. A. Hubbard, *Biol. Trace Elem. Res*., **1998**, *66*, 343.
13. W. Yang, W. Gao, B. Wang, *Med. Res. Rev*. **2003**, *23*, 346.
14. L. W. Seymour, R. Duncan, J. Strohalm, J. Kopecek, *J. Biomed. Mater. Res*., **1987**, *21*, 1341.
15. N. Miyaura, A. Suzuki, *Chem. Rev*., **1995**, *95*, 2457.
16. E. M. Flamme, W. R. Roush, *J. Am. Chem. Soc*., **2002**, *124*.
17. W. R. Roush, M. A. Adam, A. E. Walts, D. J. Harris, *J. Am. Chem. Soc*., **1986**, *108*, 3422.
18. S. V. Ley, A. W. Thomas, Angew. *Chem. Int. Ed.*, **2003**, *42*, 5400.
19. N. A. Petasis, I. A. Zavialov, *J. Am. Chem. Soc*,. **1997**, *119*, 445.
20. N. A. Petasis, A. K. Yudin, I. A. Zavialov, G. K. S. Prakash, G. A. Olah, *Synlett*, **1997**, 606.

21. T. Ishiyama, M. Murate, N. Miyaura, *J. Org. Chem.*, **1995**, *60*, 7508.
22. L. S. Liebeskind, J. Srogl, *J. Am. Chem. Soc*., **2000**, *122*, 11260.
23. R. Nishiyabu, Y. Kubo, T. D. James, J. S. Fossey, *Chem. Commun.*, **2011**, *47*, 1124.
24. R. Nishiyabu, Y. Kubo, T. D. James, J. S. Fossey, *Chem. Commun*., **2011**, *47*, 1106.
25. W. Yang, X. Gao, B. Wang, *Med. Res. Rev*., **2003**, *23*, 346.
26. N. Fujita, S. Shinkai and T. D. James, *Chem.–Asian J*., **2008**, *3*, 1076.
27. J. J. Cash, T. Kubo, A. P. Bapat, B. S. Sumerlin, *Macromolecules*, **2015**, 48, 2098.
28. O. R. Cromwell, J. Chung, Z. Guan, *J. Am. Chem. Soc*., **2015**, 137, 6492.
29. C. C. Deng. W. L. A. Brooks, K. A. Abboud, B. S. Sumerlin, *ACS Macro Lett*., **2015**, 4, 220.
30. W. Niu, C. O'Sullivan, B. M. Rambo, M. D. Smith, J. Lavigne, *J. Chem. Commun*., **2005**, 4342.
31. A. P. Bapat, D. Roy, J. G. Ray, D. A. Savin, B. S. Sumerlin, *J. Am. Chem. Soc*., **2011**, 133, 19832.
32. J. Xu, D. G. Yang, W. J. Li, Y. Gao, H. B. Chen, H. M. Li, *Polymer*, **2011**, 52, 4268.
33. M. Piest, X. Zhang, J. Trinidad, J. F. Engbersen, *J. Soft Matter*, **2011**, 7, 11111.
34. D. Tarus, E. Hachet, L. Messager, B. Catargi, V. Ravaine, R. Auzély-Velty, Macromol. *Rapid Commun*., **2014**, 35, 2089.
35. L. He, D. E. Fullenkamp, J. G. Rivera, P. B. Messersmith, *Chem. Commun*., **2011**, 47, 7497.
36. M. C. Roberts, M. C. Hanson, A. P. Massey, E. A. Karren, P. F. Kiser, *Adv. Mater*., **2007**, 19, 2503.
37. Y. Kotsuchibashi, R. V. C. Agustin, J.-Y. Lu, D.G. Hall, R. Narain, *ACS Macro Lett.*, **2013**, 2, 260.
38. N. Fujita, S. Shinkai, T.D. James, J. Asian Chem., **2008**, *3*, 1076–1091.
39. F. Jäkle, *Chem. Rev*. **2010**, *110*, 3985.
40. T.D. James, K. R. A. S. Sandanayake, S. Shinkai, Angew. *Chem. Int. Ed. Engl*. **1996**, *35*, 1910.
41. N. Y. Edwards, T. W. Sager, J. T. McDevitt, E. V. Anslyn, *J. Am.Chem. Soc*. **2007**, *129*, 13575.
42. H. Meng, P. Xiao, J. Gu, X. Wen, J. Xu, C. Zhao, J. Zhang, T. Chen, T. *Chem. Commun*. **2014**, *50*, 12277.
43. J. N. Cambre, B. S. Sumerlin, *Polymer*, **2011**, *52*, 4631.
44. F. Cheng, F. Jakle, *Polym. Chem*., **2011**, *2*, 2122.
45. G. R. Hendrickson, L. A. Lyon, *Soft Matter*, **2009**, *5*, 29.
46. L. Klouda, A. G. Mikos, *Eur. J. Pharm. Biopharm*., **2008**, *68*, 34.
47. Z. Li, J. Guan, *Expert Opin. Drug Delivery*, **2011**, *8*, 991.
48. T. R. Hoare, D. S. Kohane, *Polymer*, **2008**, *49*, 1993.
49. B. V. Slaughter, S. S. Khurshid, O. Z. Fisher, A. Khademhosseini, N. A. Peppas, *Adv. Mater*., **2009**, *21*, 3307.
50. N. E. Fedorovich, J. Alblas, J. R. de Wijn, W. E. Hennink, A. J. Verbout, W. Dhert, *Tissue Eng*., **2007**, *13*, 1905.
51. D. Buenger, F. Topuz, J. Groll, *Prog. Polym. Sci*., **2012**, *37*, 1678.
52. Y. Guan, Y. Zhang, *Chem. Soc. Rev*., **2013**, *42*, 8106.

53. E. Frankland, B. F. Duppa, Justus Liebigs, *Ann. Chem.*, **1860,** *115*, 319.
54. A. Michaelis, P. Becker, Ber. Dtsch. *Chem. Ges.*, **1880**, *13*, 58.
55. A. Michaelis, P. Becker, Ber. Dtsch. *Chem. Ges.*, **1882**, *15*, 180.
56. J. P. Lorand, J. O. Edwards, *J. Org. Chem*., **1959**, *24*, 769.
57. G.E.K. Branch, D. L. Yabroff, B. Bettmann, *J. Am. Chem. Soc*., **1934**, *56*, 937.
58. D. L. Yabroff, G. E. K. Branch, B. Bettmann, *J. Am. Chem. Soc*.,**1934**, *56*, 1850.
59. B. Bettman, B., G. E. K. Branch, D. L. Yabroff, *J. Am. Chem. Soc*., **1934**, *56*, 1865.
60. S. Soundararajan, M. Badawi, C. M. Kohlrust, J. H. Hageman, *Anal. Biochem*., **1989**, *178*, 125.
61. K.Torssell, J. H. McLendon, G. F. Somers, *Acta Chem. Scand*., **1958**, *12*, 1373.
62. H. R. Mulla, N. J. Agard, A. Basu, Bioorg. *Med. Chem. Lett.*, **2004**, *14*, 25.
63. R. P. Singhal, B. Ramamurthy, N. Govindraj, Y. Sarwar, *J. Chromatogr.*, **1991**, *543*, 17.
64. A. R. Goldberg, B. H. Northrop, *J. Org. Chem*., **2016**, *81*, 969.
65. G. Wulff, M. Lauer, H. Böhnke, Angew. *Chem. Int. Ed. A. Engl*., **1984**, *23*, 741.
66. X. Yang, M. C. Lee, F. Sartain, X. Pan, C. R. Lowe, *Chem.-Eur. J*., **2006**, *12*, 8491.
67. M. P. Hughes, B. D. Smith, *J. Org. Chem*. **1997**, *62*, 4492.
68. N. Fujita, S. Shinkai, T. D. James, *Chem. - Asian J*., **2008**, *3*, 1076.
69. J. P. Lorand, J. O. Edwards, *J. Org. Chem*. **1959**, *24*, 769.
70. G. Springsteen, B. Wang, *Tetrahedron*, **2002**, *58*, 5291.
71. M. Arzt, C. Seidler, D. Y. W. Ng, T. Weil, *Chem. - Asian J*., **2014**, *9*, 1994.
72. W. A. Marinaro, R. Prankerd, K. Kinnari, V. J. J. Stella, *Pharm. Sci*., **2015**, *104*, 1399.
73. E. L. Spitler, M. R. Giovino, S. L. White, W. R. Dichtel, *Chem. Sci*., **2011**, *2*, 1588.
74. Y. Tokunaga, H. Ueno, Y. Shimomura, T. Seo, *Heterocycles*, **2002**, *57*, 787.
75. Y. Tokunaga, H. Ueno, Y. Shimomura, *Heterocycles* **2007**, *74*, 219.
76. C. D. Roy, H. C. Brown, *J. Organomet. Chem*., **2007**, *692*, 784.
77. D. Bradley, G. Williams, M. Lawton, *J. Org. Chem*., **2010**, *75*, 8351.
78. J. Kua, P. J. Iovine, *Phys. Chem. A*, **2005**, *109*, 8938.
79. R. Haruta, M. Ishiguro, N. Ikeda, Y. Yamamoto, *J. Am. Chem. Soc*., **1982**, *104*, 7667.
80. W. R. Roush, A. G. Walts, L. K. Hoong, *J. Am. Chem. Soc*., **1985**, *107*, 8186.
81. K. A. Ketuly, A. H. A. Hadi, *Molecules*, **2010**, *15*, 2347.
82. K. Ditrich, T. Bube, R. Stürmer, R. W. Hoffmann, *Angew. Chem. Int. Ed. Engl*., **1986**, *25*, 1028.
83. D. S. Matteson, A. A. Kandil, *Tetrahedron Lett*., **1986**, *7*, 3831.
84. R. Ray, D. S. Matteson, *Tetrahedron Lett*., **1980**, *21*, 449.
85. T. Herold, U. Schrott, R. W. Hoffmann, *Chem. Ber*., **1981**, *111*, 359.
86. J. E. A. Luithle, J. Pietruszka, *J. Org. Chem*., **1999**, *64*, 8287.
87. J. E. A. Luithle, J. Pietruszka, *J. Org. Chem*., **2000**, *65*, 9194.
88. J. Pietruszka, G Solduga, Eur. *J. Org. Chem*., **2009**, 5998.
89. H. G. Kuivila, A. H. Keough, E. J. Soboczenski, *J. Org. Chem*., **1954**, *8*, 780.
90. D. Montarnal, M. Capelot, F. Tournilhac, L. Leibler, *Scienc*e, **2011**, *334*, 965.
91. W. Denissen, G. Rivero, R. Nicolaÿ, L. Leibler, J. M. Winne, F. E. Du Prez, *Adv. Funct. Mater*. **2015**, 1.

Chapter 5

PMMA and PS Vitrimers with Pending Boronic Esters

Table of Contents

Chapter 5 – PMMAand PS Vitrimers with Pending Boronic Esters

5.1 Introduction

The following chapter describes the synthesis of boronic ester containing monomers and polymers to generate PMMA and PS vitrimers based on the exchange of boronic esters. Different polymerizable diol and boronic acid/ester carrying monomers were synthesized and subsequently polymerized via radical processes. Two different divalent crosslinkers were synthesized and used to crosslink functional thermoplastics PMMA, and PS. The crosslinking process via gel formation in solution or via extrusion in bulk was analyzed and the resulting materials processed via common processing techniques such as compression, extrusion and injection molding. The systems were analyzed for their thermosetting properties (swelling tests, DMA, stress cracking experiments) as well as thermoplastic properties (rheology, recycling) and important characteristics such as modulus, T_g, tensile strength, swelling ratio, soluble fraction, stress relaxation and creep behavior, viscosities, thermal and stress cracking resistance were compared to the respective thermoplastic precursors. Finally, adhesion of incompatible polymers was tested and resulted in promising results.

5.2 General experimental methods

Chemical compounds: Chemical compounds and solvents were purchased from Sigma Aldrich, TCI Chemicals, Alfa Aesar or Acros. Solvents were either used as purchased or dried over new and oven dried molecular sieves (3 Å). Glassware was usually dried in the oven before use. Commercial monomers were passed over a column filled with basic alumina to remove inhibitors. AIBN was recrystallized from hot methanol. Commercially available thermoplastics for comparison were kindly provided by Arkema (**PMMA 1** and **PMMA 2**) or purchased from Sigma Aldrich (**PMMA 3**).

Gel permeation chromatography (GPC): GPC was performed on a Viscotek GPCmax/VE2001 connected to a triple detection array (TDA 305) from Malvern. Obtained raw data were treated with the respective standard homopolymer calibration curve (PMMA and PS) and related to the peak of toluene which was added as internal standard.

More detailed descriptions of the machines and methods used can be found in the respective sections.

5.3 Monomer syntheses

The following subchapter describes the synthesis of vinyl monomers containing pendant diol or boronic ester functionalities. Additionally, three different divalent boronic ester crosslinkers were generated.

5.3.1 Methacrylate monomer with a pending phenylboronic ester function linked through the boron atom

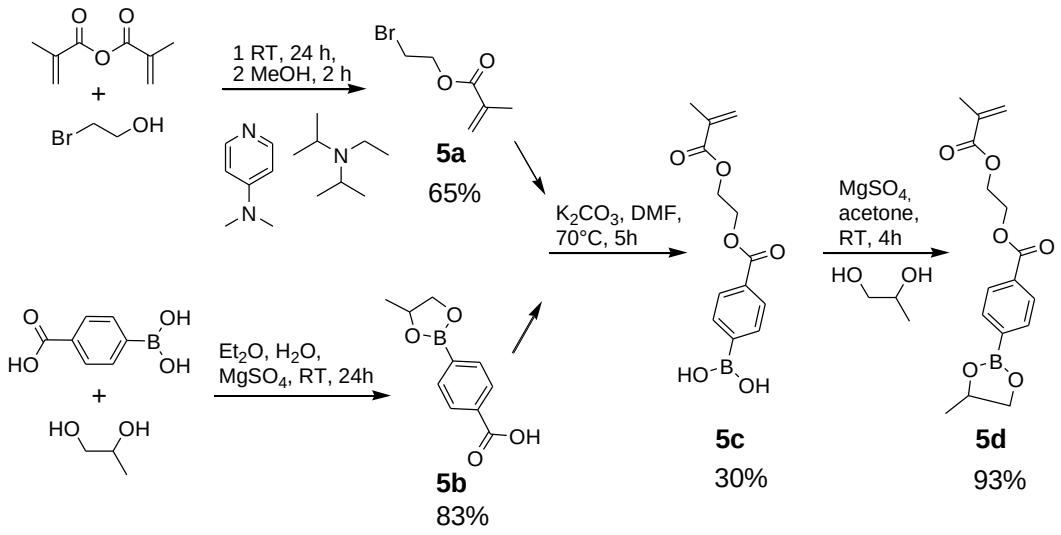

Scheme 5.1. Synthesis of a vinylic monomer carrying a pendant boronic ester functionality attached to rest of the monomer via the boron atom.

Synthesis of compound **5a**: 2-Bromoethanol (15 g, 120 mmol), DIPEA (17.1 g, 132 mmol), DMAP (147 mg, 1.2 mmol) and methacrylic anhydride (22.2 g, 144 mmol) were mixed (without the addition of any solvent) and stirred for 24 hours at room temperature. Methanol (5 mL) was added and the resulting mixture was stirred two additional hours at room temperature. Ethyl acetate (50 mL) and water (50 mL) were added. The resulting organic phase was washed with a solution of 0.5 M HCl (3 × 50 mL), a solution of 0.5 M NaOH (3 × 50 mL) and with water (1 × 50mL). The organic phase was dried over magnesium sulfate ($MgSO_4$), filtered and concentrated under reduced pressure at 50 °C to yield 18.3 g of a

slightly yellow liquid. ^{1}H-NMR analysis confirms the generation of compound **5a** and the presence of 13 mol% of ethylene glycol dimethacrylate. Yield = 65%.

^{1}H NMR ($CDCl_3$, 400 MHz): δ (ppm) 6.17 (s, 1H), 5.62 (s, 1H), 4.44 (t, J = 6.0 Hz, 2H), 3.56 (t, J = 6.0 Hz, 2H), 1.95 (s, 3H).

Synthesis of compound **5b**: 4-Carboxyphenylboronic acid (5 g, 30.1 mmol) and propane-1,2-diol (2.41 g, 31.7 mmol) were mixed in diethyl ether (30 mL) and 0.1 ml of water was added. The resulting mixture was stirred until full dissolution of the compounds. Magnesium sulfate (5 g) was added and the suspension was stirred for 24 hours at room temperature before filtration. The filtrate was concentrated under reduced pressure to yield compound **5b** as a white solid (5.15 g, 83%).

^{1}H NMR ($CDCl_3$, 400 MHz): δ (ppm) 7.97 (d, J= 8.4 Hz, 2H), 7.78 (d, J= 8.4 Hz, 2H), 4.79-4.68 (m, 1H), 4.44 (t, J = 8.4 Hz, 1H), 3.87 (d, J = 8.4 Hz, 1.6 Hz, 1H), 1.33 (d, J = 6.4 Hz, 3H).

Synthesis of compound **5c**: Compound **5a** (5 g, 25.9 mmol), compound **5b** (6.14 g, 29.8 mmol) and K_2CO_3 (10.7 g, 77.7 mmol) were mixed in 50 mL of DMF. The resulting mixture was stirred at 70 °C for 5 hours. Ethyl acetate (50 mL) and water (150 mL) were added and the organic phase was washed with water (3 × 150 mL). During washing, 300 mg of NaCl) were added to the mixture to enhance phase separation. The organic phase was dried over magnesium sulfate, filtered and concentrated under reduced pressure at 50 °C to yield a white solid. The white solid was dissolved in 50 mL of ethyl acetate and the resulting solution was washed with HCl 0.5 M (3 × 25mL) and water (1 × 50mL). The organic phase was dried over magnesium sulfate, filtered and concentrated under reduced pressure at 50 °C to yield a white solid (4.73 g). A fraction of the white solid (1.15 g) was dissolved in ethyl acetate. The resulting mixture was heated to 50 °C and 8.5 mL heptane was added. The mixture was kept 5 minutes at 50 °C before placing it in the freezer at -18 °C. After 16 hours, the precipitated white solid was collected via filtration and washed with 250 mL pentane. This procedure was repeated a second time to obtain compound **5c** (529 mg, 30% calculated for the entire batch) as white solid.

^{1}H NMR ($CDCl_3$, 400 MHz): δ (ppm) 8.31 (s, 2H), 7.91 (s, 2H), 6.02 (s, 1H), 5.67 (s, 1H), 4.57-4.45 (m, 4H), 1.87-1.79 (m, 3H).

Synthesis of compound **5d**: Compound **5c** (3 g, 10.8 mmol), propane-1,2-diol (0.86 g, 11.3 mmol) were mixed in 30 mL of diethyl ether and 0.1 mL of water was added. The resulting mixture was stirred until complete dissolution of all compounds. Magnesium sulfate (4 g) was added and the mixture was stirred for 24 hours at room temperature before filtration. The filtrate was concentrated under reduced pressure yielding compound **5d** as a white solid (3.18 g, 93%).

^{1}H NMR ($CDCl_3$, 400 MHz): δ (ppm – broad signals) 8.02 (s, 2H), 7.88 (s, 2H), 6.13 (s, 1H), 5.58 (s, 1H), 4.75-4.49 (m, 6H), 3.93 (s, 1H), 2.16 (s, 3H), 1.42 (s, 3H).

5.3.2 Methacrylate monomer with a pending phenylboronic ester function linked through the diol moiety

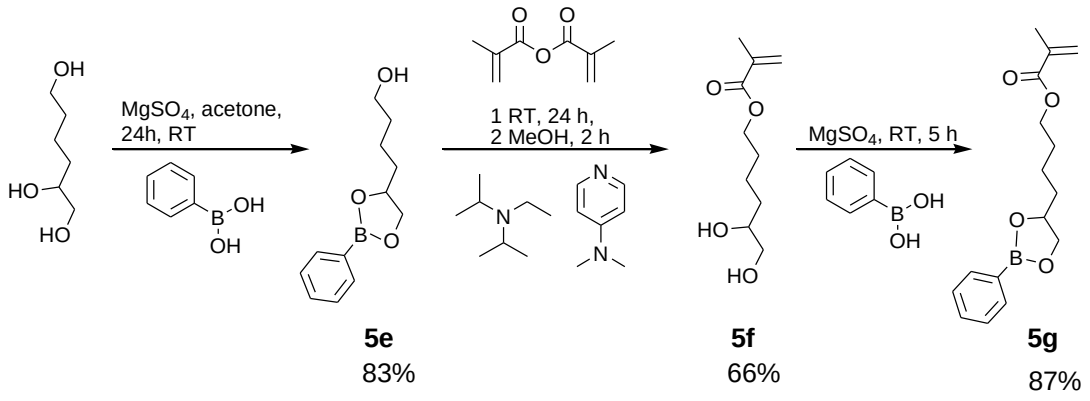

Scheme 5.2. Synthesis of a vinylic monomer carrying a pendant boronic ester functionality attached to rest of the monomer through the diol moiety.

Synthesis of compound **5e**: Hexane-1,2,6-triol (10 g, 74.5 mmol) and phenylboronic acid (9.55 g, 78.3 mmol) were mixed in 50 mL of acetone and 0.2 mL of water. Magnesium sulfate (20 g) was added and the resulting suspension was stirred at room temperature for 24 hours before filtration. The filtrate was concentrated under reduced pressure to yield compound **5e** (13.6 g, 83%) as a colorless liquid.

^{1}H NMR ($CDCl_3$, 400 MHz): δ (ppm) 7.82 (d, J = 8.0 Hz, 2 H), 7.50-7.46 (m, 1H), 7.40-7.36 (t, J = 8.0 Hz, 2H), 4.61-4.54 (m, 1H), 4.43 (dd, J = 8.8 Hz, 0.8 Hz, 1H), 3.95 (dd, J = 8.8 Hz, 2.0 Hz, 1H), 3.67 (t, J = 6.4 Hz, 2H), 1.76-1.47 (m, 6H).

Synthesis of compound **5f**: Compound **5e** (5.0 g, 22.7 mmol), DIPEA (3.23 g, 25.0 mmol), DMAP (28 mg, 0.23 mmol) and methacrylic anhydride (4.2 g, 27.3 mmol) were mixed (without the addition of solvent) and stirred at room temperature for 24 hours. Methanol (1 mL) was added and the resulting mixture was stirred at room temperature for two additional hours. Ethyl acetate (50 mL) and water (50 mL) were added. The resulting organic phase was washed with a solution of HCl 0.5 M (3 × 50 mL), a solution of NaOH (3 × 50 mL) and water (1 × 50 mL). The organic phase was dried over magnesium sulfate, filtered and concentrated under reduced pressure to obtain compound **5f** (3.03 g, 66%) as a slightly yellow liquid.

^{1}H-NMR (400 MHz, $CDCl_3$): δ (ppm) 5.98 (s, 1H), 5.45 (s, 1H), 4.09-3.90 (m, 4H), 3.56-3.27 (m, 3H), 1.81 (s, 3H), 1.68-1.27 (m, 6H).

Synthesis of compound **5g**: Compound **5f** (700 mg, 3.46 mmol) and phenylboronic acid (443 mg, 3.63 mmol) were mixed in 20 mL of diethyl ether and 0.1 mL of water. Magnesium sulfate (1 g) was added and the resulting suspension was stirred at room temperature for 5 hours before filtration. The filtrate was concentrated under reduced pressure to obtain monomer **5g** (864 mg, 87%) as a slightly yellow liquid which crystallized rapidly. The proton NMR showed some impurities.

^{1}H-NMR (400 MHz, $CDCl_3$): δ (ppm) 7.80-7.26 (m, 5H), 6.10 (s, 1H), 5.55 (s, 1H), 4.56 (m, 1H), 4.44 (m, 1H), 4.20 (m, 3H), 1.93 (s, 3H), 1.68-1.50 (m, 6H).

5.3.3 5,6-Dihydroxyhexyl methacrylate

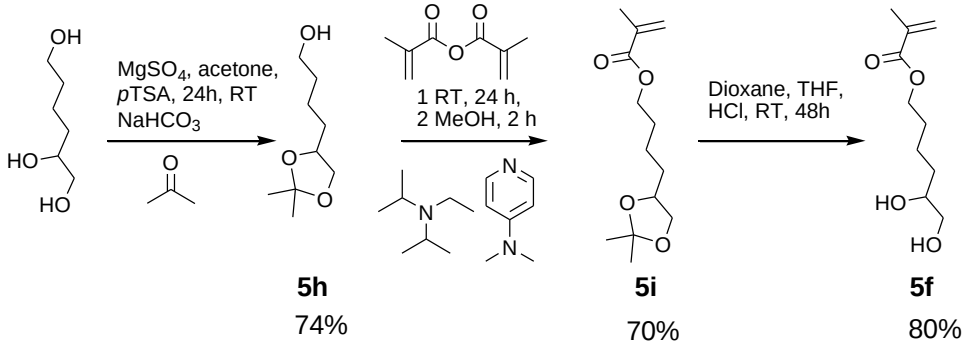

5h 74%

5i 70%

5f 80%

Scheme 5.3. Synthesis of 5,6-dihydroxyhexyl methacrylate.

Synthesis of 4-(4-hydroxybutyl)-2,2-dimethyl-1,3-dioxolane **5h**: 1,2,6-Hexanetriol (25 g, 186 mmol) was dissolved in acetone (340 mL) in the presence of $MgSO_4$ (45 g, 374 mmol). Then, *p*TSA (2.9 g, 15.7 mmol) was added slowly and the mixture was stirred at room temperature for 24 hours. $NaHCO_3$ (2.66 g, 31.7 mmol) was added and stirring was continued for 3 h at room temperature. The mixture was filtered, dried over $MgSO_4$ and concentrated under reduced pressure to yield a white slurry. Water (350 mL) was added and the organic phase was extracted with DCM (4 × 200 mL). The organic phase was dried over $MgSO_4$, filtered and concentrated under reduced pressure (25 °C) to obtain the target compound **5h** as a slightly yellow liquid (18.6 g, 74%).

^{1}H-NMR (400 MHz, $CDCl_3$): δ (ppm) 3.95-1.92 (m, 2H), 3.52-3.40 (m, 3H), 2.80 (s, 1H), 1.47-1.24 (m, 12H).

Synthesis of 4-(2,2-Dimethyl-1,3-dioxolan-4-yl)butyl methacrylate **5i**: 4-(4-Hydroxybutyl)-2,2-dimethyl-1,3-dioxolane **5h** (14.3 g, 82.2 mmol), DIPEA (11.7 g, 90.5 mmol), DMAP (100 mg, 0.82 mmol) and methacrylic anhydride (15.2 g, 98.8 mmol) were mixed and stirred for 24 h at room temperature. MeOH (5 mL) was added and the mixture was stirred for 3additional hours. Heptane (50 mL) and water (50 mL) were added and the organic phase was washed with 0.5 M HCl (3 × 50 mL), 0.5 M NaOH (3 × 50mL) and water (1 × 50mL). Then, the organic phase was dried over $MgSO_4$, filtered and concentrated under reduced pressure at 50 °C to obtain the target compound **5i** as a slightly yellow liquid (10.0 g, 70%).

^{1}H-NMR (400 MHz, $CDCl_3$): δ (ppm) 6.03 (s, 1H), 5.49 (s, 1H), 4.09-4.00 (m, 4H), 3.43 (m, 1H), 1.88 (s, 3H), 1.68-1.34 (m, 12H).

Synthesis of 5,6-dihydroxyhexyl methacrylate **5f**: 4-(2,2-Dimethyl-1,3-dioxolan-4-yl)butyl methacrylate **5i** (2.0 g, 8.26 mmol) was introduced in 55 mL of dioxane (50 mL) and THF (5 mL) before HCl (1 M, 0.5 mL and 36% 0.4 mL) was added slowly. The transparent solution was stirred for 48 hours at room temperature and DCM (100 mL) was added. The organic phase was washed with water (3 × 50 mL) and dried over $MgSO_4$, filtered and concentrated under reduced pressure to obtain the target compound **5f** as a yellow oil (1.6 g, 80%).

^{1}H-NMR (400 MHz, $CDCl_3$): δ (ppm) 5.98 (s, 1H), 5.45 (s, 1H), 4.09-3.90 (m, 4H), 3.56-3.27 (m, 3H), 1.81 (s, 3H), 1.68-1.27 (m, 6H)

5.3.4 1,4-Benzenediboronic acid bis(1,2-propanediol) ester X_1

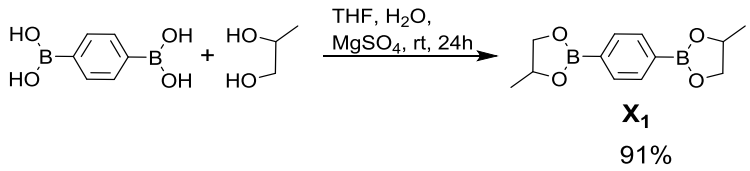

Scheme 5.4. Synthesis of the bis-dioxaborolane crosslinking agent $\mathbf{X_1}$.

Synthesis of 1,4-benzenediboronic acid bis(1,2-propanediol) ester $\mathbf{X_1}$: 1,4-Phenyldiboronic acid (3.0 g, 18.1 mmol) and 1,2-propanediol (2.82 g, 37.1 mmol) were mixed in THF (30 mL) and water (0.1 mL). $MgSO_4$ (5 g) was added and after 24 h at room temperature, the solution was filtered and concentrated under reduced pressure to obtain the target compound as a slightly yellow solid. Then, the solid was immersed into heptane and stirred for 1 hour at 50 °C, filtered and concentrated under reduced pressure to obtain the target compound $\mathbf{X_1}$ as a white solid (4.06 g, 91%).

^{1}H NMR ($CDCl_3$, 400 MHz): δ (ppm) 7.82 (s, 4H), 4.77-4.69 (m, 2H), 4.46 (dd, J = 8.8 Hz, 1.2 Hz, 2H), 3.90 (dd, J = 8.8 Hz, 1.2 Hz, 2H), 1.41 (d, J = 6.4 Hz, 6H).

^{13}C-NMR (100 MHz, THF-d_8): δ (ppm) 131.8, 71.9, 70.5, 18.9. Carbon adjacent to boron not detected.

5.3.5 1,4-Benzenediboronic acid bis(1,3-propanediol) ester X_2

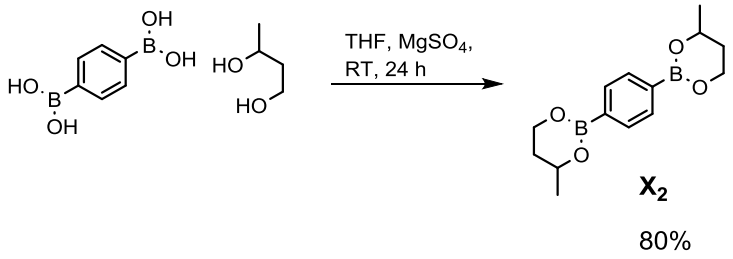

Scheme 5.5. Synthesis of the bis-dioxaborinane crosslinking agent $\mathbf{X_2}$.

Synthesis of 1,4-benzenediboronic acid bis(1,3-propanediol) ester $\mathbf{X_2}$: 1,4-Phenyldiboronic acid (3.0 g, 18.1 mmol) and butane-1,3-diol (3.43 g, 38.0 mmol) were mixed in 30 mL of THF and 0.1 mL of water. Magnesium sulfate (6 g) was added and the reaction mixture is stirred at room temperature for 24 hours, filtrated and concentrated under reduced pressure to obtain the crosslinking agent $\mathbf{X_2}$ as white solid (3.97 g, 14.5 mmol, 80%).

^{1}H NMR (THF-d_8, 400 MHz): δ (ppm) 7.65 (s, 4 H), 4.28-4.23 (m, 2 H), 4.14-4.03 (m, 4H), 2.02-1.97 (m, 2H), 1.79-1.74 (m, 2H), 1.31 (d, J = 6.4 Hz, 6H).

^{13}C NMR (THF-d_8, 100 MHz): δ (ppm) 130.5, 65.7, 59.1, 32.4, 20.4. Carbon adjacent to boron not detected.

5.4 Polymer syntheses

The following part describes the general synthetic procedures to generate diol or boronic ester functionalized thermoplastic polymers. Thermoplastic polymers were generated via reversible addition-fragmentation chain-transfer polymerization (RAFT) using 2-phenyl-2-propyl benzodithioate as chain transfer agent. Polymers were analyzed by GPC referring either to the respective homopolymer calibration curves in the presence of a known standard (toluene) or using the triple detection array and ^{1}H-NMR. Some of the polymers were synthesized several times resulting in similar characteristics such as molecular weight M_n and M_w (±5 Kg/mol), dispersity $Đ$ (±0.2) and functional group concentration (±0.15). Free radical polymerization resulted in almost every cases in permanently crosslinked materials which was most likely due to small impurities in the functional monomer (presence of a divalent methacrylate).

5.4.1 PMMA with pending boronic esters attached via the boron atom

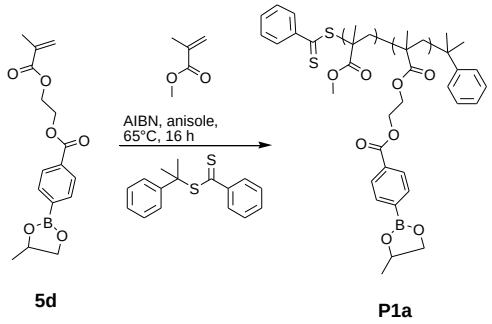

Scheme 5.6. RAFT copolymerization of MMA with monomer **5d**.

Synthesis of polymer **P1a**: Methyl methacrylate (MMA, 1.26 g, 12.6 mmol), the monomer **5d** (1 g, 3.14 mmol), 2-phenyl-2-propyl benzodithioate (PPBDT, 17.2 mg, 0.063 mmol) and AIBN (4.1 mg, 0.025 mmol) were mixed in 1.5 mL of anisole. The resulting solution was bubbled with nitrogen at room temperature for 30 minutes. The reaction mixture was heated to 65 °C for 16 hours while keeping it under protective atmosphere. After 16 hours, 2 mL of anhydrous THF was added and the polymer was precipitated into dry diethyl ether. The obtained polymer was re-dissolved in anhydrous THF, precipitated a second time into dry diethyl ether and dried under high vacuum at 50 °C overnight. Yield = 1.5 g, M_n = 43 000 g/mol, M_w = 57 000 g/mol, $Đ$ = 1.32. Ratio MMA/monomer in **5d**: *ca.* 3.7/1.

5.4.2 PMMA with diol, phenyl boronic ester or trimethylsilane moieties obtained from a functional PMMA with pending acetal groups attached via the diol radical

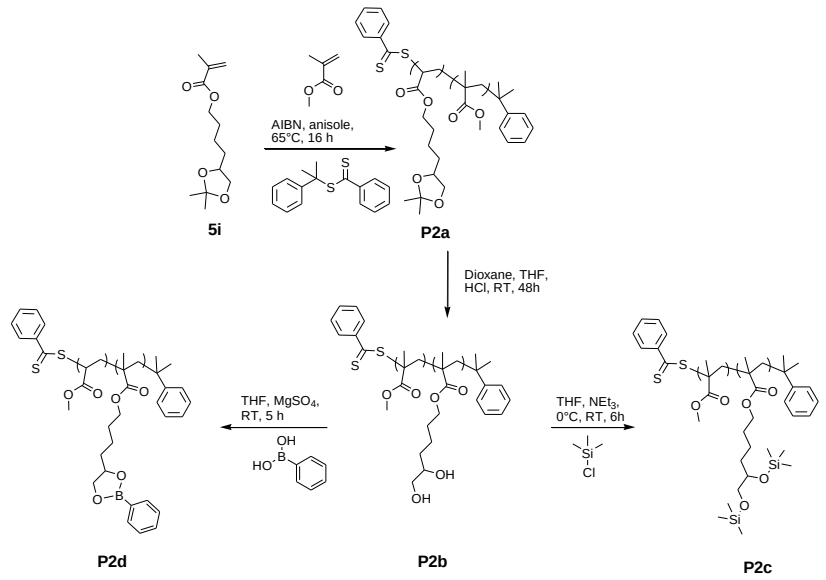

Scheme 5.7. RAFT copolymerization of MMA and monomer **5i**. Post-polymerization functionalization to obtain PMMA copolymers with pending free diol (**P2b**), boronic ester (**P2d**) and siloxane (**P2c**) functions.

Synthesis of polymer **P2a**: MMA (5.0 g, 49.9 mmol), the monomer **5i** (3.0 g, 12.5 mmol), 2-phenyl-2-propyl benzodithioate (68.0 mg, 0.25 mmol) and AIBN (16.4 mg, 0.1 mmol) were mixed in 5 mL of anisole. The resulting solution was bubbled with nitrogen at room temperature for 30 minutes. The reaction mixture was heated to 65 °C for 16 hours while keeping it under protective atmosphere. After 16 hours, 5 mL of anhydrous THF were added and the polymer was precipitated into dry diethyl ether. The obtained polymer was re-dissolved in anhydrous THF and precipitated a second time into dry diethyl ether. The polymer **P2a** was dried under high vacuum at 50 °C overnight. Yield = 5.3 g, M_n = 26 000 g/mol, M_w = 31 000 g/mol, $Đ$ =1.19. Ratio MMA/monomer in **5i**: ca 3.3/1 by ^{1}H-NMR.

Synthesis of polymer **P2b**: The polyacetal **P2a** (1.0 g) was dissolved in dioxane (50 mL) and 0.5 mL of a HCl solution (1 M) and 0.4 mL of a HCl solution (36 wt%) were added. THF (3 mL) was added and the reaction mixture was stirred at room temperature for 48 hours. The solution was concentrated under reduced pressure and the polymer was isolated by precipitation into dried diethyl ether. The resulting polymer was re-dissolved in anhydrous THF and precipitated a second time in dried diethyl ether. The polymer **P2b** was dried under high vacuum at 50 °C overnight. Yield = 0.6 mg, M_n = 18 000 g/mol, M_w = 20 000 g/mol, $Đ$ =1.11.

Via the same procedure, another boronic ester functionalized PMMA was synthesized.
P2b: Yield = 13 g, M_n = 24 000 g/mol, M_w = 27 000 g/mol, $Đ$ =1.13.

Synthesis of polymer **P2d**: Phenylboronic acid (232 mg, 1.9 mmol) and the polymer **P2b** (1.0 g) were mixed in 25 mL of anhydrous THF and water (0.1 mL) was added. The reaction mixture was stirred at room temperature until full dissolution and magnesium sulfate (4 g) was added. The reaction mixture was stirred 5 hours at room temperature before being filtered. The filtrate was concentrated under reduced pressure (viscous solution). The polymer **P2d** was isolated by precipitation of this viscous solution into dried diethyl ether and dried at 50 °C under high vacuum overnight. Yield = 10 g, M_n = 22 000 g/mol, M_w = 26 000 g/mol, $Đ$ =1.18.

Synthesis of polymer **P2c**: The polymer **P2b** (1 g) was dissolved in 20 mL THF and the reaction mixture was cooled to 0 °C. While keeping the temperature at 0 °C, triethylamine

(733 mg, 7.24 mmol) and then chlorotrimethylsilane (590 mg, 5.43 mmol) were added dropwise. The reaction mixture was allowed to warm to room temperature and stirred for 6 additional hours at room temperature. After filtration, the polymer **P2c** was isolated by precipitation into dried diethyl ether and dried under high vacuum at 50 °C overnight. Yield = 620 mg, M_n = 46 000 g/mol, M_w = 53 000 g/mol, $Đ$ =1.15 (triple detection).

Discoloration of **P2d**: Linear polymer **P2d** (1 g, ca 0.045 mmol benzodithioate functionalities) was dissolved in anhydrous THF (10 mL) and *n*-butylamine (8.2 mg, 0.11 mmol) was added. After 10 hours at room temperature, ethyl acrylate (21.2 mg, 0.22 mmol) was added. After stirring at room temperature for at least 16 hours, precipitation into dry Et_2O yielded the polymer as a white solid.

5.4.3 PMMA with pending phenylboronic ester attached via the oxygen atoms

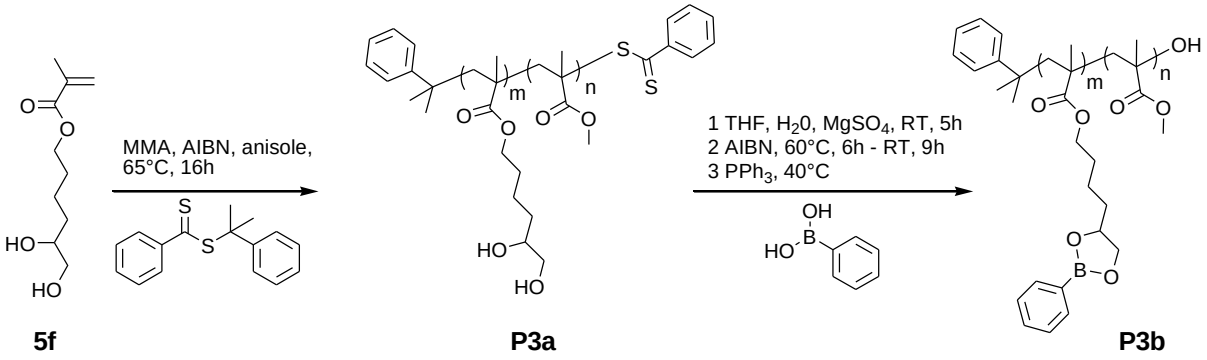

Scheme 5.8. RAFT copolymerization of MMA and monomer **5f**, and post-polymerization functionalization of the polydiol copolymer **P3**a into the corresponding poly(boronic ester) copolymer **P3b**.

Synthesis of PMMA copolymer with pending diol functionalities **P3a**: MMA (15 g, 149.8 mmol), the 5,6-dihydroxyhexyl methacrylate **5f** (7.58 g, 37.5 mmol), 2-phenyl-2-propyl benzodithioate (51.0 mg, 0.187 mmol) and AIBN (12.3 mg, 0.075 mmol) were dissolved in anisole (15 mL). The resulting mixture was bubbled with nitrogen at room temperature for 30 minutes before being heated up to 65 °C. The reaction mixture was kept under nitrogen while stirring at 65 °C. After 16 hours, 10 mL of anhydrous THF were added to the viscous oil and the mixture was precipitated into dry diethyl ether. Yield = 17.5 g. Total monomer conversion: 77%. Ratio MMA/monomer **5f**: *ca.* 3.3/1. Yield = 12.5 g, M_n = 71 000 g/mol, M_w = 96 000 g/mol, $Đ$ =1.35.

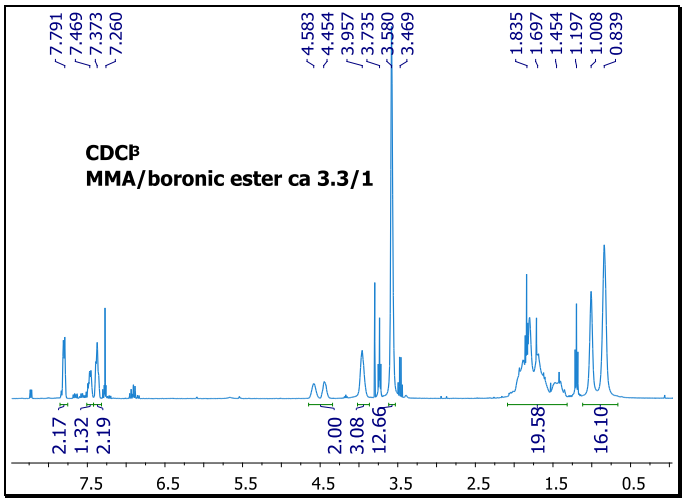

Figure 5.1. ^{1}H-NMR spectrum in $CDCl_3$ of the PMMA copolymer with pending diol functionalities **P3a**. The ratio of MMA to repeating units with a pending boronic ester function was estimated to be *ca*. 3.3/1.

Synthesis of PMMA copolymer with pending boronic ester functionalities **P3b**: The polymer **P3a** (17 g) was dissolved in anhydrous THF (250 mL) and phenylboronic acid (4.08 g, 33.5 mmol) and water (0.1 mL) were added. After 5 minutes, $MgSO_4$ (11.5 g) was added and the mixture was stirred at room temperature for 5 hours. AIBN (173 mg, 1.06 mmol) was added and the mixture heated for 6 hours at 60 °C before stirring at room temperature for 9 additional hours. Triphenylphosphine (277 mg, 1.06 mmol) was added and the reaction mixture was stirred at 40 °C for 1 additional hour. The mixture was put in a centrifuge for 30 minutes at 8500 rpm, filtered, concentrated under reduced pressure and precipitated into anhydrous Et_2O. The polymer **P3b** was dried at 100 °C under high vacuum for 16 hours. Yield = 14.5 g. M_n = 86 000 g/mol, M_w = 120 000 g/mol, $Đ$ =1.40.

Figure 5.2. Functional PMMA copolymers **P3a** and **P3b.** Pink powder = PMMA polydiol with a dithioester chain-end (corresponding to the RAFT CTA), **P3a**. White powder = PMMA poly(boronic ester) with no dithioester chain-end, **P3b**.

To generate similar molecular weight PMMA copolymers with less pending boronic ester functionalities, **P4a** and **P4b**, the following ratio of MMA/monomer **5f**/CTA/AIBN was used: 20/1/0.025/0.01 while keeping constant the vol% of anisole.

P4a: Yield = 17.0 g, M_n = 65 000 g/mol, M_w = 80 000 g/mol, $Đ$ =1.23. Ratio MMA/monomer **5f**: ca 24/1.

P4b: Yield = 14.3 g, M_n = 76 000 g/mol, M_w = 100 000 g/mol, $Đ$ =1.32.

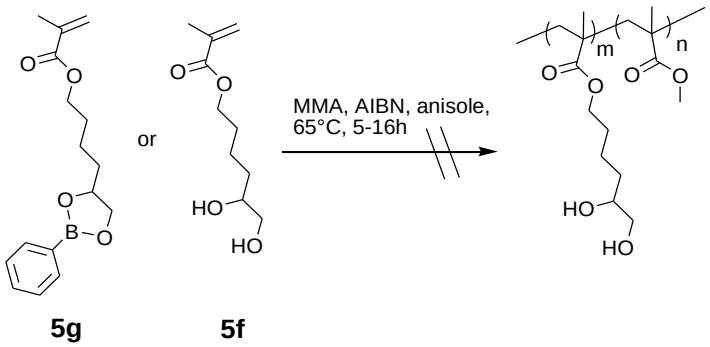

Scheme 5.9. Conventional free radical copolymerization of MMA with monomer **5f** or **5g**. All attempts led to permanently crosslinked systems.

Synthesis of a functional poly(methyl methacrylate) with pending diols or boronic esters by free radical polymerization: Free radical copolymerizations of MMA with monomers **5g** or **5f** using the protocol described for RAFT polymerizations but without the addition of the chain-transfer agent 2-phenyl-2-propyl benzodithioate were performed. Compound ratios MMA/monomer **5g** or **5f** /AIBN of 4/1/0.002 and 20/1/0.01 were tested with reaction time of 5 and 16 hours, respectively. Another test with the double amount of AIBN for the ratio MMA/monomer **5g** or **5f**/AIBN 20/1/0.02 was attempted (polymerization time of 5 hours). All reactions resulted in a slightly, but permanently crosslinked material. These materials did not dissolve after addition of THF, but swelled. No further characterization was performed on these materials. This result is likely caused by the contamination of monomers **5f** and **5g** by few mol% of ethylene glycol dimethacrylate produced as a side product during their syntheses.

5.4.4 PMMA with pending cyclohexylboronic ester attached via the oxygen atoms

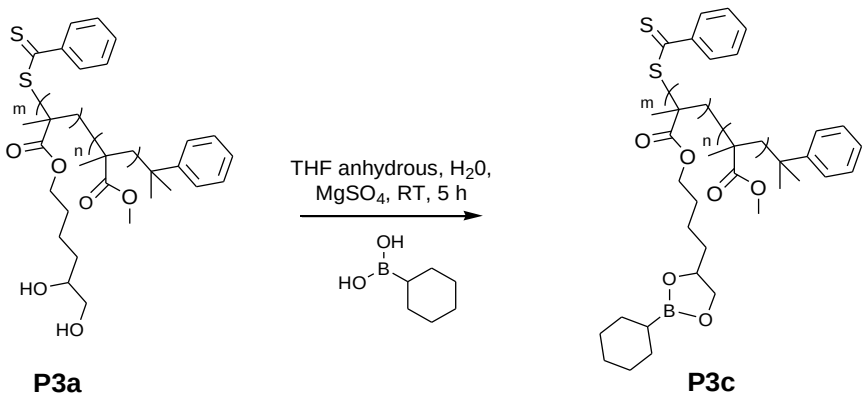

Scheme 5.10. Post-polymerization functionalization of PMMA carrying pendant diol units with cyclohexylboronic acid to result in the corresponding poly(boronic ester).

Synthesis of polymer **P3c**: Cyclohexylboronic acid (1.20 g, 9.8 mmol) and the polymer **P3a** (5.0 g) were mixed in 25 mL of anhydrous THF and water (0.1 mL) was added. The reaction mixture was stirred at room temperature until full dissolution. Magnesium sulfate (5 g) was added and the reaction mixture was stirred 5 hours at room temperature before filtration. The filtrate was concentrated under reduced pressure (viscous solution). The polymer **P3c** was isolated by precipitation of this viscous solution into dry diethyl ether and dried at 50 °C under high vacuum overnight. Yield = 4 g. M_n = 103 000 g/mol, M_w = 128 000 g/mol, $Đ$ = 1.24.

5.4.5 One-pot synthesis of a functional PMMA with pending phenylboronic ester functions linked through the oxygen atoms

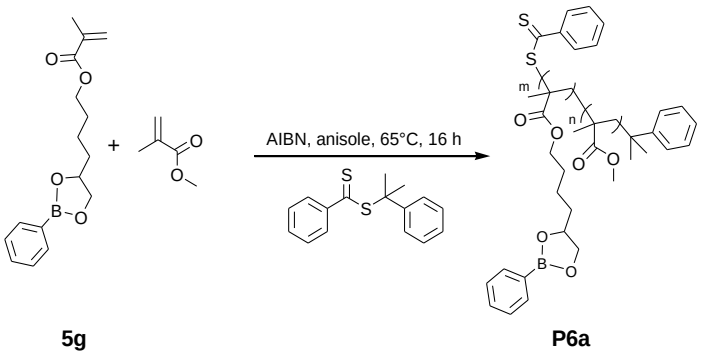

Scheme 5.11. RAFT copolymerization of MMA and monomer **5g**.

Synthesis of polymer **P6a**: MMA (1.22 g, 12.2 mmol), the monomer **5g** (880 mg, 3.05 mmol), 2-phenyl-2-propyl benzodithioate (16.7 mg, 0.061 mmol) and AIBN (4.0 mg, 0.024 mmol) were dissolved in anisole (1.2 mL). The resulting mixture was bubbled with nitrogen at room temperature for 30 minutes before being heated up to 65 °C. The reaction mixture was kept under nitrogen while stirring at 65 °C. After 16 hours, 1 mL of anhydrous THF was added to the viscous oil was and the mixture was precipitated into dry diethyl ether. Yield = 1.2 g. M_n = 24 000 g/mol, M_w = 29 000 g/mol, $Đ$ = 1.21. Ratio MMA/**5g**: 4.2/1 from ^{1}H-NMR.

5.4.6 PMMA homopolymer by RAFT polymerization

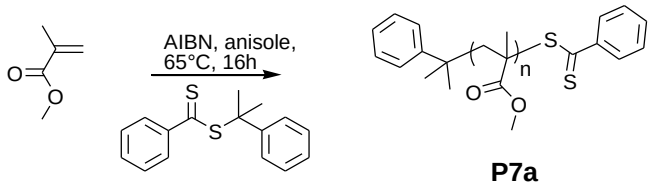

Scheme 5.12. RAFT homopolymerization of MMA.

Synthesis of PMMA homopolymer **P7a**. MMA (7 g, 69.9 mmol), 2-phenyl-2-propyl benzodithioate (19.1 mg, 0.07 mmol) and AIBN (4.6 mg, 0.028 mmol) were dissolved in anisole (5.6 mL). The resulting mixture was bubbled with nitrogen at room temperature for 30 minutes before being heated up to 65 °C. The reaction mixture was kept under nitrogen while stirring at 65 °C. After 16 hours, 5 mL of anhydrous THF were added to the viscous oil and the mixture was precipitated into dry diethyl ether. Yield = 4.2 g. Total monomer conversion: 70%. M_n = 50 000 g/mol, M_w = 60 000 g/mol, $Đ$ = 1.20.

5.4.7 Overview of PMMA and functional PMMA copolymers prepared and/or used

#	M_n (Kg/mol)	M_w (Kg/mol)	$Đ$	Average functionality f per chain (M_n)	Comonomer/ functional monomer in the copolymer (^{1}H-NMR)
Poly(methyl methacrylate)s					
P1a*	43	57	1.32	63	3.7/1
P2a*	26/22	31/28	1.19/1.27	45/39	3.3/1
P2b*	18/24	20/27	1.11/1.13	34/45	3.3/1
P2c*	46	53	1.15	74	3.3/1
P2d* **(PMMA BE 1)**	22	26	1.18	38	3.3/1
P3a** **(PMMA D 1)**	71	96	1.35	134	3.3/1
P3b** **(PMMA BE 2/3)**	86	120	1.40	139	3.3/1
P4a**	65	80	1.23	25	24/1
P4b** **(PMMA BE 4)**	76	100	1.32	28	24/1
P3c** **(PMMA BE 5)**	103	128	1.24	178	3.3/1
P6a**	24	29	1.21	36	4.2/1
P7a**	50	60	1.20	-	-
PMMA 1**	44	92	2.01	-	-
PMMA 2**	57	129	2.27	-	-
PMMA 3**	61	116	1.90	-	-
*triple detection, **homopolymer calibration curve					

Table 5.1. Overview of PMMA and functional PMMA copolymers prepared and/or used

5.4.8 Polystyrene with pending boronic esters attached via the diol moiety

Strategy 1

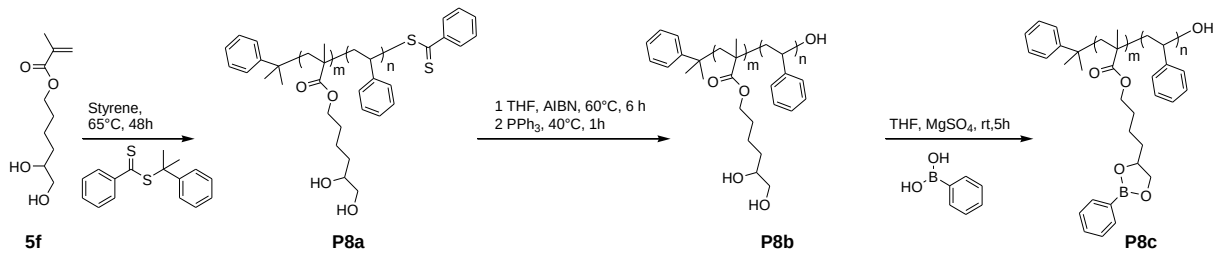

Scheme 5.13. Synthetic strategy 1 for the preparation of polystyrene copolymers with pending diol or boronic ester functions.

Synthesis of polymer **P8a**: Styrene (24.0 g, 26.4 mL, 230 mmol), monomer **5f** (11.7 g, 57.8 mmol), 2-phenyl-2-propyl benzodithioate (78.4 mg, 0.29 mmol) and AIBN (18.9 mg, 0.115 mmol) were mixed in anisole (24 mL). The resulting mixture was bubbled with nitrogen at room temperature for 30 minutes before being heated up to 65 °C. The reaction mixture was kept under nitrogen while stirring at 65 °C for 48 hours. After 48 hours, anhydrous THF (10 mL) was added and the polymer was precipitated into dry diethyl ether. This precipitation procedure was repeated and the solid was dried under reduced pressure. Yield = 15 g, M_n = 48 800 g/mol, M_w = 53 600 g/mol, $Đ$ = 1.10. Conversion monomer **5f** = 59.8%, conversion Styrene = 38.3%, ratio MMA diol/styrene: 1/2.5 (from monomer conversions).

Synthesis of polymer **P8b**: The polymer **P8a** (5 g) was dissolved in THF (40 mL) and AIBN (50 mg, 0.3 mmol) was added. The mixture was heated to 60 °C for 6 hours and was then cooled to room temperature and stirring was continued for 8 additional hours. PPh_3 (81.2 mg, 0.32 mmol) was added and after 1 hour at 40 °C the mixture was centrifuged and filtered, concentrated under reduced pressure and precipitated into dry diethyl ether. The product was obtained as a white solid. Yield = 3.5 g, M_n = 70 500 g/mol, M_w = 267 000 g/mol, $Đ$ = 3.78.

Synthesis of polymer **P8c**: The polymer **P8b** (3.0 g, 6.34 mmol diol functionalities) was dissolved in anhydrous THF (25 mL) and phenylboronic acid (812 mg, 6.66 mmol) was added. After full dissolution of all compounds, $MgSO_4$ (2.4 g, 20 mmol) was added and the reaction mixture was stirred for 5 hours at room temperature. AIBN (30 mg, 0.18 mmol) was added and the mixture was heated to 60 °C for 6 hours and was then cooled to room temperature and continued to stir for 8 more hours. PPh_3 (49 mg, 0.19 mmol) was added and after 1 hours at 40 °C the mixture was centrifuged and filtered, concentrated under reduced pressure and precipitated into dry diethyl ether. The product was obtained as a white polymer. Yield = 2.6 g, M_n = 54 300 g/mol, M_w = 67 300 g/mol, $Đ$ = 1.24. Ratio MMA diol/styrene: 1/2.7 from ^{1}H-NMR.

Strategy 2

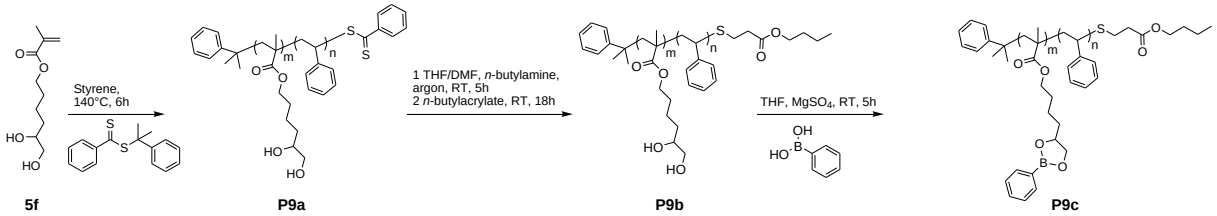

Scheme 5.14. Synthetic strategy 2 for the preparation of polystyrene copolymers with pending diol and boronic ester functions.

Synthesis of polymer **P9a**: Styrene (1 000 eq, 43 mL), **5f** (7.6 g, 100 eq) and the CTA (1 eq) were mixed in anisole (0.7 mL, internal standard) and bubbled with argon at room temperature for 30 minutes. The mixture was heated to 140 °C for 6 hours and samples were taken to follow the reaction kinetics. After 6 hours, the mixture was diluted with THF and precipitated into MeOH and dried under reduced pressure to obtain a pink solid. Yield = 35 g, 75 wt%, M_n = 74 800 g/mol, M_w = 118 000 g/mol, $Đ$ = 1.57. Conversion **5f** = 85.7%, conversion Styrene = 73.1%, ratio **5f**/styrene: 1/8.5 from conversions.

The polymerization kinetics were monitored to check for reactivity differences between styrene and the functional monomer (Figure 5.3), *i.e.* to check for a potential drift of composition along the polymer backbone. Anisole was used as internal standard, the monomer conversion was followed via ^{1}H-NMR and the chain growth via GPC using the PS homopolymer calibration. In Figure 5.3 (left side) can be seen that from the start of the polymerization, the diol containing monomer **5f** was slightly more incorporated than the styrene, as could be expected. According to this, the overall conversion at the end of the experiment was observed to be slightly higher (85.7%) for the functional monomer than for styrene (73.1%). The ratio of styrene/**5f** was calculated via ^{1}H-NMR to be 8.5/1. In total, the reaction is rather well controlled until ca 3 hours which corresponds to ca 70% total monomer conversion and after 6 hours the $Đ$ reaches 1.57.

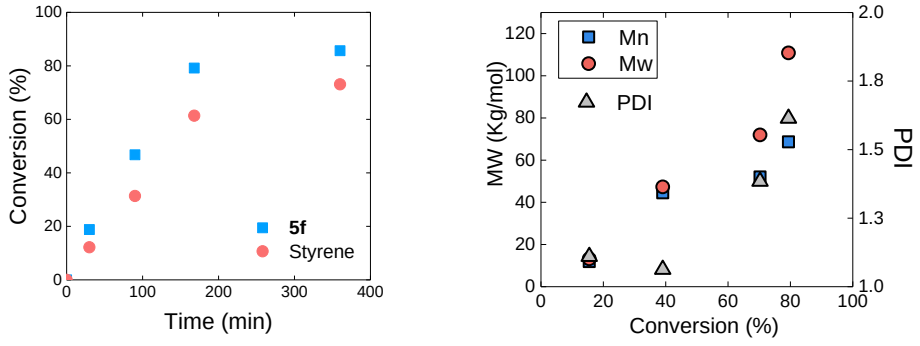

Figure 5.3. Kinetics of the RAFT copolymerization of styrene with the diol monomer **5f** via synthetic strategy 2.

Synthesis of polymer **P9b**: The polymer **P9a** was dissolved in a THF/DMF mixture (1/1, 250 mL) and reacted with *n*-butylamine (275 mg, 3.76 mmol) at room temperature under argon for 5 hours. *n*-Butylacrylate (4.8 g, 37.6 mmol) was added and stirring was continued at room temperature for 18 hours. The mixture was concentrated under reduced pressure and the colorless polymer **P9b** precipitated into MeOH. Yield = 30 g, M_n = 77 000 g/mol, M_w = 123 000 g/mol, $Đ$ =1.60.

Synthesis of polymer **P9c**: The polymer **P9b** (25 g) was dissolved in THF (50 mL) and phenylboronic acid (2.94 g, 24.1 mmol) and $MgSO_4$ (8.68 g, 72.4 mmol) were added. After 5 hours at room temperature, the mixture was centrifuged and then filtered, concentrated under reduced pressure and precipitated into dry Et_2O to yield polymer **P9c**. Yield = 25 g. M_n = 76 000 g/mol, M_w = 130 000 g/mol, $Đ$ = 1.71.

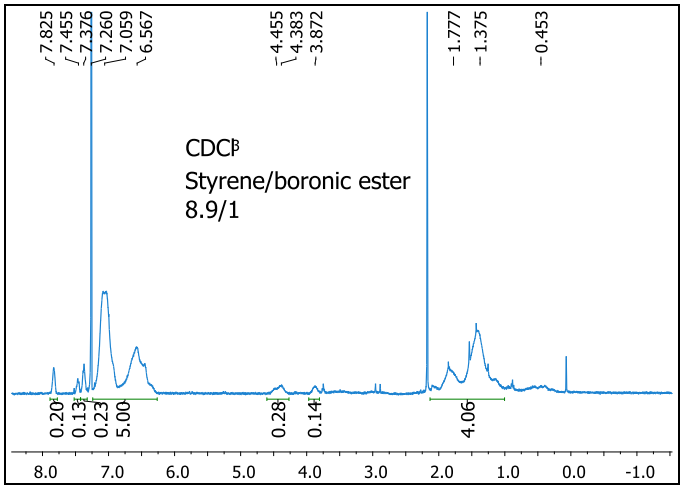

Figure 5.4. ^{1}H-NMR spectrum of the functional PS copolymer **P9c** in $CDCl_3$. The ratio of styrene to pending boronic ester was estimated to be *ca*. 8.9/1.

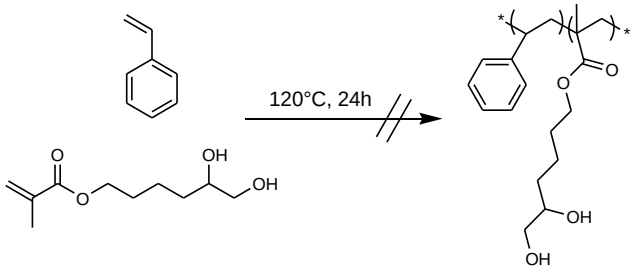

Scheme 5.15. Free radical polymerization of styrene with diol monomer **5f**. The experiment resulted in a permanently crosslinked system.

Synthesis of a functional polystyrene with pending diols via free radical polymerization: Styrene (24 g, 115.2 mmol) and monomer **5f** (11.66 g, 28.8 mmol) were mixed and bubbled

with nitrogen at room temperature for 30 minutes before being heated up to 120 °C. The reaction mixture was kept under nitrogen while stirring at 120 °C for 8 hours. After 8 hours, THF (50 mL) was added to dissolve the mixture. The mixture did not dissolve, but started to swell. Even after addition of 150 mL more THF and 18 hours at room temperature the system did not dissolve. The material was not further tested. This result is likely caused by the contamination of monomer **5f** by few mol% of ethylene glycol dimethacrylate generated during the synthesis of monomer **5f**.

#	*Mn**** (kg/mol)	*Mw**** (kg/mol)	Đ	Average functionality *f* per chain	Comonomer/functional monomer
Polystyrenes					
P8a	49	54	1.10	Diol	2.5/1*
P8b	71	267	3.78	Diol	2.5/1*
P8c (PS BE 1)	54	67	1.24	Boronic ester	2.7/1**
P9a	75	118	1.57	Diol	8.9/1**
P9b	77	123	1.60	Diol	8.9/1**
P9c (PS BE 2)	76	130	1.71	Boronic ester	8.9/1**
*via conversion, ** via ^{1}H-NMR, *** PS homopolymer calibration curve					

Table 5.2. Overview of functional polystyrenes prepared.

5.5 Vitrimer formation and gels

Two main procedures were used to transform functional thermoplastics into vitrimers (Figure 5.5). Functional PMMA and PS were dissolved in a good solvent of the polymer and the bisboronic ester crosslinker $\mathbf{X_1}$ or $\mathbf{X_2}$ was added. After gel formation the system was dried at high temperature under vacuum. Furthermore, functional PS was mixed in bulk with the bisboronic ester crosslinker $\mathbf{X_1}$ and crosslinked during extrusion.

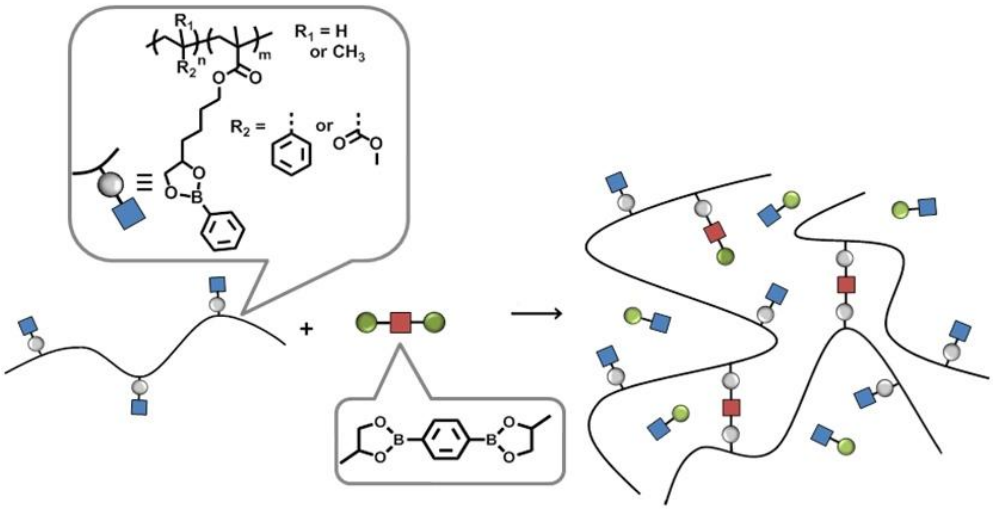

Figure 5.5. Schematic representation of the crosslinking process via exchange reaction between pending boronic esters and the bisboronic ester crosslinker $\mathbf{X_1}$. The addition of a difunctional boronic ester results in the crosslinking of a thermoplastic boronic ester functionalized PMMA or PS and the release of small boronic esters.

5.5.1 Crosslinking of functional thermoplastics in solution

5.5.1.1 General procedure

The functional polymer (10 g) was dissolved in anhydrous THF (20-40 mL) under stirring. The bisboronic ester crosslinker $\mathbf{X_1}$ or $\mathbf{X_2}$ was dissolved in anhydrous THF (0.5 to 1 mL) and added to the polymer solution. The mixture was stirred at room temperature and gel formation was observed in less than 30 minutes (Figure 5.6). The system was dried under high vacuum at 120 °C for at least 16 hours.

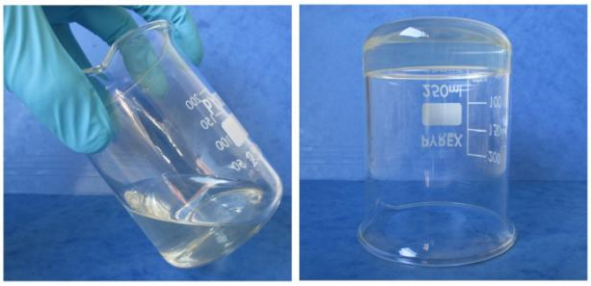

Figure 5.6. Crosslinking of **PMMA BE 3** at room temperature in solution. Left side: Solution of the functional thermoplastic in dried THF (25 wt%). Right side: The resulting vitrimer gel right after gel-formation, *ca.* 10 min after the addition of the bisboronic ester crosslinker $\mathbf{X_1}$.

5.5.1.2 Crosslinking in solution followed by rheology

The crosslinking process of the functional thermoplastic **PMMA BE 3** with *ca.* 22 mol% pending boronic esters was monitored on an Anton Paar rheometer using a cone plate geometry (50 mm) at 20 °C (Tables 5.3 and 5.4, Figures 5.7 and 5.8). Different amounts of crosslinker $\mathbf{X_1}$ were added to a solution containing a constant polymer concentration (Table 5.3). Additionally, the amount of crosslinker $\mathbf{X_1}$ was held constant while the overall polymer concentration was changed (Table 5.4). The polymer was dissolved in dried anisole and a solution of the crosslinker $\mathbf{X_1}$ was added and mixed by shaking before the mixture was placed onto the plate with a syringe (1.55 mL). The reaction time was corrected for the time it took to mix and to transfer the mixture onto the rheometer and start the experiment (1-2 minutes).

5.5.1.3 Variation of the crosslinker concentration with a constant polymer concentration

	[Polymer]	Boronic esters	Crosslinker $\mathbf{X_1}$ in 50 μL anisole	
#	wt% in 1.5 mL anisole	mmol	wt% in respect to polymer	mmol
1	12.7	0.344	2.2	0.02
2			3.3	0.03
3			4.4	0.04
4			6.2	0.056
5			8.0	0.073

Table 5.3. Concentrations of polymer and crosslinker $\mathbf{X_1}$ used to study gel formation at 20 °C.

At short reaction times (1-5 minutes), the values of G'' are superior to those of G', corresponding to a liquid regime, *i.e.* the system behaves like a fluid (Figure 5.7). During 3-4 minutes G' and G" fluctuate around a rather constant value and no gel formation can be detected. After this time, both start to increase and network formation is observed with a cross-over of G' and G" at *ca.* 5 minutes. At this point, the material becomes elastic and gel-like. The more crosslinker is added, the earlier the increase of G' is observed. The same trend follows the final value of G', which is characteristic of the increase of the crosslink density of the system.

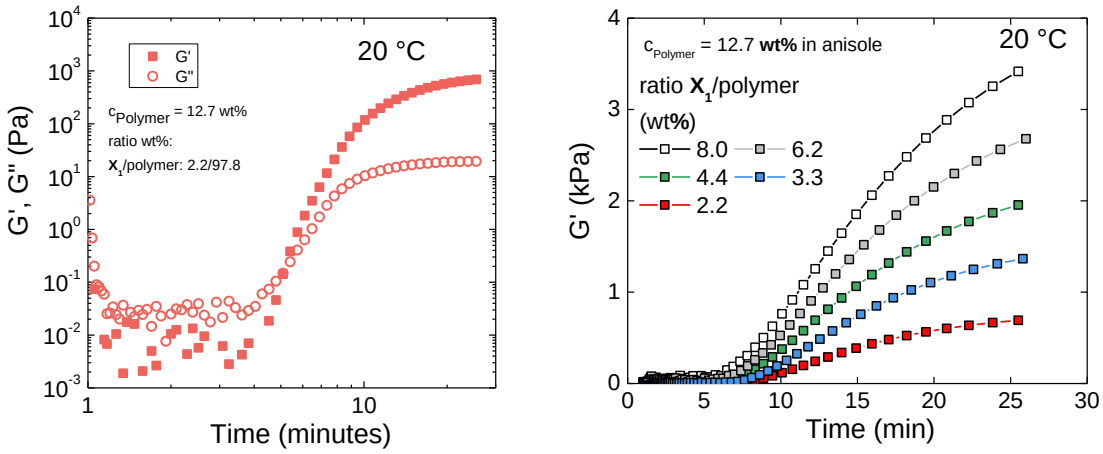

Figure 5.7. Left side: The evolution of G' and G" during the crosslinking reaction of **PMMA BE 3** (12.7 wt%) in anisole with a fixed amount of crosslinker$\mathbf{X_1}$ at 20 °C. Right side: The more crosslinker$\mathbf{X_1}$ is added, the higher the resulting G' of the vitrimer gel.

5.5.1.4 Variation of the polymer concentration at fixed molar ratio of polymer/crosslinker

	[Polymer]	Crosslinker $\mathbf{X_1}$ in 50 µL anisole
#	wt% in 1.5 mL anisole	wt% in respect to polymer
1	11.5	2.2
2	22.5	

Table 5.4. Variation of the concentration of functional thermoplastic **PMMA BE 3** with a constant molar ratio of functional thermoplastic **PMMA BE 3** to crosslinker $\mathbf{X_1}$.

The different evolution of G' as a function of time could reflect concentration effects: the more concentrated was the polymer solution, the earlier an increase in G' was observed. Both systems reached a constant G' at similar times, which likely reflects the similar ratio of polymer to crosslinker $\mathbf{X_1}$ and similar kinetics of exchange. The respective G' at complete reaction of the two vitrimer gels varied significantly which is most likely due to the difference in swelling ratio: whereas the vitrimer gel obtained from a less concentrated polymer solution exhibited a G' of about 550 Pa, the vitrimer gel obtained from a more concentrated polymer solution exhibited G' increased by a factor of 13. The less concentrated gel in Figure 5.8 was comparable to the similar swollen and crosslinked gel analyzed at constant polymer concentration (Figure 5.7). Frequency sweep experiments of both gels after reaching equilibrium under these conditions were performed with 1% deformation at 20 °C. Both vitrimer gels showed a defined G' plateau, proving their crosslinked nature. A cross-over was not detected at these frequencies and at this temperature.

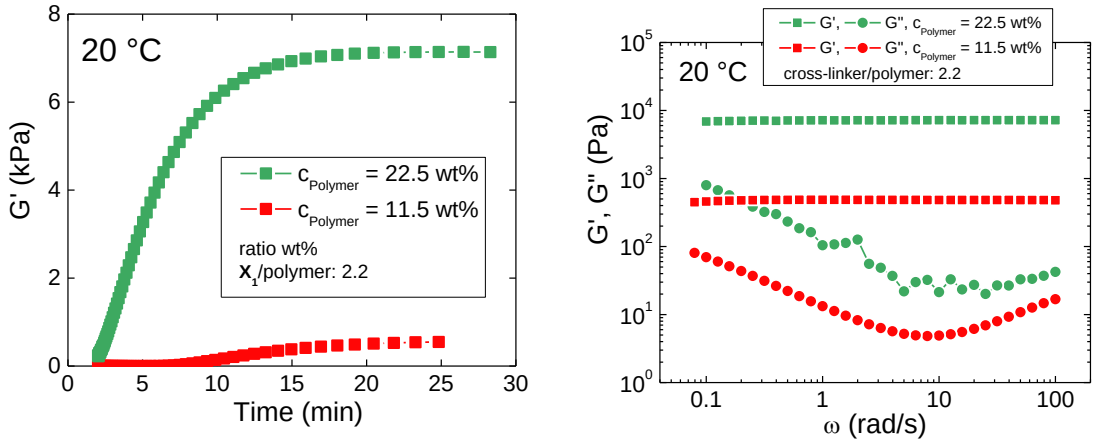

Figure 5.8. Left side: The evolution of G' as a function of time for two mixtures with different overall polymer concentration and a constant molar ratio of functional thermoplastic **PMMA BE 3** to crosslinker $\mathbf{X_1}$. Right side: Frequency sweeps at the same temperature (20 °C) of both gels after reaching a stable G' (*ca.* 25-30 minutes).

These experiments show that even at room temperature, the addition of a divalent boronic ester is sufficient to crosslink functional thermoplastic polymers containing pendant boronic ester groups via exchange reaction between boronic esters without the evaporation of generated monofunctional boronic esters. The presence of diols in these systems could not be detected. The properties of the resulting vitrimer gels can be modified at will by the addition of different amounts of crosslinker $\mathbf{X_1}$ or by changing the overall polymer concentration. The resulting vitrimer gels and their plateau at a wide range of frequencies, in frequency sweep experiments, can be seen as clear proof of their crosslinked nature.

5.5.2 Crosslinking in extrusion

Functional **PS BE 1** (3.0 g) was crosslinked using a DSM Explore batch twin-screw extruder (5 cm^3 capacity) equipped with a conical screw profile and a recirculation channel to control the residence time. The bisboronic ester crosslinker $\mathbf{X_1}$ (2.2 wt% as compared to **PS BE 1**) was manually mixed with the polymer in the powder form. The mixture was introduced into the barrel at a set temperature of 200 °C and a screw speed of 100 rpm. Upon addition, the measured force increased and 2 minutes after complete addition the measured force stabilized (Figure 5.9). This constant regime corresponds to the equilibrium state of the exchange between the monofunctional pending groups and the difunctional crosslinker $\mathbf{X_1}$, *i.e.* a terminated crosslinking process. The polymer was extruded by opening the valve and the extruded material was collected (2.7 g). This PS vitrimer was subsequently re-extruded via the

same procedure (Figure 5.9). Extruded samples were collected again and their crosslinked nature was confirmed by swelling tests (Table 5.12).

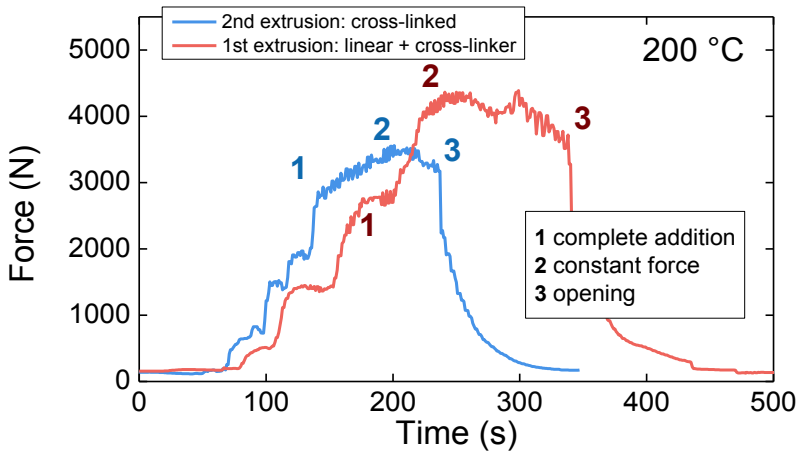

Figure 5.9. Evolution of the force as function of time during crosslinking and (re)extrusion of the **PS BE 1** material.

5.5.3 Overview of generated vitrimers

Thermo-plastic	M_n (kg/mol)	M_w (kg/mol)	$Đ$	Monomer/ functional monomer	Crosslinker $\mathbf{X_n}$ (wt%)	Vitrimer
Poly(methyl methacrylates) (PMMA)						
BE 1	22	26	1.19	3.3/1	2.2*	**BE V1**
BE 2	86	120	1.40	3.3/1	1.0*	**BE V2**
BE 3	86	120	1.40	3.3/1	2.2*	**BE V3**
BE 4	76	100	1.32	Ca 24/1	2.2*	**BE V4**
BE 5	103	128	1.24	3.3/1	2.2*	**BE V5**
BE 3	86	120	1.40	3.3/1	2.2**	**BE V6**
D 1	71	96	1.35	3.3/1	2.2*	**D V1**
Polystyrenes (PS)						
BE 1	54	67	1.24	2.7/1	2.2*	**BE V1**
BE 2	76	130	1.71	8.9/1	2.2*	**BE V2**

Table 5.5. Overview table of thermoplastic precursors and their corresponding boronic ester/diol vitrimers.

5.5.4 Additional experiments with vitrimer gels

5.5.4.1 Gel-formation with small molecules and complementary functionalized polymers

Vitrimer formation in solution was qualitatively studied by mixing either a linear functional polymer **P2a,c,d** with the bisboronic ester crosslinker $\mathbf{X_1}$ or by mixing equal solutions of

P2a,c,d with solutions of complementary functional polymer **P1a** (Table 5.6; *cf.* Figures 5.7 and 5.8 for polymer structures).

Experiment	Compound 1	Compound 2	Observation
Polymer + Small Molecule			
1	**P2a**	**X_1**	No gel
2	**P2c**	**X_1**	No gel
3	**P2d**	**X_1**	Gel
Polymer + Polymer			
4	**P2a**	**P1a**	No gel
5	**P2c**	**P1a**	No gel
6	**P2d**	**P1a**	Gel

Table 5.6. Gel-formation tests in dried THF by mixing differently functionalized thermoplastics with small difunctional crosslinker $\mathbf{X_1}$ or with a thermoplastic polymer **P1a** functionalized with complementary boronic ester functions.

Mixing of linear functional polymers and bisboronic ester crosslinker $\mathbf{X_1}$: The functional polymer **P2a,c,d** (100 mg, 0.16-0.18 mmol functional groups) was dissolved in anhydrous THF (1.0 mL) in a small glass vial closed with a septum. Upon full dissolution, the bisboronic ester crosslinker $\mathbf{X_1}$ (4.5 mg, 0.018 mmol) in anhydrous THF (0.2 mL) was added via syringe at room temperature. The reaction mixture was heated to 50 °C. After 1 hour at 50 °C, gel formation was observed for mixture **3**, but not for control experiments **1** and **2** (Figure 5.10).

Mixing of complementary functional polymers: The polymers **P2a,c,d** (100 mg, 0.16-0.18 mmol functional groups) and the polymer **P1a** (100 mg, 0.15 mmol functional groups) were separately dissolved in vials containing anhydrous THF (0.6 mL each). Once they were fully dissolved, different mixtures were generated by mixing one solution of one of the polymers **P2a,c,d** with a solution of **P1a** (0.6 mL each) via syringe. Gel formation was observed for mixture **6** after less than 5 minutes at room temperature. The fact that the gel seemed inhomogeneous will have to be studied in more detail. Gel formation was not observed for control experiments **4** and **5**, even after 7 days at room temperature (Figure 5.10).

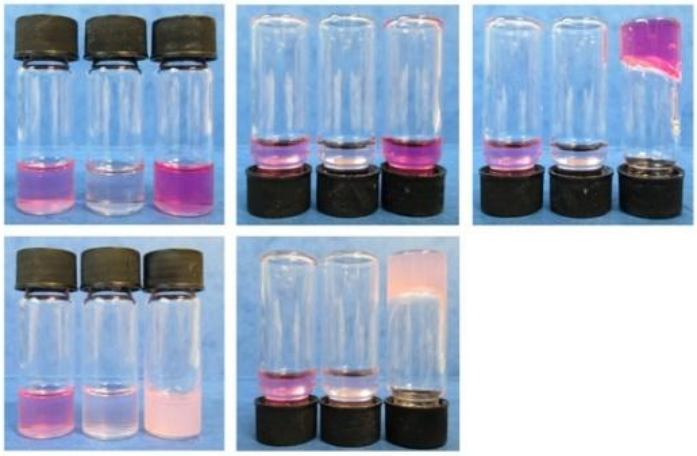

Figure 5.10. In each pictures, from left to right, solutions containing **P2a**, **P2c** and **P2d**. Top row: Experiments 1-3 (left to right) mixing with crosslinker $\mathbf{X_1}$. Left and center pictures: before addition of $\mathbf{X_1}$, right picture: after addition of $\mathbf{X_1}$. Bottom row: Experiments 4-6 (left to right) mixing with functional polymer **P1a**. Left picture: before addition of **P1a**, right picture: after addition of **P1a**.

Both sets of experiments show that boronic ester vitrimer gels can be generated by two different procedures. Either a small molecule containing two or more boronic ester functions ($\mathbf{X_1}$) is added to a solution of functional thermoplastic or complementary functional thermoplastic polymers are mixed. Control experiments with pending diols protected as trimethylsilanes or acetals did not give gels, proving that the observed gel formation is governed by the dynamic boronic ester exchange reaction.

5.5.4.2 De-crosslinking of vitrimer gels

To verify the chemical nature and the dynamic of the here presented boronic ester crosslinks, de-crosslinking experiments on gels with an excess of free diol were performed. Two gels were generated using the procedure described above for experiments **3** and **6** (see Table 5.6). After gel formation, an excess of 1,2 propanediol was added to each gel to degrade the network via boronic ester transesterification with the boronic ester crosslinks that assure the connectivity of the vitrimer networks (Table 5.7).

Mixture	**1,2 propane diol**		**Network Degradation time**
	***V* (mL)**	***n* (mmol)**	**(min)**
3	0.2	2.7	10
6	0.5	6.8	30

Table 5.7. De-crosslinking of vitrimer gels. Amount of added free diols and network degradation time.

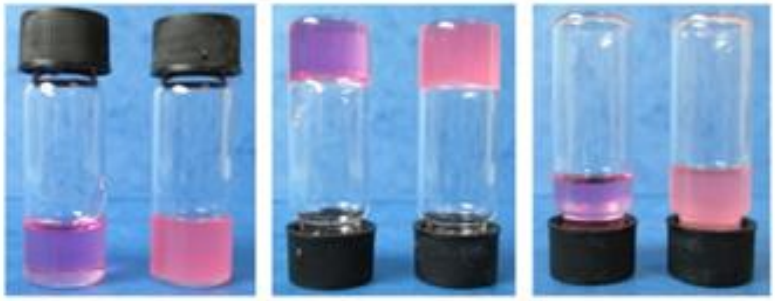

Figure 5.11. De-crosslinking of vitrimer gels. Left vial: mixture 3, right vial mixture 6. Pictures (left and center): Gels before addition of free diol, solutions after addition of free diol (right).

Both gels dissolved completely after rather short times (10 and 30 minutes) at room temperature without stirring (Figure 5.11). The de-crosslinked systems were analyzed by GPC and results compared to precursor polymers (if available) assuming complete reaction of pending boronic esters with diols (Table 5.8). Whereas the de-crosslinked network from **P2d** (**3**) was compared to polymer **P2b**, the de-crosslinked system with **P2d** and **P1a** (**6**) could only be compared to **P2b** and the boronic ester containing precursor **P1a**. The fact that once formed, these networks can be degraded via simple addition of a diol, and that the resulting polymers displayed comparable MW and distribution as their precursors prove the absence of side reactions during network formation under these conditions as well as the fact that only boronic ester crosslinks were formed.

System	Pending functionality	M_n (Kg/mol)	M_w (Kg/mol)	$Đ$
P2b*	Diol	24	27	1.21
P2d*	Boronic ester	22	26	1.19
P1a*	Boronic ester	43	57	1.32
De-crosslinked **3****	Diol	18	22	1.21
De-crosslinked **6****	Diol	60	68	1.13
*triple detection, **PMMA homopolymer calibration				

Table 5.8. GPC data of vitrimer precursors and of the respective de-crosslinked polymers.

5.5.4.3 Sticking and qualitative self-healing of vitrimer gels

Two gels were generated using the same procedure as described above for experiment **3**. One of the gels was generated with the discolored polymer **P2d**. After 24 hours at room temperature, the gels were taken out of their flasks and put in contact in a bigger sealed flask (Figure 5.12). The two gels stuck together immediately. After 2 hours at room temperature the upper colorless gel could not be separated from the lower pink gel by lifting it up with a

tweezer. After 5 hours, creep was observed and the uncolored gel seemed to become pinkish. After 24 hours, the two gels were completely fused together proving the dynamic nature of boronic ester vitrimers.

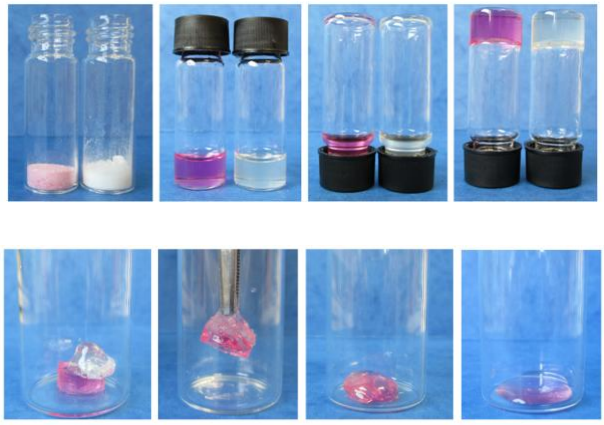

Figure 5.12. Top row: gel formation of pink (left vial) and discolored (right) **PMMA BE 3** in dried THF. Bottom row: Sticking of gels at room temperature, from left to right: after contact, after 2 hours, 5 hours and 24 hours.

PMMA BE 3 (5.0 g) was dissolved in anhydrous THF (20 mL) and the crosslinking agent $\mathbf{X_1}$ (110 mg) was added. Gel formation was observed after 15 minutes at room temperature (Figure 5.13). The gel was "broken" with a spatula (1st image) and kept at room temperature for 2 days (2nd image). Then, the gel was put upside down (3rd image) and creep was observed (4th image after 2 more days, 5th image after 4 more days).

Figure 5.13. Gel formation by mixing **PMMA BE 3** and $\mathbf{X_1}$ and subsequent creep at room temperature. First image: gel broken with a spatula. 2nd and 3rd images: after 48 hours, 4th image: 96 hours, 5th image: 192 hours.

Both the sticking of two gels and the observed self-healing/flow of a gel qualitatively confirm the dynamic character of the vitrimers based on boronic ester exchange reactions. The swollen gels flow at room temperature due to the fast exchange between pending monofunctional boronic esters and boronic ester crosslinks. The presence of small quantities of diol in these systems cannot be excluded. By increasing the crosslink density and the molecular weight of the network forming chains, the creep of the system can be slowed down.

5.6 Processing of PMMA and PS thermoplastics and vitrimers containing pending boronic esters

Once crosslinked via gel-formation in solution and subsequent drying or by reactive extrusion, vitrimers were processed via compression molding or injection molding techniques.

5.6.1 Sample preparation by compression molding

The PMMA and PS vitrimers were either ground into powder by hand or cut into small pieces and placed into a metal mold which was covered on both sides with a Teflon layer of *ca.* 0.5 to 1 mm thickness (Figure 5.14). The total was put into a preheated hydraulic press and brought into loose contact with the upper heating plate. After 5 minutes equilibration, a pressure of 3 to 5 tons was applied and held for 2-30 minutes at the selected temperature. Then, the pressure was released and the (cooled) sample was de-molded by simple pressing with a spatula or fingers.

Figure 5.14. Processing and reprocessing of **PMMA BE V3** by compression molding. The colorless powder was compression molded at 150 °C for 30 minutes under a load of 3-5 tons.

5.6.2 Sample preparation by injection molding

The mold (dumbbell or disc shape) was preheated to the desired temperature (150 °C for thermoplastic polymers and 180 °C for vitrimers). The vitrimer (ca 3.0 g) was either ground into powder or manually cut into small pieces and added to the cold injection barrel. The injection barrel was heated to 200 °C (*ca.* 2 minutes) and equilibrated for 1 more minute. Then, a pressure of 12 bar was applied in 4 consecutive steps. Step 1: from 0-12 bar in 3

seconds, step 2-4: holding 12 bar for 3×30 seconds and finally releasing the pressure. The mold was cooled down with a water-cooling circuit (*ca.* 3 minutes) and the mold was ejected manually at *ca.*60 °C. The mold was opened (by hand) and the sample was de-molded using a spatula or razor blade. The exact time to fill the mold under these conditions is 15-20 seconds for all tested vitrimers (Figure 5.14). For PMMA vitrimers a shorter total injection sequence of ca 20 seconds before cooling was successfully applied, too.

If samples with special geometry were needed, *e.g.* a rectangular shape for DMA, they were cut at *ca.* 110 °C from injection molded discs using a punch. All studied vitrimer materials were compression and injection moldable. The higher the crosslink-density, the easier the samples could be de-molded. For low molecular weight systems (**PMMA BE V1** and precursor) and more polar materials (**PMMA D V1** and precursor) severe problems were encountered. It seemed that the high concentration of diols dramatically increased adhesion to the mold causing problems during mold opening and de-molding.

5.7 Characterization of PMMA and PS vitrimers with pending boronic esters

5.7.1 Calorimetry

The materials glass transitions were analyzed by differential scanning calorimetry (DSC) and compared to their thermoplastic counterparts. Sequences of temperature ramps (heating, cooling, heating) from -25 °C to 220 °C were performed at 10 °C min^{-1} using a TA Instruments Q1000. The first heating ramp was performed to reset the sample's thermo-mechanical history. Usual sample size was 4 to 12 mg. The following transition temperatures were measured.

System	T_g (°C)
PMMA BE V1	84
PMMA BE V3	93
PMMA BE V4	93
PMMA BE V4*	99
PMMA D V1	92
PS BE 2	86
PS BE V2	98
*after 4 injections	

Table 5.9. T_g of PMMA and PS vitrimers and of the thermoplastic precursor **PS BE 2**.

The measured glass transition temperatures of the vitrimer materials were in general slightly lower compared to those of the corresponding homopolymers reported in literature.[2] The copolymerization with the functional comonomer (pending hexyl group) lowered the T_g by a few degree, *e.g.* for **PMMA BE V3** with a T_g of 93 °C (Table 5.9). The system with only 4 mol% functionalization **PMMA BE V4** had a T_g of 93 °C after the first reprocessing, but its T_g increased to 99 °C after four steps of processing. One of the possible explanations of this increase might be the evaporation of remaining small molecules (small boronic esters released during crosslinking). By comparing the functionalized thermoplastic precursor **PS BE 2** and its corresponding vitrimer **PS BE V2**, one finds that the T_g increased by forming the vitrimer (Table 5.9 and Figure 5.15).

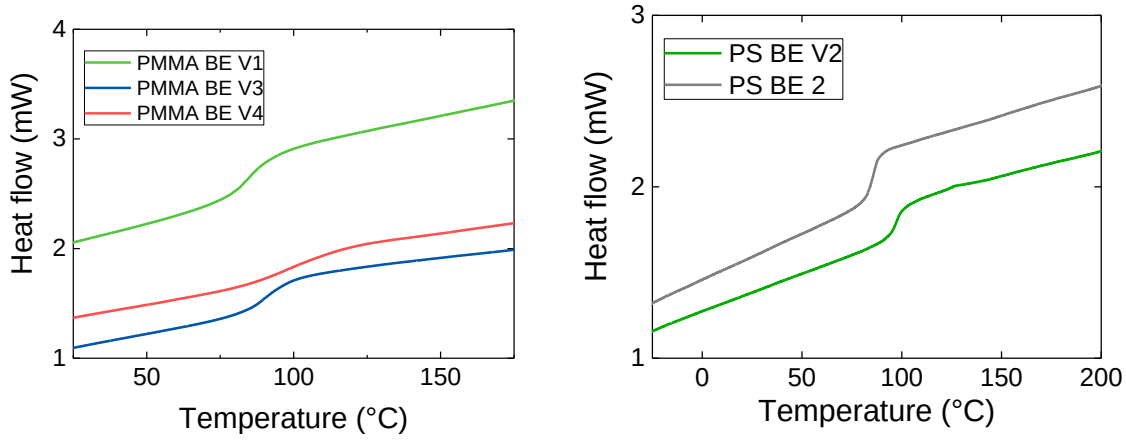

Figure 5.15. Second cycle DSC data of tested vitrimers. The first cycle was used to reset the samples thermal history. Left side: PMMA systems, right side: PS systems.

5.7.2 Swelling tests

Usually crosslinked materials show increased solvent resistance and do not dissolve in good solvents of the network forming chains (Tables 5.10-5.13). Depending on the crosslink density, networks swell more or less. On the other hand, thermoplastic polymers normally dissolve in good solvents of the polymer chains and thus have inferior solvent resistance as compared to crosslinked networks. Vitrimers were tested for their swelling behavior in self-designed swelling tests. As by definition of vitrimers, the crosslinks are dynamic, tests to de-crosslink swollen vitrimers with an excess of small molecule diols were conducted. Injection molded samples were immersed in a dried solvent at room temperature and weighted after a characteristic time. Then, they were dried under high vacuum at 120 °C until complete

dryness. The swelling ratio and soluble fraction of the vitrimer materials were calculated according to equations 5.1 and 5.2:

$$Swelling\ ratio = \frac{Mass\ swollen - Mass\ dried}{Mass\ dried}$$

Equation 5.1.

$$Soluble\ fraction = 1 - (\frac{Mass\ dried}{Mass\ dry})$$

Equation 5.2.

Sample	Number of injections	Mass dry (mg)	Mass swollen (mg)	Swelling ratio	Mass dried (mg)	Soluble fraction (%)
1	1	356	1979	4.7	350	1.7
2	1	256	1562	5.4	245	4.3
3	3	240	1430	5.0	239	0.4
4	3	198	1149	4.8	197	0.5

Table 5.10. Swelling experiments, in 10 mL of anhydrous THF for 24 hours, of **PMMA BE V3** samples processed once or three times by injection molding.

Sample	Number of injections	Mass dry (mg)	Mass swollen (mg)	Swelling ratio	Mass dried (mg)	Soluble fraction (%)
1	1	130	680	4.2	130	0
2	1	106	589	4.6	105	0.9
3	1	99	636	5.6	97	2.0
4	4	142	710	4.0	141	0.7
5	4	202	1206	5.0	200	1.0
6	4	216	1210	4.6	216	0

Table 5.11. Swelling experiments, in 10 mL of anhydrous THF for 72 hours, of **PMMA BE V4** samples processed once or four times by injection molding.

Sample	Number of extrusions	Mass dry (mg)	Mass swollen (mg)	Swelling ratio	Mass dried (mg)	Soluble fraction (%)
1	2	81.5	2131	27.0	76	6.7
2	2	184	3874	21.7	171	7.0
3	2	151	3610	23.1	150	0.7

Table 5.12. Swelling experiments, in 6 mL of anhydrous DCM for 24 hours, of **PS BE V1** samples crosslinked by reactive extrusion and processed a second time by extrusion.

Sample	Injections	Mass dry (mg)	Mass swollen (mg)	Swelling ratio	Mass dried (mg)	Soluble fraction (%)
1	1	320	780	2.5	311	2.8
2	1	186	485	2.7	178	4.3
3	1	201	523	2.7	194	3.5
PMMA D 1	1	200	Dissolved completely			

Table 5.13. Swelling experiments of injected **PMMA D V1** samples in 10 mL dried toluene for 24 hours at 80 °C under argon.

In all cases, the soluble fractions are rather small with less than 7% of solubles, proving the crosslinked nature and the increased solvent resistance of these systems. The swelling ratio of systems **PMMA BE V3** and **V4** which differ in the concentration of pending functionalities, but not in the added amount of crosslinker? was observed to be rather similar proving their comparable crosslink density and the efficient incorporation of the crosslinker in both cases. Increased solvent resistance holds for systems with pending diols, too. When treating the thermoplastic precursor **PMMA D 1** under the same conditions, complete dissolution is observed whereas the vitrimer swells but stays insoluble. To further compare the solvent resistance between vitrimers and their thermoplastic homologues, the following experiment was performed. **PMMA BE V3** (1.5 g) and thermoplastic PMMA **P7a** (1.4 g) were compression molded at 150 °C for 1.5 hours in an infrared KBr mold with a weight of 5 Kg. Both samples were cured at 70 °C for 16 hours in an oven under atmospheric conditions. The cylindric (pink) samples were separately immersed in 15 mL of anhydrous THF for 24 hours at 24 °C followed by 3 hours at 60 °C (Figure 5.16). The thermoplastic PMMA **P7a** dissolved almost completely after 24 hours at room temperature and last traces of the solid dissolved completely after heating to 60 °C for 3 hours while the vitrimer remained insoluble. Instead, it was observed that the resulting gel filled the entire bottom part of vial. By turning the vials, the gel started to flow (see studies on gels). The resulting mixture of the linear **P7a** was pink while the liquid phase of the vitrimer mixture was almost colorless proving that soluble fraction was rather small as measured in the swelling tests described above (Table 5.10).

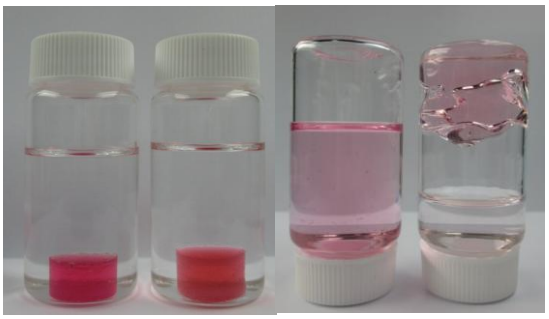

Figure 5.16. Left sample: thermoplastic PMMA **P7a**, right sample: **PMMA BE V3**. Left image: at t= 0.5 min., right image: after 24 hours at 24°C and 3 h 42 min at 60°C.

5.7.3 Polymer recycling via selective de-crosslinking

Samples of the vitrimers **PMMA BE V3**/**V4** and **PS BE V2** (50-250 mg polymer, n eq. functional groups) were immersed in THF and 1,2 propanediol (50-150 n eq.) was added. After *ca.* 18 hours at room temperature without stirring, all tested samples were completely dissolved. After dissolution, the clear solution was filtered (no residue in the filtrate after rinsing with anhydrous THF) and analyzed via GPC. The molecular weight of the crosslinked/(re)processed/de-crosslinked samples was compared to the respective precursor polydiols (**P3a** and **P4a**) and polyboronic ester precursors (**P3b** and **P4b**). For both PMMA systems tested the detected molecular weight of the de-crosslinked samples increased by a factor of not more than 15% (M_n) (Table 5.14). The dispersity increased even less.

#	M_n (Kg/mol)	Mw (Kg/mol)	Đ	Processing
		PMMA BE V3		
P3a**	71	96	1.35	-
P3b**	86	120	1.40	-
PMMA BE V3$^+$	75	105	1.40	1 inj.
PMMA BE V3$^+$	76	108	1.42	3 inj.
		PMMA BE V4		
P4a**	65	80	1.23	-
P4b**	69	84	1.22	-
PMMA BE V4$^+$	75	97	1.29	1 inj.
PMMA BE V4$^+$	76	101	1.33	4 inj.
		PS BE V2		
P9a	75	118	1.57	-
P9b	77	123	1.60	-
P9c	76	130	1.71	-
PS BE V2$^+$	76	129	1.70	2 extr.

$^+$de-crosslinked by addition of an excess of 1,2 propanediol

Table 5.14. GPC analyses of thermoplastic precursors and cleaved vitrimers: **PMMA BE V3** and **V4** were (re)processed by injection molding and **PS BE V2** by extrusion.

PMMA vitrimers processed up to 4 times did not show any sign of degradation or coupling side reactions (Figure 5.17). Similar results were obtained for the PS system. The molecular weight (M_n) and the $Đ$ were observed to stay almost constant compared to their precursors. These results indicate that the introduced boronic esters are stable in the polymer matrix during network formation and processing conditions (up to 200 °C, high shear rates) and that they stay exchangeable. As a consequence, the polymer constituting the vitrimers can be selectively recovered, opening new ways to recycle permanent networks and composites.

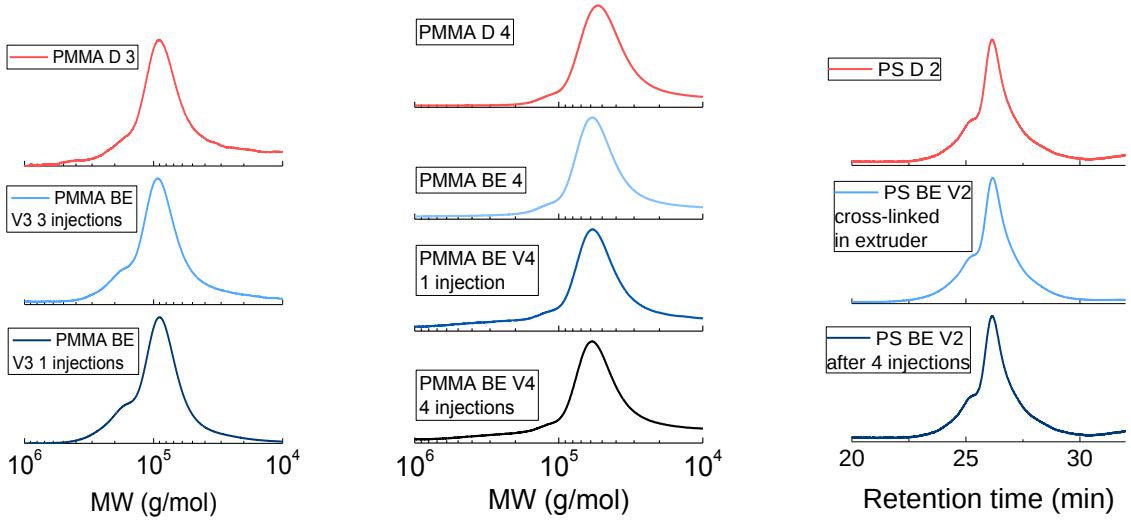

Figure 5.17. GPC raw data of thermoplastic precursors and de-crosslinked **PMMA BE V3**, **V4** and **PS BE V2** polymers.

5.7.4 Dynamic mechanical analysis (DMA)

PMMA and PS vitrimers with pending boronic esters/diols were analyzed for their structural stability by ramping the temperature (Figures 5.18 and 5.19). Once thermoplastic materials pass their characteristic transition temperature, they usually flow under their own weight, lose their 3D integrity and eventually rupture. In contrast, permanently crosslinked systems present a higher structural stability at high temperature. They possess a rubbery plateau at temperatures higher than their transition temperature, which is strongly dependent on the crosslink density. Dynamic mechanical analysis was carried out using a TA Instruments Q800 in tension mode and vitrimers were analyzed and compared to their thermoplastic counterparts. Temperature ramps were performed at a constant rate of 3 °C/min from -25 °C to 220 °C for compression and injection molded PMMA and PS samples with a maximum strain amplitude of 1% at a fixed frequency of 1 Hz (Figures 5.18 and 5.19).

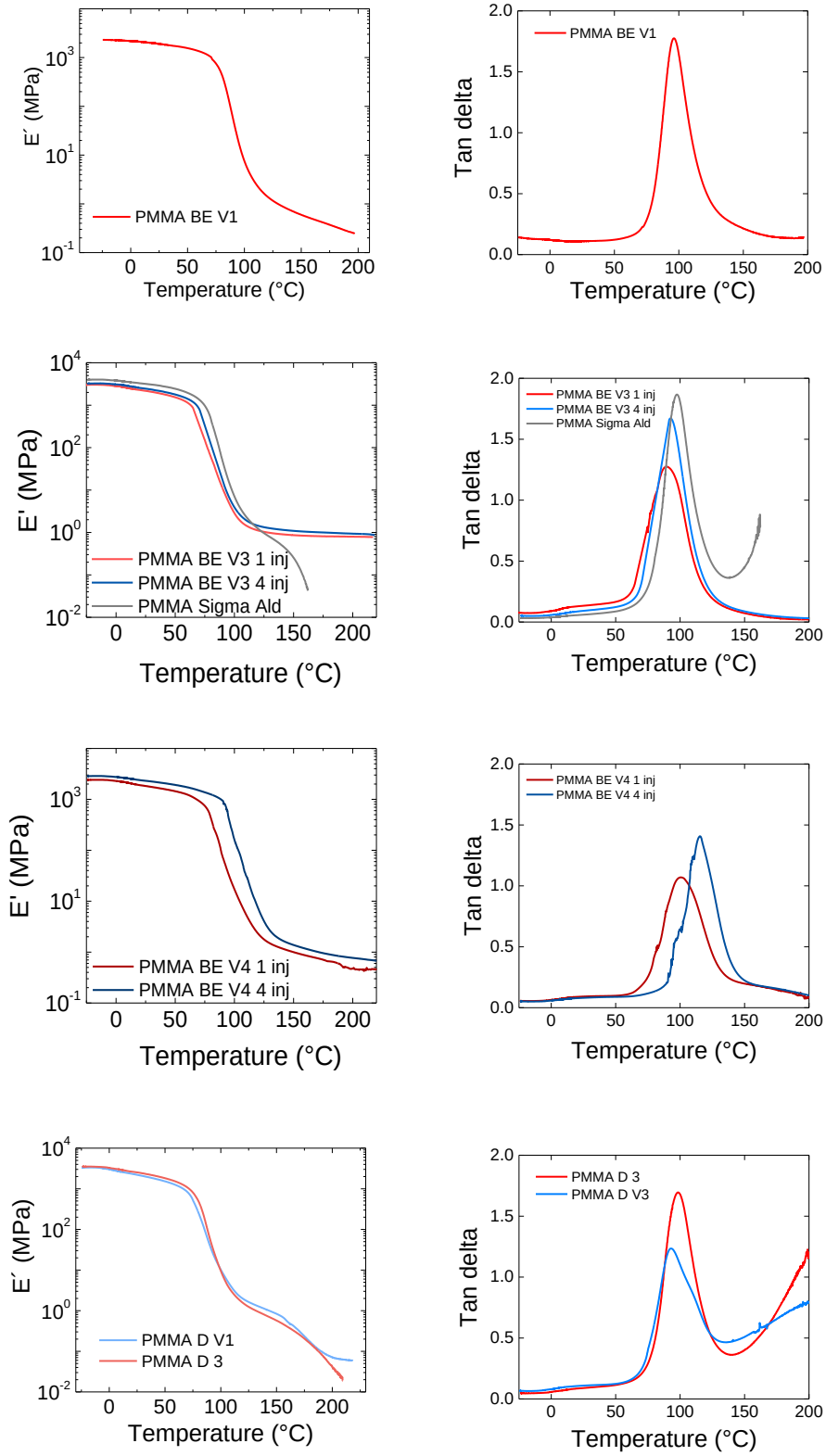

Figure 5.18. Dynamic mechanical analysis of PMMA vitrimers and their thermoplastic precursors at 3°C/min in tensile testing mode. Left side: Storage modulus. Right side: Tan delta. From top to bottom: Compression molded **PMMA BE V1.** Injection molded **PMMA BE V3** and 4 times processed sample. Injection molded commercially available **PMMA 3**. Injection molded **PMMA BE V4** and 4 times processed sample. Injection molded **PMMA D V1** and its thermoplastic precursor.

At temperatures below T_g the vitrimers exhibited similar behavior as their thermoplastic precursors. With storage moduli between 2.0-3.5 GPa they are comparable to values of the homopolymers reported in literature and to their thermoplastic precursors (Figures 5.18 and 5.19). For PMMA samples, the T_g of a commercially available homopolymer **PMMA 3** (98 °C) was slightly higher than the T_g of the **PMMA BE V3** vitrimer (90 °C), which is most likely due to the incorporation of the pending boronic ester functionalities. By decreasing the comonomer concentration, the T_g of **PMMA BE V4** increased (100 °C). Processing seems to have an annealing effect and *e.g.* for system **PMMA BE V4**, the T_g increased from the first to the 4th cycle of re-processing to 114 °C. For the polystyrene vitrimer, an increase of the T_g of the vitrimer (*ca.* 101 °C) as compared to the functional precursor (ca 96 °C) was observed, as can be anticipated with crosslinking (Figure 5.19). The same trend was found in DSC measurements.

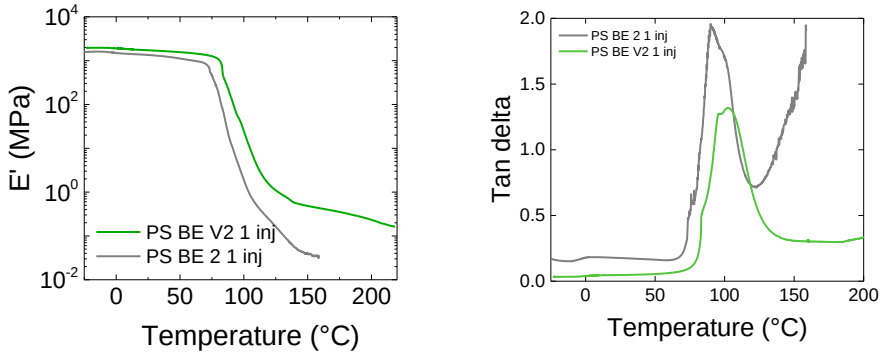

Figure 5.19. Dynamic mechanical analysis at 3°C/min in tensile testing mode. Compression molded **PS BE V2** and its thermoplastic precursor. Left side: Storage modulus. Right side: Tan delta.

In all cases, it was observed that above T_g, the vitrimer systems possess an increased structural stability as compared to their thermoplastic counterparts. The commercial **PMMA 3** as well as the functional PS thermoplastic, did not show a rubbery plateau above their T_g. Once the characteristic transition temperature is passed, they start to flow immediately and eventually brake. The vitrimer systems showed, depending on the molecular weight, the crosslink density and the nature of the polymer, a plateau-like regime which is characteristic of crosslinked systems. They did not lose their structural integrity under the testing conditions and the storage modulus stayed rather constant, with the exception of PMMA diol vitrimer, **PMMA D V1**, and **PMMA BE V1**. Even after several cycles of reprocessing, these systems remained crosslinked. and processable For systems which exchange very fast, *e.g.* due to low crosslink density, small molecular weight or a high concentration of pending diols (**PMMA BE V1** and **PMMA D V1**) (Figure 5.18), the systems flow-behavior was more similar to the

thermoplastic. This is the case for the **PMMA D V1** where the increase in structural stability compared to its linear precursor is not visible before very high temperatures (>200 °C). A similar behavior was observed for **PMMA BE V1** obtained from a low molecular functional PMMA (M_n =22 000 g/mol; Đ = 1.18). Nevertheless, even if the modulus decreased rather constantly it was still higher than the modulus of the higher molecular weight linear **PMMA 3** (M_n =61 000 g/mol; Đ = 1.90). Direct comparison with the linear precursor **PMMA BE 1** was not possible, because all of the processed samples broke either during de-molding or fixation in the DMA due to the too low molecular weight of this polymer.

5.7.5 Tensile testing and recycling

An advantage of thermoplastic materials is that above a material specific temperature (T_g, T_m), their viscosity drops of several orders of magnitude within a rather narrow temperature window, allowing processing, (re-)shaping and recycling. Chemically crosslinked polymers cannot be (re)processed because their crosslinks inhibit flow of the polymer chains. To test the vitrimers mechanical properties and their re-processability and recyclability, tensile tests followed by re-processing and re-testing were performed. Uniaxial tensile tests were performed at room temperature on dumbbell-shaped specimens using an Instron 5564 tensile machine mounted with a 2 kN cell. For each generation, 3-5 specimens were tested at a fixed crosshead speed of 1.5 mm/min . Vitrimer and thermoplastic (for comparison purposes) samples were injection molded and then cut into dumbbell shape with a punch at ca 110 °C. Engineering stress-strain curves were obtained through measurements of the tensile force F and crosshead displacement Δl by defining the engineering stress as $\sigma = F/S_0$ and the strain as $\gamma = \Delta l/l_0$, where S_0 and l_0 are the initial cross-section and gauge length of the specimens, respectively. The Young's modulus was determined as the initial slope of the engineering stress-strain curves. Characteristic parameters such as stress at break and strain at break were investigated for all systems.

Following tensile testing, the vitrimer materials were manually cut down to small fragments with a cutter and reprocessed via compression molding (**PMMA BE V1**, **V3**) or injection molding (**PMMA BE V3**, **V4** and **PS BE V1**) in order to test their recyclability over several generations (the first generation corresponding to the original, once processed specimens) (Figure 5.20 to Figure 5.23). This procedure of tensile testing and re-processing was repeated 3 to 4 times for each material. In some cases, commercially available thermoplastics and/or

functional precursors were tested via the same processing and testing procedure for comparison. For clarity, the totality of results is reported in the form of bar diagrams and characteristic (single) stress strain curves are shown for **PMMA BE V1**, and **V3** .

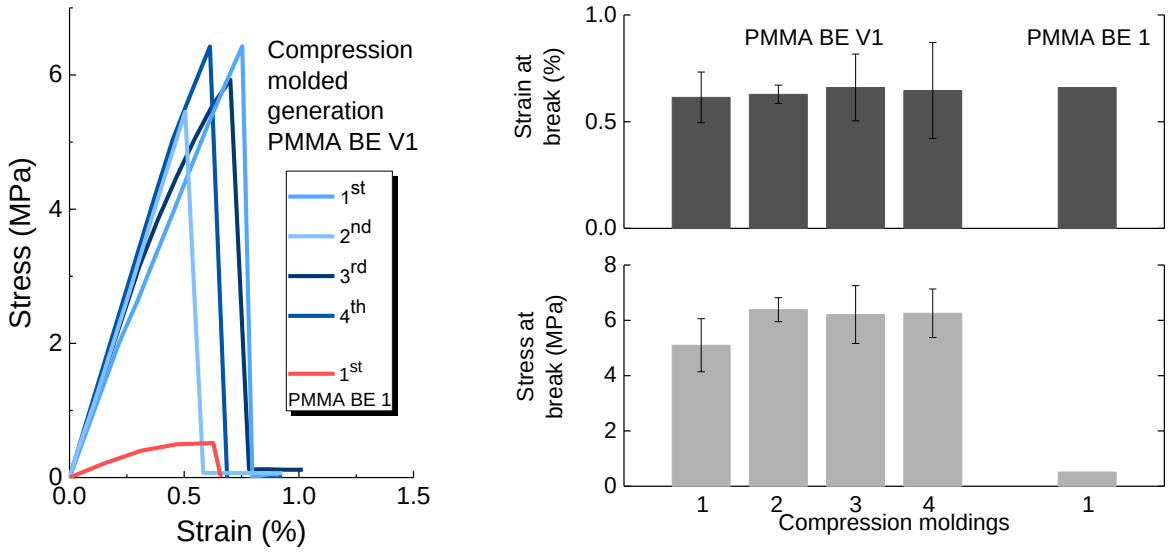

Figure 5.20. Tensile testing and re-processing of **PMMA BE V1** via compression molding for 30 minutes at 150 °C under a load of 3-5 tons. The functional thermoplastic precursor was processed via the same procedure. Left side: stress – strain curves raw data. Right side: Histogram of average values for all sample generations.

All of the tested PMMA vitrimers were recyclable. For all systems, the results show that characteristic values such as Young's modulus, stress at break and elongation at break did not vary significantly after several re-processing steps via the same processing method (compression or injection molding) (Figure 5.20 to Figure 5.22). For example the stress and strain at break of **PMMA BE V1** stayed constant around 5.5 MPa and 0.6%, respectively, even after a total of four re-processing steps via compression molding at 150 °C for 30 min (Figure 5.20). Compared to its low molar mass functional thermoplastic precursor, crosslinking enhanced mechanical strength by a factor of *ca.* 11 (0.5 MPa stress at break of **PMMA BE 1**). The linear precursor was tested only once, because the other five prepared samples broke either during de-molding or fixation in the grids. However, compared to literature, the results obtained for this vitrimer were very poor.[3]

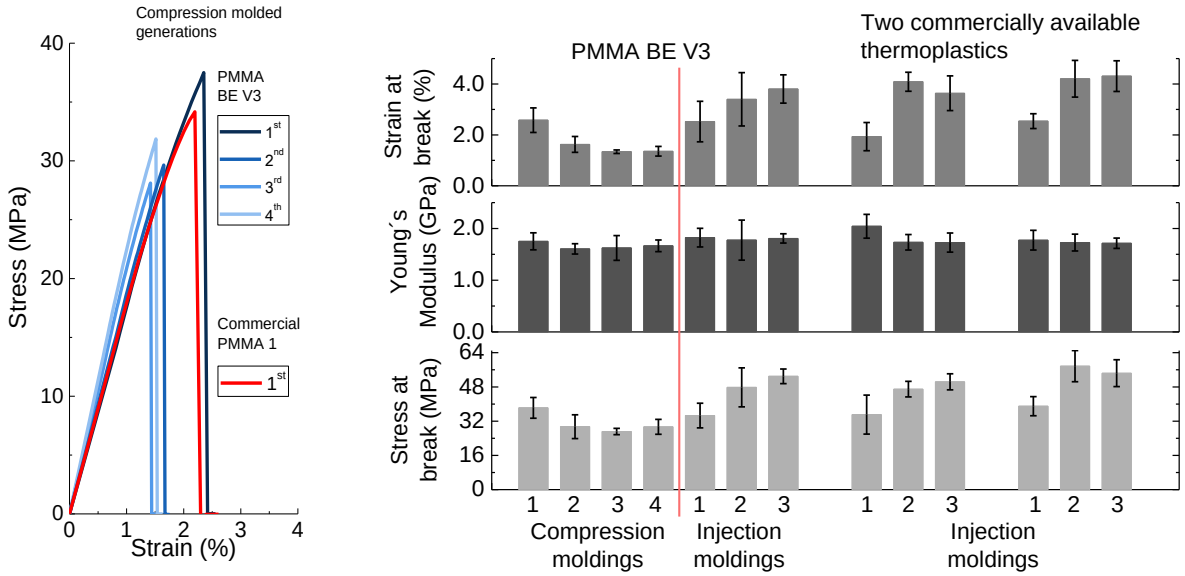

Figure 5.21. Tensile testing and re-processing of **PMMA BE V3** via compression molding for 30 minutes at 150 °C under a load of 3-5 tons (4 generations) and via injection molding at 200 °C with a pressure of 12 bar (3 more generations). The two commercially available thermoplastic precursors were processed via the same procedure. Left side: Stress-strain curve raw data. Right side: histogram of average values of all sample generations.

Compression molded **PMMA BE V3** (150 °C, 30 min) with a higher molecular weight of network forming polymer chains showed an increase of mechanical properties with stresses at break between 26 to 38 MPa (Figure 5.21). The characteristic values decrease after the second recycling of about 20% for stress at break and 40% for strain at break. Further recycling resulted in rather stable characteristic values. The determined Young's modulus stayed constant for all generations. When changing the processing method to injection molding (200 °C, *ca.* 3 min), mechanical properties of the former compression molded material increased steadily and finally reach values close to the literature (50 MPa and 2-3%).[3] Processing the two commercial references **PMMA 1** and **2** via the same procedure, resulted in materials with comparable properties. Additionally to the processing temperature, small defects possibly due to less efficient mixing in the compression molding set-up might have been the reason of this discrepancy between processing methods.

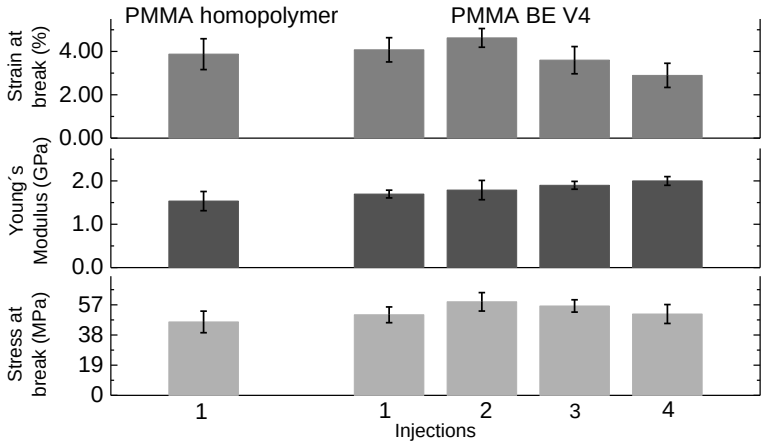

Figure 5.22. Tensile testing and re-processing of **PMMA BE V4** and an in-the-lab-synthesized PMMA homopolymer via injection molding at 200 °C with a pressure of 12 bar.

Figure 5.22 presents the recycling via injection molding of **PMMA BE V4** and the PMMA homopolymer **P7a** The values between homopolymer and vitrimer are comparable. In addition, and despite the fact that this vitrimer has *ca.* 5 times less pending functional groups than **PMMA BE V3** (and a similar molecular weight), all characteristic values measured were very comparable and therefore closed to reported to the literature values.[3]

PS systems were tested via the same injection molding procedure (Figure 5.23). As for the PMMA BE vitrimers, the properties stayed unchanged even after a total of four re-processing steps. Data were comparable between vitrimer and its functional thermoplastic precursor. However, values were rather weak compared to data reported in literature for PS materials.[4,5] This is, because most PS systems possess rather high dispersions of molecular weight (Đ > 3) and branching, whereas the here reported vitrimer exhibited a rather well defined molecular weight and low Đ of *ca.* 1.7.

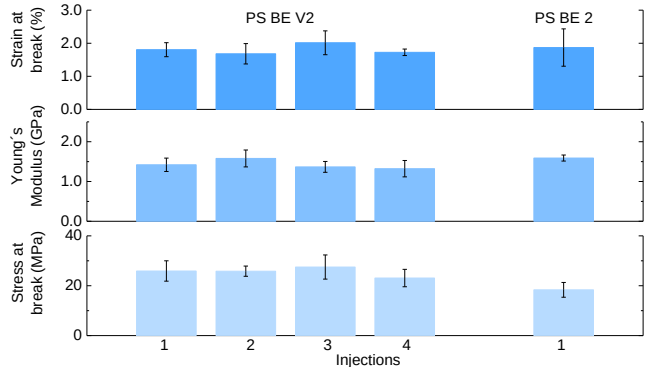

Figure 5.23. Tensile testing and re-processing of **PS BE V2** via injection molding at 200 °C with a pressure of 12 bar. The functional thermoplastic precursor was processed via the same procedure.

As discussed before, processing issues such as inefficient mixing during compression molding and other limitations such as low pressure (12 bar) and manual de-molding in injection molding processing significantly influence tensile testing results. In most of the cases the comparison with either commercially available thermoplastics or linear precursors processed via the same conditions in our laboratory showed similar properties as the respective vitrimers. Nevertheless, when comparing low molecular weight **PMMA BE V1** with its linear precursor, an improvement of the tensile properties in favor of the vitrimer was observed.

5.7.6 Rheological characterization

The rheological properties of thermoplastics depend among others parameters on their molecular weight, structure (branching), friction and processing conditions. Rheology can give detailed information about the structure and characteristics of materials, and especially for thermoplastics interesting properties such as viscosity, creep-recovery behavior and relaxation time can be measured. By definition, chemically crosslinked polymers can neither flow nor relax stress and thus no viscosity can be measured. In the following section, vitrimer

properties such as modulus, creep-recovery behavior, relaxation behavior, relaxation time and viscosity were investigated and compared to their thermoplastic precursors in rheological measurements. Vitrimers were analyzed on an ARES G2 from TA Instruments in parallel plate geometry using plates of 25 mm diameter in a convection oven. Samples were either compression or injection molded directly into a disc shape and placed in the preheated geometry under air. After 5 minutes of equilibration, an initial normal force of 10-15 N was applied and the system equilibrated for at least 5 more minutes before the experiment was started. For all systems, the normal force decreased during equilibration and experiment to equilibrate around 0 N. As for tensile properties, the vitrimers were compared to their linear precursors and tested in different experiments such as multi frequency sweeps, creep-recovery and stress relaxation experiments. For tests on the same sample but at different temperatures, usually the highest temperature was chosen as starting condition. After the run was terminated, the furnace was cooled down to the target temperature. The gap was set to automatically equilibrate to 1 N normal force and once a stable gap was reached, the whole set-up was equilibrated for 5 more minutes and the normal force was re-set to ca 10-15 N. After re-equilibration for at least 5 minutes the experiment was started. Prior to creep-recovery experiments a conditioning method was performed on every material at the respective temperature to allow the strain-controlled machine to correlate applied strain to the targeted stress.

Figure 5.24 displays a strain sweep experiment which was done prior to any other testing to assure that the frequency sweep experiments with 1% deformation were still in the systems linear regime. For the **PMMA BE V3**, the moduli do not change significantly at this temperature (170 °C) before a shear strain of 8%..

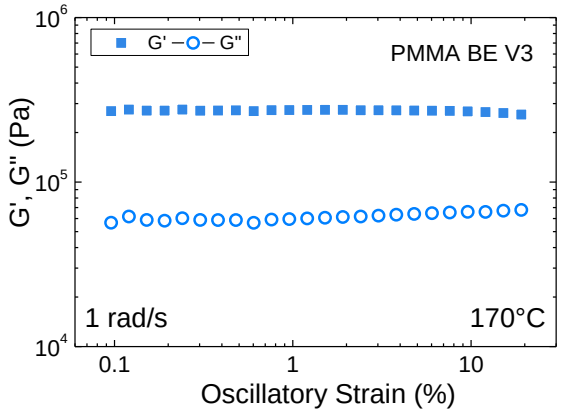

Figure 5.24. Determination of the linear regime of **PMMA BE V3** at 170 °C.

5.7.6.1 Frequency sweep experiments

Frequency sweeps were carried out by decreasing the angular frequency ω from 100 to 0.01 rad.s^{-1} with the strain amplitude γ_0 fixed at 1%. Experiments were performed at different temperatures for vitrimers and their thermoplastic precursors. For all tested PS and PMMA vitrimers a cross-over was detected, proving that these materials relax stress under the testing conditions. Angular frequency was converted to time via the following equation 5.3:

$$f\,(Hz) = \omega\,(rad.s^{-1})/2\pi \text{ and } t\,(s) = f^{-1}$$

Equation 5.3

For **PMMA BE V3** four different temperatures were tested (Figure 5.25). For a fixed frequency, the lower the temperature (170 °C) the higher was G'. At high and moderately high frequencies, *ca.* from 100 - 1 rad/s, the system possessed a pseudo-plateau which can be interpreted as characteristic for an associated system. At lower frequencies, G' decreased more rapidly and eventually crosses G" at the cross-over point, the systems longest relaxation time. The higher the temperature, the more this pseudo-plateau and the samples cross-over were shifted to higher frequencies, *i.e.* the system relaxed faster due to an accelerated exchange reaction of crosslinks and pending monofunctional groups.

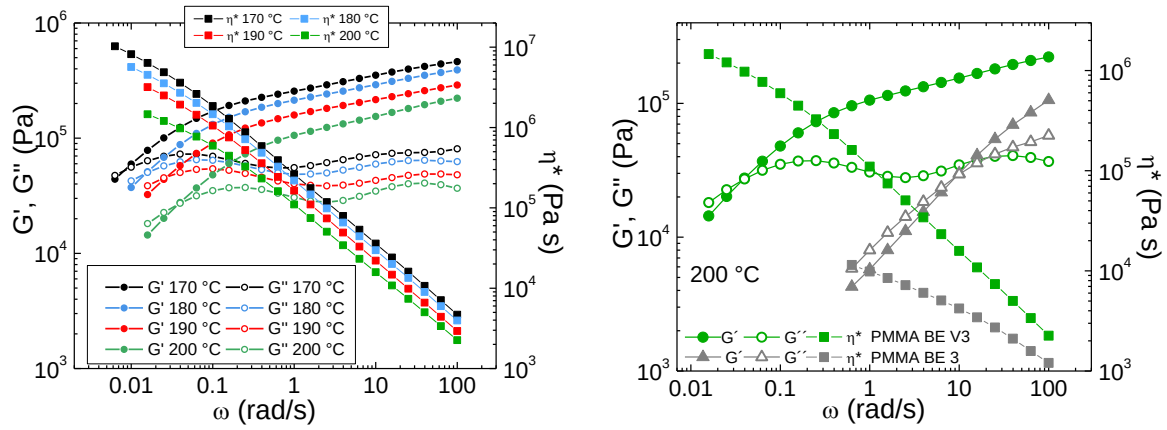

Figure 5.25. Left side: Frequency sweep experiments in parallel plate geometry of **PMMA BE V3** at different temperatures. Right side: Comparison with the thermoplastic precursor.

By comparing the vitrimer with its functional precursor under the same conditions, one observes that both G' and G" were higher for the vitrimer (as observed in DMA) at a given frequency due to its crosslinked nature and that the thermoplastic precursor did not exhibit a pseudo-plateau (Figure 5.25). Additionally, one finds that the relaxation processes (cross-over) was slowed down by a factor of *ca.* 2 order of magnitudes for the vitrimer. At 200 °C

and 1 rad.s^{-1}, the linear precursor has a complex viscosity of $\eta^* = 1x10^4$ Pa.s whereas the vitrimer has $\eta^* = 1x10^5$ Pa.s (Figure 5.25). Figure 5.26 showed that the **PMMA BE V4** material which has less boronic ester pending groups than **PMMA BE V3** possessed a more pronounced plateau at frequencies between 100 - 0.2 rad s^{-1}. The fact that less exchangeable partners are available in the **PMMA BE V4** system slowed down the exchange reactions and thus the relaxation process resulting in a cross-over at lower frequencies $\omega_{crossover} = 0.031$ rad s^{-1} for the **PMMA BE V4** system as compared to $\omega_{crossover} = 0.036$ rad s^{-1} for **PMMA BE V3**. These frequencies can be converted (equation 5.3) into relaxation time of 203 s and 175 s for **PMMA BE V4** and **PMMA BE V3**, respectively (200 °C). G' of the two PMMA BE vitrimers at the same temperature and high frequencies (100 - 1 rad.s^{-1}) were comparable (Figures 5.25 and 5.26) and can be interpreted as proof for their similar crosslink-density as observed in swelling tests.

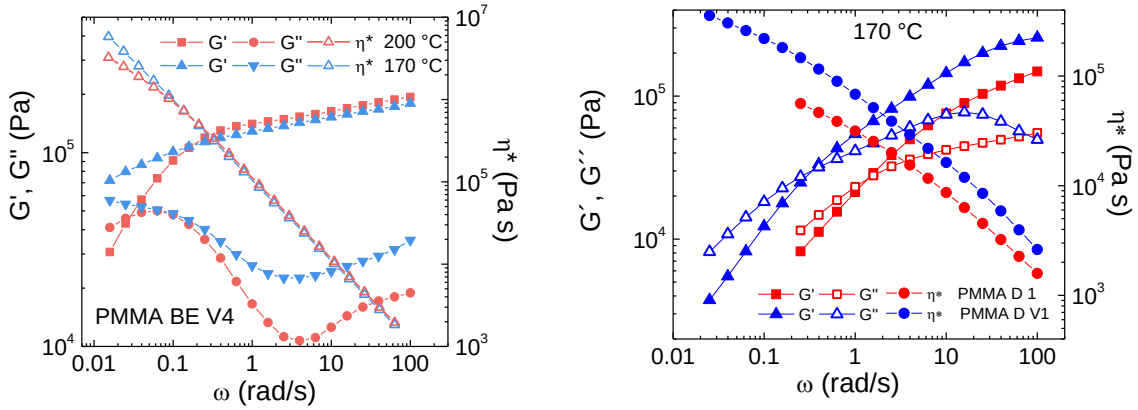

Figure 5.26. Left side: Frequency sweep experiments in parallel plate geometry of **PMMA BE V4** at 170 °C and 200 °C. Right side: **PMMA D V1** and its thermoplastic precursor at 170 °C.

Similarly to its boronic ester homologue, the cross-over of the **PMMA D V1** at 170 °C was shifted to lower frequencies, *i.e.* longer relaxation times, as compared to its linear precursor. Due to the high concentration of pending diols and the very high rate of boronic ester transesterification with 1,2-diols, the shift is less than 1 order of magnitude and no pseudo-plateau was observed at high frequencies. Complex viscosities as low as $\eta^* = 7x10^4$ Pa.s at 1 rad.s^{-1} for the vitrimer and $\eta^* = 3x10^4$ Pa.s for the linear polydiol were measured. In general, the same trends were observed for the PS systems. The difference in complex viscosity of the vitrimer **PS BE V1** and its thermoplastic precursor under the same conditions was more pronounced with $\eta^* = 1x10^4$ Pa.s vs $\eta^* = 5x10^2$ Pa.s at 1.6 rad/s (Figure 5.27).

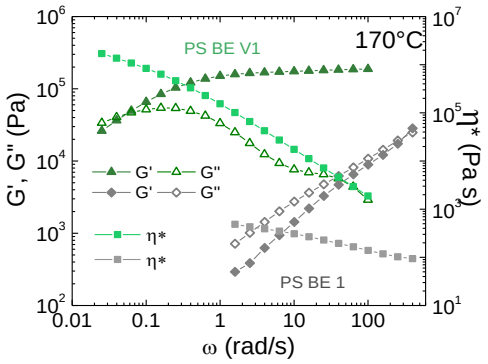

Figure 5.27. Frequency sweep experiments in parallel plate geometry of **PS BE V1** and its functional thermoplastic precursor at 170 °C..

The **PS BE V2** (ca. 10 mol% of repeating units with pending boronic esters) relaxed faster than the **PMMA BE V3** (ca. 22 %mol of repeating units with pending boronic esters) despite its lower concentration of exchangeable pending groups (Table 5.15). Several parameters govern the relaxation of these systems, one of them being the friction of the polymer backbone which is known to be smaller for PS than for PMMA of similar molecular weight.

System	T (°C)	$t_{crossover}$ (s)	η^* (Pa s) at 1 rad s^{-1}
PMMA BE 3	200	0.7	$1x10^4$
PMMA BE V3	200/190/180/170	175/233/393/757	$1x10^5/1.6x10^5/2.1x10^5/2.6x10^5$
PMMA BE V4	200	203	$1.4x10^5$
PMMA D 1	170	4.4	$3x10^4$
PMMA D V1	170	19	$7x10^4$
PS BE 2	170	0.02	$1x10^3$
PS BE V2	170	121	$4x10^4$

Table 5.15. Crossover times and complex viscosities of tested vitrimer systems.

5.7.6.2 Creep-recovery experiments

To analyze the flow behavior of the reported vitrimer systems, creep-recovery experiments were performed by applying a constant shear stress to the sample and releasing this shear stress after a given time. The systems elongation under stress and after stress release was monitored and in some cases consecutive creep-recovery cycles were performed.

Upon application of a shear stress of 1000 Pa, **PMMA BE V1** immediately deforms elastically of about 0.45-0.6% (Figure 5.28). Using the following expression, the elastic deformation can be converted to the elastic modulus which corresponds to the modulus observed in the stress relaxation experiment at the same temperature (150 °C).

$$\frac{\sigma}{\gamma} = G = \frac{1000\ Pa}{0.0048} = 0.21\ MPa$$

Equation 5.4.

The system continues to elongate and reached a steady regime almost immediately. From the slopes of the straight creep curves, the viscosities were determined at different temperatures and found to be as low as 10^6 Pa.s at 160 °C.[6]

$$\eta_{160\ °C} = \sigma/\text{slope} = 1000\ \text{Pa}/0.109\% = 9.2 \times 10^5\ \text{Pa.s}$$

Equation 5.5.

Interestingly, the mono logarithmic plot of the obtained viscosities versus the inverse time results in a straight line (Figure 5.28). The systems viscosity (η) can thus be described by a simple Arrhenius law (η_0 = materials constant, E_a = activation energy, R = gas constant, T = temperature):

$$\eta = \eta_0 \exp\left(\frac{E_a}{RT}\right)$$

Equation 5.6.

The activation energy of the system was calculated to be 33 kJ/mol. After release of the stress, only the elastic deformation was recovered proving that the exchange reaction actually allowed the vitrimer to flow and that the network reached a new equilibrium topology. The actual creep can be determined once the deformation stabilized after stress release and was observed to be as high as almost 100% at 160 °C under these conditions.

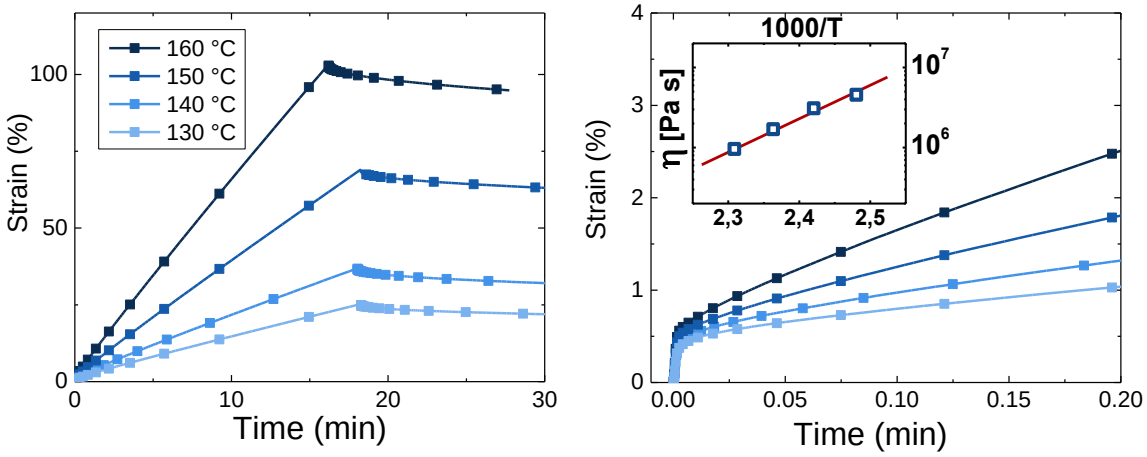

Figure 5.28. Left side: Creep-recovery experiments in parallel plate geometry of **PMMA BE V1** at different temperatures. Right side: Zoom-in on elastic region and viscosities.

By changing the molecular weight the flow behavior can be modified. For example vitrimer **PMMA BE V2** was deformed under constant stress of 3500 Pa for 10 minutes and let recover

for 10 minutes (Figure 5.29). This procedure was repeated several times at 150 °C and 130 °C. The higher the temperature, the faster the system flows. After an initial annealing of *ca.* 50 minutes and *ca.*59% real creep, the creep-curves became identical and the experiment was continued to an elongation of up to 147%. The viscosity obtained from the slopes was calculated to be 2×10^7 Pa.s at 150 °C (Figure 5.29).

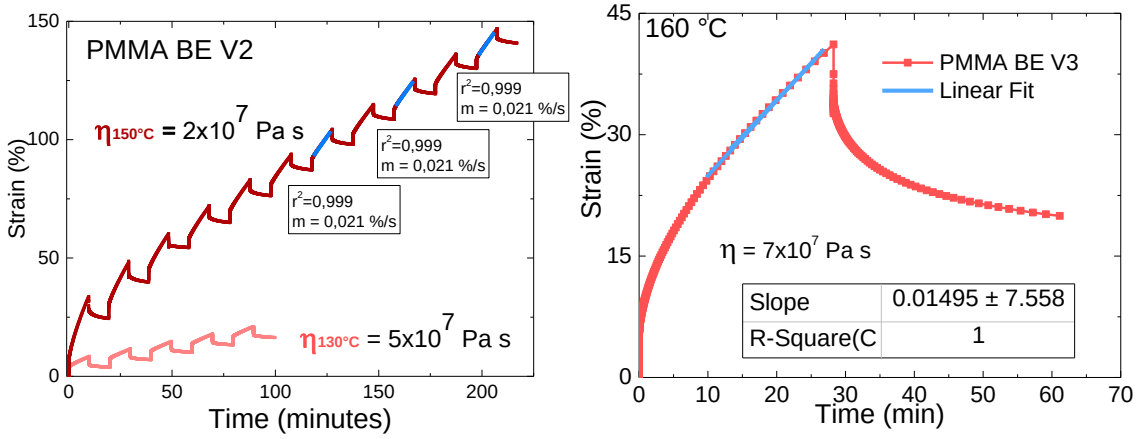

Figure 5.29. Left side: Consecutive creep-recovery experiments in parallel plate geometry of **PMMA BE V2** at 150 °C and 130°C. Right side: Creep-recovery of **PMMA BE V3** at 160 °C.

PMMA BE V3 was tested under a shear stress of 10 kPa at 160 °C (Figure 5.32). The transition between the elastic regime and a linear flow regime was more pronounced due to entanglements. The system crept less and after stress release the system recovered more than the initial elastic deformation. A viscosity of 7×10^7 Pa.s was calculated. As observed in the multi frequency sweep experiments, **PMMA BE V4** was less dynamic and thus had a higher viscosity of ca. 1×10^7 Pa.s at 200 °C (Figure 5.30 ; Table 5.16). The **PMMA D V1** crept remarkably fast to 80% deformation in less than 3 minutes under small load. Figure 5.30 shows that its creep behavior is stress dependent, *i.e.* the smaller the applied shear stress, the smaller the creep and viscosities of 2×10^6 Pa.s for 300 and 1800 Pa were estimated at 150 °C (Figure 5.30). Under the rather high stress of 3500 Pa, the system might be outside of its linear regime and the estimated viscosity drops by a factor of 2 to 6×10^5 Pa.s (shear thinning).

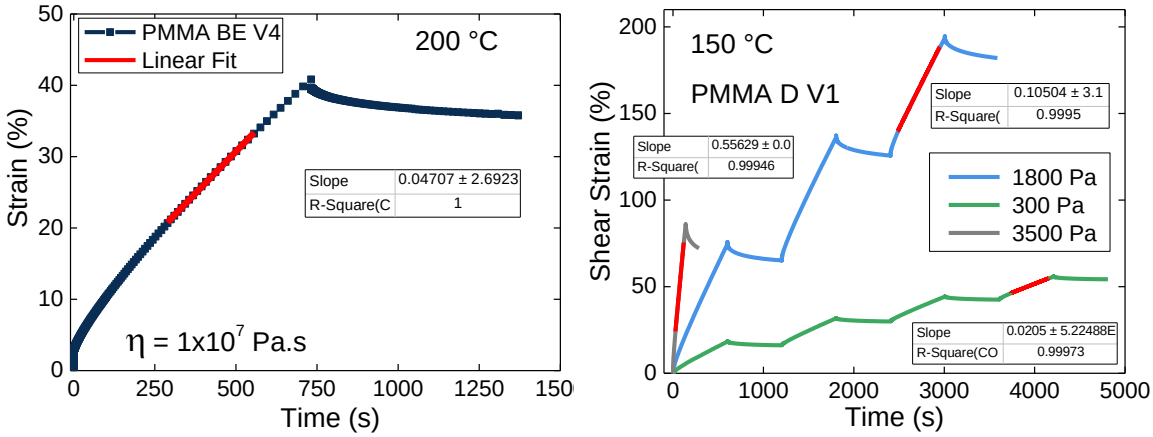

Figure 5.30. Left side: Creep-recovery experiment in parallel plate geometry of **PMMA BE V4** at 200 °C. Right side: Consecutive creep-recovery experiments of **PMMA D V1** at 150 °C under different shear stresses.

System	η_{creep} (Pa s) at Temperature (°C)					Stress
	130 °C	140 °C	150 °C	160 °C	200 °C	(Pa)
PMMA BE V1	$5x10^6$	$3x10^6$	$2x10^6$	$1x10^6$	-	1 000
PMMA BE V2	$*5x10^7$	-	$*2x10^7$	-	-	3 500
PMMA BE V3	-	-	-	$7x10^7$	-	10 000
PMMA BE V4	-	-	-	-	$1x10^7$	5 000
PMMA D V1	-	-	$2x10^6$	-	-	300
PMMA D V1	-	-	$2x10^6$	-	-	1 800
PMMA D V1	-	-	$6x10^5/*5x10^5$	-	-	3 500/3 500
PS BE V2	-	-	$*7x10^6$	-	-	3 500
*from consecutive creep-recovery						

Table 5.16. Viscosities of vitrimers tested in creep-recovery experiments.

Under the same stress, a consecutive creep-recovery experiment with an identical sample of **PMMA D V1** was able to flow more than 100% deformation in less than 8 minutes (Figure 5.31). The actual flow after recovery was around 80%. The viscosity calculated from the last creep-curve was 5×10^5 Pa.s and thus comparable to the one for the single creep-recovery experiment above. **PS BE V2** can flow, too. Viscosities of 7×10^6 Pa.s were estimated from consecutive creep-recovery experiments at 150 °C (Figure 5.31). Under similar conditions, the system creeps thus slower than **PMMA BE V1** (2×10^6 Pa.s), but faster than for example **PMMA BE V2** (5×10^7 Pa.s).

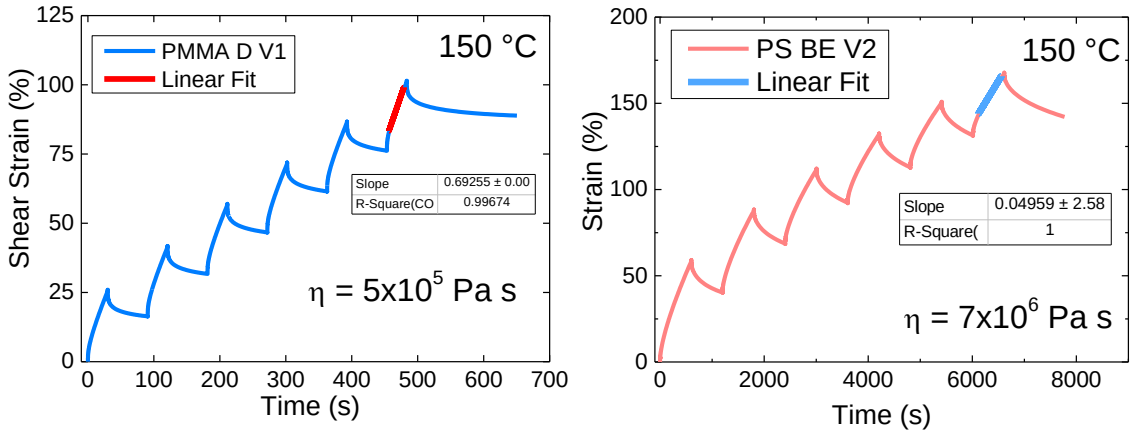

Figure 5.31. Consecutive creep-recovery experiments of **PMMA D V1** (**left side)** and **PS BE V2 (**right side) at 150 °C.

5.7.6.3 Stress relaxation experiments

Stress relaxation experiments were performed by applying a constant shear strain and monitoring the force to hold the sample at this constant strain. The time of 0.1 seconds after starting the experiment was chosen as t=0, because at this point the gap between the upper and lower plates was observed to be constant. All tested vitrimers relaxed stress. As seen above in frequency sweep and creep-recovery experiments, the dynamics of the material, *i.e.* stress relaxation via exchanging crosslinks and pending groups, can be modified by changing temperature, molecular weight, crosslink density and concentration of functionalities. All of the studied PMMA vitrimers based on boronic ester exchange relax stress (Figure 5.32). First presented epoxy/acid and epoxy/anhydride vitrimers (Leibler, *Science*, **2011**) were described by a Maxwell model with

$$\frac{G_{(t)}}{G_{(0)}} = e^{-\frac{t}{\tau}}$$

Equation 5.7.

and thus by only one relaxation time τ which equals the relaxation of ca 63% initial stress. With the aim to facilitate comparison of relaxation times between vitrimers reported in the literature and here presented vitrimers, this value was chosen.

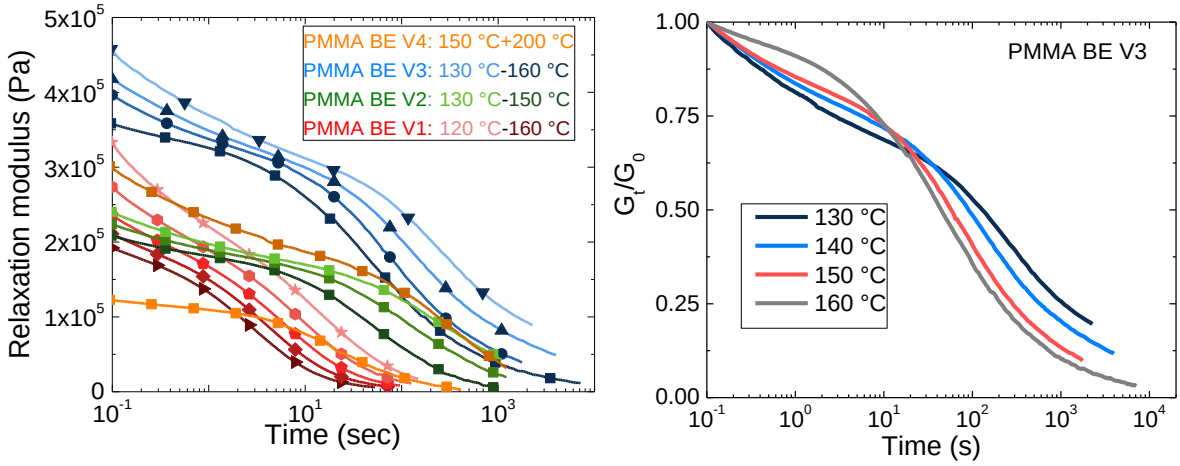

Figure 5.32. Left side: Stress relaxation cures of PMMA BE V1-V4 at different temperatures. Right side: Normalized relaxation curves of PMMA BE V3 at different temperatures.

The relaxation curves have two regimes (Figure 5.32). In the first regime, the system relaxes chain segments between crosslinks and dangling chain ends. Then, the system relaxes entirely through covalent bond exchange between the crosslinks and pending monofunctional groups. At higher temperatures, the first mode is less distinct, because the chain ends/chain segments have already relaxed. The initial modulus is proportional to the crosslink density at the same temperature as can be observed by comparing **PMMA BE V2** (0.2 MPa) and **V3** (0.4 MPa). To compare different systems, the modulus is plotted in Figure 5.33 for the 4 studied PMMA BE vitrimers at 150 °C. The low molecular weight system **PMMA BE V1** relaxed very fast (τ_{rel} = <5 seconds) at 150 °C whereas **PMMA BE V4** needed *ca.* 180 seconds. Vitrimers **PMMA BE V2** and **V3** relaxed 63% initial stress at 150 °C in 63 seconds and 122 seconds respectively. Depending on the experiments period, the remaining stress decreased to very small numbers. Increasing the temperature accelerated stress relaxation and even the slowest relaxing system, **PMMA BE V4**, had very short characteristic relaxation times of 33 seconds at 200 °C (Figure 5.32). From the chosen characteristic relaxation time at 63% of relaxed stress and the initial modulus, viscosities were calculated (equation 5.8). In Figure 5.33 viscosities at 150 °C are presented and are as low as 1.0×10^6 Pa.s for **PMMA BE V1** and 5.6×10^7 Pa.s for **PMMA BE V4**.

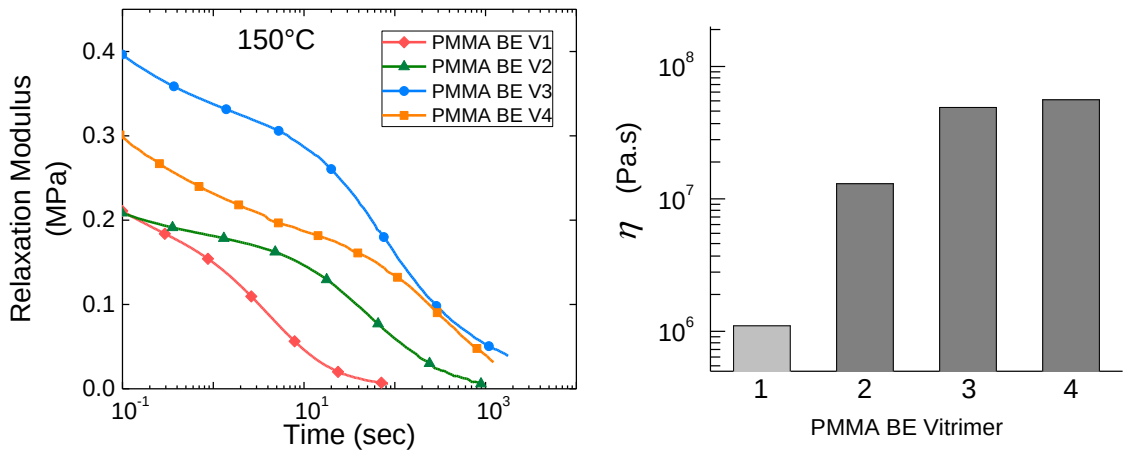

Figure 5.33. Left side: Comparison of stress relaxation data of **PMMA BE V1-V4** at 150 °C. Right side: Corresponding viscosities (**equation 5.7**) from stress relaxation measurements.

From Figure 5.34, it can be seen that vitrimers with boronic esters containing a cyclohexyl boronic acid moiety, **PMMA BE V5,** instead of the aromatic phenyl ring, did not show a significant different relaxation behavior (117 seconds) as compared to similar **PMMA BE V3** (122 seconds) (Figure 5.33). Mixing the bis-dioxaborinane (6-membered ring boronic ester) crosslinker $\mathbf{X_2}$ with **PMMA BE 3** resulted in a material with an accelerated relaxation process (<8 seconds). A possible explanation might be related to the fact that 6-membered boronic esters are more stable as compared to 5-membered species. As a result, the **PMMA BE V5**, might present a significantly lower crosslinking density due to a less efficient exchange between the pendant dioxaborolanes and the bis-dioxaborinane crosslinker $\mathbf{X_2}$ during vitrimer formation. This hypothesis is partially confirmed by the initial relaxation modulus of **PMMA BE V6** (0.2 MPa), which is twice lower than that of **PMMA BE V3**. Swelling experiments should allow to further confirm this hypothesis.

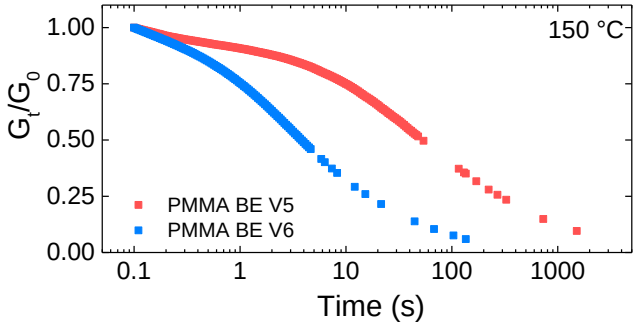

Figure 5.34. Normalized relaxation curves of **PMMA BE V5** and **PMMA BE V6** at 150 °C.

From the relaxation times (τ_{rel}) and the initial relaxation modulus $G_{0.1\ s}$, one can estimate a viscosity from stress relaxation experiments η_{rel} via the following expression (Table 5.17).[6]

$$\eta_{rel}\,(Pa.s) = G_{0.1\ s}\,(Pa) \times \tau_{rel}\,(s)$$

Equation 5.8.

Systems PMMA BE	T (°C)	τ_{rel} (s)*	$G_{0.1\ s}$ (MPa)	η_{rel} (10^6 Pa s)
V1	160/150/140/130/120	3.8/5.3/6.8/8.2/10.1	0.19/0.21/0.23/ 0.27/0.33	0.7/1.1/1.6/2. 2/3.3
V2	150/140/130	62/147/265	0.21/0.22/0.24	13/32/64
V3	160/150/140/130	94/122/215/354	0.36/0.4/0.42/0 .46	34/49/90/163
V4	200/150	33/187	0.12/0.3	40/56
V5	150	117	0.22	26
V6	150	7.4	0.2	1.5

*at 63% relaxed stress

Table 5.17. Viscosities of vitrimers from stress relaxation measurements.

The here presented viscosities from stress relaxation measurements match the viscosities obtained to creep-recovery experiments rather well. In general, the values obtained in creep-recovery experiments are slightly higher. For example at 150 °C, the viscosity of vitrimer **PMMA BE V1** was calculated to be 1.1×10^6 Pa.s by stress relaxation experiments and 2.0×10^6 Pa.s by creep-recovery experiements. The same holds for **PMMA BE V3** with 3.4×10^7 Pa.s (stress relaxation) and 7.0×10^7 Pa.s (creep-recovery) at 160 °C.

5.7.7 Environmental stress cracking

The environmental stress cracking failure of a plastic is caused by external and/or internal stresses and surface active substances.[8-11] These stress cracking agents, which can be alcohols, soaps, dyes, moisture containing agents, etc, interact with the surface of the plastic generating and accelerating the process of brittle-crack formation. Stress cracking can cause severe problems in long-term application devices and depends on several factors, such as environment (substances, temperature, light), load (stresses) and processing conditions. A solution to enhance stress cracking resistance is crosslinking. To demonstrate that vitrimers (**PS BE V2**) are more resistant to environmental stress cracking than their thermoplastic precursors (**PS BE 2**), materials were tested using a TA Instruments Q800 DMA in three

point bending geometry. Environmental conditions were simulated by placing rectangular compression molded samples (150 °C, 5 minutes, length of 30 mm, width of 15.8 mm, thickness of 1.4 mm) on the two lower tips of a demounted three point bending set-up in a mixture of 300 mL of ethanol/water (9/1) at room temperature (Figure 5.35).

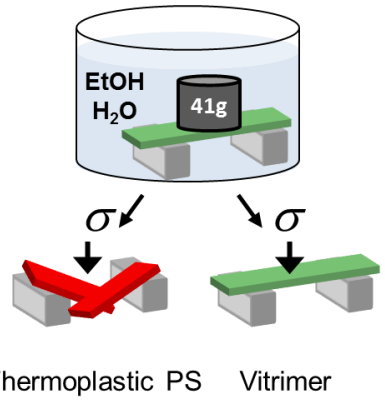

Figure 5.35. Schematic representation of stress cracking experiments with **PS BE V2** and its functional thermoplastic precursor, **PS BE 2**.

Stress was applied by positioning a cylindrical weight (41 g/120 g/250 g) in the center of the samples for different time intervals. Afterwards, the samples were dried on both sides with a paper towel and let dry at air and room temperature for 20 minutes. The dried samples were placed in a three point bending set-up in DMA and the force was ramped at 3 N/min to 18 N (upper limit of the machine) at 35 °C. Additionally to testing different immersion times under the same load, higher loads were applied on the vitrimer (Figure 5.36).

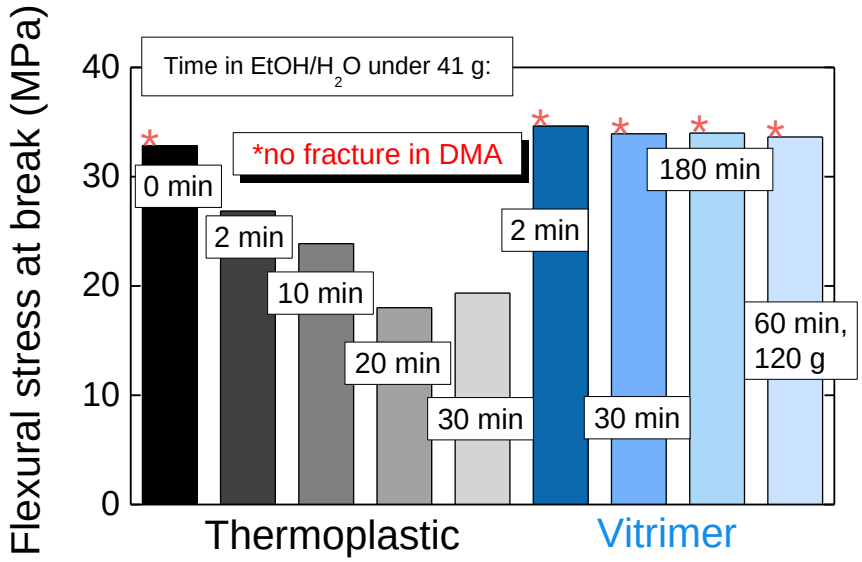

Figure 5.36. Environmental stress cracking experiments of **PS BE V2** and its functional thermoplastic precursor, **PS BE 2**.

Non-immersed **PS BE 2** thermoplastic samples did not fracture under the testing conditions (Figure 5.36). After immersion for 2 minutes in the stress cracking agent, the sample broke at a flexural stress of 26.7 MPa. By increasing the immersion time and keeping the load unchanged the flexural stress at break decreased to *ca.* 19.3 MPa after 30 minutes. In comparison, the vitrimer did not break after treatment under the same conditions. After 30 minutes in the stress cracking agent and under identical load, the applied force was not sufficient to fracture the sample. Similarly, no fracture was observed for samples after 3 hours using the same weight and after 60 minutes with a 3 times heavier weight (Figure 5.36). Eventually, when increasing the weight to 250 g, the vitrimer sample broke in the stress cracking agent after 5 minutes of immersion. Compared to their linear **PS BE 2** precursors? and as reported for crosslinked systems, the vitrimers showed increased environmental stress cracking resistance. Even rather high concentrations of water (10 vol%) did not result in instabilities of the vitrimers, which could have been caused by a potential partial hydrolysis of boronic ester links. All samples, thermoplastic precursors and vitrimers became slightly white and blurry on the surface after immersion for longer times (>20 minutes) in the stress cracking agent.

5.7.8 Thermo gravimetric analysis (TGA)

To test whether the implemented boronic esters are stable in the PMMA matrix, TGA measurements on a TG 209 F1 Libra from Netzsch were performed. Therefor, the temperature was either ramped at 10 °C/min or was hold in isothermal mode at 180 °C or 200 °C. Conditions were set to simulate air conditions with a ratio of nitrogen/air of 4/1. **PMMA BE V3** was tested after crosslinking in solution and drying and after processing once via injection molding. The vitrimer after processing was found to be more temperature resistant as its unprocessed homologue (Figure 5.37). During injection molding traces of small molecules (monomers, solvent, generated boronic esters) are evaporated resulting in a later but steeper mass loss. At 400 °C – 450 °C both tested samples showed a weight loss of at least 90%. After an initial weight loss of ca 2.5% after 25 minutes, the isotherms of the injection molded vitrimers at 180 °C and 200 °C were rather stable, proving the heat-stability under processing conditions of the PMMA BE vitrimers (Figure 5.37).

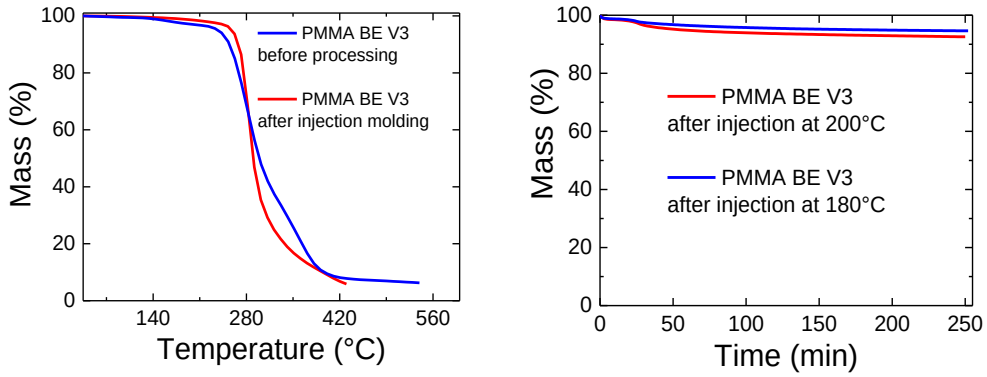

Figure 5.37. Thermogravimetric analysis of **PMMA BE V3**. Temperature ramp at 10°C/min (left side) and isotherms at 180°C and 200°C (right side).

5.7.9 Comparative infrared studies after immersion in water

The stability towards hydrolysis of pending and network forming boronic esters in the vitrimer materials was investigated. As PMMA is more hydrophilic than PS, PMMA was selected for these series of test. An injection molded disc-shape sample of **PMMA BE V3** was immersed in normal tab water at room temperature for 3 months. To hold the sample under water, a small metal weight was placed on one edge of the sample. After this period, the sample was dried with a paper towel and the hydrolysis of boronic esters was studied and compared to its not-immersed counterpart and the **PMMA D 3** linear precursor by FT-IR in absorbance mode (Figure 5.38). The commercially available PMMA from Sigma Aldrich **PMMA 3**, **PS BE V2** and its diol precursor were analyzed without immersion in water. Spectra from 1,2 butanediol and the pure $\mathbf{B_1D_2}$ were taken to confirm the peak assignation.

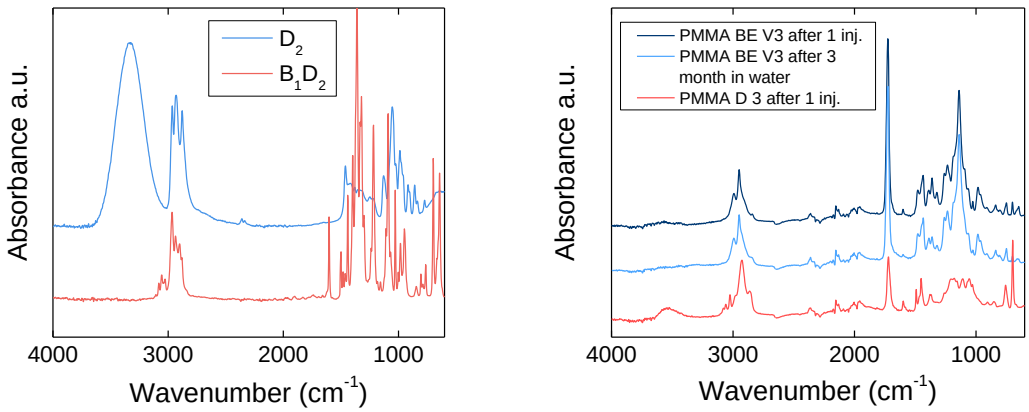

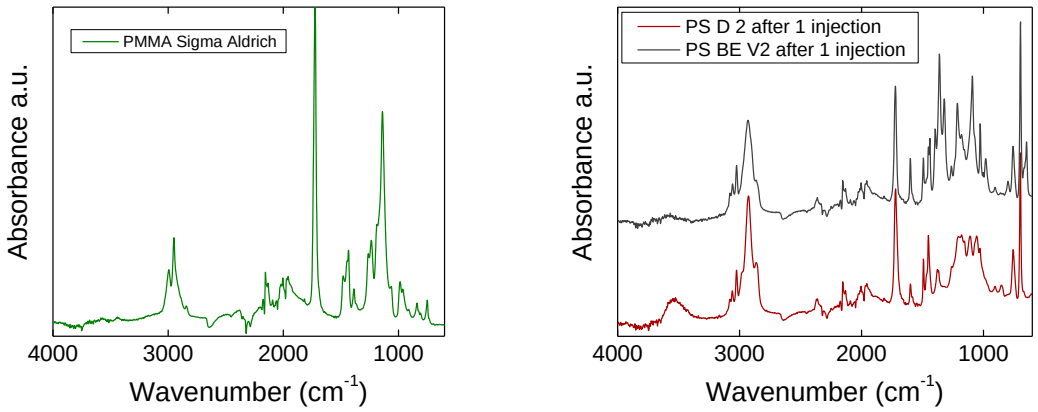

Figure 5.38. FT-IR spectra of boronic esters containing small molecules or polymers. Top left: Highly pure B_1D_2 dioxaborolane and 1,2-butanediol. Top right: PMMA BE V3 after 1 injection (as injected) and after 3 month immersion in water at room temperature, PMMA D 3 as injected for comparison. Bottom left: PMMA 3. Bottom right: PS D 2 and PS BE V2 after injection molding.

To investigate whether boronic esters were hydrolyzed to boronic acids and diols, the peak at around 3330 cm^{-1} which is significant for the OH stretching in 1,2 butanediol and did not overlap with other signals was monitored. In the corresponding small molecule boronic ester **B_1D_2** no diol signal was detected (Figure 5.38). In the spectra of **PMMA D 3**, the OH stretching signals were clearly detectable. In the spectra of the not immersed **PMMA BE V3** diol signals were not detectable, but some noise can be seen in the relevant region. The immersed **PMMA BE V3** did not change color, nor shape during immersion. Its spectrum shows even less noise and is, in this region, comparable to the commercially available homopolymer PMMA. Regarding the PS samples, a clear difference between the systems with pending diols and pending boronic esters was detected. These results prove that even after 3 month in water at room temperature, the pending and network forming boronic esters are stable and not prone to hydrolysis. Although the noise in the region around 3330 cm^{-1} could be explained by the hydrolysis of very small amounts of boronic esters at the surface of the sample, the hydrophobicity of the polymer matrix inhibits the water to enter the system and the crosslinks stay intact.

5.7.10 Adhesion tests between PMMA and PS vitrimers

Welding of specimens of the same thermoplastic polymer is well known. Usually, the material is heated above a material characteristic transition temperature (T_g or T_m) while bringing in contact the specimen in the desired shape. In general, this process proceeds by creep and the formation of entanglements/crystallizable regions across the interface. However, many

thermoplastic polymers do not adhere and stick to species of other thermoplastics. Even at elevated temperatures where they flow, they are not weldable resulting in severe problems for applications where blending and coating of different materials would be of advantage. Using a dynamic covalent exchange reaction which can interact across interfaces of crosslinked networks, we aimed to show that vitrimers with different polymer backbones can be welded together. In detail, we tested the adhesion of samples of **PMMA BE V3** with **PS BE V1**. As comparison, thermoplastic counterparts were tested for their weldability via the same procedure.

Thermoplastic **PMMA BE 3** and **PS BE 1** with pendant boronic ester functions and their corresponding vitrimers **PMMA BE V3** and **PS BE V1** were tested for adhesion by compression molding (Figure 5.39). Prior to testing, the samples were processed by compression molding into rectangular shape (width = 4.15 mm, length = 2.5 cm, thickness = 1.5 mm) at 150 °C for 30 min. under a total load of 3 tons. The thermoplastic materials were tested individually as comparison (right after processing, not welded) and after welding to each other. Vitrimers were tested after welding only. For each experiment, at least 2 samples were tested via the following procedure: each sample was put in a rectangular mold (used for processing) and after equilibration of 5 minutes, the molds were pressed with Teflon layers on the exterior of the molds to avoid direct contact with the press. After 30 minutes at 150 °C and 3 tons total load, the samples were de-molded. Overlap length was set to 5 mm and the total length of the sample in between the clamps was set to 2.5 cm.

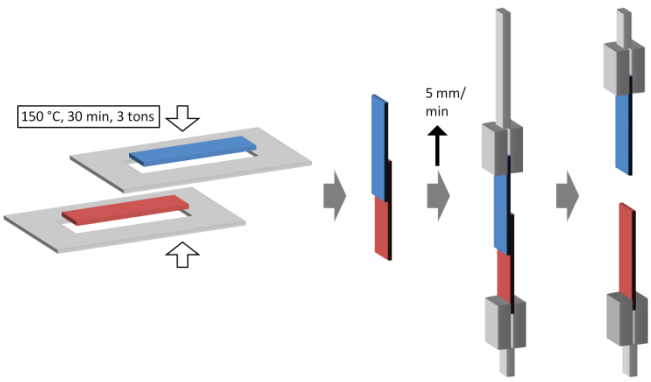

Figure 5.39. Welding of PMMA and PS thermoplastics and vitrimers via compression molding.

Both the PMMA and the PS thermoplastics were tested for their tensile properties right after processing. As expected from tensile testing results with dumbbell shaped specimen (recycling), the PMMA has superior properties than the PS. PMMA and PS thermoplastics

adhered to each other and could be placed between the grips of the traction machine and tested. Their elongation at rupture and their force at break were observed to be inferior to the individual thermoplastics (Figure 5.40). When welding the respective vitrimer samples, adhesion was enhanced by a factor of *ca.* 2 for both elongation and force at break. Interestingly, the welded vitrimer samples broke in the bulk and not in the overlap section of the two different materials, meaning that adhesion was stronger than the bulk material. Indeed, the force at break of the welded vitrimers was almost as high as the one of the single PS material, which might be limiting the determination of the adhesion between these two vitrimers.

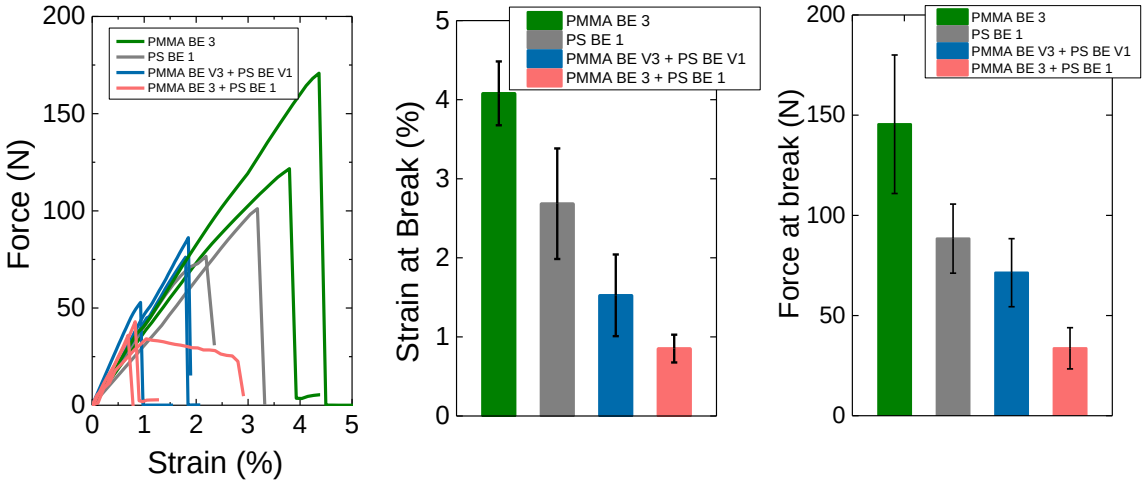

Figure 5.40. Welding of PMMA and PS systems. From left to right: Force strain curves of welding experiments, strain at break (%) and force at break (N).

The "as processed" PMMA and PS samples broke at 146 N and 89 N respectively and thus were more stable than all welded samples which broke at 72 N for the welded vitrimers and 34 N for the welded thermoplastics. Interesting is the difference of the welded vitrimers and thermoplastic samples: an increase of 112% of the force at break was observed for the vitrimers. All welded samples will be limited by their PS part as the least stable component and yet the welded vitrimers reach 81% of the force at break of the pristine PS samples? whereas the welded thermoplastics broke at 38%. The strain at break followed the same trend and the overall moduli did not change. Covalent dynamic exchanges of boronic esters in polymer matrices allow the welding of normally poorly sticking different polymer materials.

5.8 Conclusions

This chapter describes the generation and characterization of vinyl vitrimers based on the dynamic exchange of boronic esters. Methacylic monomers bearing either an aryl boronic acid or a 1,2-alkyl diol moiety were synthesized via different strategies. Thermoplastic PMMA and PS with pending diol or boronic ester functionalities were generated via controlled radical polymerization techniques (RAFT). Vitrimers were generated via two different approaches. Functional thermoplastic PMMA and PS polymers were crosslinked in solution or in bulk (reactive extrusion) with two different bisboronic esters. The crosslinking reaction was studied in more details by rheology of PMMA systems in dried anisole and the resulting gels were analyzed for self-healing, creep and reversibility of the network forming bonds. Vitrimers were processed via techniques which are common in industry, such as extrusion and injection/compression molding into different shapes, *e.g.* dumbbell, disc or bars. The PMMA and PS vitrimers swell in good solvents of their respective thermoplastic precursors and show very small soluble fractions even after several cycles of processing/testing and recycling. Even after several steps of re-processing, gels of PMMA and PS vitrimers could be de-crosslinked in the presence of an excess of monofunctional diol, confirming the good thermal and chemical resistance of the boronic ester bond. Compared to their thermoplastic precursors, the here reported vitrimers show only slightly decreased glass transition temperatures (PMMA), but enhanced three dimensional stability above the glass transition temperature (T_g). In rheological measurements, they reveal a pseudo-plateau regime depending on their functionality, crosslink density and molecular weight. They creep and relax stress and have viscosities in the range of 10^5–10^7 Pa.s between 130-200 °C. Once crosslinked, the vitrimers could be re-processed several times showing good and comparable mechanical properties for each re-processed generation, but also compared to the respective thermoplastic precursors. The most hydrophilic system, PMMA vitrimer, was tested for hydrolysis of network forming boronic ester bonds. Even after immersion in water for 3 month at room temperature, no diol species could be detected in infrared spectra of the specimen. PS systems were tested for their environmental stress cracking resistance and an increase in stress cracking resistance was detected compared to the thermoplastic precursor. Additionally, we showed that polymers which usually poorly adhere to each other (PMMA and PS) can be welded together using vitrimer technology. It can be envisioned that vitrimer systems find use in applications were enhanced chemical, mechanical and thermal resistance coupled with re-processability, malleability or recyclability are needed. Especially, for

approaches which are normally limited due to poor adhesion between surfaces, boronic ester vitrimer technology might open the door for totally new possibilities. In general, such applications could be in Wind-mills, 3D printing, cars, dental restoration, cables, electrical switches, composite matrices, facades and windows, liquid transport, bathtubs, adhesives, coatings, lenses and frame of optical glasses, LCD displays, laser cutting or fabrication of microfluidic devices.

5.9 References

1. S. Yu, R. Zhang, Q. Wu, T. Chen, P. Sun, *Adv. Mate*r., **2013**, 25, 4912.
2. J. R. Fried, "Polymer Science & Technology 3rd edition", Prentice Hall, **2014**.
3. W. M. Cheng, G. A. Miller, J. A. Manson, R. W. Hertzberg, L. H. Sperling, *J. Mater. Sci*., **1990**, *25*, 1979.
4. H. W. McCormick, F. M. Brower, L. Kin, *J. Poly: Sci*., **1959**, 87.
5. B. H. Bersted, T. G. Anderson, *J. Appl. Polym. Sci*., **1990**, *39*, 499.
6. J. Ferry, "Viscoelastic Properties of Polymers", Wiley, New York **1980**.
7. J. Scheirs, "Compositional and Failure Analysis of Polymers", J. Wiley & Sons, Chichester **2000**.
8. D. Wright, "Environmental Stress Cracking of Plastics", RAPRA Technology Ltd., Shawbury **1996**.
9. J. Lagaron, N. M. Dixon, B. J. Kip, *Macromolecules*, **1998**, 31, 5845.
10. J. Lagaron, J. Pastor, B. Kip, *Polymer*, **1999**, 40, 1629.
11. K. Kendall, Phys. D: *Appl. Phys*., **1975**, 8, 512.

General Conclusion

General Conclusion

In the here presented work, the concept of vitrimers was transferred to polymeric systems with exclusively carbon-carbon bond in their backbones, such as PMMA and PS. Different known and unknown dynamic covalent exchange reactions based on boron or nitrogen containing bonds were investigated. Kinetic studies on model compounds were performed under various conditions via nuclear magnetic resonance spectroscopy or gas chromatography. Three general considerations were identified to be very important parameters for the kinetic studies of the considered exchange reactions. 1) The purity of the starting compounds in order to avoid side reactions and/or parallel processes possibly leading to the same outcome as the studied reaction. 2) The use of protective conditions during model experiments and dryness of solvents, especially in the presence of hydrolytically labile compounds such as imines and boronic esters 3) The adaptation of analytical methods to the rate of exchange of the studied dynamic covalent reactions, in order to allow collection of sufficient data during the reaction and detection of all important species.

Three reported dynamic covalent exchange reactions were studied as well as two non reported dynamic covalent exchanges. The mixing of aldehydes and amines yielded imines in good yields and high purity (>=97%). Transimination mediated imine exchange was observed in chloroform, but proceeded slower than expected at rather high amine content (ca. 10 mol%) under air, but closed conditions. Under the same conditions, but in the presence of aldehydes instead of amines, the system needed less time to reach equilibrium. Imine exchange in the presence of traces of free amines and aldehydes was studied in bulk at 60 °C under protective atmosphere and proceeded very fast with an equilibration time shorter than 10 minutes. With this set-up hydrolysis was not observed. Interestingly, and to our knowledge not yet reported, is the reaction between imines and aldehydes. When mixing a dried aldehyde with an imine, the corresponding exchange products were detected even at room temperature in $CDCl_3$. In the protected set-up, with less than 1 mol% free amine and no detectable traces of water (^{1}H-NMR) the bulk exchange between an imine and an aldehyde equilibrated in less than three hours at 60 °C. Other than for the exchange between two imines, the equilibrium composition of species was not stoichiometric owing to different thermodynamic stability of aldehydes and imines. Two solvents, namely trichlorobenzene and toluene, were tested as reaction medium under air in closed systems in the presence of molecular sieves. For both tested imine/aldehyde reactions, similar activation energies of around 30 kJ/mol were estimated.

Due to small traces of amines (and aldehydes), and although hydrolysis can be excluded in the bulk reactions (argon atmosphere), the exact mechanism of the reaction in the imine/imine and imine/aldehyde exchanges are not entirely elucidated. Further work will have to be performed synthetically to obtain compounds with even higher purities and the analytical methods will have to be adapted to the nature of compounds (polarity – GC column) and the speed of reaction (^{1}H-NMR).

Highly pure boronic esters were synthesized and purified via a sequential washing and distillation. The hydrolytic stability and hydrolysis process of different dioxaborolanes and dioxaborinanes, cyclic 5- and 6-membered boronic esters respectively, were investigated. The association constant and dissociation constants were estimated via proton and boron nuclear magnetic resonance spectroscopy and qualitatively related to the structural characteristics of the compounds. Depending on the substitution pattern of the boronic ester, and the chemical structure of the diol, boronic esters are known to exhibit different hydrolytic stabilities. The role of humidity was investigated by running a series of experiments between two pure boronic esters under unprotected atmosphere, *i.e.* in small glass vials closed with a septum . In general, it can be concluded that a lower Lewis acidity and a higher hydrolytic stability leads to a decreased rate of exchange due to lower reactivity of the boron atom and a lower content of free diols. For example, halogen substituted phenylboronic dioaxaborolanes exchange very fast at room temperature (< 10 minutes) and were used to generate a 3x3 library within fifteen minutes at room temperature. In contrast to this, pinacol-derived species do not exchange at all under the tested conditions which is attributed both to their very high steric hindrance and hydrolytic stability. Boronic ester transesterification was studied in depth for cyclic 5- and 6-membered species in solution and in bulk under protective argon atmosphere. As reported in the literature, this exchange reaction is very rapid and difficult to quantify. With the aim to measure characteristic reaction parameters, such as the rate constant of reaction and the activation energy, a new approach was tested that allowed extending the time required to reach equilibrium without affecting the speed of exchange. The exchange of boronic esters through transesterification in the presence of small, known and purposely added quantities of diols allowed measuring the rate constant of transesterification. Rate constants of boronic ester transesterification were estimated (dioxaborolanes at room temperature in DCM: $k = 0.145\ M^{-1}\ s^{-1}$) and an activation energy of 28.1 kJ/mol (in toluene/MeCN) was calculated. The role of traces of water was further studied by addition of known amounts of water to pure boronic ester mixtures. The more water was added, the faster the exchange proceeded.

Surprisingly, and very interestingly, it was demonstrated that highly pure dioxaborolanes can undergo exchange under protective atmosphere in the absence of any detectable diol, water or other impurities. The exact mechanism of this apparent metathesis reaction between dioxaborolanes remains to be elucidated. Two possibilities at least can be envisaged: an indirect pathway through successive transesterifications with undetected traces of diols, or a direct exchange between dioxaborolanes. Indeed, when two highly pure boronic esters were mixed in bulk in the "protective" set-up, as was used for imines and aldehydes, 2x2 libraries were generated in reasonable time scales (*ca.* 60 min at 150 °C), while the absence of (detectable) hydrolysis and diols was confirmed by ^{1}H-NMR spectroscopy at the beginning and at the end of reaction. A rate constant of $k = 21\ M^{-1}\ s^{-1}$ for the bulk reaction at 60 °C was found and an activation energy of as low as 15.9 kJ/mol was estimated from experiments at different temperatures,.

With the aim to generate polymer networks containing the investigated exchange chemistries, a styrene derivative containing an aldehyde/imine function, a methyl methacrylate diol and different boronic ester monomers were synthesized, purified and characterized. Model controlled radical polymerizations (RAFT) were performed to check the stability and compatibility of these functionalities with radical (co)polymerization processes. In all cases, functional thermoplastic polymers could be obtained. However, the polymerization of the imine functionalized styrene derivative led to copolymers with higher dispersities, indicating that some side reactions, likely branching through transfer, occurred during radical polymerization. Controlled radical copolymerization with the other functional monomers led to well defined copolymers with narrow molecular weight distributions. For imine based materials polymerizable diimine crosslinker was synthesized and vitrimer materials were generated by copolymerization of this crosslinker, with the styrene derivative carrying an aldehyde function and methacrylates or styrene monomers. Another approach to generate vitrimers was applied to thermoplastics functionalized with pending imines or aldehydes, which consisted in the addition of a divalent imine crosslinker, in solution or extrusion, to the functional copolymers. Gel formation was observed for a imine-aldehyde material at room temperature. Chemically crosslinked materials were dried and their crosslinked, yet dynamic nature, was confirmed with several tests. Dried imine-based vitrimers were compression molded into different shapes according to the utilized mold. The higher was the imine content in these materials, the more colored (yellowish/reddish) they became and the longer was the processing time. Yet, the vitrimers were transparent like the parent poly(methyl methacrylate)

and polystyrene polymers and did not show any inhomogeneities. Solubility/swelling experiments in good organic solvents were performed. Vitrimers exhibited low soluble fractions <10% with swelling ratios corresponding to their crosslink densities. Additionally, the crosslinking density was shown to be stable even after several steps of re-processing. DMA measurements confirmed the crosslinked nature, with elevated storage moduli and rubbery plateaus above the glass transition temperature, both correlated to the crosslink density of the materials. The glass transition temperatures of the vitrimers were found to be (slightly) lower compared to the corresponding commercially available polymer matrices, due to the incorporation of pending groups. Stress relaxation and creep-recovery experiments of the systems confirmed the above made conclusions. Stress relaxation curves exhibited, depending on molecular weight of network forming chains and crosslink density, a two-mode relaxation. The first mode was attributed to relaxing chains ends and segments between crosslinks, followed by a second relaxation mode controlled by dynamic covalent exchanges. Cyclic processing by compression and/or injection molding with subsequent tensile testing at room temperature revealed the re-processability and recyclability of the here presented vitrimers. The mechanical properties such as stress and strain at break could be restored by compression molding. Despite the fact that these materials are processable, malleable and recyclable, side reactions of imines, especially at high temperatures cannot be excluded and rather long processing times had to be used. Furthermore, stress relaxation and creep is rather slow for materials made of network forming chains with decent molecular weight (important for mechanical properties) and more than 2 crosslinks per chain. To enhance the dynamic character of these systems and shorten processing time, more work has to be performed on both the exchange itself (acceleration) and the high temperature stability of the functionalized polymers.

Vitrimers containing boronic esters were generated via two approaches: gel formation and drying or crosslinking during extrusion. Different crosslinkers with boronic ester functionalities (5-or 6-membered rings) were synthesized and used to crosslink functionalized thermoplastics with pending boronic esters. Gel formation was observed and the crosslinking process was studied in more detail in anisole at room temperature for PMMA materials. Gels were studied for their ability to flow and self-heal. Chemically crosslinked gels were dried and their crosslinked yet dynamic nature was confirmed in swelling tests and DMA. Dried vitrimers could be processed via compression or injection molding. Obtained samples were uncolored (PMMA and PS) even after up to 4 cycles of (re-) processing. The

vitrimers were transparent and did not show any inhomogeneities. Whereas the parent thermoplastics however (PMMA and PS) easily dissolved under the testing conditions it was observed that the vitrimers do not dissolve. Important parameters such as swelling ratio and soluble fraction were estimated and the vitrimer systems exhibited low soluble fractions, below 7%. Additionally, the crosslinking density was shown to be stable even after several steps of re-processing in DMA measurements. As for the materials containing imines, the glass transition temperatures of the boronic ester vitrimers were found to be (slightly) lower compared to the corresponding commercially available matrices. However, at lower concentrations of pending groups and after several steps of re-processing, the glass transition temperatures become more similar. Although chemically crosslinked, the vitrimers relaxed stress and cross-over frequencies were observed for all tested systems at temperatures resembling processing conditions, *i.e.* not higher than 200 °C. At high frequencies, the obtained complex viscosities of vitrimers and commercially available thermoplastics are comparable. Stress relaxation and creep-recovery experiments confirmed the dynamic nature of the vitrimers and a two mode relaxation process was also observed with these systems. From creep-recovery, stress relaxation and frequency sweep experiments, viscosities ranging from 10^5-10^7 Pa.s at 150 °C could be estimated. Cyclic processing by compression and/or injection molding with subsequent tensile testing at room temperature revealed the re-processability and recyclability of the here presented boronic ester vitrimers. The mechanical properties such as stress and strain at break did not change significantly even after up to 4 re-processings (injection molded), however they were lower than values reported in literature. Tests with commercially available thermoplastics were performed under the same conditions resulting in similar results meaning that the processing conditions and not the materials by themselves were responsible of this behavior. The stability of boronic esters under processing conditions was confirmed by cleavage experiments on the recycled specimens. An excess of free diol was added to a swollen four time re-processed piece and after a relatively short time, the former crosslinked gel was dissolved completely. GPC results confirm the rather small impact of processing on the cleaved thermoplastic chains. An increased stress cracking resistance of polystyrene vitrimers was confirmed in a mixture of ethanol/water at room temperature. In a 3-point bending set-up, thermoplastic precursors showed decreased resistance after as little as 2 minutes of immersion time. The vitrimers however, did not fracture even after 3 hours in the stress cracking agent. In this work, the concept of vitrimers was transferred to polymers containing C-C bonds in their backbones only. The here presented materials show vitrimer-characteristic properties such as insolubility and

dimensional stability at high temperatures, yet they relax stress, are processable via commonly used techniques like injection molding and can be recycled and welded. They possess increased stress cracking resistance as it is common for crosslinked systems and can overcome barriers for welding of incompatible polymer matrices. Thanks to its universal applicability, the here presented easily adaptable, robust and fast exchange of highly pure boronic esters can be transferred to a variety of other polymer backbones.

Résumé

Résumé

Les vitrimères sont des matériaux à la fois réticulés et insolubles mais également façonnables, malléables et recyclables. Cette combinaison de propriétés très intéressantes est due à des liaisons dynamiques covalentes qui, à une certaine température, commencent à se réorganiser par un processus associatif tout en gardant le nombre de points de réticulation constants (Figure 1.9). Les vitrimères se comportent donc comme des thermodurcissables sous leur transition vitreuse, mais sont capables de relaxer les contraintes et de couler une fois chauffés haut dessus de cette valeur. A l'inverse des thermoplastiques, et grâce aux échanges dynamiques covalents associatifs, la viscosité des vitrimères suit une loi d'Arrhenius comme la silice. Les premiers vitrimères étaient basés sur des réactions de transestérification en présence de catalyseurs zinc dans des systèmes époxy/acide et époxy/anhydride.

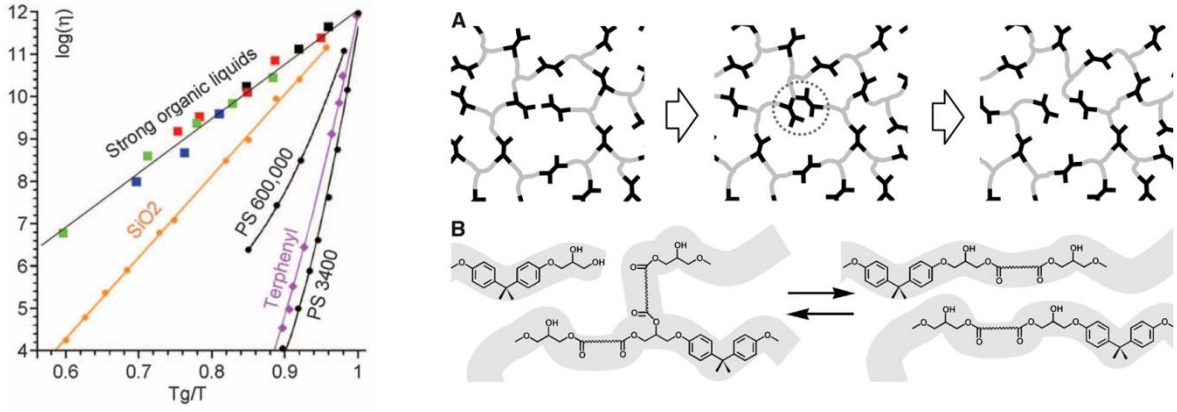

Figure 1.9. Sur la gauche: Angell fragility plot. Les points en couleur correspondent aux vitrimères. Sur la droite: Regroupement des liaisons dynamiques covalentes. Le taux de réticulations reste constant. [Leibler and co-workers, *Science*, **2011**]

Plusieurs autres types de vitrimères ont vu le jour depuis ces premiers matériaux et le concept de vitrimères a été appliqué à d'autres systèmes, comme les composites, les hybrides (liaisons hydrogènes) et les cristaux liquides. D'autres réactions d'échange ont également été étudiées afin d'accélérer les processus d'échanges des liaisons covalentes. Jusqu'à présent quasiment tous les systèmes vitrimères contenaient les fonctions échangeables intégrées dans leur chaine principale. Cependant, la grande majorité des polymères commerciaux ont des squelettes contenant uniquement des liaisons carbone-carbone, qui ne sont pas échangeables.

Le but de cette thèse est d'appliquer le concept des vitrimères aux polymères dont la chaine principale est constituée de liaisons C-C . Dans ce cadre, plusieurs défis ont été relevés, notamment l'étude de nouvelles réactions d'échanges. Ces réactions doivent être stables sous les conditions de polymérisation radicalaire et compatible avec les polymères (les acrylates et les polystyrènes). En transformant des thermoplastiques en vitrimères, les liaisons échangeables doivent être résistantes aux températures élevées pendant le moulage par compression ou par injection, mais également lors de l'extrusion. Du fait de certains problèmes associés aux catalyseurs métalliques (oxydation, toxicité, prix, compatibilité chimique) les réactions d'échanges étudiées et développées ne nécessitent pas l'emploi de catalyseur.

Plusieurs réactions d'échanges dynamiques basées sur les liaisons C=N et B-O ont été développées et étudiées lors de cette thèse. Le deuxième chapitre traite de la synthèse de molécules modèles et de l'étude des échanges entre imines, des échanges entre imines et amines, et introduit les échanges imine/aldéhyde et la possibilité d'utiliser des aldéhydes pour catalyser les échanges entre imines. Les premiers suivis cinétiques ont été réalisés par RMN du proton avec des solvants secs. Malgré un tube RMN bien fermé, une dégradation des imines a pu être observée, probablement liée à l'hydrolyse de ces composés par d'infimes traces d'eau dans le solvant ou dans l'atmosphère.

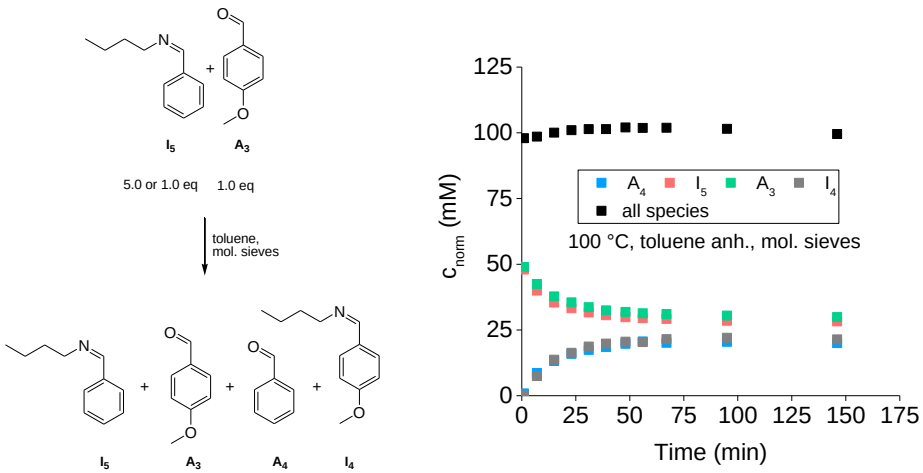

Figure 2.9. Sur la gauche: Réaction d'échange entre l'imine **I_5** et l'aldéhyde **A_3** réalisée dans le toluène en présence de tamis moléculaire. Sur la droite: Données obtenues lors du suivis cinétiques de cette réaction.

Pour éviter la dégradation des imines, des suivis cinétiques ont été réalisés avec d'autres solvants moins hygroscopiques, séchés et en présence de tamis moléculaire. Les suivis cinétiques par chromatographie en phase gazeuse n'ont montré aucune dégradation des imines

et une énergie d'activation de 33 kJ/mol a été mesurée pour l'échange imine-aldéhyde dans le toluène une (Figure 2.9). Pour complètement exclure l'hydrolyse et connaitre le taux exact d'amines et d'aldéhydes dans les imines utilisés pour les suivis cinétiques, une autre méthode a été mise en place. Des solutions concentrées d'imines ont été analysées par RMN du proton, et des traces d'amines et d'aldéhydes ont été observées et quantifiées. Des réactions d'échange entre deux imines et entre une imine et un aldéhyde ont ensuite été réalisées dans des tubes Schlenk sous argon sec. La réaction entre deux imines à 60 °C était en équilibre stœchiométrique après moins de 10 minutes. Sous les mêmes conditions, la réaction imines-aldéhyde était finie en moins de 3 heures. Dans les deux cas l'absence de dégradation des imines et l'absence d'eau ont été confirmées avant et après la réaction d'échange par chromatographie en phase gazeuse (standard interne) et RMN du proton. Ces résultats montrent que les réactions d'échanges avec des imines en masse peuvent être très rapides à une température moindre. Cependant le rôle exact des traces d'amines et d'aldéhydes sur le mécanisme d'échange reste à étudier. Notamment la synthèse doit être améliorée afin d'obtenir des molécules modèles présentant une pureté encore plus élevée.

Dans le chapitre trois, la réaction d'échange imine-aldéhyde a été utilisée pour créer des vitrimères. Un dérivé styrénique portant une fonction benzaldéhyde a été synthétisé. Deux approches ont été utilisées pour créer des vitrimères, soit par réticulation de thermoplastiques portant des fonctions aldéhyde ou imine pendantes, soit par polymérisation radicalaire de monomères fonctionnels avec des agents de réticulation contenant des fonctions imine (Figure 3.1). Des thermoplastiques avec des groupements pendants imines ou aldéhydes ont été générés par polymérisation radicalaire conventionnelle ou contrôlée. Ces thermoplastiques ont ensuite été réticulés en ajoutant une molécule diimine en solution ou en extrusion. Pour la synthèse des réseaux en présence de monomères, ceux-ci ont été polymérisés en présence d'une diimine portant des fonctions vinyliques. Les réseaux obtenus ont été gonflés et lavés à plusieurs reprises pour retirer les impuretés.

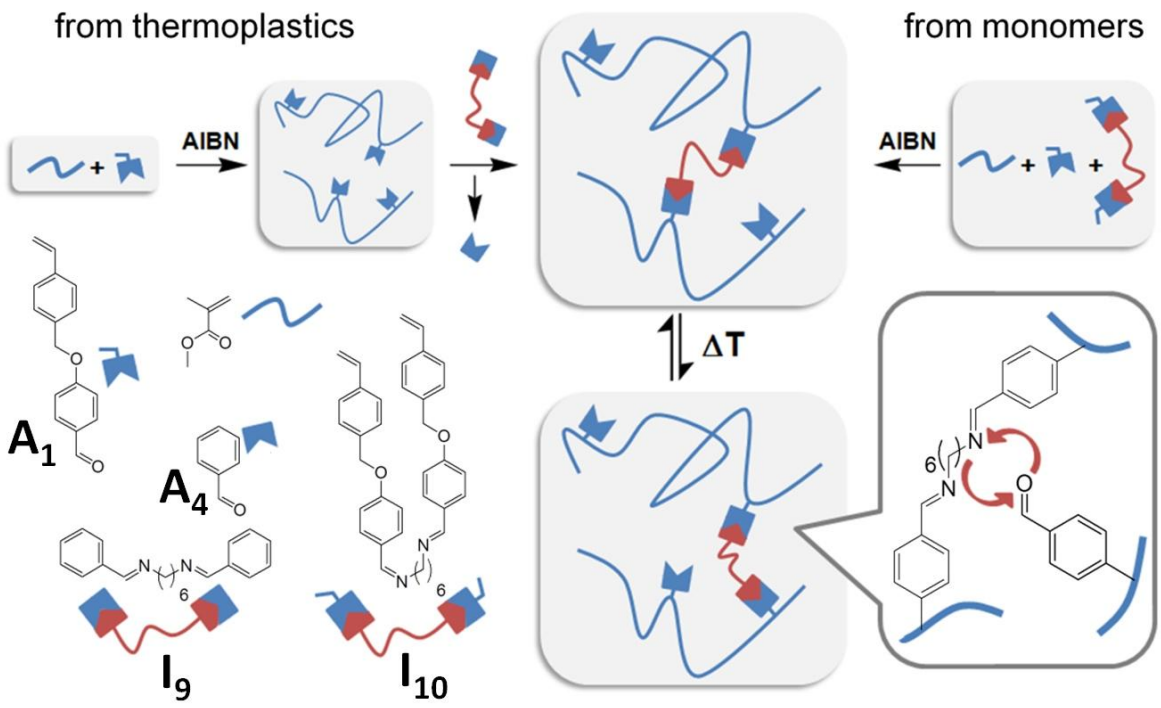

Figure 3.1. Deux stratégies ont été mises en place pour générer des réseaux vitrimères. Sur la gauche: La réticulation de thermoplastiques fonctionnals. Sur la droite: La synthèse des réseaux à partir de monomères.

Des expériences de solubilité/gonflement et d'analyse dynamique mécanique ont été réalisées afin de confirmer les effets de la réticulation. Les matériaux obtenus spnt insolubles dans des solvants organiques et le taux de gonflements est relié au nombre de point de réticulations. Ces matériaux sont façonnables par moulage par compression et leur taux de réticulation est resté inchangé après plusieurs cycles de moulage. D'autres expériences, comme la relaxation de contrainte et le fluage ont confirmé que ces matériaux ont des propriétés viscoélastiques comme les thermoplastiques. Ces vitrimères peuvent être recyclés par moulage par compression jusqu'à quatre fois sans perte significative de leurs propriétés mécaniques, telles la contrainte ou l'élongation à la rupture.

Dans le chapitre quatre, deux réactions dynamiques covalentes basés sur la liaison B-O ont été étudiées: la transestérification entre un ester boronique et un diol 1,2- ou 1,3- ainsi que la réaction d'échange entre deux esters boroniques. Ces deux réaction d'échanges impliquant des esters boroniques ont été suivie par chromatographie en phase gazeuse. Des esters boroniques très purs (>99.99 mol%) ont été synthétisés, purifiés et stockés sous atmosphère inerte. En rajoutant de l'eau dans les solutions d'esters boroniques (cycles à 5 et 6 atomes) leur stabilité vis à vis de l'hydrolyse a pu être mesurée et la constante de dissociation calculée. Des courbes d'étalonnage en chromatographie en phase gazeuse ont été élaborées en analysant les esters

boroniques à différentes concentrations . Les échanges entre un diol 1,2 et différents esters boroniques aromatiques ont été réalisés. Cet échange est extrêmement rapide à température ambiante, ce qui ne nous a pas permis de mesurer les constantes de vitesses associées . Afin d'obtenir des données cinétiques précises, une nouvelle stratégie a été mise en place. La transesterification des dioxaborolanes (esters boroniques présentant un cycle à 5 atomes) a été effectuée sous argon en ajoutant des taux de diol très précis dans un mélange contenant deux esters boroniques purs. La vitesse de la réaction d'échange a ainsi pu être mesurée et quantifiée. De la même manière, l'ajout d'eau aux mélanges d'esters boroniques en solution à permis d'observer des réactions d'échange à température. Toutefois, à température ambiante et sous atmosphère inerte, aucune réaction d'échange entre deux esters boroniques purs n'a pu être observée à des concentration de 100 mM en ester boronique et pour des temps de réactions allant jusqu'à trois heures.

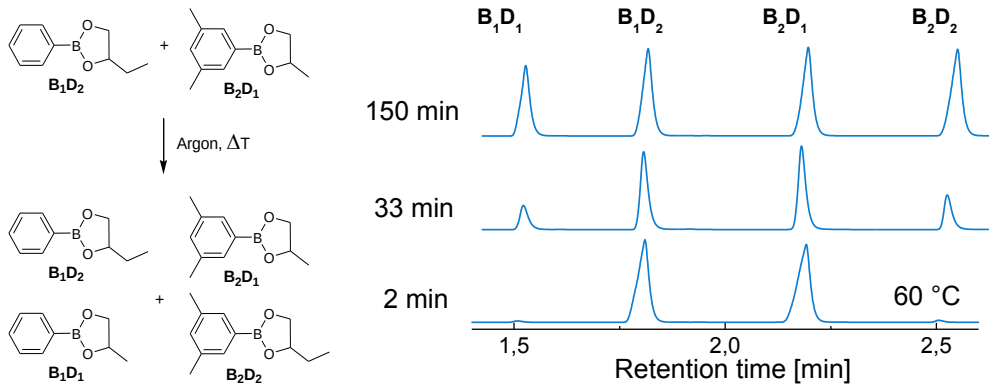

Figure 4.19. Sur la gauche: Réaction d'échange de deux esters boroniques très purs en l'absence de solvant sous argon et sans traces détectables de diol ou d'eau. Sur la droite: Suivi cinétique, par chromatographie en phase gazeuse, de la réaction à 60 °C.

La constante de vitesse et l'énergie d'activation de la transesterification des diols 1,2 avec les dioxaborolanes ont pu être mesurées. Dans les mêmes conditions d'analyse, mais sans solvant, l'échange entre deux esters boroniques (sans trace détectables de diol et d'eau) a été effectué (Figure 4.19). Comme pour les imines et aldéhydes, la réaction d'échange à 60°C était extrêmement rapide. Une énergie d'activation de 15 kJ/mol a été calculée pour cette nouvelle réaction et l'absence d'hydrolyse a été confirmée par RMN du proton.

Une stratégie additionnelle a été d'effectuer ces réactions d'échanges sous atmosphère non protégée, *i.e.* en présence d'air Dans ces conditions, l'échange entre deux esters boroniques en solution à une concentration globale de 100 mM a été observé et quantifié (Schéma 4.7).

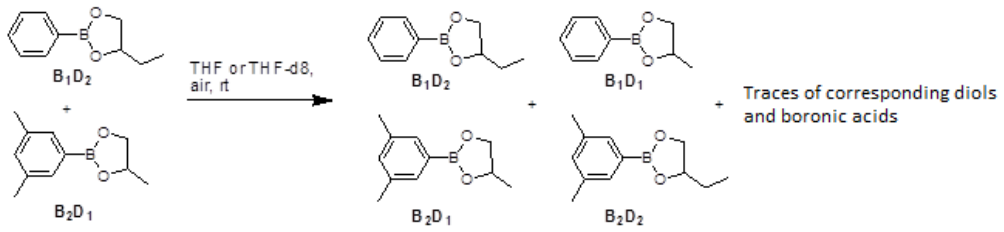

Schema 4.7. Formation d'un mélange de quatre esters boroniques différents par réaction d'échange entre deux esters boroniques (dioxaborolanes) en solution en présence d'humidité (air).

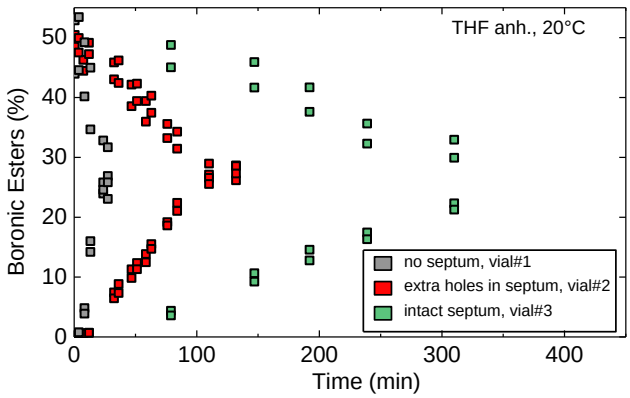

Figure 4.26. Le temps d'équilibre de la réaction d'échange entre deux esters boroniques peut être modifié par la présence d'eau dans l'atmosphère.

Dans cette série d'expériences, des esters boronique purs ont été mélangés dans des flacons fermés avec des septums. En modifiant la taille des trous dans les septums, et en allant d'un septum non troué à l'absence complète de septum, l'apparition des deux esters boroniques mixtes peut être accélérée de façon très significative. Les résultats montrent que plus l'eau est présente dans le solvant, plus les esters boroniques sont hydrolysés, et la transesterification avec des diols libres résultants rapide (Figure 4.26). En mélangeant trois esters boroniques différents, l'apparition d'un mélange de neuf esters boroniques a été constatée après environ 10 minutes. D'autres esters boroniques plus ou moins stable, en fonction de leurs structures chimiques, ont été synthétisés et testés dans les mêmes conditions. Afin de créer des vitrimères avec de faibles viscosités, la réaction d'échange entre esters boroniques a été introduite dans des matrices poly(méthacrylate de méthyle) (PMMA) et polystyrène (PS).

Dans le chapitre cinq, la synthèse de polymères thermoplastiques PMMA et PS fonctionnalisés avec des groupements pendants esters boroniques ou diols est présentée. Différentes stratégies de synthèses ont été étudiées et des tests de réticulations avec des esters boroniques divalents ont été réalisés en solution ou en extrusion (Figure 5.5).

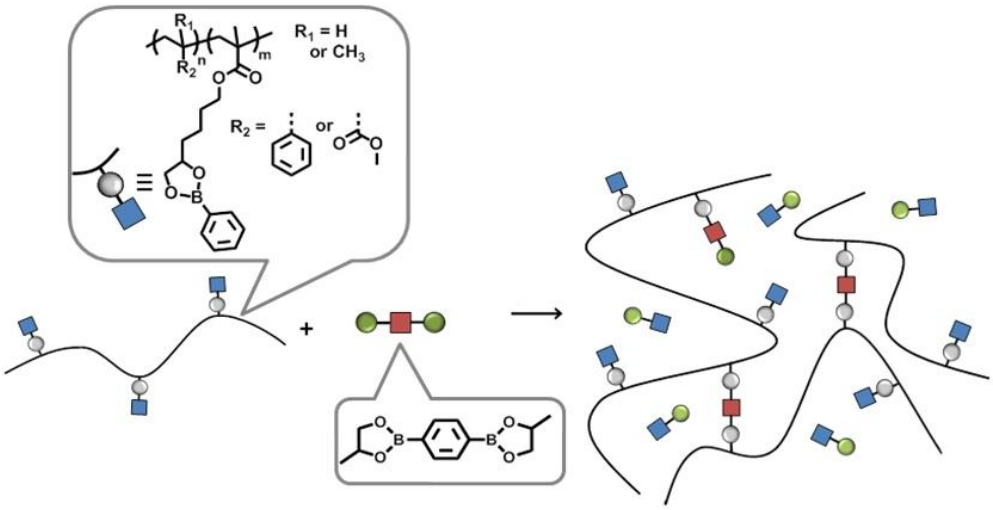

Figure 5.5. Formation de vitrimères reposant sur la chimie des esters boroniques par réticulation de thermoplastiques PMMA et PS fonctionnels via réaction d'échange entre les fonctions ester boronique pendantes et un réticulant di(ester boronique).

La formation de gels a été suivie/analysée en rhéologie. Plus la concentration du réticulant était importante, plus le module G' final était élevé. Après le séchage, les réseaux ont été façonnés par moulage par compression ou par injection (Figure 5.15). Comme pour les vitrimères basés sur les imines/aldéhydes, des tests de gonflements ont montré un taux d'insoluble extrêmement élevé. L'analyse dynamique mécanique a confirmé la réticulation de ces matériaux en montrant des plateaux caoutchouteux.

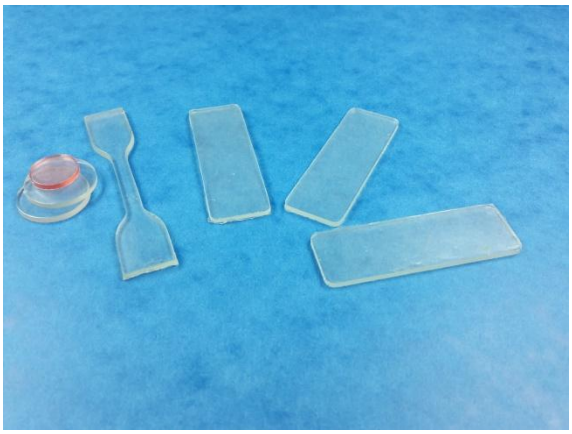

Figure 5.15. Des vitrimères façonnés par moulage par injection ou compression. Sur la gauche et l'haltère: **PMMA BE V3**. Sur la droite: **PS BE V2**.

En rhéologie, les matériaux vitrimères présentent des viscosités finies plus élevées que celles de leurs précurseurs thermoplastiques fonctionnels. Pourtant, à une température supérieure à leur transition vitreuse ces systèmes sont capables de relaxer les contraintes et de fluer. Les vitrimères basés sur des esters boroniques sont recyclables par moulage par compression et

par injection et présentent des propriétés mécaniques comparables à celles de thermoplastiques de masses molaires comparables. Les vitrimères PS ont été testés pour leurs propriétés « environmental stress cracking ». Comme des réseaux polymères conventionnels, les vitrimères ont une résistance plus importante que leurs précurseurs thermoplastiques. Même après plusieurs cycles de moulage, des vitrimères basés sur la chimie des esters boroniques ont pu être complètement "dé-réticuler" par une méthode de gonflement en présence d'un excès de diol libre. Ces expériences montrent la stabilité des esters boroniques à haute température pendant le processus de mise en forme.

Dans cette thèse, des réactions d'échange reposant sur les liens covalents dynamiques imines et esters boroniques ont été étudiées. Des paramètres importants, comme la constante de dissociation de certaines molécules, la constante de vitesse d'échange et l'énergie d'activation, ont été mesurés. Des monomères porteurs de liaisons échangeables ont été synthétisés et polymérisés. Des vitrimères avec des liaisons C-C dans la chaine principale ont été créés (à partir de thermoplastiques ou monomères). Ces matériaux sont réticulés et insolubles avec un plateau caoutchouteux mais également façonnables et recyclables par moulage par compression ou par injection. Ces vitrimères peuvent relaxer les contraintes et couler à une température supérieure à celle de leur transition vitreuse. Des tests de traction montrent que leurs propriétés mécaniques ne subissent pas de baisse significative après plusieurs cycles de recyclage par moulage par injection (systèmes reposant sur les esters boroniques).

Même après plusieurs cycles de moulage, les vitrimères basés sur la chimie des esters boroniques peuvent être complètement dé-réticulés, signe de leur stabilité à haute température, notamment lors des étapes successives de mise en forme. Ces vitrimères ont une résistance supérieure dans les conditions "d'environmental stress cracking" comme des réseaux polymères conventionnels.

Summary: With the aim to generate vitrimers from commonly used thermoplastics with carbon-carbon based backbones, such as PMMA and PS, dynamic covalent exchange reactions relying on Schiff's bases and boronic esters were investigated. Two different approaches, *i.e.* crosslinking in solution or in extrusion, were used. These materials are processable via extrusion, compression and injection molding like their thermoplastic counterparts. The crosslinked nature of these systems was confirmed by solubility tests and DMA. Rheological measurements revealed the vitrimers ability to flow and viscosities between 10^5-10^7 Pa.s for boronic ester based PMMA vitrimers were measured. Consecutive tensile testing/reprocessing sequences proved the full recyclability of these vitrimers, and selective cleavage of the vitrimer networks followed by precise chemical analyses showed the thermal and chemical stabilities of vitrimers relying on boronic ester bonds. The stress cracking resistance of these vitrimers was significantly higher than that of parent thermoplastics, as can be expected for crosslinked systems.

Keywords: vitrimers, dynamic covalent chemistry, crosslinked polymers, processing, recyclability

Résumé: Dans l'optique de préparer des vitrimères à partir des thermoplastiques communément utilisés, tels le PMMA et le PS, des réactions d'échange dynamiques reposant les liens imine et esters boroniques ont été étudiées. Des paramètres importants comme la constante de dissociation de certaines molécules, la constante de vitesse et l'énergie d'activation ont été mesurées. Des monomères porteurs de liaisons échangeables ont été synthétisés et polymérisés. Des vitrimères, avec des liaisons C-C dans la chaine principale, ont été créés par différentes stratégies (PMMA et PS). Ces matériaux sont réticulés et insolubles avec un plateau caoutchouteux mais également façonnables et recyclables par moulage par compression ou par injection. Ces vitrimères peuvent relaxer les contraintes et couler à une température supérieure à celle de leur transition vitreuse. Des viscosités de 10^5-10^7 Pa.s ont été estimées pour les vitrimères PMMA reposant sur la chimie des esters boroniques. Des tests de traction montrent que leurs propriétés mécaniques de ces matériaux ne subissent pas de baisse significative après plusieurs cycles de recyclage par moulage par injection. Même après plusieurs cycles de moulage, les vitrimères basés sur la chimie des esters boroniques peuvent être complètement dé-réticulés, signe de leur stabilité à haute température lors du moulage. Ces vitrimères ont une résistance supérieure dans les conditions "d'environmental stress cracking" comme des réseaux polymères conventionnels.

Mots-clés: vitrimères, chimie dynamique covalente, polymères réticulés, mise en forme, recyclabilité.